POWER-LAW FLUID FLOWS OVER A TRUNCATED CONE IN A NON-DARCY POROUS MEDIUM

A THESIS SUBMITTED TO
NATIONAL INSTITUTE OF TECHNOLOGY WARANGAL, (T.S.)
FOR THE AWARD OF THE DEGREE OF
DOCTOR OF PHILOSOPHY
IN
MATHEMATICS

BY
ABHINAVA SRIVASTAV
(Roll No. 718064)

UNDER THE SUPERVISION OF
Dr. CH. RAMREDDY

DEPARTMENT OF MATHEMATICS
NATIONAL INSTITUTE OF TECHNOLOGY
WARANGAL-506004, INDIA

OCTOBER 2021

C E R T I F I C A T E

This is to certify that the thesis entitled "**Power-law Fluid Flows over a Truncated Cone in a Non-Darcy Porous Medium**" submitted to National Institute of Technology Warangal, for the award of the degree of ***Doctor of Philosophy***, is a bonafide research work done by **Mr. ABHINAVA SRIVASTAV** under my supervision. The contents of this thesis have not been submitted elsewhere for the award of any degree.

Dr. Ch. Ramreddy
Assistant Professor
Department of Mathematics
National Institute of Technology Warangal
Telangana State, INDIA

.

DECLARATION

This is to certify that the work presented in the thesis entitled **"Power-law Fluid Flows over a Truncated Cone in a Non-Darcy Porous Medium"**, is a bonafide work done by me under the supervision of **Dr. CH. RAMREDDY** and has not been submitted elsewhere for the award of any degree.

I declare that this written submission represents my ideas in my own words and where others' ideas or words have been included, I have adequately cited and referenced the original sources. I also declare that I have adhered to all the principles of academic honesty and integrity and have not misrepresented or fabricated or falsified any idea / data / fact / source in my submission. I understand that any violation of the above will be a cause for disciplinary action by the Institute and can also evoke penal action from the sources which have thus not been properly cited or from whom proper permission has not been taken when needed.

Abhinava Srivastav

Roll No. 718064

Date: 21/10/2021

Dedicated to

My Parents

Krishan Kumar Srivastav and Neelam Srivastava

Family & Friends

ACKNOWLEDGEMENTS

I am most grateful to God for giving me his grace to achieve all I have so far. I feel very privileged that I got a chance to start my research work under the unique supervision of Dr. Ch. Ramreddy, Assistant Professor of Mathematics, National Institute of Technology Warangal, India. I am indebted for his invaluable guidance and constant encouragement throughout the preparation of this thesis and his involvement and meticulous supervision while my work was in progress. With his inimitable qualities as a good teacher, he chiseled my path towards perfection. Ever since I met him, he has been a perpetual source of motivation, inspiration, encouragement and enlightenment. He is responsible for making the period of my research work as an educative and enjoyable learning experience. The thesis would not have seen the light of the day without his unrelenting support and cooperation. I deem it a privilege to have worked under his amiable guidance. My vocabulary is inadequate to express my gratitude. I also thank to his wife Smt. Ch. Geetha Ramreddy, for her hospitality and her patience during our elongated discussions.

I thank the Chairman of the Doctoral Scrutiny Committee and the Head of the Department, Dr. P. Muthu, members of the Doctoral Scrutiny Committee, Prof. J. V. Ramana Murthy, Prof. D. Srinivasacharya, Department of Mathematics and Dr. S. Ravi Chandra, Department of Computer Science and Engineering for their valuable suggestions, moral support and encouragement while my work was in progress.

I am greatly indebted to Prof. Y. N. Reddy, Prof. K. N. S. Kasi Viswanadham, Prof. Debashis Dutta, Department of Mathematics for their affectionate support and encouragement throughout my research period. Also, I thank all the Faculty members and the office non-teaching staff of the Department of Mathematics, for their valuable suggestions and help during this journey.

I express my sincere thanks to the Director, National Institute of Technology, Warangal for awarding me Institute Fellowship (MoE/MHRD, GoI) to carry out my research work. I express my sincere thanks to Dean (Academic), National Institute of Technology, Warangal and his staff for their valuable support through out my research work.

I owe my special thanks to Dr. Ch. Venkata Rao, Dr. P. Naveen, Dr. G. Shiva Kumar Reddy, Dr. Om Prakash Meena and Dr. Dipak Barman for their support and guidance. I thank Mr. K. Sita Ramana, Mr. Raghvendra Pratap Singh, Mr. Atul Kumar Shriwastva, Mr. R. Shravan Kumar, Mrs. Smriti Tiwari, Mr. Har Lal Saran, Mr. Subhabrata Rath, Mr. Nitish Gupta, Miss. Nidhi Humnekar, Mr. B. Rajender and all other research colleagues in the Department of mathematics and my friends, who helped me during my Ph.D. for being cooperative and also for making my every moment of stay in the NITW campus fruitful and enjoyable.

My deepest gratitude to my Parents, Krishan Kumar Srivastav and Neelam Srivastava and siblings Ayushi Srivastava and Abhijeet Srivastav for their continuous support and constant encouragement over the years. All of their love and affection have been motivating force behind what I am today. Without their help and encouragement, I would not have finished this thesis.

Abhinava Srivastav

A B S T R A C T

The heat transfer characteristics in natural/mixed convective flow of non-Newtonian fluids (particularly power-law fluids, power-law nanofluids and power-law hybrid nanofluids) are very important because of its significant applications in engineering and science. Fluids like molten plastics, glues, pulp, slurries etc., are described by the Ostwald-de Waele type of power-law fluids. The heat transfer problems in different power-law fluids subject to the convective boundary condition are more extensive and these occur in various realistic situations. In the mathematical models of these type of power-law fluids, the physical systems become slightly more complicated leading to the complex interactions of the fluid flow and heat transfer mechanism. In this thesis, an attempt has been made to analyze the flow of different power-law fluids over a truncated cone placed in a non-Darcy porous medium with various important effects. The flow governing equations and boundary conditions are changed into dimensionless form by introducing suitable non-dimensional variables. The resulting system of equations is then solved numerically by employing combined approach of local non-similarity and spectral local linearisation method (SLLM). The error analysis and convergence test have been conducted to examine the accuracy of this combined numerical approach. In addition to this, the obtained numerical results are also validated and compared with the existing results in some special cases and the outcomes are observed to be in a very good agreement.

This thesis consists of SEVEN chapters. Chapter - 1 is introductory in nature and gives motivation to the investigations carried out in the thesis. A survey of pertinent literature is presented to exhibit the importance of the problems considered. The basic governing equations of the flow and physical quantities related to power-law fluids, power-law nanofluids and power-law hybrid nanofluids along with the details of used methodology, are given. In the case of nanofluids and hybrid nanofluids, the Tiwari and Das model is adopted to examine the fluid flow. Chapter - 2 consists of a numerical investigation on the flow of stratified power-law fluids over a convectively heated truncated cone in a non-Darcy porous medium with nonlinear convection and thermal dispersion effects. Chapter - 3 deals with the entropy generation and Bejan number estimation in power-law fluid flows. Chapter - 4 gives a combined study of linear, quadratic and nonlinear thermal radiation in the flow of power-law fluids. Chapter - 5 explores the inspection of power-law nanofluid flows in which Titanium alloy and multi wall Carbon nanotubes are used separately as nanoparticles whereas water is taken as the base fluid. Chapter - 6 reports the convective flow analysis of power-law hybrid nanofluids and these fluids are formed with the two nanoparticles together, namely, Titanium alloy and multi wall Carbon nanotubes along with water. In all the above

chapters, a truncated cone placed in a non-Darcy porous medium is used as the geometry. The obtained numerical results are exhibited graphically to illustrate the effects of various parameters, nanoparticle volume fraction and streamwise coordinate on the dimensionless velocity, temperature, heat transfer rate and skin friction coefficient. Chapter - 7 includes the main conclusions of the earlier chapters and the directions in which further investigations may be carried out.

NOMENCLATURE

A^*	Stratification intensity control parameter
b	Empirical constant
Bi	Biot number
Be	Bejan number
Br	Brinkman number
C_f	Skin friction coefficient
C_p	Specific heat capacity
d	Pore diameter
Ds	Thermal dispersion parameter
E_f	Error norm for velocity
E_θ	Error norm for temperature
Fs	Non-Darcy parameter (Forchheimer number)
g	Gravitational acceleration
Gr^*	Modified Grashof number
h_f	Convective heat transfer coefficient
k, k_m	Thermal conductivity
k_d	Dispersion thermal conductivity
k_e	Effective thermal conductivity
K_p	Intrinsic permeability
K^*	Modified permeability
$\bar{k}$	Mean absorption coefficient
L_x	Numerical approximation at infinity
n	Power-law index
Nu_x	Local Nusselt number
Ns	Dimensionless entropy generation rate
N_x	Collocation points in η direction
N_1	Dimensionless entropy generation due to heat transfer
N_2	Dimensionless entropy generation due to fluid friction
O	Origin of coordinate system
p	Fluid pressure
Pe	Peclet number
Pr	Prandtl number
$\overrightarrow{q}$	Darcian velocity
r	Radius of truncated cone
Ra	Rayleigh number
Re	Reynolds number
S	Scaling parameter
S_T	Thermal stratification parameter
S_g'''	Dimensional entropy generation rate

$\left(S_g'''\right)_0$	Characteristic entropy generation rate
T	Temperature
T_f	Convective wall temperature
u_*	Characteristic velocity
u	Velocity in x direction
v	Velocity in y direction
$\bar{x}$	Modified streamwise coordinate

Greek Symbols

α	Molecular diffusivity
α_d	Thermal diffusivity
α_1	Nonlinear convection parameter
$\beta_0\,,\beta_1$	First and second order thermal expansion coefficients
ϵ	Viscous dissipation parameter
η	Dimensionless variable in y-direction
γ	Inclination of angle
χ	Mechanical dispersion coefficient
λ	Mixed convection parameter
θ	Dimensionless temperature
θ_w	Temperature ratio
$\phi\,,\phi'$	Nanoparticle volume fraction
ϕ^*	Porosity of the medium
μ	Dynamic viscosity
μ^*	Consistency index of power-law fluid
μ'	Effective viscosity
ν	Kinematic viscosity
ρ	Density
σ	Stefan-Boltzmann constant
ψ	Stream function
τ	Shear stress
ξ	Dimensionless streamwise coordinate
Ω	Dimensionless temperature difference

Subscripts

f	Fluid
nf	Nanofluid
hnf	Hybrid nanofluid
s	Solid particle
w	Wall condition
∞	Ambient condition

Superscript

$'$	Differentiation with respect to η

Contents

[1]Case(a): Published in "**International Journal of Applied and Computational Mathematics**" 7(3), 1–17, (2021), Case(b): Published in "**Heat Transfer**" 50(3), 2380–2402, (2021).

[2]Case(a): Published in "**Journal of Thermal Analysis and Calorimetry**", June 2021, DOI: 10.1007/s10973-021-10823-1, Case(b): Published in "**International Journal of Ambient Energy**", July 2021, DOI: 10.1080/01430750.2021.1951838.

[3]Case(a): Communicated to "**International Communications in Heat and Mass Transfer**", Case(b): Communicated to "**International Journal of Thermal Sciences**".

[4]Case(a): Accepted in "**Discontinuity, Nonlinearity, and Complexity**", January 2021, Case(b): Published in "**Indian Journal of Physics**", March 2021, DOI: 10.1007/s12648-021-02055-8.

[5]Case(a): Published in "**Computational Thermal Sciences: An International Journal**" 13(5), 31–43, (2021), Case(b): Communicated to "**International Journal for Numerical Methods in Fluids**".

Chapter 1

Preliminaries and Review

1.1 Introduction

The area of fluid dynamics surrounds the movement in different liquids and gases, the forces behind this movement and the interlinkage of the fluids with solids. Fluid dynamics can be treated as a centre of many engineering and science sectors and it is involved in almost each direction of our day-to-day survival. From the field of aerodynamics and related movable vehicles to the motion of biological fluids in the human body, the weather forecast, the efficiency of microfluidic gadgets, all require a proper comprehension of this subject. Since fluid dynamics contains complex flow studies and carries widespread applications, it is proved to be a broad area with various exciting and challenging problems related to recent advancement in engineering and science. The search for extensive grip in this area has not only stimulated the evolution of the subject but has also given the breakthrough in the assisting fields, such as applied mathematics, numerical computation and experimental techniques. The foundational postulates of fluid dynamics are the conservation laws namely conservation of mass, Newton's second law of motion and first law of thermodynamics. A large number of problems in fluid dynamics have claimed the attention of mathematicians, physicists, and engineers for many years. As a result, an enormous body of established results has been accumulated steadily but remains scattered in the literature.

Convective heat transfer, or simply, convection is the study of heat transport processes affected by the flow of fluids and has gained significant importance in recent times. In general, the convection process is classified into two processes. If any outsider source is responsible for the fluid motion, then it is called forced convection and if no such external induced flow is supplied and the flow takes place due to effect of a density difference resulting from changes in temperature in a body force field such as the gravitational field, then it is called free or natural convection. When both free and forced convection effects are significant and neither of the two can be neglected, the process is called mixed convection. The phenomenon of free and mixed convection occurs in many technical and industrial problems such as cooling of electronic equipment, materials processing, and drilling operations. Apart from these applications, the free convection has also been used to explain the connection between skin disease and respiratory disease such as eczema and asthma respectively whereas the mixed convection has an important role in controlling the temperature of a medium. For more details on the convective heat transfer, one can refer the text book by Bejan [9].

1.2 Porous Medium

A medium (or material) which contains voids is termed as porous medium whose skeletal portion is usually called the frame or matrix. In general, a fluid (liquid or gas) is typically filled in these pores and the solid matrix with the fluid is called a fluid-saturated porous medium. A porous medium is normally distinguished by porosity defined as the fraction of the volume of void spaces over the total volume (between 0 and 1). Examples of porous media are very wide ranging from natural substances (e.g., soil, rocks and biological tissues) to artificial ones (e.g., cements and ceramics) and different properties of these materials are only rationalized by treating these as porous media.

Porous medium concept is used in different areas of engineering and applied science, for example, petroleum, construction or material science, filtration, geomechanics, soil mechanics, acoustics, etc. Thus, flow of fluids (Newtonian or non-Newtonian) in porous medium exerts a huge amount of interest among researchers and has been emerged as a separate area

of research. In particular, if the temperature and moisture distribution over agricultural fields are studied with this approach then these ideas can be used in the control of environment pollution. Keeping all these in mind, many different fluid models have been developed and a few of them are analysed to explain fluid flow properties through non-Darcy porous media in different books by Pop and Ingham [98], Nield and Bejan [88], and Vafai [124]. Further, the boundary layer assumptions have been successfully applied to these models and a good amount of related work over the last a few decades have been done for a wide variety of geometries. The Darcy model and a series of its modifications have attained much acceptance in comparison with other models.

Darcy Model

In 1856, Darcy [25] was the first who gave a governing equation to analyse the fluid flow in upstanding porous column. This equation depicts a stabilization of pressure gradient and viscous force. Mathematically,

$$\overrightarrow{q} = -\frac{K_p}{\mu}(\nabla p - \rho\, g), \tag{1.1}$$

where $\overrightarrow{q}$ is known as Darcian velocity, K_p, p, g, ρ and μ are termed as intrinsic permeability of the medium, fluid pressure, acceleration due to gravity, density and coefficient of viscosity respectively. This law provides better consistency with experimental observations for $1-D$ flows in low porosity system. Since this law does not involve inertial effects, it is applicable only for seepage flows $[Re = O(1)]$.

Darcy-Brinkman Model

It is assumed that the flow through an anisotropic porous medium with notable permeability must reduce to the viscous flow in a limit. In view of this, Brinkmann [88] realised the necessity to consider the viscous force employed by a flowing fluid on a dense swarm of spherical particles immersed in a porous mass and joined the term $\mu'\,\nabla^2 V$ to stabilize the pressure gradient. Here, μ' is the effective viscosity given by $\mu' = \mu[1-2.5(1-\phi^*)]$, in which

ϕ^* is porosity. From experiments, it is confirmed that this Brinkmann model is valid for the high porosity medium. The governing equation for this model can be written as

$$-\left[\nabla p - \rho g\right] = \frac{\mu}{K_p}\overrightarrow{q} - \mu'\nabla^2\overrightarrow{q}. \tag{1.2}$$

Darcy-Forchheimer Model

In 1901, Forchheimer made some assessment and suggested that inertial effects may be considered with the incorporation of the square of velocity in the momentum equation. So, the adjustment in Darcy′s equation can be given as

$$\left[1 + \frac{\rho\, b\, \sqrt{K_p}}{\mu}|\overrightarrow{q}|\right]\overrightarrow{q} = -\frac{K_p}{\mu}\left[\nabla p - \rho g\right], \tag{1.3}$$

where b is the non-dimensional drag coefficient which differs with the porous medium characteristics. Many more versions of modifications in this model can be seen in the literature. The validation along with associated restrictions of these models are properly described by Nield and Bejan [88].

1.3 Newtonian and Non-Newtonian Fluids

"A Newtonian fluid is the fluid which exhibits a viscosity that remains constant regardless of any external stress that is placed upon it, such as mixing or a sudden application of force. One example is water, since it flows the same way, in spite of whether it is left alone or agitated vigorously [7]." In other words, "Newtonian fluids are those that obey Newtons law relating shear stress and shear rate with a simple material property (the viscosity) dependent on basic thermodynamic variables such as temperature and pressure, but independent of flow parameters such as shear rate and time [7]." Convective heat transfer in 'Newtonian fluid' and 'Newtonian fluid saturated porous media' has been widely examined since the middle of the last century by incorporating various physical effects.

"A non-Newtonian fluid can be defined as a fluid with viscosity as a variable dependent on applied force or stress [52]." Corn starch dissolved in water is one of the routine examples of a non-Newtonian fluid, which occurs in day-to-day survival. Opposite to the Newtonian fluids, the non-Newtonian fluids become thicker or thinner when stress is applied. Therefore, a great amount of work has been brought forth to illustrate the nonlinear relationship between the rate of strain and stress in non-Newtonian fluid models. But there is no single fluid flow model which undoubtedly exhibits all the properties of real fluids. During the last century, several fluid models (viscoelastic fluids, dusty fluids, micropolar fluids, couple stress fluids, Casson fluids etc.) were proposed to characterize the real fluid behaviour. Among these, Ostwald-de Waele power-law fluid model, proposed by Ostwald [90] and de Waele [128] gained much importance. It is the one which characterizes the flow pattern of polymers, glass, cosmetic products, grease, and many more, and it has substantial applications in many engineering industries such as manufacturing processes, oil reservoir and chemical engineering, etc. These power-law fluids can be studied under following points:

1.3.1 Power-law Fluids

"A power-law fluid is a type of generalized non-Newtonian fluids for which the shear stress τ_{xy} can be expressed as

$$\tau_{xy} = \mu^* \left| \frac{\partial u}{\partial y} \right|^{n-1} \frac{\partial u}{\partial y}, \tag{1.4}$$

where μ^* is called the consistency coefficient and n is the power-law index. The dimension of μ^* depends on the value of n which is non-dimensional. When $n = 1$, the equation represents a Newtonian fluid with a dynamic coefficient of viscosity μ^*. Therefore, the deviation of n from unity indicates the degree of deviation from Newtonian behaviour [90, 128]." One may interpret the physical behaviour of the fluid by appealing to an effective viscosity. For $n > 1$, the fluid is dilatant (e.g., suspensions of sand) or shear-thickening fluids in which apparent viscosity at high shear rates. For $n < 1$, the fluid is pseudoplastic (e.g., polymer solutions) or shear-thinning fluids that have a lower apparent viscosity at higher shear rates. Shenoy [110] presented many interesting studies on convective heat transport in non-Newtonian power-law

fluids saturated porous media in connection with geothermal and oil reservoir engineering applications.

1.3.2 Power-law Nanofluids

In the last few decades, several works in the field of power-law fluids and nanotechnology have attracted many investigators due to its broad-ranging applications. Nanofluids are classified as the engineered colloids containing base fluid and nanoparticles. The suspension of nanoparticles without sedimentation in the base fluid makes them different from regular particles and this happens mainly because of their small size (10^{-9} meter). Water, polymeric solutions, organic liquids etc., are frequently used base fluids whereas chemically stable metals (e.g., Copper, Aluminium, Gold and Titanium) and metal oxides (e.g., Alumina, Titania and Silica) along with Carbon in its different form (e.g., Graphite, Diamond and Carbon nanotubes) are utilised as important nanoparticles. The nanoparticle insertion in the base fluid even at low volume concentrations, results into significant enhancement of the thermal performance. During last few decades, the exploration of nanofluids has attracted immense enthusiasm from researchers, because of its tremendous applications in computing technologies, communication, medicines, lasers, high power X-rays, optical devices, electronics, scientific measurement, material processing, material synthesis, etc. The detailed introduction and applications of nanofluids can be seen in the textbook by Das *et al.* [27].

1.3.3 Power-law Hybrid Nanofluids

A hybrid nanofluid is formed by taking a base fluid with two different types of nanoparticles dispersed in it. Each of these nanoparticles strengthen the important properties of other one. Various metals e.g., Aluminium, Copper, Titanium and their alloys possess large thermal conductivities. Although few nanoparticles have lesser thermal conductivity in comparison to metallic ones, but these possess various important properties e.g., chemical inertness and stability. So, it can be expected that the insertion of metallic nanoparticle in another

nanofluid may enhance the significant properties of the resultant mixture with sustained stability of the nanofluid. The detailed information about hybrid nanofluids can be found in the paper of Sarkar *et al.* [105] where the recent developments and challenges of hybrid nanofluids are included.

There are mainly two different popular models in this area: (i) Tiwari-Das model [123], and (ii) Buongiorno model [11]. These models have been used frequently by several researchers to investigate the heat transfer enhancement process.

Tiwari-Das model

Tiwari and Das [123] developed a model to analyse the behaviour of nanofluids by taking the volumetric fraction of nanoparticles (ϕ) into the consideration. In this model, viscosity of the nanofluid (μ_{nf}), density of the nanofluid (ρ_{nf}) and thermal diffusivity of the nanofluid (α_{nf}) are given by

$$\mu_{nf} = \frac{\mu_f}{(1-\phi)^{2.5}},\ \rho_{nf} = (1-\phi)\rho_f + \phi\rho_s,\ \alpha_{nf} = \frac{k_{nf}}{\rho C_{pnf}},$$

where

$$\rho C_{pnf} = (1-\phi)\rho C_{pf} + \phi\rho C_{ps},\ \frac{k_{nf}}{k_f} = \frac{(k_s+2k_f)-2\phi(k_f-k_s)}{(k_s+2k_f)+\phi(k_f-k_s)}.$$

Here, μ_f is the viscosity of the base fluid, ρ_f is the density of the base fluid, ρ_s is the density of the solid particle, k_{nf} is the effective thermal conductivity of the nanofluid, C_{pf} and C_{ps} are the heat capacities whereas k_f and k_s are the thermal conductivities of the base fluid and nanoparticle, respectively.

Buongiorno model

Buongiorno [11] proposed an analytical model for convective transport in nanofluids, which incorporates the effects of Brownian diffusion and thermophoresis. Contrary to the Tiwari-

Das model [123], that focuses on volumetric fraction of nanoparticles, Buongiorno model pays more attention to Brownian motion and thermophoresis effects. The arbitrary motion of nanoparticles within the base fluid is called Brownian motion, and this results from continuous collisions between nanoparticles and molecules of the base fluid. Along with this, particles can also be diffused under the influence of a temperature gradient. This phenomenon is called thermophoresis, and is the particle equivalent of the renowned Soret effect for gaseous or liquid mixtures. This Buongiorno model has been used in recent works by many researchers.

With the Tiwari-Das model it is worth noting that the nanoparticle volume fraction is taken to a constant, unlike, in the Buongiorno model it needs to be calculated. In case of nanofluids and hybrid nanofluids, the Tiwari and Das model is adopted throughout the thesis.

1.4 Solution Procedure

The governing equations of convective heat transport in Newtonian and/or non-Newtonian fluids are essentially coupled and nonlinear partial differential equations (PDEs). In general, these nonlinear PDEs cannot be easily solved analytically, therefore some numerical method should be adopted. Various numerical methods, including the finite element methods, finite difference methods, finite volume methods, spectral methods, shooting methods, boundary element methods, homotopy analysis method, cubic spline collocation method, etc., have been used by several researches to solve the boundary value problems. Among these, we apply a novel and rapid convergence approach named as the *Spectral Local Linearisation Method* (SLLM) [76] together with the non-similarity procedure [115, 74] to solve the governing differential equations in the present thesis. Initially, SLLM has been introduced by Motsa [76] and it is a combination of local linearisation technique and spectral collocation method. This procedure carries many beneficial properties that make it relevant for the approximate solutions of differential equations. A few outstanding theoretical results on the various spectral methods, for solving the coupled system of highly nonlinear differential

equations defined on both regular and irregular domains, have been discussed by Gottlieb and Orszag [40]. A brief step-wise detail of this solution procedure can be given in the following points:

1. First, incorporating the non-similarity approach:
    - Reduce the **r** number of nonlinear coupled PDEs into a system of nonlinear coupled ordinary differential equations (ODEs) by introducing the auxiliary variables to the partial derivatives of the unknown functions.
    - With this approach, one can obtain 2**r** number of nonlinear coupled ODEs which are to be solved concurrently along with the boundary conditions.
2. Next, the set of resulting 2**r** number of nonlinear coupled ODEs is linearised using the local linearisation method. For this,
    - To generate the iteration scheme, local linearisation is applied about the unknown function (the previous iteration) to the i^{th} nonlinear equation presuming that all other functions are known.
    - To get a decoupled iteration scheme, the Gauss-Seidel approach of decoupling linear algebraic system is taken into consideration.
3. To solve this iterative scheme, Chebyshev spectral collocation method [12] is utilized. In this method, we use the following steps:
    - The transformation $\frac{\eta}{S} = \frac{\tau + 1}{2}$, $-1 \leq \tau \leq 1$, is incorporated to change the domain $[0, S]$.
    - Discretize the new domain $[-1, 1]$ employing the Gauss-Lobatto collocation points.
    - Approximate the unknown functions and their derivatives in terms of Chebyshev polynomials $T_w(\tau) = \cos[w \ \cos^{-1}\tau]$ at the collocation points.
    - Replace these expressions in the system of linearised differential equations to get the matrix system.

4. Finally, solve the resultant matrix system iteratively by starting with the initial approximations.

1.5 Literature Review

The study of free and mixed convective flows gives one of the fundamental frameworks in the mechanism of heat transfer and so it is an area of appreciable conceptual and experiential curiosity. Natural convection plays a significant role in various industries, for example, chemical processing apparatus designing, emergence and diffusion of smog, temperature distribution, wetness in farm lands and thicket of fruit trees. It also occurs in the context of destruction to crops on account of chilling and contamination of the surroundings. The mixed convection takes place in several technological and commercial areas, for example, electric gadget unheated by air coolers, nuclear reactor cooling in time of any crisis situation, a heat exchanger situated in a low-velocity atmosphere, solar panels etc.

Convective flows over a vertical surface placed in a porous medium is one of the fundamental and classical problems in the heat transfer theory. It has fascinated a substantial amount of attentiveness from several researchers owing to the broad applications such as geothermal systems, energy-storage units, heat insulation, heat exchangers, drying technology, catalytic reactors, nuclear waste repositories, etc. The literature relevant to the convective flows over different surface geometries in Darcy and non-Darcy porous media has been reported by Ingham and Pop [51], Nield and Bejan [88] and Vafai [124] among others (also see the citations therein).

The presence of convective boundary condition in any heat transport mechanism gives important and convenient platform to control the situations in the heat exchangers, reactors and gas turbine related construction sites due to its pragmatic character. In several day-to-day implementations which demand surface heating or cooling, the existence of convective heat exchange between the neighbouring fluid and surface cannot be ignored, and it is an extremely important phase in industry related to thermal material processing. This operation

involves the transfer of heat to the fluid via any enclosed surface with a certain heat capacity, which gives a convective heat transfer coefficient. To explain this, a novel mechanism for the laminar thermal boundary layer flow along a flat plate is introduced by Aziz [4]. Hayat *et al.* [46] discussed the thermal radiation impact on the stagnation point flow past a movable surface with the convective boundary condition. Influence of a magnetic field under the convective boundary condition has been analysed by Murthy *et al.* [81] for a thermally stratified nanofluid flow over a vertical surface in a non-Darcy porous medium.

Non-Newtonian fluids are very extensive in the environment and industrial processes and it would be no magnification to assert that flow of Newtonian fluids is the anomaly rather than the law. The interest of learning about non-Newtonian fluid flow has attracted the researchers from many decades ago [63]. The power-law fluids are the time independent non-Newtonian fluids (generalized Newtonian fluid). Broadly, we classify the power-law fluids into two categories: shear thickening (dilatant) and shear thinning (pseudoplastic). The viscosity of the fluid increases with stress for the first and decreases for the later one. Several investigators have shown much attention to non-Newtonian fluids in view of their applications in various aspects of the industrial processing, design of equipment, chemical and allied processes such as cosmetics, synthetic polymers, biological fluids, synthetic lubricants etc. These fluids reveal complex rheological nature which is not accomplished by Newtonian fluids. The viscosity in two type of power-law fluids, shear thinning (pseudoplastic) and shear thickening (dilatant), decreases and increases with stress respectively.

Due to wide application of power-law fluids in modern science and technology, Shenoy [110] and Cheng [16] explored the influence of pertinent parameters for applicable geometries. Non-Darcy mixed convective flow of power-law fluids over an isothermal vertical plate with suction/injection effect has been examined by Ibrahim *et al.* [50]. Free convection from a cone/flat plate in a non-Darcy porous medium saturated by the power-law fluid, has been analysed by Kairi and Murthy [55]. Further, Srinivasacharya and Reddy [119] scrutinized the importance of chemical reaction and radiation on the power-law fluid flow along a vertical plate embedded in a porous medium in the presence of variable temperature and concentration conditions. The study of power-law fluid also takes part as a significant role in the

medical science to find the characteristic of blood flow in arteries and veins. In view of these, Kumar and Diwakar [64] have developed a mathematical model to investigate the blood flow via an artery with stenosis. The role of local production of thermal energy through viscous stress mechanism of power-law fluid flow due to buoyancy forces has been evaluated in detail by Khidir *et al.* [61]. Kairi [53] concluded that the increment in the radius of slender paraboloid in a porous medium reduces the Nusselt number for all shear thickening and thinning fluids. Recently, the influence of activation energy in a power-law fluid flow over a permeable inclined plate is studied by Ramreddy and Naveen [101] (also see the citations therein) and they have shown that the results are significant in the different mechanisms of ignition, technologies related to aerosol and polymeric mixtures at high temperature.

The available literature reveals that the power-law fluid flow studies can serve as a useful productive tool to solve engineering and industrial problems. There are some works available in the literature, namely, Na and Chiou [82], Gorla *et al.* [39] and Cheng [18] where researchers explored the studies related to power-law fluid flow over truncated cone maintained at uniform wall temperature and/or subject to uniform heat flux conditions. But, many engineering and industrial problems e.g., processing of melted plastics at a large level, edible items or slurries and polymers etc., require free convective transport in a power-law fluid flow from vertical surfaces subjected to the convective boundary condition in porous media. This motivates investigators to analyse the power-law fluid flow problems in detail as it helps us to understand various effects like: (i) ratio of internal thermal resistance of truncated cone surface to the thermal resistance of boundary layer in terms of Biot number, and (ii) effectiveness of non-uniform pore level velocity over temperature field within the specific porous medium in terms of thermal dispersion parameter. In view of this, the similarity solutions of power-law fluid flows past a convectively heated vertical surface have been obtained by Ece and Buyuk [31]. Khan and Gorla [59] discussed the power-law fluid flows over a convectively heating vertical wedge which are useful in thermal engineering sector, in particular, geothermal systems, ground water pollution, crude oil extractions and storage of nuclear waste etc.

It is well established from the literature survey and experiments that the Boussinesq

approximation is appropriate only for a few fluid flows where very less variations in temperature gradient exist. So, the density variation is less and the buoyancy controls the movement. In this approximation, the density is taken as constant everywhere except in the buoyancy force term. When the temperature difference between surface and ambient fluid is noticeably great, the mathematical models established by involving linear density relation does not give proper result. In other words, a few thermal systems, e.g. solar collector and nuclear reactor which are handled at much higher temperatures and so the density relation with temperature loses its linearity nature $\rho = \rho_\infty [1 - \beta_0(T - T_\infty)]$ (See, Pop and Ingham [98]). The resultant nonlinearity contrast in temperature-dependent density relationship $\rho = \rho_\infty [1 - \beta_0(T - T_\infty) - \beta_1(T - T_\infty)^2]$ (for more details, Partha [93] and citations therein may be referred) strongly influences the fluid flow and heat transfer characteristics, and termed as nonlinear density temperature relationship (specifically, nonlinear convection or nonlinear Boussinesq approximation). Partha [93] examined the effect of cross-diffusion, double dispersion and nonlinear convection in a viscous fluid flow, whereas this work has been extended by Kameswaran *et al.* [57] in which thermophoretic effect is discussed in the absence of cross-diffusion effects. Nonlinear convection over an impulsive stretching sheet has been examined numerically by Motsa *et al.* [77] (see the references therein). A broad span of problems in the field of geophysical and energy industries such as geophysical flows, thermal insulation etc., requires convective flow analysis of non-Newtonian fluids in a porous medium [88].

Thermal dispersion effect in a non-Darcy porous medium is important because of the existence of inertial effects. In non-uniform geometries, particularly in the packed beds, flow of fluid through curvy paths led to the thermal dispersion at pore level of the involved porous media. In view of the mechanism of thermal dispersion effect, Cheng [21] and Plumb [96] provided a model for the fluid flow and heat transfer in porous media by taking these effects into consideration. Also, Hong *et al.* [48] conducted the theoretical studies extensively on thermal dispersion effect by treating $\dfrac{\chi du_\infty}{\alpha} = \chi Pe_\chi$ as a single parameter Ds. By adopting the similar representations, Kairi and Murthy [54] conducted the study of free convective flow of non-Newtonian fluids from a vertical flat plate with the thermal dispersion. Numerical

study for the same fluid flow but without prescribing the temperature and concentration on the vertical surface has been presented by Srinivasacharya *et al.* [117] and they concluded that the obtained similarity solutions are valid only for small values of X - location (i.e. $0 < X < 1$). On the other hand, Lai and Kulacki [65] concluded the similar results of Hong *et al.* [48] without treating $\frac{\chi du_\infty}{\alpha}$ as single parameter Ds. In a precise way, they treated $\frac{\chi du_\infty}{\alpha}$ as χPe_χ instead of Ds, by assigning the experimental value for χ within $\left[\frac{1}{7}, \frac{1}{3}\right]$. However, Murthy [79] and his collaborators [57] conducted further comprehensive study on the validity of thermal dispersion under different flow conditions over various surface geometries and revealed the fact that it enhances the heat transfer rate (for sake of brevity only a few references are cited here).

The study related to thermal stratification with its consequences in different porous media has gained significant recognition in modern times in view of its major applications in heat exchangers for solar hot water storage tanks to use in domestic purposes. Dake and Harleman [24] gave the analytical and laboratory studies of thermal stratification in lakes. The widely used model of solar domestic hot water systems requires heat exchanger involvement in order to transfer heat from solar collector (contains hot fluid) to storage tank (contains water). One can refer to the works of Knudsen and Simon [62] for more details. In view of these applications, Narayana *et al.* [86] and Cheng [17] conducted independent studies on the free convective flows over vertical flat plate and vertical wavy surface, respectively, with dilatant and pseudoplastic fluids and concluded that the total Nusselt number value for wavy surface is more in comparison to the smooth surface. RamReddy *et al.* [100] investigated the effects of linear and nonlinear stratification on mixed convective flow in a porous medium and concluded that the stratification significantly affects the heat and mass transfer rates and delays the boundary layer separation (also see the references given there). Vasu *et al.* [127] emphasized the significance of entropy generation, thermal dispersion and nonlinear temperature density relationship on the thermally stratified fluid flow over a vertical plate embedded in a porous medium.

The locally produced thermal energy due to viscous stress mechanism, commonly known as viscous dissipation, influences forced, mixed and free convective flows for fluid saturated

porous medium and clear viscous fluids. For the uniform forced convective flows along a plane surface, its effects in the presence of wall temperature distribution have been discussed by Magyari *et al.* [67]. Aydin and Kaya [3] explained viscous dissipation impact in the convective flows over an isothermal vertical plane surface immersed in non-Darcy and Darcy porous media respectively. An expression to show the rate of change of kinetic energy using upscaled momentum equation has been well established by Salama [103]. El-Amin *et al.* [34] employed the Darcy-Brinkman model for the explanation of flow field by involving viscous dissipation in a novel form. Megahed and Reddy [73] described the theoretical and numerical studies related to viscous dissipation on the flow of viscoelastic fluid.

The effect of thermal radiation in different fluid flows, is very useful in the nuclear plants, gas turbines, various propulsion devices for aircraft, missiles, satellites, space vehicles, etc. Also, the thermal radiation may play an essential role in controlling the heat transfer in industries where the quality of final product depends on the heat controlling factors to some extent. Mixed convective flow analysis along a vertical plate with the companionship of nonlinear radiation has been properly analysed by Murthy *et al.* [80]. Also, Chen [15] examined the effect of linear thermal radiation on the flow of power-law fluid with electrical properties. The linear radiation effect in a MHD non-Darcy porous medium using numerical techniques has been studied by Srinivasacharya *et al.* [118]. Simultaneous impact of the nonlinear thermal radiation and MHD in a stagnation point flow of power-law fluids has been investigated by Hayat *et al.* [44]. Megahed [72] discussed the impact of constant heat flux on power-law fluid flows exposed to the linear thermal radiation. Srinivasacharya and Reddy [120] addressed the role of mixed convection study in a power-law fluid flow with chemical reaction and nonlinear radiation impacts. The usefulness of linear thermal radiation on the natural convective flow past a truncated cone has been scrutinized by Elbashbeshy *et al.* [35]. RamReddy and Naveen [101] analysed the effect of linear thermal radiation and activation energy for power-law fluid flows in the presence of convective heating.

The second law of thermodynamics gives an idea of optimization in the design of different devices involved in the thermal field by making the sum of thermal and frictional entropy generation rates minimum. To get an optimal set of operating and design conditions, one

can minimize the system's irreversibility. There is a basic difference between transfer of energy into a system in the form of heat and doing the same by work. Both can be of equal quantity but after being a part of system's energy, these have much distinct character. This can be seen as the amount of energy involved in the process of energy transport (e.g., heat transfer), energy character and its change in the course of transport activity. So, in order to measure this character along with its possible decay in the process of energy transfer, entropy plays a very significant part. The entropy generation analysis has great importance in the manufacturing and upgrading of various thermofluidic components e.g., turbines, heat exchangers, pumps, energy storage systems etc. To explain these applications, Bejan [8] studied the effectiveness of various factors involved in the entropy generation in different thermal systems. Khan and Gorla [60] considered the non-Newtonian fluid flows over a horizontal plate immersed in a porous medium and performed the second law analysis. Das *et al.* [26] explained the combined effect of Navier slip, convective heating and magnetic field on the analysis of entropy generation (for more details, see the citations therein).

In recent past, a good amount of interest is developed in the scientific and research community to deal nanofluids along with convective flow studies [81, 42, 84]. Khan and Khan [58] used Buongiorno type of power-law nanofluids to discuss the boundary layer flow involving a new mass flux condition (also see the citations therein). Dogonchi and Ganji [30] explored the impact of Cattaneo-Christov heat flux on the flow of a MHD nanofluid with thermal radiation and Joule heating. Further, many useful references related to nanofluids are collected in the books by Das *et al.* [27] and Minkowycz *et al.* [75]. The review papers by Kakac and Pramuanjaroenkij [56] and Fan and Wang [36] also gave a detailed reference list. Chougule and Sahu [22] investigated the thermal performance of radiators experimentally using Carbon nanotube-water nanofluid. The non-Newtonian nature of nanofluid containing MWCNTs nanoparticles has been experimentally verified by Liu *et al.* [66]. The numerical investigation of the entropy generation on MHD mixed convective flow of Cu-water nanofluid with partial slip influence has been done by Chamkha *et al.* [13]. Similarly, Rashad *et al.* [102] performed a numerical investigation related to impact of the heat sink, source size and location on the entropy generation and MHD free convection flow. The effect of partial slips

on entropy generation analysis has been given by Shashikumar *et al.* [107].

Selimefendigil and Chamkha [106] performed the numerical investigation related to the free convection in a triangular annulus containing hybrid nanofluid. Also, the preparation and thermal properties including heat transfer and friction factor have been provided by many researchers [111, 121]. On the other hand, these hybrid nanofluids have a broad range of significant application in the domestic and technical fields e.g., refrigerators, transformers, brake fluids for different type of automobiles etc. The analysis of heat transfer in Ag-CuO/water hybrid nanofluid has been done by Hayat [45]. Sozen *et al.* [114] discussed the improvement in heat recovery unit performance where working fluid is taken as CuO-ZnO/water hybrid nanofluid. Recently, Basha *et al.* [6] revealed the impact of suction/injection parameter on skin friction coefficient for Ag-MgO/water hybrid nanofluid flow.

The limited literature related to this power-law fluid flow model over a truncated cone in a non-Darcy porous medium under different conditions motivates us to explore it. Also, considering the important applications of these different power-law fluids in real world, the flow studies over a truncated cone have been analysed in this thesis. In addition, various important effects and nanoparticles are incorporated in different types of analysis. The problems considered in this thesis are outlined in the next section.

1.6 Aim and Scope

The objective of the present thesis is to explore the flow behaviour of different non-Newtonian fluids, namely, power-law fluids, power-law nanofluids and power-law hybrid nanofluids over a truncated cone in a non-Darcy porous medium. The study focuses on the attributes of various effects such as Biot number, thermal dispersion, thermal stratification, nonlinear convection, viscous dissipation, thermal radiation, nanoparticle volume fraction, streamwise coordinate, mixed convection and non-Darcy parameters. The problems considered in the thesis are properly explored for the two flow cases: (i) free convection and (ii) mixed convection.

1.7 Outline of the Thesis

This thesis consists of SEVEN chapters.

Chapter - 1 consists of preliminary knowledge and provides inspiration to the explorations given in the thesis. An overview of relevant literature is supplied to portray the significance of the problems undertaken. The basic governing equations of the flow and physical quantities related to power-law fluids, power-law nanofluids and power-law hybrid nanofluids along with the details of used methodology (local non-similarity technique [115] and spectral local linearisation method [76]) are given.

A numerical investigation of the flow of a stratified power-law fluids over a convectively heated truncated cone with nonlinear convection and dispersion effect, is presented in Chapter - 2. The non-dimensional velocity and temperature profiles are displayed graphically for different values of the Biot number, nonlinear convection, thermal stratification and thermal dispersion parameters. In addition, the variation in non-dimensional heat transfer rate and skin friction coefficient is also presented and discussed for various values of pertinent parameters.

Chapter - 3 deals with the entropy generation rate and Bejan number estimation in power-law fluid flows over a truncated cone embedded in a non-Darcy porous medium in the presence of viscous dissipation, thermal dispersion and nonlinear convection. The effect of pertinent parameters on the non-dimensional velocity and temperature profiles is portrayed. Along with the rate of heat transfer and entropy generation, Bejan number study is also incorporated and all these are analysed through graphs.

A combined analysis of linear, quadratic and nonlinear thermal radiation in the flow of power-law fluids over a truncated cone in a non-Darcy porous medium, is examined in Chapter - 4. The obtained numerical results are exhibited graphically to demonstrate the influence of each thermal radiation parameter on the dimensionless velocity and temperature profiles in every case. Further, the effect of these parameters on the non-dimensional heat transfer rate and skin friction coefficient versus streamwise coordinate is also explored and

displayed through graphs.

In Chapter - 5, an attempt has been made to investigate the power-law nanofluid flows over a truncated cone in a non-Darcy porous medium. The Titanium alloy and multi wall Carbon nanotubes are used separately as nanoparticles and water is taken for the base fluid. The impact of volume fraction of these nanoparticles on dimensionless velocity, temperature, heat transfer rate and skin friction coefficient is explored properly. The effect of streamwise coordinate on the velocity and temperature profiles is also carried out separately and some interesting results have been obtained.

Chapter - 6 reports a study of power-law hybrid nanofluid flows over a truncated cone placed in a non-Darcy porous medium. The power-law hybrid nanofluids are formed with two nanoparticles together, namely, Titanium alloy and multi wall Carbon nanotubes along with water as the base fluid. The obtained numerical results are exhibited graphically to illustrate usefulness of the nanoparticle volume fraction and streamwise coordinate on dimensionless velocity, temperature, heat transfer rate and skin friction coefficient.

In all the above chapters (2 - 6), the nonlinear governing boundary layer equations and the boundary conditions are changed into dimensionless form by introducing suitable non-dimensional variables. The resulting system of equations is then solved numerically by employing combined approach of local non-similarity and spectral local linearisation method (SLLM). Initially, non-similarity technique [115] is used to obtain the system of ordinary differential equations by employing the three levels of truncation. Later, the SLLM [76] is used to solve the resultant system of ordinary differential equations. It consists of the following three steps:

(i) first, an innovative linearisation procedure locally based on quasi-linearisation technique is used to linearise the nonlinear components of the obtained ordinary differential equations after applying local non-similarity technique;

(ii) next, the Chebyshev spectral collocation method is adopted to transform the set of linearised ordinary differential equations into the set of algebraic equations in the matrix form;

(iii) finally, this matrix system is solved iteratively using appropriate initial approximations (which are taken to satisfy the boundary conditions).

The error analysis and convergence test have been conducted to examine the accuracy of this spectral method. In addition to this, the obtained numerical results are also validated and compared with the existing results in some special cases and the outcomes are observed to be in a very good agreement.

The main conclusions of the earlier chapters and the directions in which further investigations may be carried out are indicated in Chapter - 7.

List of references is given at the end of the thesis. The references are arranged in an alphabetical order and according to this order, citations appear in the text. In each chapter, the details which are already presented in the earlier chapters are avoided. Since a detailed review of the existing literature is presented in the introductory chapter itself, in each of the next chapters, only a brief introduction to the concerned problem is given. Also, the physical meaning of the various parameters is given in the chapters repeatedly for the easy readability of readers.

A substantial portion of the research problems dealt in the thesis is already published/accepted for publication in reputed journals. The remaining portion is communicated for publication. The complete information is as following:

List of papers published

1. "Efficient spectral method for stable stratified power-law fluid flows with dispersion over convectively heated truncated cone in a non-Darcy porous medium", ***International Journal of Applied and Computational Mathematics***, Vol. 7(3), pp. 1-17, (2021).

2. "Effect of dispersion on thermally stable stratified power-law fluids over the vertical frustum of a cone in a non-Darcy porous medium: Flow separation", ***Heat Transfer***, Vol. 50(3), pp. 2380-2402, (2021).

3. "Aqueous Titanium alloy-MWCNTs hybrid nanofluid flow in a non-Darcy porous medium", ***Computational Thermal Sciences: An International Journal***, Vol. 13(5), pp. 31-43, (2021).

4. "Numerical study and error estimation in power-law nanofluid flow over vertical frustum of a cone", ***Indian Journal of Physics***, March 2021. DOI: 10.1007/s12648-021-02055-8.

5. "The second law analysis in free convective flow of pseudoplastic and dilatant fluids over a truncated cone with viscous dissipation: Forchheimer model", ***Journal of Thermal Analysis and Calorimetry***, June 2021. DOI: 10.1007/s10973-021-10823-1.

6. "Entropy generation estimation in pseudoplastic and dilatant fluid flows over a vertical plate and frustum of a cone", ***International Journal of Ambient Energy***, July 2021. DOI: 10.1080/01430750.2021.1951838.

List of papers accepted

7. "Analysis of Ostwald-de Waele power-law nanofluid flow in a non-Darcy porous medium with an efficient spectral algorithm", Accepted for publication in ***Discontinuity, Nonlinearity, and Complexity***, January 2021.

List of papers communicated

8. "Case wise study of thermal radiation in dilatant and pseudoplastic fluid flows: A detailed numerical approach", Communicated to ***International Journal of Thermal Sciences***.

9. "Numerical estimations in a power-law fluid flow with thermal radiation: A complete case study", Communicated to ***International Communications in Heat and Mass Transfer***.

10. "Flow study of a power-law hybrid nanofluid using spectral method: Local non-similarity approach", Communicated to ***International Journal for Numerical Methods in Fluids***.

Chapter 2

Stable Stratified Power-law Fluid Flows over Convectively Heated Truncated Cone Embedded in a Non-Darcy Porous Medium [1]

2.1 Introduction

Ostwald-de Waele power-law fluid model [90, 128] is one among the best established models dealing with various daily life applications. The combined study of pseudoplastic and dilatant fluids helps to obtain a complete analysis of deviation from the Newtonian behaviour. The importance of flow studies in a porous medium is well established and it has attracted a significant amount of attention in the recent times. Convective boundary condition is playing a vital role in different kinds of complex flow studies involved in laboratories and industries. Besides, it is more realistic and general, especially in various technologies and industrial operations such as textile drying, transpiration cooling process, laser pulse heating and so

[1] Case(a): Published in "**International Journal of Applied and Computational Mathematics**" 7(3), 1–17, (2021), Case(b): Published in "**Heat Transfer**" 50(3), 2380–2402, (2021).

on. Cheng [19] discussed the double diffusion from a truncated cone in a non-Newtonian fluid saturated porous medium with variable heat and mass fluxes. Also, he explained various effects on heat and mass transfer by natural convection from the same geometry in a fluid-saturated porous medium with variable wall temperature and concentration [20]. Free convection from a cone/flat plate in a non-Darcy porous medium saturated by a power-law fluid, has been analysed by Kairi and Murthy [55].

In this chapter, the natural and mixed convective flow of stratified power-law fluids over a convectively heated truncated cone situated in a non-Darcy porous medium, are studied in detail. In addition, the significance of thermal dispersion and nonlinear thermal convection effects is also discussed. Along with these, the mixed convection is explained carefully for both opposing and aiding flow cases. For this purpose, the combined local non-similarity and spectral local linearisation methods are utilized and the influence of pertinent parameters is shown through graphs. It is concluded from the literature survey that this work is not attained much regard though it has several notable applications in multiple directions of engineering and science and so it is attempted here.

2.2 Mathematical Analysis

Consider the convective flow over a truncated cone immersed in a power-law fluid saturated non-Darcy porous medium with thermal dispersion and convective boundary condition. The physical model with coordinate system is displayed in Fig. 2.1. The leading edge of the truncated cone is kept at a distance x_0 from the origin O, where x and y axes are taken along and normal to the surface of the truncated cone, respectively. The free stream velocity is taken as u_∞ and it is assumed that the ambient medium temperature is linearly stratified as $T_\infty(\bar{x}) = T_{\infty,0} + A^*\bar{x}$, where the modified streamwise coordinate $\bar{x}$ is defined as $\bar{x} = x - x_0$ and the parameter A^* is used to control the stratification intensity. The fluid temperature is taken as T_f, and the truncated cone surface is either heated ($T_f > T_\infty(\bar{x})$) or cooled ($T_f < T_\infty(\bar{x})$). In addition, this fluid flow is taken for granted to be two dimensional and steady along with the laminar behaviour and the porous medium is assumed to be homo-

geneous and isotropic. The flow intensity is taken to be moderate and the permeability of the medium is presumed to be less in order to explore the applicability of the Forchheimer flow model and negligence of boundary effect. Also, the nonlinear temperature density variations bring a significant influence on the flow field due to notably large changes in temperature between the surface of the truncated cone and ambient fluid.

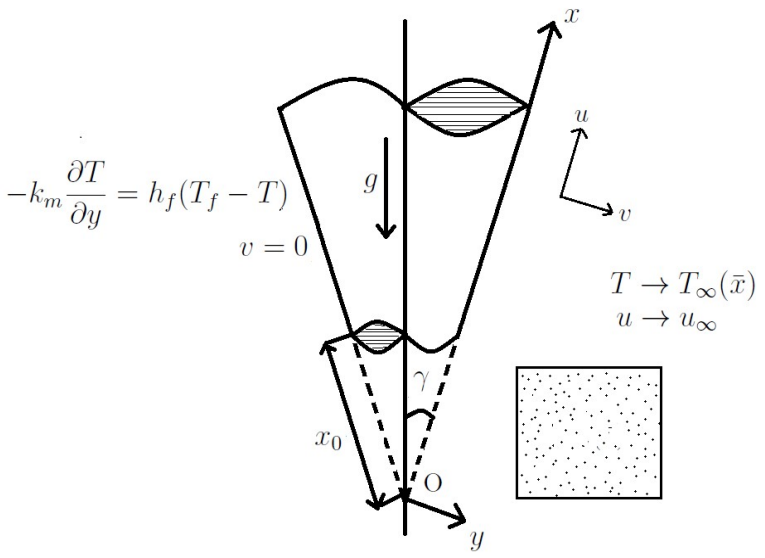

Figure 2.1: *Physical model and coordinate system.*

One more assumption involved is that the boundary layer thickness is very small in comparison with the local radius of the truncated cone. So, the two radii, namely, local radius at a point located in the boundary layer and the radius of truncated cone can be approximated by $r = x\,sin\gamma$ (see Singh *et al.* [113]). Therefore, the equations and boundary conditions involved will be valid only in the region $x_0 < x < \infty$. Hence, the above assumptions are physically realistic in nature with more relevance in practical situations.

Taking the boundary layer hypothesis into consideration together with the above-mentioned approximations and assumptions, the governing equations for the fluid flow over a truncated

cone are given by

$$\frac{\partial(ru)}{\partial x}+\frac{\partial(rv)}{\partial y}=0, \tag{2.1}$$

$$\frac{\partial u^n}{\partial y}+\frac{bK^*}{\nu}\frac{\partial u^2}{\partial y}=\frac{K^*g}{\nu}\left\{\left[\beta_0+2\beta_1(T-T_\infty(\bar{x}))\right]\frac{\partial T}{\partial y}\right\}\cos\gamma, \tag{2.2}$$

$$u\frac{\partial T}{\partial x}+v\frac{\partial T}{\partial y}=\frac{\partial}{\partial y}\left(\alpha_*\frac{\partial T}{\partial y}\right), \tag{2.3}$$

and the boundary conditions can be written as

$$\begin{aligned} v=0,\ -k_m\frac{\partial T}{\partial y}&=h_f(T_f-T) \quad \text{at} \quad y=0,\\ u\to u_\infty,\ T&\to T_\infty(\bar{x}) \quad \text{as} \quad y\to\infty, \end{aligned} \tag{2.4}$$

where ν, h_f, b, γ, g, T, k_m, u_∞ and (u,v) denote the kinematic viscosity, convective heat transfer coefficient, empirical constant, inclination of angle, acceleration due to gravity, temperature, thermal conductivity, free steam and Darcian velocities, respectively. A variable quantity $\alpha_*=\alpha+\alpha_d$ is used to denote the sum of the molecular diffusivity α and the thermal diffusivity $\alpha_d=\chi ud$ followed by Plumb [96], where χ denote the coefficient of mechanical dispersion whose value is based on experiments and d represents the pore diameter. Next, we have considered the thermal expansion coefficients of first and second order, namely, β_0 and β_1 respectively. Here n is the power-law index (for $n<1$, the fluid is pseudoplastic; for $n>1$, the fluid is dilatant; and for $n=1$, the fluid is Newtonian). K^* is the modified permeability and by following Christopher and Middleman [23], and Dharmadhikari and Kale [28], its expression is given by

$$K^*=\frac{1}{2\,c_t}\left(\frac{n\phi^*}{3n+1}\right)^n\left(\frac{50K_d}{3\phi^*}\right)^{\frac{n+1}{2}},$$

where ϕ^* is the porosity of the medium, $K_d=\dfrac{\phi^{*3}d^2}{150(1-\phi^*)^2}$, and

$$c_t=\begin{cases}\frac{25}{12},\\ \dfrac{2}{3}\left(\dfrac{8n}{9n+3}\right)^n\left(\dfrac{10n-3}{6n+1}\right)\left(\dfrac{75}{16}\right)^{3(10n-3)/(10n+11)}\end{cases}.$$

The stream function ψ is introduced in such a way that it satisfies the equation of continuity (2.1). Mathematically,

$$u = \frac{1}{r}\frac{\partial \psi}{\partial y} \quad v = -\frac{1}{r}\frac{\partial \psi}{\partial x}. \tag{2.5}$$

In this chapter, two types (cases) of problems are considered: (a) free/natural convection and (b) mixed convection.

2.2.1 Case(a): Natural Convection

The flow is assumed to be a natural convective flow which is caused by only buoyancy forces and without any external agent. Hence, the velocity of the external flow becomes zero ($i.e., u_\infty = 0$). The non-dimensional relations utilized to get the non-dimensional form of equations (2.2)-(2.4) are

$$\xi = \frac{\bar{x}}{x_0}, \;\; \eta = \frac{y}{\bar{x}}\, Ra^{\frac{1}{2}}, \;\; f(\xi,\eta) = \frac{Ra^{-\frac{1}{2}}}{\alpha\, r}\psi(\xi,\eta), \;\; \theta(\xi,\eta) = \frac{T(\xi,\eta) - T_\infty(x - x_0)}{(T_f - T_{\infty,0})}, \tag{2.6}$$

where ξ is streamwise coordinate, η is the dimensionless variable in $y-$direction and $Ra = \frac{\bar{x}}{\alpha}\left(\frac{\rho\,\beta_0\, g\, K^*\, cos\gamma\,(T_f - T_{\infty,0})}{\mu}\right)^{\frac{1}{n}}$ is the local modified Darcy-Rayleigh number.

Using these transformations (2.6) in the equations (2.2) to (2.3) and the boundary conditions (2.4), the non-dimensional form of the above equations become

$$\left[n\,(f')^{n-1} + 2\,Gr^* f'\right] f'' = (2\,\alpha_1\theta + 1)\theta', \tag{2.7}$$

$$\theta'' + (f'\,\theta'' + f''\,\theta')\,Ds + \left(\frac{\xi}{\xi+1} + 0.5\right) f\theta' - S_T\,\xi\, f' = \xi f'\frac{\partial\theta}{\partial\xi} - \xi\frac{\partial f}{\partial\xi}\theta', \tag{2.8}$$

along with its transformed boundary conditions

$$2\,\xi\,(\xi+1)\left(\frac{\partial f}{\partial \xi}\right)_{\eta=0}+(3\,\xi+1)f(\xi,0)=0,\ \theta'(\xi,0)-Bi\,\xi^{\frac{1}{2}}\,[\theta(\xi,0)\ -1\ +S_T\,\xi]=0,$$
$$f'(\xi,\eta)\to 0,\quad \theta(\xi,\eta)\to 0\ \ as\ \ \eta\to\infty. \tag{2.9}$$

Here, prime indicates the differentiation in respect of η and $Gr^*=\dfrac{b\,K^*}{\nu}\left(\dfrac{\alpha Ra}{\bar{x}}\right)^{2-n}$, $\alpha_1=\dfrac{\beta_1}{\beta_0}(T_f-T_{\infty,0})$, $Ds=\dfrac{\chi dRa}{\bar{x}}$, $S_T=\dfrac{A^*x_0}{(T_f-T_{\infty,0})}$, $Bi=\dfrac{h_f\sqrt{x_0}}{k_m}\left(\dfrac{\bar{x}}{Ra}\right)^{\frac{1}{2}}$ represent the modified Grashof number, nonlinear density-temperature parameter, thermal dispersion parameter, thermal stratification parameter and Biot number respectively. When $\xi\to 0$ (i.e., $x\to x_0$), this problem is converted to the flow problem past a vertical plate. Similarly, when $x_0=0$, ξ becomes very large which is utilized to obtain the same problem with the full cone as a geometry.

Non-dimensional representation of the Nusselt number $Nu_x=-\dfrac{\bar{x}}{k}\dfrac{(k+k_d)}{(T_f-T_{\infty,0})}\left[\dfrac{\partial T}{\partial y}\right]_{y=0}$ and the skin friction coefficient $C_f=\dfrac{2}{\rho\,u_*^2}\left[\mu\dfrac{\partial u}{\partial y}\right]_{y=0}$ is

$$\frac{Nu_{\bar{x}}}{Ra^{\frac{1}{2}}}=-\left[Ds\,f'(\xi,0)+1\right]\theta'(\xi,\,0),\qquad \frac{1}{2}\frac{Ra^{\frac{1}{2}}}{Pr}C_f=f''(\xi,0). \tag{2.10}$$

Here u_* and μ denote the characteristic velocity and the dynamic viscosity respectively, k_e (the effective thermal conductivity of the medium) is the sum of k_d (the dispersion thermal conductivity) and k (the molecular thermal conductivity), and Pr denotes the Prandtl number.

Numerical Solution

The governing equations (2.7)-(2.8) along with the boundary conditions (2.9) are solved numerically using spectral local linearisation method (SLLM) together with the non-similarity approach. The details are given below:

Local Similarity and Non-similarity Approaches:

It is used to convert the set of nonlinear partial differential equations (2.7)-(2.8) and the boundary conditions (2.9) into a set of nonlinear ordinary differential equations and boundary conditions by employing the three levels of truncation (for more details, one can refer [115, 74]). When $\xi << 1$, the preliminary approximation is found from the local similarity equations and insignificant terms involving $\xi\dfrac{\partial}{\partial\xi}$ are removed. Consequently, the local similarity equations for the first level truncation of equations (2.7)-(2.8) are

$$\left[n\ (f')^{n-1} + 2\,Gr^* f'\right] f'' - (2\,\alpha_1\theta + 1)\theta' = 0, \tag{2.11}$$

$$\theta'' + (f''\,\theta' + f'\,\theta'')\,Ds + \left(\frac{\xi}{\xi+1} + 0.5\right) f\theta' - S_T\,\xi\,f' = 0, \tag{2.12}$$

and the corresponding boundary conditions (2.9) are

$$\begin{gathered} f(\xi,0) = 0,\ \theta'(\xi,0) + Bi\,\xi^{\frac{1}{2}}\,[1 - \theta(\xi,0)\ - S_T\,\xi] = 0, \\ f'(\xi,\eta) \to 0, \quad \theta(\xi,\eta) \to 0 \ \ as \ \ \eta \to \infty. \end{gathered} \tag{2.13}$$

The parameter ξ contained in the governing equations and boundary conditions can be regarded as assigned constant at any streamwise location along the surface. As a result, the governing equations transformed by the local similarity method can be treated as a system of ordinary differential equations with partial non-similar effects retained in the momentum equation and the boundary conditions. Here, the solutions are different for different values of the streamwise coordinate ξ. This can be seen by assigning different values to ξ along the surface and plotting the respective boundary layer distributions.

On the other hand, the non-similar terms on the right-hand side of equations (2.7)-(2.9) are vanished in the local similarity procedure. The local similarity postulation requires ξ to be close to zero. Otherwise, the whole term in the bracket on the right-hand side of equations (2.7)-(2.9) must be minimal to justify the exclusion of non-similar terms. The validity of the latter assumption, however, is subject to uncertainty and this is a weakness of the local similarity procedure.

The second level truncation involves the use of new variables $U = \dfrac{\partial f}{\partial \xi}, V = \dfrac{\partial \theta}{\partial \xi}$, by which the local non-similarity nonlinear ODEs are derived to get the previously omitted terms. Hence, updated governing equations are

$$\left[n\ (f')^{n-1} + 2\,Gr^* f'\right] f'' - (2\,\alpha_1\theta + 1)\theta' = 0, \tag{2.14}$$

$$\theta'' + (f''\,\theta' + f'\,\theta'')\,Ds + \left(\frac{\xi}{\xi+1} + 0.5\right) f\theta' - S_T\,\xi\,f' - \xi\,V\,f' + \xi\,U\,\theta' = 0, \tag{2.15}$$

with boundary conditions

$$\begin{aligned} (3\,\xi+1)f(\xi,0) + 2\,(\xi+1)\,\xi\,U(\xi,0) &= 0,\\ \theta'(\xi,0) + Bi\,\xi^{\frac{1}{2}}\,[1 - S_T\,\xi\ - \theta(\xi,0)] &= 0,\\ f'(\xi,\eta) \to 0, \quad \theta(\xi,\eta) \to 0 \ \ as \ \ \eta &\to \infty. \end{aligned} \tag{2.16}$$

Finally, in the last truncation level, equations (2.14)-(2.16) are differentiated in respect of ξ and all partial derivatives of U and V are removed. Therefore, the final equations are

$$\begin{aligned} n\,(f')^{n-1}\,U'' + n(n-1)\,(f')^{n-2}\,f''U' + 2Gr^*(U''f' + f''U') -\\ -V' - 2\,\alpha_1(\theta V' + V\theta') = 0, \end{aligned} \tag{2.17}$$

$$\begin{aligned} V'' + Ds(f'V'' + f''V') + \left(\frac{1}{2} + \frac{\xi}{\xi+1}\right) fV' - f'V + \xi UV' - \xi U'V +\\ Ds(U''\theta' + U'\theta'') + \left(\frac{1}{2} + \frac{\xi}{\xi+1}\right) U\theta' - S_T f' - \xi S_T U' + \theta' U + \frac{1}{(\xi+1)^2} f\theta' = 0, \end{aligned} \tag{2.18}$$

with boundary conditions

$$\begin{aligned} 3f(\xi,0) + (7\xi+3)U(\xi,0) &= 0,\\ V'(\xi,0) - Bi\xi^{\frac{1}{2}}V(\xi,0) + 0.5\,Bi\xi^{-\frac{1}{2}}[1-\theta(\xi,0)] - 1.5\,Bi\xi^{\frac{1}{2}}S_T &= 0,\\ U'(\xi,\eta) \to 0, \quad V(\xi,\eta) \to 0 \ \ as \ \ \eta &\to \infty. \end{aligned} \tag{2.19}$$

The two-equation model involves four coupled equations [i.e., (2.14)-(2.15) and (2.17)-(2.18)] that need to be solved simultaneously in conjunction with the two sets of boundary

conditions [(2.16) and (2.19)]. Therefore, the local non-similarity procedure preserves the non-similar terms in original governing equations and boundary conditions because we are dropping the non-similar terms from its auxiliary equations only. Since the original governing equations remain intact, the local non-similarity solution is expected to be more accurate than the local similarity solution.

Spectral Local Linearisation Method (SLLM):

The SLLM is based on developing a decoupled iterative scheme that is then chronologically solved using spectral methods. Local linearisation is applied to the equations before generating the iterative scheme in a manner similar to the Gauss-Seidel approach of decoupling linear algebraic systems. Consider a system of n nonlinear ordinary differential equations in n unknown functions $Y_j(\eta)$, $j = 1, 2, 3, ..., n$ written as a sum of its linear and nonlinear terms as follows:

$$L_j[Y_1, Y_2, ..., Y_n] + N_j[Y_1, Y_2, ..., Y_n] = 0, \qquad j = 1, 2, 3, ..., n. \tag{2.20}$$

Let the subscripts r and $r+1$ represent the previous and current iteration, respectively. Local linearisation of N_j at the previous iteration about Y_j is then carried out as follows:

$$N_j[Y_1, Y_2, ..., Y_n] = N_j[Y_{1,r}, Y_{2,r}, ..., Y_{n,r}] + \frac{\partial N_j}{\partial Y_j}[Y_{1,r}, Y_{2,r}, ..., Y_{n,r}](Y_j - Y_{j,r}), \tag{2.21}$$

using this, at the current iteration with $Y_j = Y_{j,r+1}$, equation (2.20) becomes

$$\begin{aligned} L_j[Y_{1,r+1}, Y_{2,r+1}, ..., Y_{n,r+1}] + \frac{\partial N_j}{\partial Y_j}[Y_{1,r}, Y_{2,r}, ..., Y_{n,r}]Y_{j,r+1} \\ = \frac{\partial N_j}{\partial Y_j}[Y_{1,r}, Y_{2,r}, ..., Y_{n,r}]Y_{j,r} - N_j[Y_{1,r}, Y_{2,r}, ..., Y_{n,r}]. \end{aligned} \tag{2.22}$$

Following the Gauss-Sidel approach, whereby the updated solutions $Y_k(k < j)$, obtained at previous equations are utilised to get a solution Y_j at the current iteration level $Y_{j,r+1}$, the

local linearisation iteration scheme can be generated as follows:

$$\begin{aligned}
&L_1[Y_{1,r+1}, Y_{2,r+1}, ..., Y_{n,r+1}] + \frac{\partial N_1}{\partial Y_1}[...]Y_{1,r+1} \\
&\quad = \frac{\partial N_1}{\partial Y_1}[...]Y_{1,r} - N_1[Y_{1,r}, Y_{2,r}, ..., Y_{n,r}], \\
&L_2[Y_{1,r+1}, Y_{2,r+1}, ..., Y_{n,r+1}] + \frac{\partial N_2}{\partial Y_2}[...]Y_{2,r+1} \\
&\quad = \frac{\partial N_2}{\partial Y_2}[...]Y_{2,r} - N_2[Y_{1,r+1}, Y_{2,r}, ..., Y_{n,r}], \\
&\qquad \vdots \\
&L_n[Y_{1,r+1}, Y_{2,r+1}, ..., Y_{n,r+1}] + \frac{\partial N_n}{\partial Y_n}[...]Y_{n,r+1} \\
&= \frac{\partial N_n}{\partial Y_n}[...]Y_{n,r} - N_n[Y_{1,r+1}, ..., Y_{n-1,r+1}, Y_{n,r}],
\end{aligned} \tag{2.23}$$

where [...] at the j^{th} iteration represents $[Y_{1,r+1}, Y_{2,r+1}..., Y_{j-1,r+1}, Y_{j,r}, ..., Y_{n,r}]$. Hence, starting from an initial approximation $Y_{1,0}, Y_{2,0}, ..., Y_{n,0}$, the iterative scheme (2.23) is solved until convergence is reached for all the unknowns. Utilising this procedure, the iterative scheme for four coupled equations [(2.14)-(2.15) and (2.17)-(2.18)] along with two sets of boundary conditions [(2.16) and (2.19)] is generated as following:

$$f''_{r+1} + a_{1,r} f'_{r+1} = K_{1,r}, \tag{2.24}$$

$$\theta''_{r+1} + b_{1,r} \theta'_{r+1} = K_{2,r}, \tag{2.25}$$

$$U''_{r+1} + x_{1,r} U'_{r+1} = K_{3,r}, \tag{2.26}$$

$$V''_{r+1} + y_{1,r} V'_{r+1} + y_{2,r} V_{r+1} = K_{4,r}, \tag{2.27}$$

where

$$a_{1,r} = \frac{n(n-1) f''_r \left(f'_r\right)^{n-2} + 2Gr^* f''_r}{n \left(f'_r\right)^{n-1} + 2Gr^* f'_r},$$

$$K_{1,r} = \frac{\theta_r' + 2\alpha_1\theta_r\theta_r' + n(n-1)f_r''\left(f_r'\right)^{n-1} + 2Gr^* f_r'' f_r'}{n\left(f_r'\right)^{n-1} + 2Gr^* f_r'},$$

$$b_{1,r} = \frac{Dsf_{r+1}'' + \left(\frac{1}{2} + \frac{\xi}{\xi+1}\right) f_{r+1} + \xi U_r}{1 + Dsf_{r+1}'},$$

$$K_{2,r} = \frac{\xi S_T f_{r+1}' + \xi f_{r+1}' V_r}{1 + Dsf_{r+1}'},$$

$$x_{1,r} = \frac{n(n-1)\left(f_{r+1}'\right)^{n-2} f_{r+1}'' + 2Gr^* f_{r+1}''}{2Gr^* f_{r+1}' + n\left(f_{r+1}'\right)^{n-1}},$$

$$K_{3,r} = \frac{V_r' + 2\alpha_1\theta_{r+1}' V_r + 2\alpha_1\theta_{r+1}V_r'}{n\left(f_{r+1}'\right)^{n-1} + 2Gr^* f_{r+1}'},$$

$$y_{1,r} = \frac{Dsf_{r+1}'' + \left(\frac{1}{2} + \frac{\xi}{\xi+1}\right) f_{r+1} + \xi U_{r+1}}{1 + Dsf_{r+1}'},\ y_{2,r} = \frac{-f_{r+1}' - \xi U_{r+1}'}{1 + Dsf_{r+1}'},$$

$$K_{4,r} = \frac{-Ds\left(U_{r+1}'\theta_{r+1}'' + U_{r+1}''\theta_{r+1}'\right) - \left(\frac{3}{2} + \frac{\xi}{\xi+1}\right) U_{r+1}\theta_{r+1}' + \xi S_T U_{r+1}' + S_T f_{r+1}' - \frac{1}{(\xi+1)^2} f_{r+1}\theta_{r+1}'}{1 + Dsf_{r+1}'},$$

with linearised boundary conditions

$$\begin{aligned}
f_{r+1}(\xi,0) &= -\frac{2\xi(\xi+1)}{3\xi+1}U_r(\xi,0),\\
\theta_{r+1}'(\xi,0) - \xi^{\frac{1}{2}}Bi\,\theta_{r+1}(\xi,0) &= -Bi\xi^{\frac{1}{2}} + Bi\xi^{\frac{3}{2}}S_T,\\
U_{r+1}(\xi,0) &= -\frac{3}{7\xi+3}f_{r+1}(\xi,0),\\
V_{r+1}'(\xi,0) - Bi\xi^{\frac{1}{2}}V_{r+1}(\xi,0) &= -\frac{1}{2}Bi\xi^{\frac{-1}{2}} + \frac{1}{2}Bi\xi^{\frac{-1}{2}}\theta_{r+1}(\xi,0) + \frac{3}{2}Bi\xi^{\frac{1}{2}}S_T,\\
f_{r+1}'(\xi,\eta) \to 0,\ \theta_{r+1}(\xi,\eta) \to 0,\ U_{r+1}'(\xi,\eta) \to 0,\ V_{r+1}(\xi,\eta) \to 0,\ as\ \ \eta \to \infty.
\end{aligned} \tag{2.28}$$

Since the coefficient parameters and the right-hand side of these equations are known (from previous iterations), it can easily be solved using any numerical method. Here, the equations are solved using the Chebyshev spectral collocation method (Canuto *et al.* [12]). This

method is based on approximating the unknown functions by the Chebyshev interpolating polynomials in such a way that they are collocated at the Gauss-Lobatto points defined as

$$\tau_m = \cos\frac{\pi m}{N_x}, \qquad m = 0, 1, ..., N_x, \tag{2.29}$$

where N_x is the number of collocation points.

The Chebyshev polynomials are defined on the interval $[-1, 1]$. So, the physical region $[0, \infty)$ is transformed into the region $[-1, 1]$ using the domain truncation technique in which the problem is solved on the interval $[0, S]$ instead of $[0, \infty)$. This leads to the mapping

$$\frac{\eta}{S} = \frac{\tau + 1}{2}, \qquad -1 \leq \tau \leq 1, \tag{2.30}$$

where S is the scaling parameter which is used to invoke the boundary condition at ∞.

The unknown functions $Y_{j,r+1}$ are approximated at the collocation points as

$$Y_j(\tau) = \sum_{k=0}^{N_x} Y_j(\tau_k) T_k(\tau_m), \quad \frac{d^{\mathbb{Z}}}{d\eta^{\mathbb{Z}}} Y_j(\tau) = \sum_{k=0}^{N_x} \mathbf{D}_{km}^{\mathbb{Z}} Y_j(\tau_k), \quad m = 0, 1, ..., N_x, \tag{2.31}$$

where T_k is the k^{th} Chebyshev polynomial given by $T_k(\tau) = \cos[k\ \cos^{-1}\tau]$, $\mathcal{D}$ is the Chebyshev spectral derivative matrix such that $\mathbf{D} = (2/S)\mathcal{D}$ and $\mathbb{Z}$ is the order of differentiation.

After substituting (2.30)-(2.31) into the linearised form of equations (2.24)-(2.28), the required solution is given by

$$\tilde{\mathbf{Y}}_i = \tilde{\mathbf{B}}_{i-1}^{-1} \tilde{\mathbf{R}}_{i-1}, \tag{2.32}$$

In equation (2.32), $\tilde{\mathbf{B}}_{i-1}$ is a square matrix of order $(4N_x + 4)$ and $\tilde{\mathbf{Y}}_i$, $\tilde{\mathbf{R}}_{i-1}$ are the column matrices of order $(4N_x + 1)$. In a simplified way, the matrix representation of equations (2.24)-(2.27) can be given as

$$\boldsymbol{A_1}\, \boldsymbol{F} = \boldsymbol{B_1},$$
$$\boldsymbol{A_2}\, \boldsymbol{\Theta} = \boldsymbol{B_2},$$
$$\boldsymbol{A_3}\, \boldsymbol{U} = \boldsymbol{B_3},$$

$$\boldsymbol{A_4}\,\boldsymbol{V} = \boldsymbol{B_4},$$

where

$$\begin{aligned}
&\boldsymbol{A_1}=\boldsymbol{D^2}+\text{diag}(a_{1,r})\boldsymbol{D}, \quad \boldsymbol{B_1}=K_{1,r},\\
&\boldsymbol{A_2}=\boldsymbol{D^2}+\text{diag}(b_{1,r})\boldsymbol{D}, \quad \boldsymbol{B_2}=K_{2,r},\\
&\boldsymbol{A_3}=\boldsymbol{D^2}+\text{diag}(x_{1,r})\boldsymbol{D}, \quad \boldsymbol{B_3}=K_{3,r},\\
&\boldsymbol{A_4}=\boldsymbol{D^2}+\text{diag}(y_{1,r})\boldsymbol{D}+\text{diag}(y_{2,r})\boldsymbol{I}, \quad \boldsymbol{B_4}=K_{4,r},
\end{aligned}$$

where $\boldsymbol{I}$ is the $(N_x+1)^{th}$ order identity matrix and $\boldsymbol{F}$, $\boldsymbol{\Theta}$, $\boldsymbol{U}$ and $\boldsymbol{V}$ are the vectors containing f, θ, U and V values evaluated at the Gauss - Lobatto (collocation) points. In this way, the solution of system of equations along with the boundary conditions are obtained by making use of appropriate initial approximations and the fluid flow behaviour is studied.

Validation and Residual Error Analysis:

To validate the numerical solution obtained by using the method as described in the above section, the solutions about different values of ξ have been computed for residual errors. The residual error analysis is performed in MATLAB by taking 50 collocation points in η-direction ($i.e.\, N_x = 50$) and $L_x = 10$ is fixed in the η-direction to get the asymptotic nature at infinity. These residuals are defined as the norm of the difference between two successive iterations, and it is said to have convergence when the norms are less than a given tolerance level. The convergence property is shown by using the following expressions for the error in the fluid velocity and fluid temperature at $(r+1)^{th}$ level

$$\begin{aligned}
E_f &= max||f_{r+1,i} - f_{r,i}||_\infty, \quad 0 \le i \le N_x,\\
E_\theta &= max||\theta_{r+1,i} - \theta_{r,i}||_\infty, \quad 0 \le i \le N_x.
\end{aligned} \tag{2.33}$$

Figs. 2.2(a)-2.3(b) are prepared to display the variation in the norm of residual error with iterations for equations (2.14) and (2.15) with different ξ. The residual error is decreased with increase in iterations and its very less value for different values of ξ shows the faster convergence and accuracy of the present method (for more details, one can refer the work

of Motsa *et al.* [78]). Hence, the validation of this spectral local linearisation method is justified.

Results and Discussions

Apart from the above-said residual error estimations, to check the accuracy of computations and the exactness of formulation, the results of this problem in the case of wall temperature condition ($\theta(\xi, \eta) = 1$ as $Bi \to \infty$) for vertical plate (i.e. $\xi \to 0$) when $Ds = 0$, $\alpha_1 = 0$ and $S_T = 0$ are also compared with the results of Plumb and Huenefeld [97] and the exact results (see Nakayama *et al.* [83] and citations therein) for the Newtonian fluid case. These comparisons show that the results are matching at a very good extent as displayed in Table (2.1). Further, the behaviour of temperature and velocity profiles along with the skin friction coefficient and heat transfer rate for various values of streamwise coordinate ξ are given in the tabular form for pseudoplastic fluid and dilatant fluid in Table (2.2) and Table (2.3) respectively. From these results, it is self-evident that the solutions are not similar. This flow model reveals some of the interesting observations regarding the boundary layer flows in the practically feasible range of important parameters and these are very useful in various emerging applications.

Table 2.1: *Comparative analysis of* $-\theta'(\xi, 0)$ *for different values of* Gr^* *when* $\xi \to 0$, $Ds = 0$, $\alpha_1 = 0$, $S_T = 0$, $Bi \to \infty$ *and* $n = 1$ *(Newtonian fluid).*

Gr^*	Present	Exact [83]	Plumb [97]
0	0.44390437	0.4439	0.44390
0.01	0.44231590	0.4423	0.44232
0.1	0.42968906	0.4297	0.42969
1	0.36616650	0.3662	0.36617
10	0.25748252	0.2513	0.25126
100	0.16190872	0.1519	0.15186

Table 2.2: *The non-dimensional velocities, temperatures, Nusselt number and skin friction coefficients for various values of* ξ *when* $Gr^* = 1.0$, $Ds = 0.5$, $\alpha_1 = 1.0$, $Bi = 1.0$, $S_T = 0.01$ *and* $n = 0.8$ *(pseudoplastic fluids).*

ξ	$f'(\xi,0)$	$\theta(\xi,0)$	$\frac{Nu_{\bar{x}}}{Ra^{\frac{1}{2}}}$	$\frac{1}{2}\frac{Ra^{\frac{1}{2}}}{Pr}C_f$
0.1	0.4497	0.4778	0.2019	-0.1734
0.2	0.5169	0.5375	0.2592	-0.2155
0.3	0.5513	0.5727	0.2965	-0.2447
0.4	0.5730	0.5984	0.3235	-0.2683
0.5	0.5894	0.6185	0.3474	-0.2877
0.6	0.6033	0.6341	0.3628	-0.3035
0.7	0.6200	0.6428	0.3838	-0.3128

Table 2.3: *The non-dimensional velocities, temperatures, Nusselt number and skin friction coefficients for various values of* ξ *when* $Gr^* = 1.0$, $Ds = 0.5$, $\alpha_1 = 1.0$, $Bi = 1.0$, $S_T = 0.01$ *and* $n = 1.2$ *(dilatant fluids).*

ξ	$f'(\xi,0)$	$\theta(\xi,0)$	$\frac{Nu_{\bar{x}}}{Ra^{\frac{1}{2}}}$	$\frac{1}{2}\frac{Ra^{\frac{1}{2}}}{Pr}C_f$
0.1	0.4896	0.4561	0.2137	-0.1626
0.2	0.5494	0.5194	0.2728	-0.2017
0.3	0.5830	0.5551	0.3126	-0.2277
0.4	0.6062	0.5798	0.3430	-0.2474
0.5	0.6239	0.5986	0.3677	-0.2632
0.6	0.6382	0.6138	0.3884	-0.2764
0.7	0.6501	0.6265	0.4063	-0.2877

The variation in the non-dimensional velocity, temperature, heat transfer rate and skin friction coefficient for different Bi is portrayed graphically in Figs. 2.4(a)-2.4(d) where all

other parameters are given fixed values. Bi is defined as the proportion of internally heated resistance in the truncated cone surface to the boundary layer heated resistance. Fig. 2.4(a) depicts the fluid velocity increments with higher values of Bi and the dilatant fluid is more influenced in comparison with the pseudoplastic fluid. In Fig. 2.4(b), the influence of Bi on temperature profiles is displayed which shows that the higher values of temperature are obtained with the increment in Biot number. It is clear from this figure that the temperature is more for both the fluids when the surface is subjected to wall temperature condition (i.e., $\theta(\xi, 0) = 1 - \xi\, S_T$ which is obtained when $Bi \to \infty$) in comparison with the convectively heated surface (as shown in Boundary condition (2.9)). The variation in Nusselt number with the nonlinear convection parameter α_1 for various values of Biot number is shown in Fig. 2.4(c). From this figure, the domination of dilatant fluid over the pseudoplastic fluid is observed and also the higher rate of heat transfer is noticed with an increment of Bi. Similarly, in Fig. 2.4(d), the change in skin friction coefficient with α_1 for different values of Bi is displayed. Less negative values are obtained for the dilatant fluid with an increment of Bi and this negativity increases with the Biot number increment. This type of analysis where the temperature of surface is fixed in later stage, may be very useful in many applications because if the surface temperature is fixed initially, it may further result into damage of materials involved in the experiment or even in industry.

The variation in the non-dimensional velocity, temperature, Nusselt number and skin friction coefficient for different values of the thermal dispersion parameter Ds is depicted in Figs. 2.5(a)-2.5(d). Thermal dispersion raises the potency of non-uniform pore level velocities on the temperature field in a certain porous medium. In addition, the importance of integrated variations in the temperature and velocity profiles to the heat transportation can also be seen with the help of thermal dispersion. It is found from the Fig. 2.5(a) that there is increment in velocity when the thermal dispersion is present in the case of dilatant and pseudoplastic fluids. Likewise, Fig. 2.5(b) portrays that there is again increment in the temperature profiles for non-zero values of Ds. Due to higher flow velocities in the porous medium, the thermal dispersion dominates molecular diffusion. Hence, a detailed analysis must be given about its impact on the heat transfer properties in this study. In view of

this, the impact of Ds with α_1 on Nusselt number is shown in Fig. 2.5(c). With enhanced values of Ds, the heat transfer is also enhanced for both the dilatant and pseudoplastic fluids. The values for dilatant fluid are found to be more. The influence of Ds on the skin friction coefficient with α_1 is displayed in Fig. 2.5(d). When Ds is increased, less negative skin friction is observed for the two fluids. The magnitude of Ds is higher for pseudoplastic fluid than that of the dilatant fluid.

In the Figs. 2.6(a)-2.6(d), the significance of S_T on non-dimensional velocity of the fluid flow, temperature, heat transfer rate and skin friction coefficient is depicted. There is decrement in the velocity and temperature profiles in the case of increasing values of stable stratification (i.e., for $S_T > 0$) for both dilatant and pseudoplastic fluids. Due to S_T increment, density of the fluid is increased which results the decrement in the convective flow and so the velocity profiles are decreased and this effect is less for pseudoplastic fluid. Also, in the presence of S_T, the temperature variation between the surface of the truncated cone and the marginal fluid decreases, which thickens the thermal boundary layer resulting into temperature profile decrement. In Fig. 2.6(c), the impact of stratification on Nusselt number with α_1 is shown for dilatant and pseudoplastic fluids. Increase in S_T values results into the decrement of Nusselt number for both the fluids. Nusselt number is noticed to be less in the case of pseudoplastic fluid. Fig. 2.6(d) shows the impact of stratification on the skin friction coefficient with α_1 and increment in S_T makes skin friction values less negative for dilatant and pseudoplastic fluids and there is rapid variation with α_1 values.

The effect of α_1 on the dimensionless velocity and temperature is displayed in Figs. 2.7(a)-2.7(b). The nonlinear convection parameter shows a non-linearity relationship between the temperature and density. Physically, $\alpha_1 > 0$ refers the expression $T_f > T_\infty$, so the truncated cone surface gives significant amount of heat to the fluid flow region. The presence and absence of α_1 are taken to analyse its influence when other parameters are assigned specific values. Fig. 2.7(a) displays that the presence of α_1 makes velocity to increase and this effect is less for the pseudoplastic fluid. Fig. 2.7(b) displays the temperature decrements in the presence of α_1 for both the fluids and these decrements are found to be more in the case of pseudoplastic fluid. As α_1 increases, from Figs. 2.4(c)-2.4(d) and Figs. 2.5(c)-2.5(d), it is

evident that the Nusselt number and skin friction are less affected for pseudoplastic fluids than the dilatant fluids in the presence/absence of either convective boundary condition or thermal dispersion. With the increment in α_1, the Nusselt number is identified to be more for pseudoplastic fluid when compared to dilatant fluid with/without S_T as displayed in Fig. 2.6(c). The behaviour of skin friction coefficient is noticed to be opposite to that of the Nusselt number as shown in Fig. 2.6(d) with the enhancement of α_1.

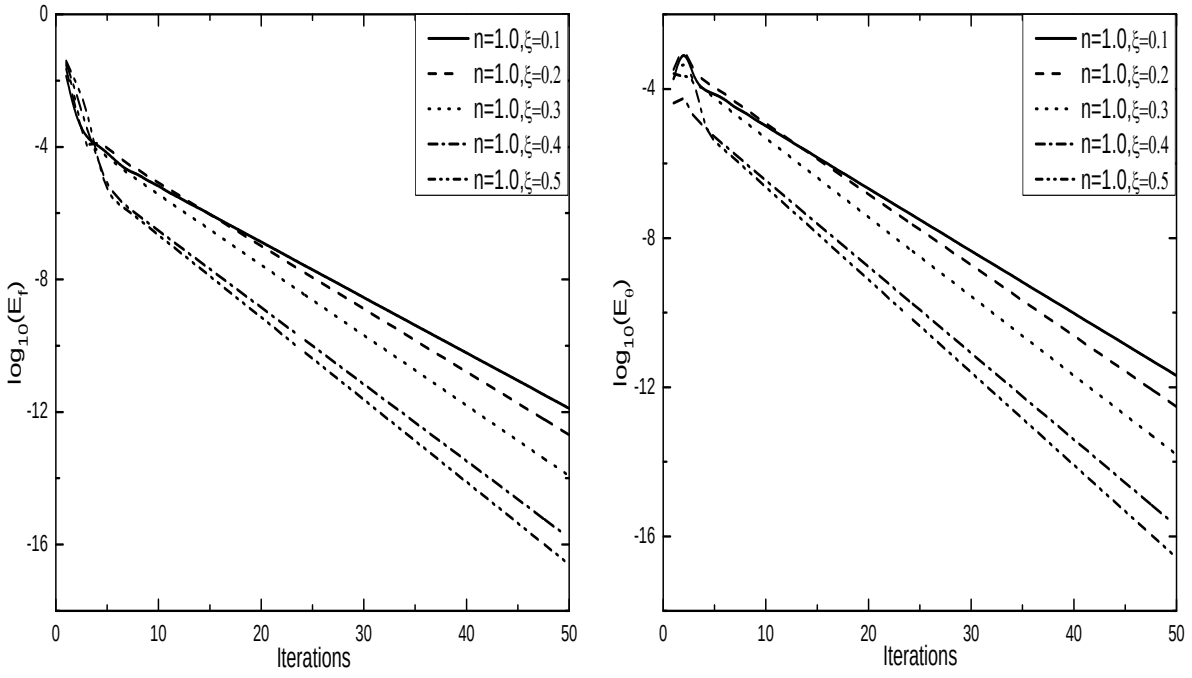

(a) (b)

Figure 2.2: *Residual errors over iterations for Newtonian fluid when* $Ds = 1.0$, $\alpha_1 = 0.1$, $Gr^* = 0.01$, $Bi = 1.0$, $S_T = 0.01$.

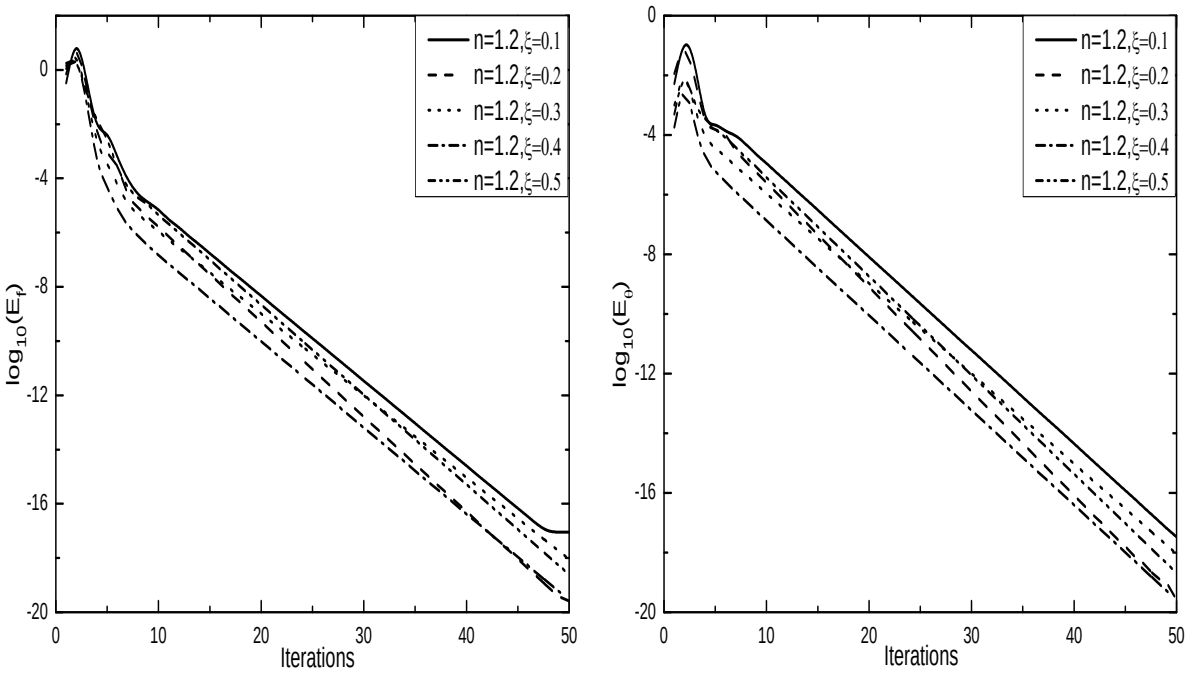

(a) (b)

Figure 2.3: *Residual errors over iterations for non-Newtonian fluid when* $Ds = 0.5$, $\alpha_1 = 0.1$, $Gr^* = 0.01$, $Bi = 1.0$, $S_T = 0.01$.

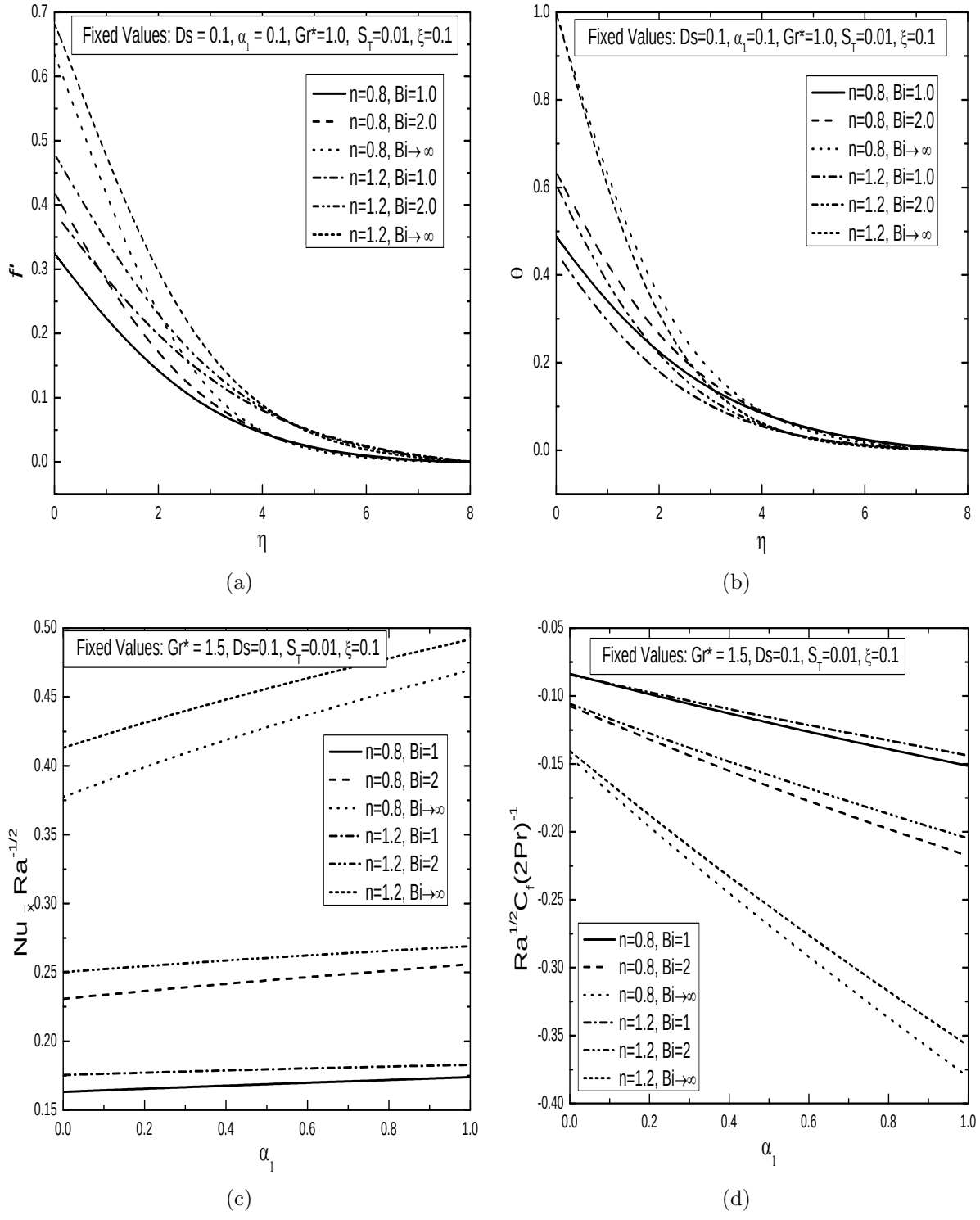

Figure 2.4: *Effect of Biot Number* (Bi) *on non-dimensional (a) velocity, (b) temperature, (c) Nusselt number and (d) skin friction coefficient profiles for different values of* n.

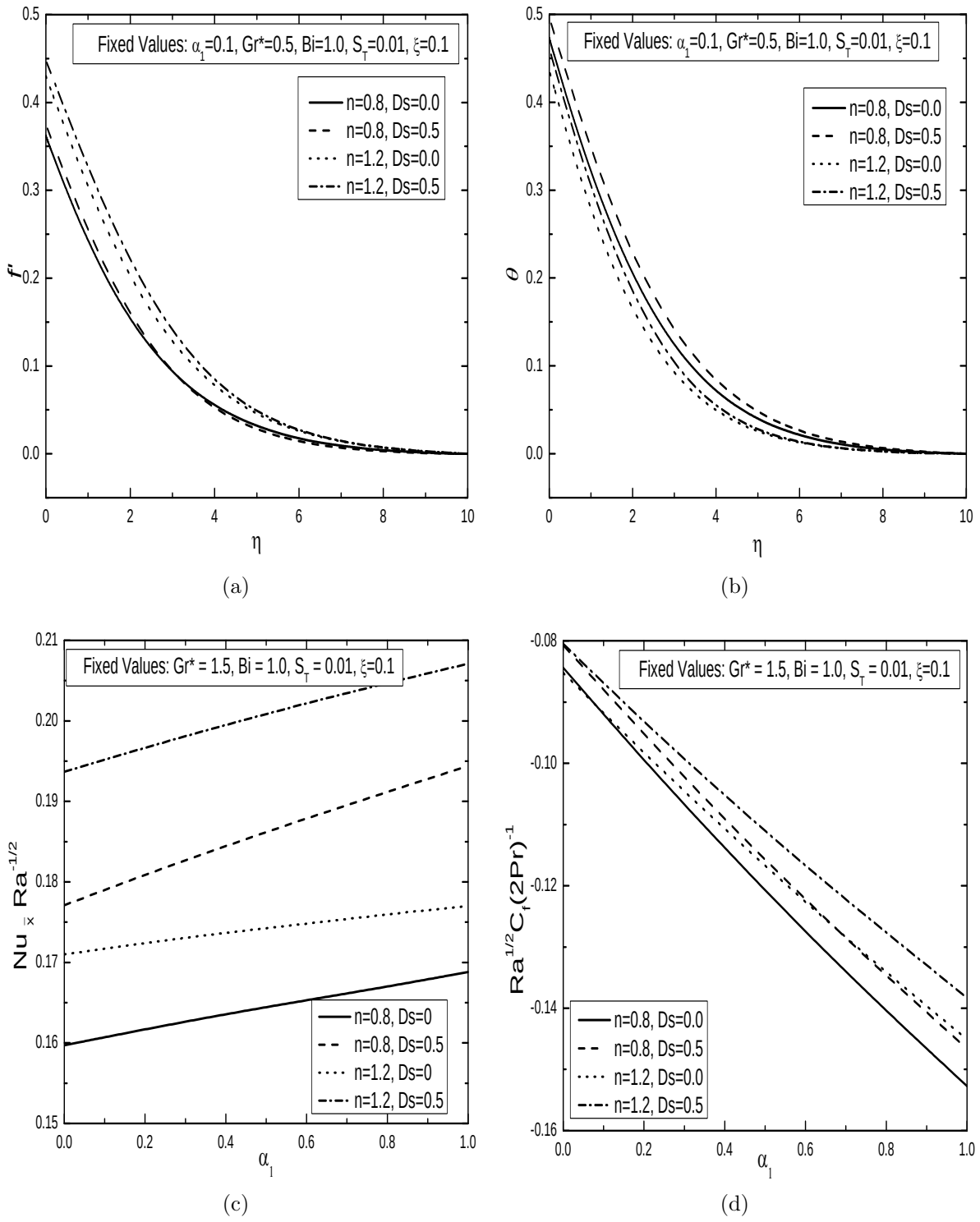

Figure 2.5: *Effect of thermal dispersion parameter* (Ds) *on non-dimensional (a) velocity, (b) temperature, (c) Nusselt number and (d) skin friction coefficient profiles for different values of* n*.*

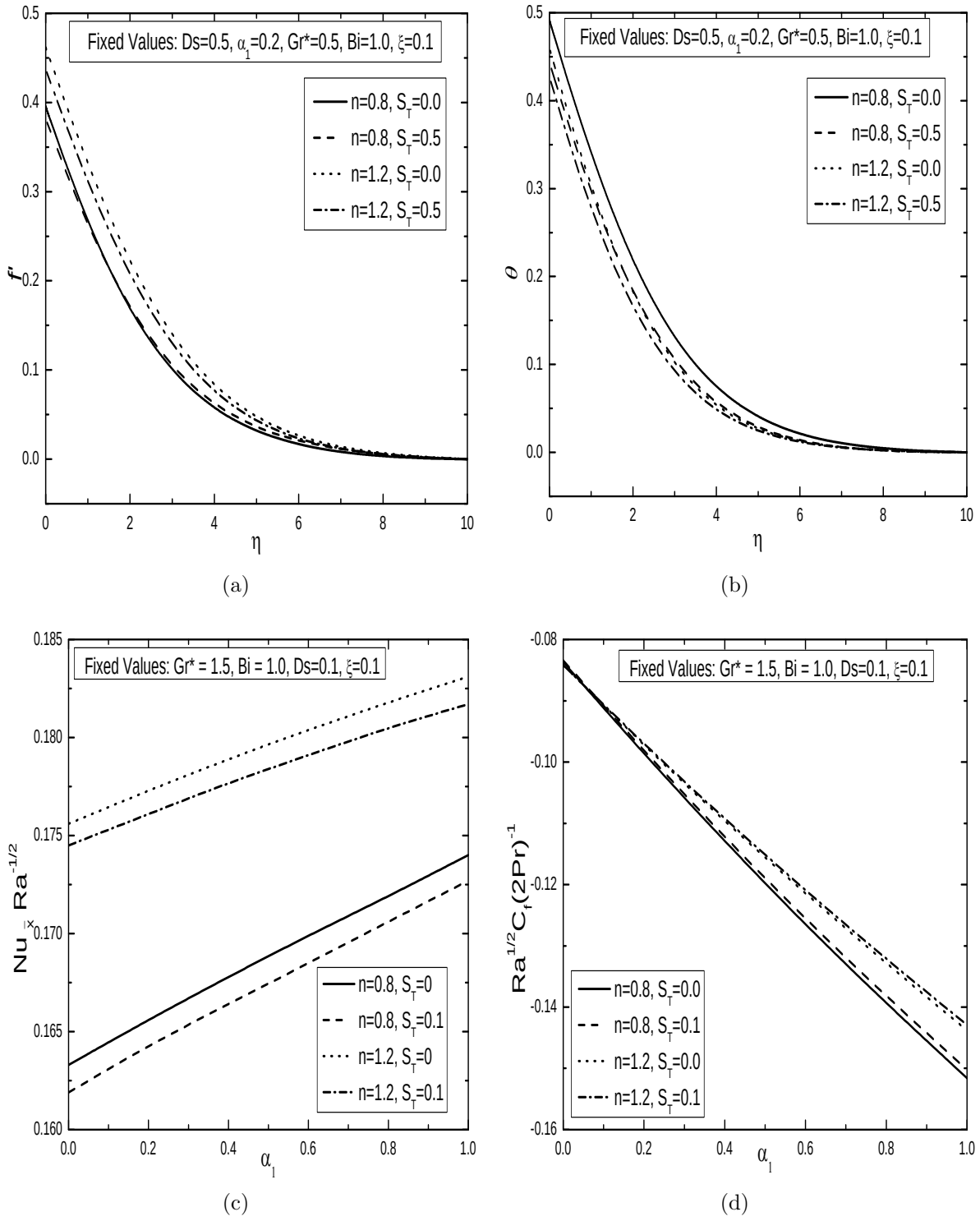

Figure 2.6: *Effect of thermal stratification parameter (S_T) on non-dimensional (a) velocity, (b) temperature, (c) Nusselt number and (d) skin friction coefficient profiles for different values of n.*

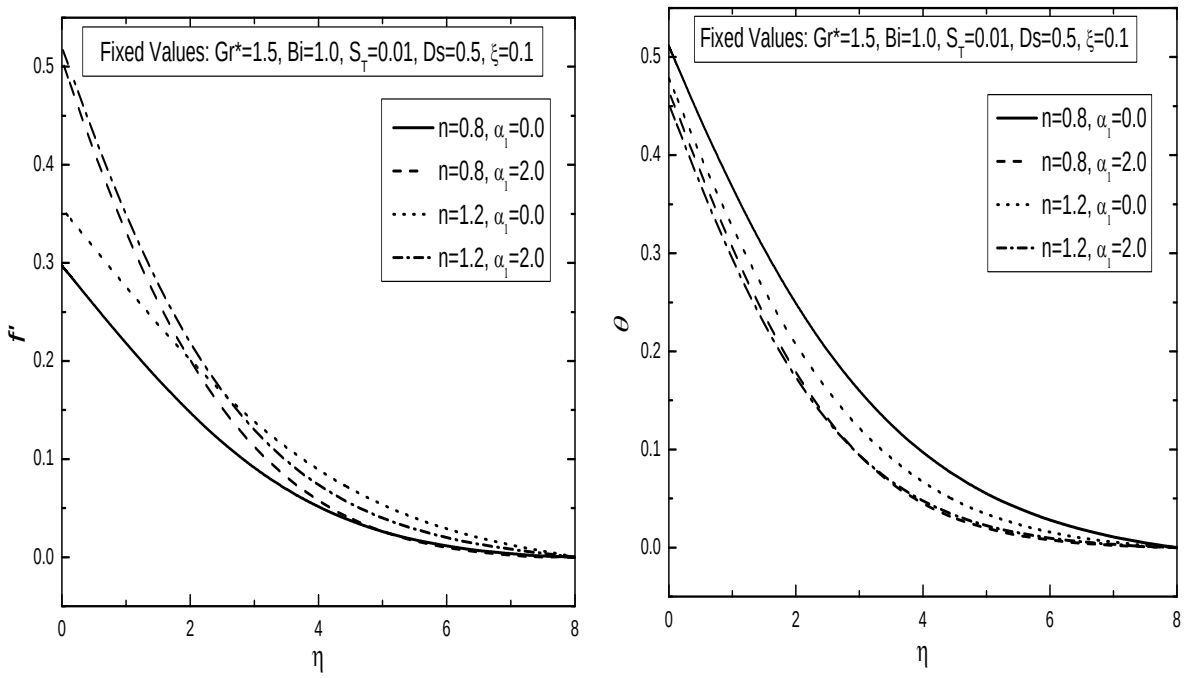

Figure 2.7: *Effect of nonlinear convection parameter* (α_1) *on non-dimensional (a) velocity and (b) temperature profiles for different values of* n.

2.2.2 Case(b): Mixed Convection

The flow is assumed to be a mixed convective flow, which arises from both buoyancy forces and an external flow with the velocity u_∞. To get the non-dimensional form of the system of equations (2.2) - (2.3) and boundary conditions (2.4), the dimensionless transformations are given below

$$\begin{aligned} \xi = \frac{\bar{x}}{x_0}, \;\; \eta = \frac{y}{\bar{x}}\, Pe^{\frac{1}{2}}, \;\; \psi(\xi,\eta) = \alpha\, r\, Pe^{\frac{1}{2}}\, f(\xi,\eta), \\ T(\xi,\eta) = T_\infty(\bar{x}) + (T_f - T_{\infty,0})\; \theta(\xi,\eta), \end{aligned} \tag{2.34}$$

where $Pe = \dfrac{u_\infty \bar{x}}{\alpha}$ is the local Peclet number.

Using these transformations (2.34) in the equations (2.2) to (2.3) and the boundary conditions (2.4), the non-dimensional form of the above equations become

$$n\; (f')^{n-1}\, f'' + 2\, Fs\, f' f'' = \lambda^n (1 + 2\,\alpha_1 \theta)\theta', \tag{2.35}$$

$$(1 + Ds\, f')\theta'' + Ds\, f''\, \theta' + \left(\frac{1}{2} + \frac{\xi}{\xi+1}\right) f\theta' - \xi\, S_T\, f' = \xi \left(f' \frac{\partial \theta}{\partial \xi} - \frac{\partial f}{\partial \xi}\theta' \right), \tag{2.36}$$

along with the boundary conditions

$$\begin{aligned} (3\,\xi + 1) f(\xi,0) + 2\,\xi\,(\xi+1)\left(\frac{\partial f}{\partial \xi}\right)_{\eta=0} = 0, \;\; \theta'(\xi,0) = -Bi\, \xi^{\frac{1}{2}} \left[1 - \theta(\xi,0)\; - \xi\, S_T\right], \\ f'(\xi,\eta) \to 1, \quad \theta(\xi,\eta) \to 0 \;\; as \;\; \eta \to \infty. \end{aligned} \tag{2.37}$$

Here, $Ra = \dfrac{\bar{x}}{\alpha}\left(\dfrac{\rho\, \beta_0\, g\, K^*\, cos\gamma\, (T_f - T_{\infty,0})}{\mu}\right)^{\frac{1}{n}}$, $\lambda = \dfrac{Ra}{Pe}$, $Fs = \dfrac{b\, K^*\; u_\infty^{2-n}}{\nu}$, $Bi = \dfrac{h_f \sqrt{x_0}}{k_m}\left(\dfrac{\bar{x}}{Pe}\right)^{\frac{1}{2}}$, $\alpha_1 = \dfrac{\beta_1}{\beta_0}(T_f - T_{\infty,0})$, $S_T = \dfrac{A^* x_0}{(T_f - T_{\infty,0})}$, and $Ds = \dfrac{\chi d u_\infty}{\alpha}$. The symbol Ra is the local modified Darcy-Rayleigh number, λ is the mixed convection parameter, Fs is the non-Darcian parameter(Forchheimer number), Bi is the Biot number, α_1 is the nonlinear density-temperature parameter, S_T is the thermal stratification parameter and Ds is the thermal dispersion parameter.

Non-dimensional form of the Nusselt number $Nu_{\bar{x}} = -\dfrac{\bar{x}}{k}\dfrac{(k+k_d)}{(T_f - T_{\infty,0})}\left[\dfrac{\partial T}{\partial y}\right]_{y=0}$ and the skin friction coefficient $C_f = \dfrac{2}{\rho\, u_\infty^2}\left[\mu\dfrac{\partial u}{\partial y}\right]_{y=0}$, is given by

$$\frac{Nu_{\bar{x}}}{Pe^{\frac{1}{2}}} = -\left[1 + Ds\, f'(\xi,0)\right]\theta'(\xi,\,0), \qquad \frac{1}{2}\frac{Pe^{\frac{1}{2}}}{Pr}C_f = f''(\xi,0). \tag{2.38}$$

Results and Discussion

In this part, the numerical findings related to the solution of equations (2.35)-(2.36) subject to the boundary conditions (2.37) by the method mentioned in the previous section for various values of physical parameters, are discussed. All the computations in this solution procedure have been carried out with 50 collocation points (*i.e.*, $N_x = 50$) in η-direction and $L_x = 20$ is used for numerical approximations at infinity in η-direction. To verify the correctness of the formulation and accurate calculations further, the outcomes of present problem subject to the wall temperature condition (i.e., $Bi \to \infty$) in the case of vertical plate (i.e., $\xi \to 0$) when $Fs = 0$, $Ds = 0$, $\alpha_1 = 0$, and $S_T = 0$, are also compared with the results (similarity solutions) of Cheng [95] and Chaoyang *et al.* [14] in the case of aiding and opposing flows for the Newtonian fluids. Further, a comparison is also done with the work of Chaoyang *et al.* [14] for non-Newtonian fluids by taking $n = 0.5$ for the pseudoplastic fluid and $n = 1.5$ for the dilatant fluid. The comparison in all these cases is matching at a good extent which is shown in Tables (2.4)-(2.5), respectively. Due to the emerging applications in diverse fields, we are also interested in the analysis of fluid flow and heat transfer rate results. In this study, all the results for power-law fluids, are analysed for both the aiding and opposing flow situations. Also, these results reveal a few interesting facts involving boundary layer flow field and heat transfer rate for physically realistic values of pertinent parameters.

Table 2.4: *Comparison of* $-\theta'(\xi, 0)$ *for various values of* λ *when* $Fs = 0$, $\xi \to 0$, $Ds = 0$, $\alpha_1 = 0$, $Bi \to \infty$ *and* $S_T = 0$*: Newtonian fluid case* ($n = 1$)*.*

λ	Cheng [95]	Chaoyang *et al.* [14]	Present
0.0	0.5641	0.5641	0.564189
0.5	0.6473	0.6473	0.647396
1.0	0.7205	0.7205	0.720584
3.0	0.9574	-	0.957475
4.0	-	1.025	1.055796
8.0	-	1.354	1.380081
10.0	1.5160	-	1.516269
20.0	2.0660	-	2.066331
-0.2	0.5269	0.5269	0.526943
-0.4	0.4865	0.4865	0.486565
-0.6	0.4420	0.4420	0.442053
-0.8	0.3916	0.3916	0.391697
-1.0	0.3320	0.3320	0.332057

Table 2.5: *Comparison of* $-\theta'(\xi, 0)$ *for various values of* λ *when* $Fs = 0$, $\xi \to 0$, $Ds = 0$, $\alpha_1 = 0$, $Bi \to \infty$ *and* $S_T = 0$*: non-Newtonian fluid cases by taking* $n = 0.5$ *and* $n = 1.5$ *respectively.*

λ	Chaoyang *et al.* [14]	Present	Chaoyang *et al.* [14]	Present
0.0	0.5641	0.56418958	0.5641	0.56418958
0.5	0.8209	0.82170383	0.6034	0.60339901
1.0	0.9303	0.92963529	0.6634	0.66337472
4.0	1.301	1.30068542	1.018	1.01758150
8.0	1.610	1.60971523	1.380	1.38021127

The variation in the dimensionless velocity, temperature, Nusselt number and skin friction coefficient for pseudoplastic ($n < 1$) and dilatant ($n > 1$) fluids with increasing values of the Biot number is displayed in Figs. 2.8(a)-2.9(d). The Biot number denotes the ratio of internal thermal resistance of the surface of truncated cone to the thermal resistance of the boundary layer. It is to be noted that the first four graphs i.e., Figs. 2.8(a)-2.8(d), are drawn for the opposing flow case ($\lambda = -3$) and the next four figures i.e., Figs. 2.9(a)-2.9(d), are plotted for the aiding flow case ($\lambda = 3$). In all these plots, all the other parameters are given a fixed value and only Biot number is changed. It is observed from Fig. 2.8(a) that the increment of Biot number increases velocity and the influence is more in the case of dilatant fluid. But, from Fig. 2.9(a), it is evidently visible that the Biot number effect is much more in aiding flow case as velocity touches the higher values (as expected) in comparison with the opposing flow case. The physical reason behind this difference in the velocity between these two fluid flow cases is that the presence of favourable pressure gradient in the aiding flow case. In Figs. 2.8(b) and 2.9(b), the Biot number effect on temperature profiles are shown and the temperature is more for higher values of the Biot number. The effect is almost same for both the opposing and aiding flow cases as there is no direct involvement of mixed convection parameter in energy equation. The variations in the non-dimensional heat transfer rate (Nusselt number) with respect to λ for different values of the Biot number are shown in Figs. 2.8(c) and 2.9(c). It is seen from the opposing flow graph that the Nusselt number variation is very less in the case of pseudoplastic fluid when compared to the dilatant fluid and the heat transfer is more for higher Biot number. The similar behaviour is found for aiding flow but the Nusselt number values are much more for higher values of the Biot number in this case. Similarly, in Figs. 2.8(d) and 2.9(d), variation in the skin friction coefficient in respect of λ for varying values of the Biot number is shown. In opposing flow case, the magnitude of skin friction coefficient is more for the dilatant fluid in comparison with the pseudoplastic fluid for all the values of Biot number and it increases with the higher values of the Biot number. In aiding flow case, the behaviour is found to be similar to opposing flow with the larger magnitude of skin friction coefficient. When $Fs = 0$, $n = 1$ and $\xi \to 0$, the present investigation gives the results of Vasu *et al.* [127], who have conducted similar analysis for the nonlinear convective flow of thermally stratified Newtonian

fluid along a vertical plate in a porous medium in the presence of thermal dispersion and convective boundary condition, and important results are also noted there.

The effect of nonlinear convection parameter (α_1) on the dimensionless velocity, temperature, Nusselt number and skin friction coefficient for opposing and aiding flow cases are shown in Figs. 2.10(a)-2.11(d). This nonlinear convection parameter deals with the nonlinearity in the density temperature relationship. Due to this reason, it is also termed as nonlinear density temperature parameter. As in the previous case, the first four graphs i.e., Figs. 2.10(a)-2.10(d) are drawn for the opposing flow case ($\lambda = -3$) and the next four graphs i.e., Figs. 2.11(a)-2.11(d) are plotted in the case of aiding flow ($\lambda = 3$) and the effect of α_1 on both the fluids i.e., pseudoplastic ($n < 1$) and dilatant ($n > 1$) fluids are shown in single figure. The three different values of α_1 are used to study its effect and all the other parameters are assigned a physically valid fixed value in all these graphs. In the physical sense, $\alpha_1 > 0$ refers the relation $T_f > T_\infty$, so the surface of truncated cone will produce remarkable quantity of heat to the fluid flow region. It is seen from Fig. 2.10(a) that due to increment in α_1, the velocity is increased and its influence is more in the case of dilatant fluid. But, from Fig. 2.11(a), it is clearly visible that the effect of α_1 is much more in aiding flow, which is similar to the Biot number case. In Figs. 2.10(b) and 2.11(b), the effect of α_1 on temperature profiles are shown and the temperature is more for higher values of α_1. The effect is almost same for both opposing and aiding flows due to the same reason stated in above effect. The variations in Nusselt number with respect to λ for different values of the nonlinear convection parameter are shown in Figs. 2.10(c) and 2.11(c). It is pointed out from the opposing flow graph that the Nusselt number variation is very less in the case of pseudoplastic fluid when compared to the dilatant fluid and increment in α_1 gave higher heat transfer rate. The similar behaviour is found for aiding flow but the values of heat transfer rate are much more for higher values of α_1 in this case. Similarly, in Figs. 2.10(d) and 2.11(d), the variations in skin friction coefficient in respect of λ for fixed values of α_1 are shown. In opposing flow case, as nonlinear convection parameter is increased, the skin friction coefficient values approach to its higher magnitude and this effect is more in dilatant fluids when compared to the pseudoplastic fluids. The similar behaviour is seen in aiding

flow but magnitude of skin friction coefficient is more in this case. Finally, it is concluded from these graphs that the heat transfer rate is less and skin friction is more for both these fluids when the linear Bousinesq approximation is employed in comparison to the nonlinear Bousinesq approximation.

Effect of thermal dispersion parameter (Ds) on the dimensionless velocity, temperature, Nusselt number and skin friction coefficient for both the pseudoplastic ($n < 1$) and dilatant ($n < 1$) fluids, is shown in Figs. 2.12(a)-2.12(d) for opposing flow case and in Figs. 2.13(a)-2.13(d) for aiding flow case. Basically, this effect brings up the effectiveness of non-uniform pore level velocity on the temperature field inside the particular porous medium. Also, it shows the significance of combined changes in velocity and temperature profiles to the heat transportation. The different values of Ds are used to study its effect and all other parameters are fixed to a certain value within their physical ranges, in all these graphs. It is found from the Figs. 2.12(a) and 2.13(a) that the velocity profiles are increased in the presence of dispersion parameter for both these fluids in opposing and aiding flow cases. As expected, the velocity is more in the case of aiding flow. Similarly, the temperature profiles are also increased in the presence of Ds as shown in Figs. 2.12(b) and 2.13(b). Since the flow velocity becomes high enough in the porous medium, there is a domination of thermal dispersion over molecular diffusion. So, it is crucial to give a satisfactory record of its influence on the heat transfer characteristics in power-law fluid saturated non-Darcy porous medium. The effect of dispersion parameter on Nusselt number for opposing ($\lambda = -3$) and aiding ($\lambda = 3$) flow cases is shown in Figs. 2.12(c) and 2.13(c), respectively. With higher values of Ds, the heat transfer is increased in both the flow cases for pseudoplastic and dilatant fluids and it is more in the case of aiding flow. The influence of dispersion parameter on the skin friction coefficient with respect to λ is shown in Figs. 2.12(d) and 2.13(d). Due to increment in Ds, more variation in the skin friction is observed in opposing flow case but reverse behaviour is seen in the aiding flow case for both these power-law fluids. The magnitude of skin friction coefficient is more in the case of aiding flow in comparison with the opposing flow case. As a conclusion, more heat transfer rate and less skin friction coefficient are observed in the presence of thermal dispersion when compared to its absence in the power-law fluid flows.

Also, we can say that the effect of thermal dispersion is significant when the inertial effect is frequent and its negligence can result into a decent amount of error.

The velocity profiles of pseudoplastic and dilatant fluids in the absence and presence of stable stratification for various values of λ are depicted in the Figs. 2.14(a)-2.14(d). It is significant to perceive the existence of flow separation in this study. More gain in the velocity of dilatant fluid is seen when compared to the pseudoplastic fluid. As the value of λ changes from zero to negative values, the flow separation occurs. The boundary layer separation takes place when the flow direction is reversed in the nearest part of the boundary layer to the surface or main edge. In other words, the point in the middle of forward and backward flow, where shear stress is zero, is also termed as the separation point. For positive values of λ, the velocity is more in comparison to that of the forced convection ($\lambda = 0$) for both these fluids. On the other hand, it is comparatively less in the case of negative λs. Also, it is evident from these graphs that the separation of flow is less in the presence of thermal stratification but it is more in the absence of thermal stratification.

In Figs. 2.15(a)-2.16(a), the effect of thermal stratification parameter (S_T) on non-dimensional temperature in the fluid flow is depicted for both opposing and aiding flow cases respectively. The temperature profiles are influenced with the presence of stable stratification (i.e., for $S_T > 0$) and these are decreased with an increment in S_T. In the presence of S_T, the resultant temperature difference between the surface of truncated cone and the ambient fluid is reduced, and it results into thickening of thermal boundary layer which is responsible for decrements in the temperature profiles. In Figs. 2.15(b) and 2.16(b), the impact of thermal stratification on the heat transfer is shown and it is observed to be completely different for both the fluids (pseudoplastic and dilatant). In the case of opposing flow, the heat transfer is increased linearly with more negatives λ for the pseudoplastic fluid and rapid increase is found for the dilatant fluid. With higher values of the stratification parameter, the heat transfer is decreased for both the pseudoplastic and dilatant fluids. The similar behaviour is found in the case of aiding flow but the linear behaviour related to pseudoplastic fluid is lost and the heat transfer is more in comparison with the opposing flow for a particular value of stratification parameter. The impact of stratification on skin friction coefficient with λ

is shown in Figs. 2.15(c) and 2.16(c), and it is observed that due to increment in S_T, the skin friction values are less negative in opposing flow case and the linear nature of change is found with negative λ's for the pseudoplastic fluid and rapid change is observed for the dilatant fluid. In aiding flow case, the linear behaviour related to pseudoplastic fluid is lost and magnitude of skin friction coefficient is more in comparison with the opposing flow for a certain value of S_T. Opposite to previous flow case, more negative skin friction is found with the increment in stratification parameter in this case. In this way, it can be said that the thermal stratification significantly affects the heat transfer rate of power-law fluids besides delay the boundary layer separation. The results are in tune with the observation made in references [RamReddy *et al.* [100]; Vasu *et al.* [127] and citations therein].

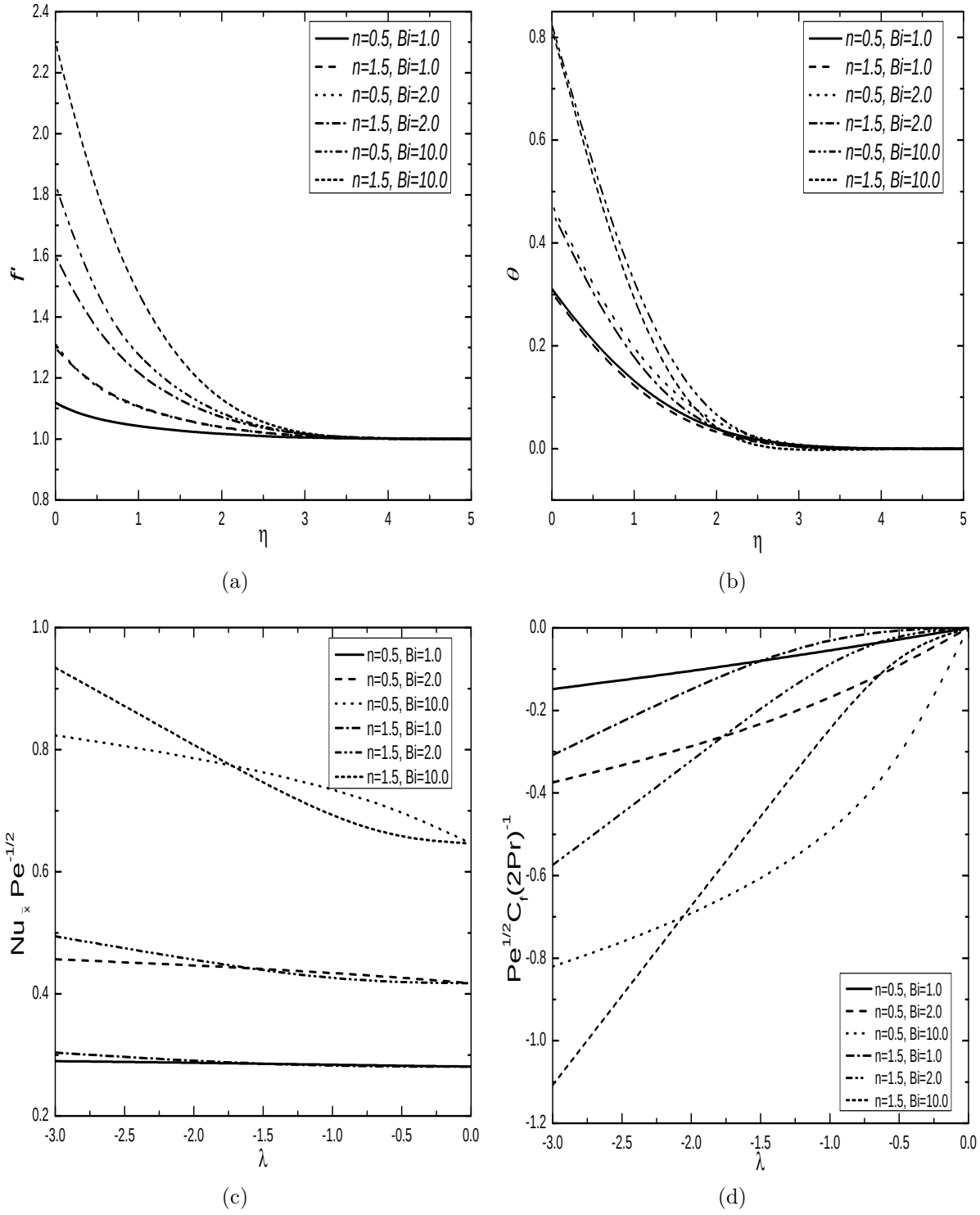

Figure 2.8: *Effect of Biot number Bi for the two values of n on (a) velocity, (b) temperature, (c) Nusselt number and (d) skin friction coefficient in the case of opposing flow with the fixed values* $Ds = 0.3$, $\alpha_1 = 2.0$, $Fs = 0.5$, $\xi = 0.1$, $S_T = 0.01$.

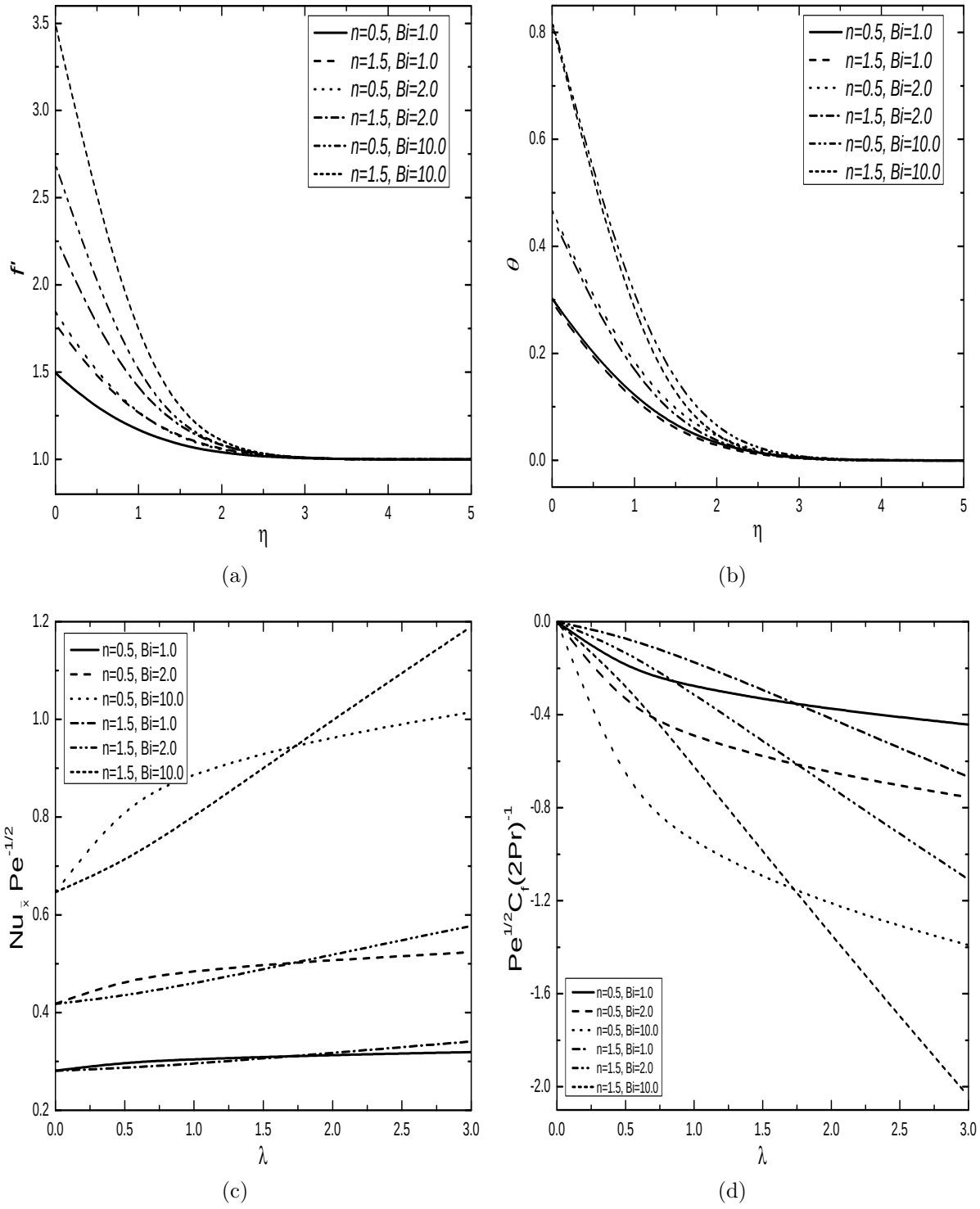

Figure 2.9: *Effect of Biot number Bi for the two values of n on (a) velocity, (b) temperature, (c) Nusselt number and (d) skin friction coefficient in the case of aiding flow with the fixed values* $Ds = 0.3$, $\alpha_1 = 2.0$, $Fs = 0.5$, $\xi = 0.1$, $S_T = 0.01$.

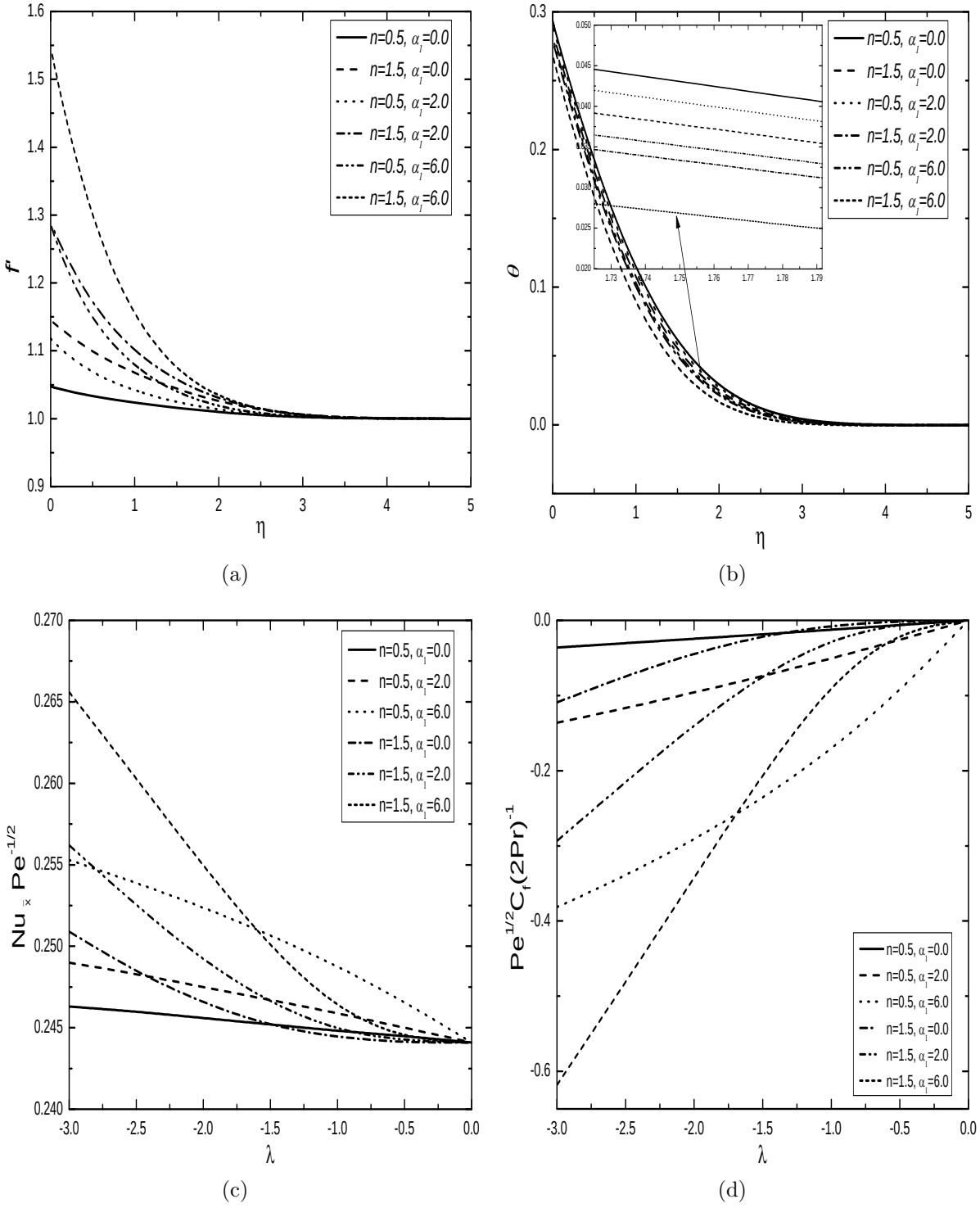

Figure 2.10: *Effect of* α_1 *for the two values of* n *on (a) velocity, (b) temperature, (c) Nusselt number and (d) skin friction coefficient in the case of opposing flow with the fixed values* $Ds = 0.1$, $Bi = 1.0$, $Fs = 0.5$, $\xi = 0.1$, $S_T = 0.01$.

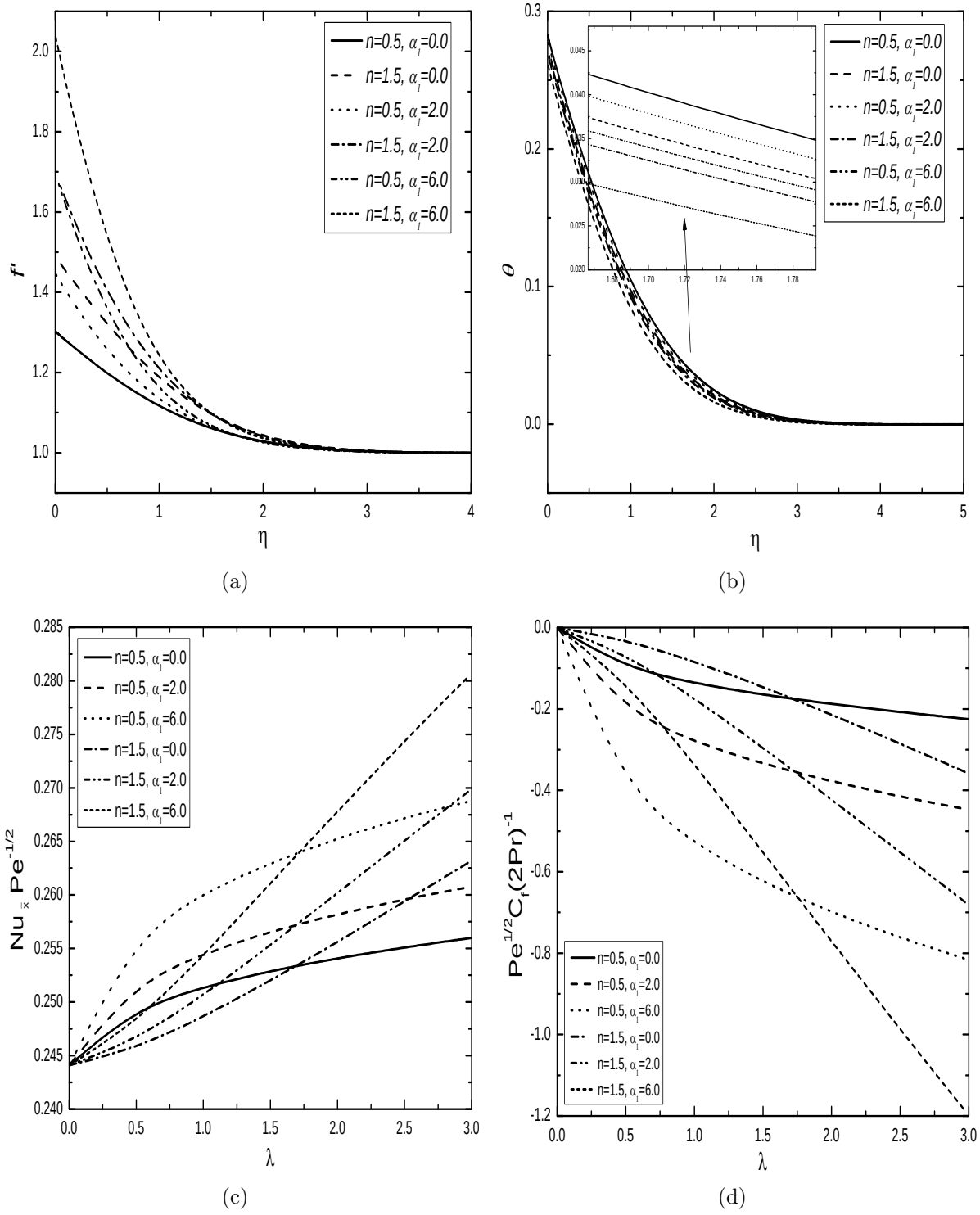

Figure 2.11: *Effect of* α_1 *for the two values of* n *on (a) velocity, (b) temperature, (c) Nusselt number and (d) skin friction coefficient in the case of aiding flow with the fixed values* $Ds = 0.1$, $Bi = 1.0$, $Fs = 0.5$, $\xi = 0.1$, $S_T = 0.01$.

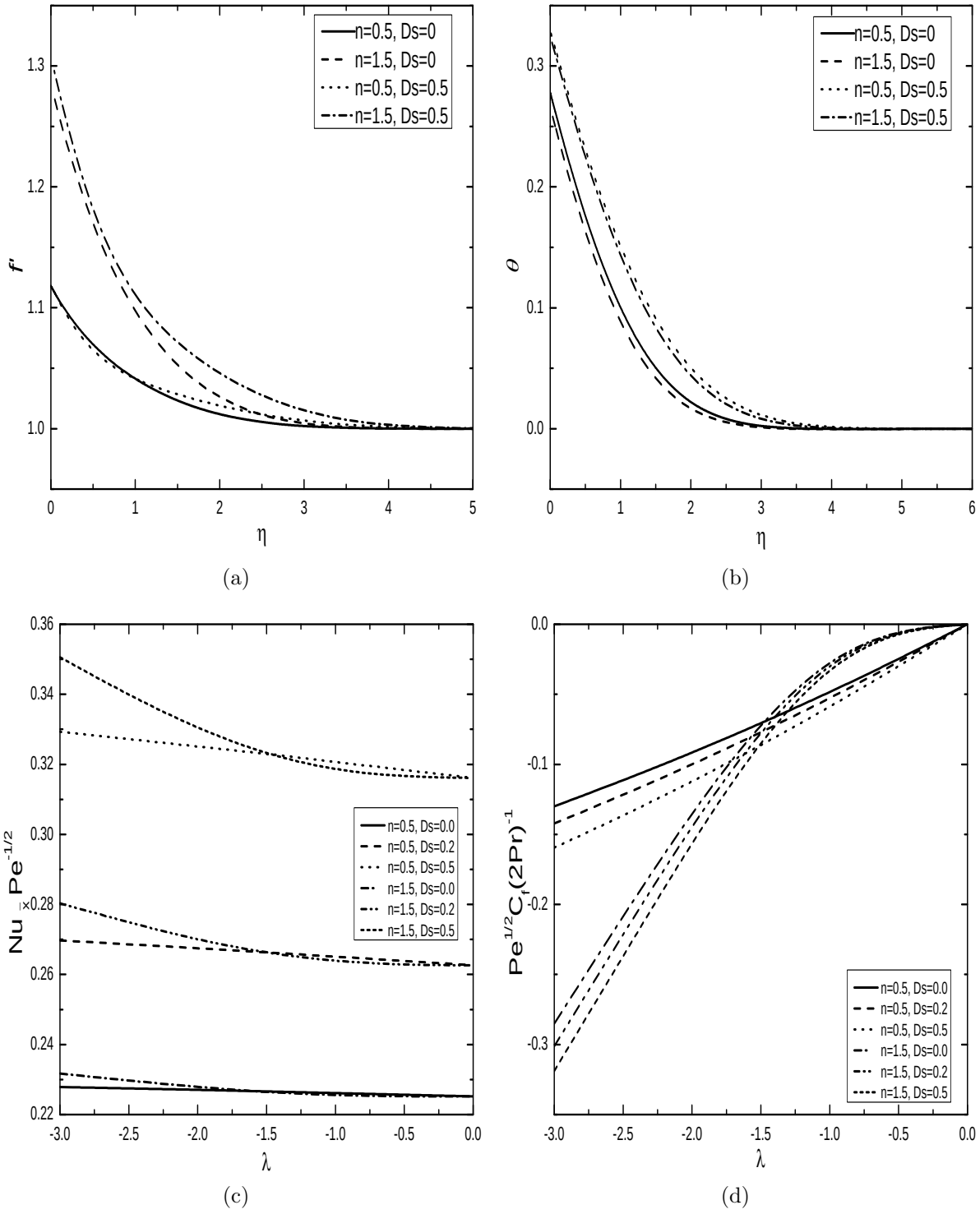

Figure 2.12: *Effect of dispersion parameter Ds for the two values of n on (a) velocity, (b) temperature, (c) Nusselt number and (d) skin friction coefficient in the case of opposing flow with the fixed values* $\alpha_1 = 2.0$, $Bi = 1.0$, $Fs = 0.5$, $\xi = 0.1$, $S_T = 0.01$.

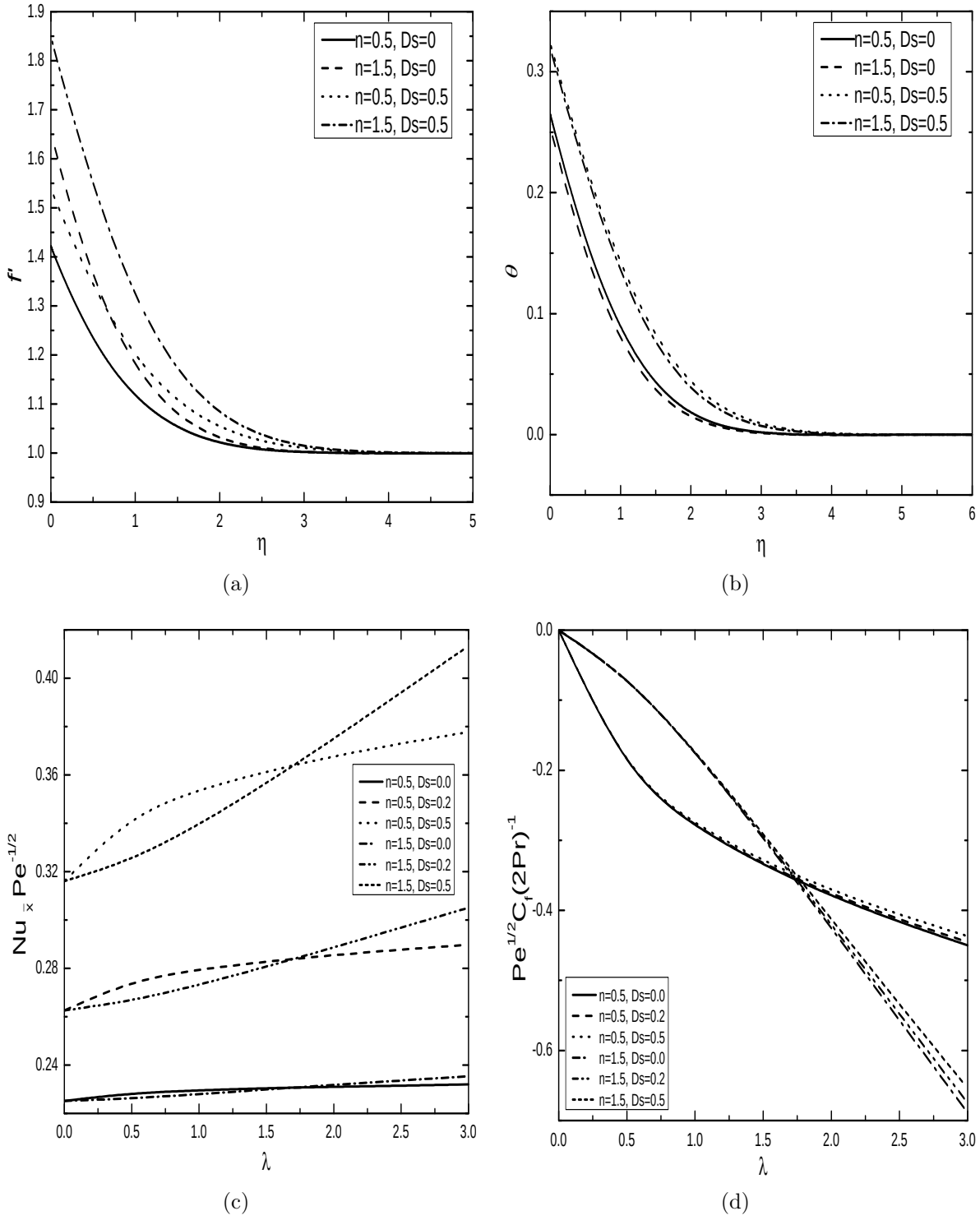

Figure 2.13: *Effect of dispersion parameter Ds for the two values of n on (a) velocity, (b) temperature, (c) Nusselt number and (d) skin friction coefficient in the case of aiding flow with the fixed values* $\alpha_1 = 2.0$, $Bi = 1.0$, $Fs = 0.5$, $\xi = 0.1$, $S_T = 0.01$.

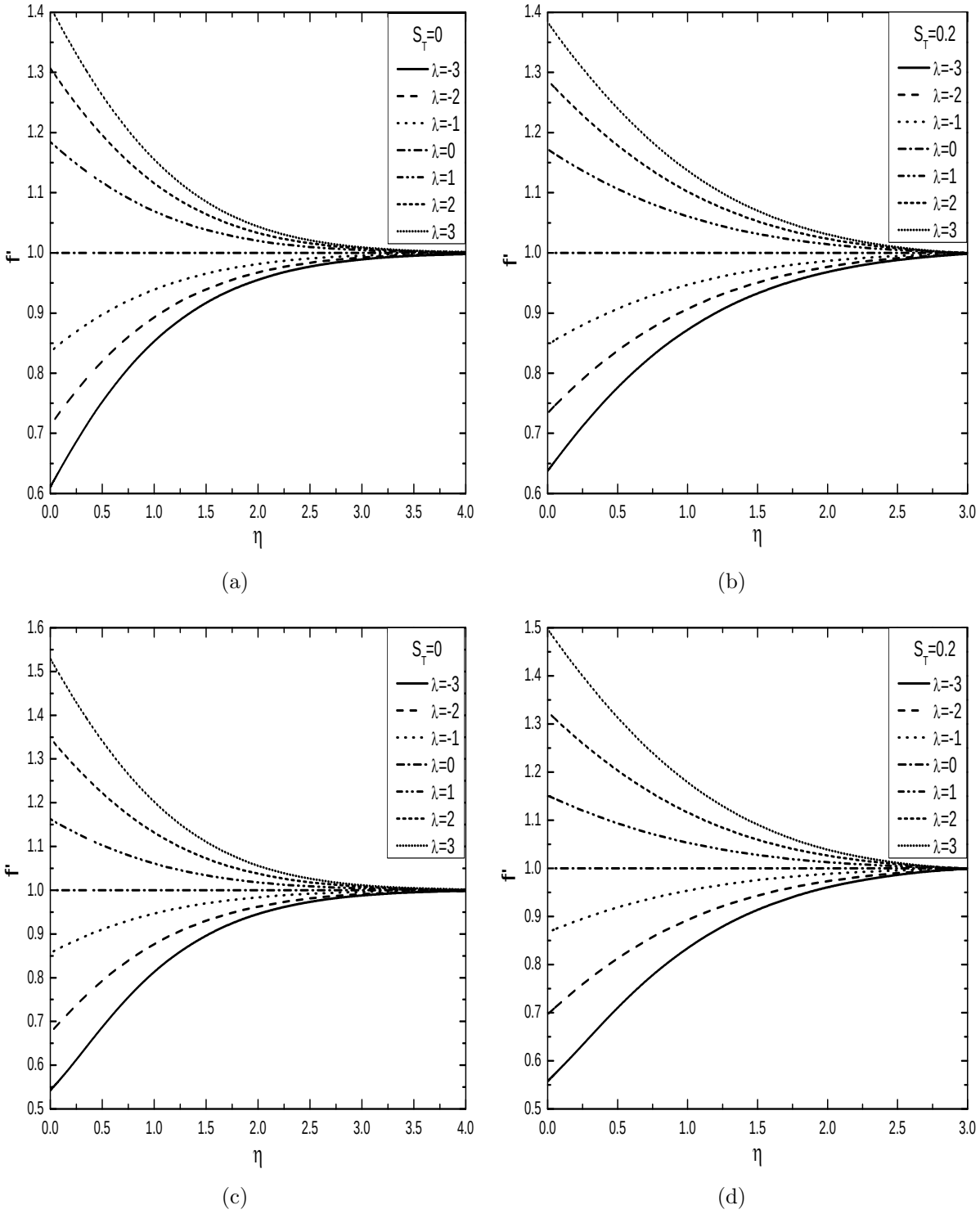

Figure 2.14: *Effect of stratification parameter S_T on the velocity profiles in opposing and aiding flow cases for (a),(b) pseudoplastic ($n = 0.8$) and (c), (d) dilatant ($n = 1.2$) fluids respectively when $Ds = 0.5$, $\alpha_1 = 2.0$, $Fs = 1.0$, $\xi = 0.1$, $Bi = 1.0$.*

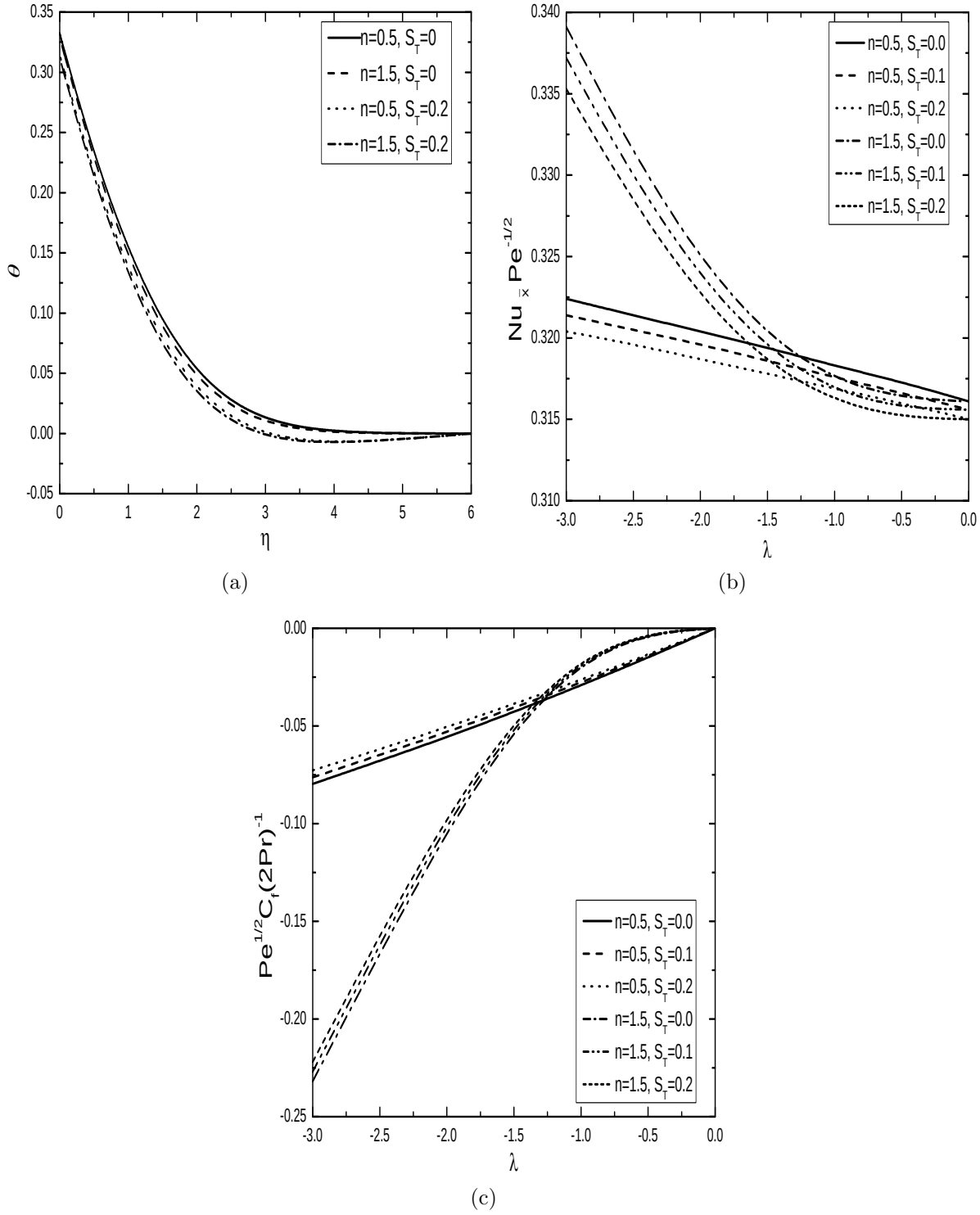

Figure 2.15: *Effect of stratification S_T for the two values of n on temperature, Nusselt number and skin friction coefficient in the case of opposing flow with the fixed values $Ds = 0.5$, $\alpha_1 = 2.0$, $Fs = 1.0$, $\xi = 0.1$, $Bi = 1.0$.*

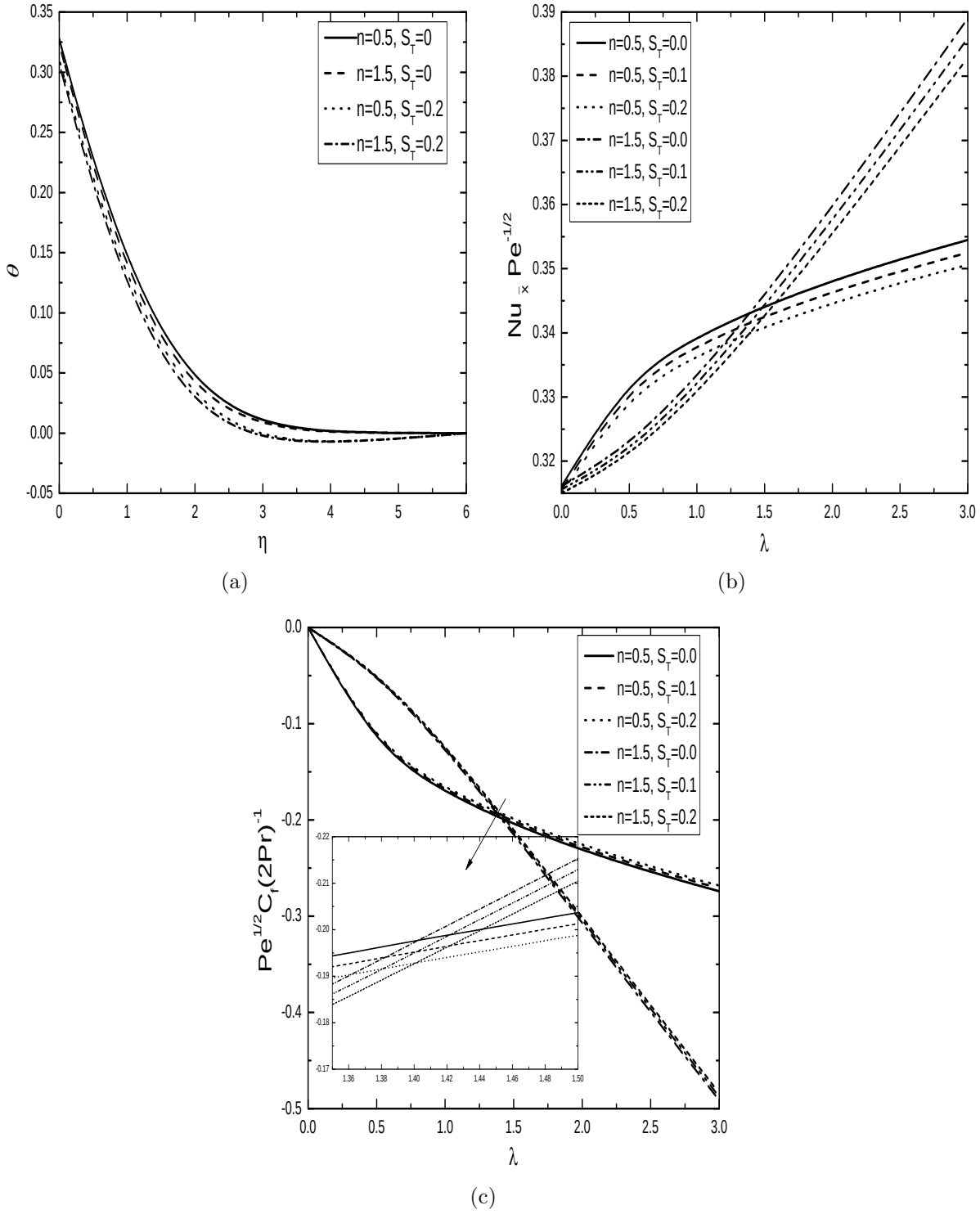

Figure 2.16: *Effect of stratification S_T for the two values of n on temperature, Nusselt number and skin friction coefficient in the case of aiding flow with the fixed values $Ds = 0.5$, $\alpha_1 = 2.0$, $Fs = 1.0$, $\xi = 0.1$, $Bi = 1.0$.*

2.3 Conclusions

In this chapter, the effect of nonlinear density-temperature and thermal dispersion parameters on the thermally stable stratified power-law fluid flows over a convectively heated truncated cone in a non-Darcy porous medium, is discussed in detail for the two cases: (a) natural convection and (b) mixed convection. Consideration of the thermally stratified power-law fluids over a truncated cone with convective heating enhanced the number of non-dimensional parameters considerably thereby increasing the nonlinear complexity of the present problem. So, the governing equations are handled by the combination of local non-similarity and spectral local linearisation approaches. These kinds of analysis play very important part in the area of polymeric mixtures maintained at very high temperatures, aerosol technology etc., and these all are related to temperature-dependent density. The conclusive remarks of this work in both the cases (a) and (b) for physically suitable values of flow governing parameters, are:

Case (a): Natural Convection

- The velocity, temperature and Nusselt number are increased for larger Bi but the skin friction coefficient is reduced for pseudoplastic and dilatant fluids.
- Thermal stratification parameter influences temperature, velocity and rate of heat transfer in a similar way and all these face decrement with higher values of S_T. But, the different trend is seen in the case of skin friction coefficient.
- The thermal dispersion parameter increases temperature, velocity, heat transfer rate and skin friction coefficient with its presence.
- The impact of nonlinear convection parameter α_1 on the velocity and temperature profiles is opposite in nature as its presence gives increment in the velocity profiles, and decrement in the temperature profiles.

Case (b): Mixed Convection

- The velocity, temperature and heat transfer rate are found to be more for higher Biot number but the skin friction coefficient is less for both the pseudoplastic and dilatant fluids.

- The impact of nonlinear convection parameter is almost as Biot number. Also, the heat transfer rate is less and skin friction coefficient is more for both the fluids when the linear Boussinesq approximation is employed in comparison with the nonlinear Boussinesq approximation.

- The effect of dispersion parameter on velocity, temperature and heat transfer is same as of stratification but opposite nature is found for the skin friction coefficient with respect to the flow behaviour.

- The separation of flow is found to be less in the thermally stratified fluids but it is more in the thermally unstratified fluids. Also, thermal stratification significantly affects the heat transfer rate of power-law fluids besides delay in the boundary layer separation.

- The flow separation is more in the pseudoplastic fluid in comparison to the dilatant fluid.

Chapter 3

Second Law Analysis on Power-law Fluid Flows over a Truncated Cone with Viscous Dissipation: Forchheimer Model [1]

3.1 Introduction

The entropy generation analysis in flow studies over vertical surfaces are very useful due to its regular involvement in various industrial applications such as geothermal reservoirs, cooling of nuclear reactors, thermal insulation and petroleum reservoirs. In particular, the entropy generation analysis builds optimization ideas to prepare the blueprint of many gadgets involved in thermal field by making the total of frictional and thermal entropy generation rates minimum. Also, the criteria of optimal design in thermal systems by minimizing their entropy generation involve the flow studies over vertical surfaces. In this regard, Bejan [10] studied the effectiveness of various factors involved in entropy generation in thermal systems.

[1] Case(a): Published in "**Journal of Thermal Analysis and Calorimetry**", June 2021, DOI: 10.1007/s10973-021-10823-1, Case(b): Published in "**International Journal of Ambient Energy**", July 2021, DOI: 10.1080/01430750.2021.1951838.

In addition to this, the impact of nonlinear convection, viscous dissipation and thermal dispersion plays very crucial role in these types of flow studies. El-Amin *et al.* [33] considered the power-law fluid flow over a plane surface to investigate the impact of viscous dissipation which is related to the locally produced thermal energy.

In recent times, Sheikholeslami *et al.* [109] demonstrated the heat transfer and entropy generation by considering nanofluid flow via heat exchanger. Recently, Noreen and Ain [89] investigated the entropy generation for electroosmotic flow across a non-Darcy porous medium by peristaltic pumping. Saleem and El-Aziz [104] performed the second law analysis in a power-law fluid flow past an exponentially movable plane with slip impacts. Srinivasacharya and Bindu [116] discussed the entropy generation for micropolar fluid in an inclined channel. The impact of viscous energy dissipation on electro-magnetohydrodynamic flow and heat transfer of a third-grade fluid using a Darcy-Brinkman-Forchheimer model, has been explained by Zhang *et al.* [130]. Entropy optimization of non-Newtonian fluids and study of Darcy-Forchheimer flows can be found in the papers by Nayak *et al.* [87] and Shaw *et al.* [108].

The problem of convective transport of power-law fluid flows over a truncated cone embedded in a non-Darcy porous medium is analysed in this chapter. Further, the nonlinear Boussinesq approximation and thermal dispersion are incorporated. As per the authors' knowledge, the present study has not been addressed in the literature even though it has many industrial applications due to involvement of cone-shaped bodies.

3.2 Mathematical Analysis

In this chapter, the effect of viscous dissipation, nonlinear convection and thermal dispersion on free and mixed convective flows over a truncated cone immersed in a Forchheimer type of non-Darcy porous medium saturated by dilatant and pseudoplastic fluids, is considered. The physical model with coordinate system is displayed in Fig. 3.1. The leading edge of the truncated cone is kept at a distance x_0 from the origin O, where x and y axes are taken along

and normal to the surface of the truncated cone, respectively. The ambient medium and wall temperatures are taken as T_∞ and T_w respectively together with the modified streamwise coordinate $\bar{x}$, which is defined as $\bar{x} = x - x_0$ for the truncated cone.

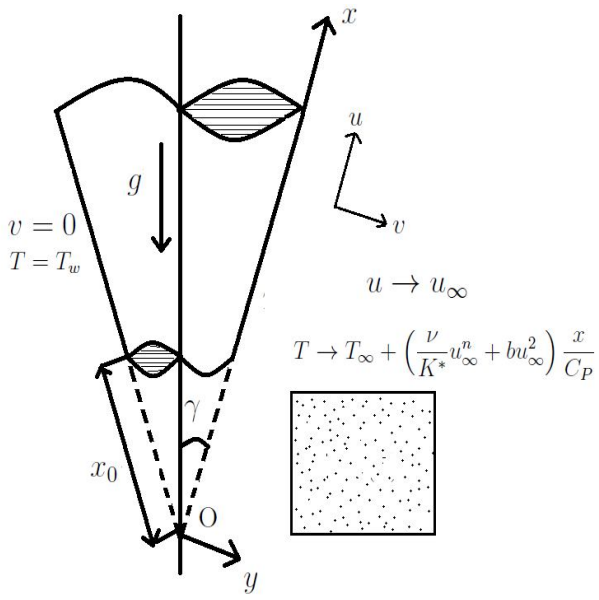

Figure 3.1: *Physical model and coordinate system.*

Taking the boundary layer hypothesis into the consideration along with the general and basic approximations and assumptions related to truncated cone as mentioned in *Chapter-2*, the governing equations for the fluid flow over a truncated cone are given by [39, 55, 85]

$$\frac{\partial(ru)}{\partial x} + \frac{\partial(rv)}{\partial y} = 0, \tag{3.1}$$

$$\frac{\partial u^n}{\partial y} + \frac{bK^*}{\nu}\frac{\partial u^2}{\partial y} = \frac{K^* g\cos\gamma}{\nu}\left\{\beta_0 + 2\beta_1(T - T_\infty)\right\}\frac{\partial T}{\partial y}, \tag{3.2}$$

$$u\frac{\partial T}{\partial x} + v\frac{\partial T}{\partial y} = \frac{\partial}{\partial y}\left(\alpha_*\frac{\partial T}{\partial y}\right) + \frac{\nu u}{K^* C_P}\left(u^n + \frac{bK^*}{\nu}u^2\right), \tag{3.3}$$

subject to

$$\begin{aligned} v(x,\,y) = 0, \qquad T(x,\,y) = T_w \qquad\qquad \text{at} \qquad y = 0, \\ u(x,\,y) \to u_\infty,\;\; T(x,\,y) \to T_\infty + \left(\frac{\nu}{K^*}u_\infty^n + bu_\infty^2\right)\frac{x}{C_P} \quad \text{as} \quad y \to \infty, \end{aligned} \tag{3.4}$$

where ν is the kinematic viscosity, γ is the angle inclination, g is the gravitational acceleration, T is the temperature, b is the empirical constant, C_P is the specific heat capacity, β_0 and β_1 are the 1^{st} and 2^{nd} order thermal expansion coefficients, (u, v) and u_∞ denote the Darcian and free stream velocities, respectively. Also, $\alpha_* = \alpha + \alpha_d$ where α is the molecular diffusivity and $\alpha_d = \chi u d$ is the thermal diffusivity. Here, χ is the mechanical dispersion coefficient and d is the pore diameter. K^* is the modified permeability in the porous medium and it depends on the power-law index (n). It is important to mention that an assumption of constant ambient temperature along with this type of modeling of viscous dissipation (u^2-type) gives an inconsistent solution. It is because the constant ambient temperature condition does not satisfy the energy equation. It is a well-known deficiency in the modeling of viscous dissipation in a porous media and there has been much argument on whether to include the work done due to pressure in such a model. This inconsistency is resolved by allowing the ambient temperature to vary with x.

In this chapter also, two types (cases) of problems are considered: (a) free/natural convection and (b) mixed convection.

3.2.1 Case(a): Natural Convection

Since natural convective flows are caused by only buoyancy forces and there is no involvement of any external agent. Hence, the external flow velocity becomes zero ($i.e., u_\infty = 0$). So, the non-dimensional relations used to get the non-dimensional form of equations (3.2)-(3.4) are

$$\xi = \frac{\bar{x}}{x_0}, \;\; \eta = \frac{y}{\bar{x}}\,Ra^{\frac{1}{2}}, \;\; \psi(\xi,\eta) = \alpha\, r\, Ra^{\frac{1}{2}}\, f(\xi,\eta), \;\; T(\xi,\eta) = T_\infty + (T_w - T_\infty)\,\theta(\xi,\eta), \tag{3.5}$$

where $Ra = \dfrac{\bar{x}}{\alpha}\left(\dfrac{\rho\,\beta_0\,g\,K^*\,cos\gamma\,(T_w - T_\infty)}{\mu}\right)^{\frac{1}{n}}$ is the local modified Darcy-Rayleigh number.

On substituting the transformations (3.5) in the equations (3.2) to (3.3), the non-dimensional form of these equations become

$$n\ (f')^{n-1}\,f'' + 2\,Gr^*\,f'f'' = (1 + 2\,\alpha_1\theta)\theta', \tag{3.6}$$

$$\begin{aligned}(1 + Ds\,f')\theta'' + Ds\,f''\,\theta' + \left(\frac{1}{2} + \frac{\xi}{\xi+1}\right) f\theta' + \epsilon\xi f'\left[(f')^n + Gr^*\,(f')^2\right] \\ = \xi\left(f'\frac{\partial\theta}{\partial\xi} - \frac{\partial f}{\partial\xi}\theta'\right),\end{aligned} \tag{3.7}$$

The boundary conditions (3.4) in their transformed forms can be written as

$$\begin{aligned}2\,\xi\,(\xi+1)\left(\frac{\partial f}{\partial\xi}\right)_{\eta=0} + (3\,\xi+1)f(\xi,\,\eta) = \ 0, \quad \theta(\xi,\,\eta) = 1 \ \ as \ \ \eta = 0, \\ f'(\xi,\eta) \to 0, \quad \theta(\xi,\eta) \to \ 0 \ \ as \ \ \eta \to \infty.\end{aligned} \tag{3.8}$$

Here, the differentiation with respect to η is indicated by primes. In usual notations, $Gr^* = \dfrac{b\,K^*}{\nu}\left(\dfrac{\alpha\,Ra}{\bar{x}}\right)^{2-n}$, $\epsilon = \dfrac{\nu\,x_0}{K^*\,C_P\,(T_w - T_\infty)}\left(\dfrac{\alpha\,Ra}{\bar{x}}\right)^n$, $\alpha_1 = \dfrac{\beta_1}{\beta_0}(T_w - T_\infty)$, and $Ds = \dfrac{\chi dRa}{\bar{x}}$. Here, Gr^* is the modified Grashof number, ϵ is the viscous dissipation parameter, α_1 is the nonlinear density-temperature parameter and Ds is the thermal dispersion parameter. When $x_0 = 0$, ξ becomes very large and this limiting case is used to get the fluid flow problem over a full cone. Likewise, when $\xi = 0$ (i.e., $x = x_0$), the present problem reduces to fluid flow problem along a vertical plate.

Non-dimensional form of the heat transfer coefficient, commonly known as Nusselt number $Nu_{\bar{x}} = -\dfrac{\bar{x}}{k}\dfrac{(k + k_d)}{(T_w - T_\infty)}\left[\dfrac{\partial T}{\partial y}\right]_{y=0}$ is given by

$$\frac{Nu_{\bar{x}}}{Ra^{\frac{1}{2}}} = -\left[1 + Ds\,f'(\xi,0)\right]\theta'(\xi,\,0), \tag{3.9}$$

where the addition of dispersion thermal conductivity k_d and molecular thermal conductivity k is used as the effective thermal conductivity of the porous medium.

The available amount of energy in any system related to industrial or engineering processes, is destroyed by entropy generation and so this property plays a significant role in these fields. It is therefore important to determine the entropy generation rate in any system so that the operation efficiency of the system can be optimized. The dimensional form of the expression for entropy generation related to the present flow problem is written as

$$S_g''' = \frac{K^*}{T_\infty^2}\left(\frac{\partial T}{\partial y}\right)^2 + \frac{\nu}{K^*\, C_P\, T_\infty}\left(u^{n+1} + \frac{bK^*}{\nu}u^3\right). \tag{3.10}$$

The characteristic entropy generation is defined as $\left(S_g'''\right)_0 = \dfrac{K^*}{T_\infty^2}\dfrac{(T_w - T_\infty)^2}{\bar{x}^2}$ and so the non-dimensional form of entropy generation $Ns = \dfrac{S_g'''}{\left(S_g'''\right)_0}$ can be written as

$$\frac{Ns}{Ra} = \theta'^2 + \frac{Br}{\Omega}\xi\left[(f')^{n+1} + Gr^*(f')^3\right], \tag{3.11}$$

where $Br = \dfrac{\alpha\,\nu\,x_0}{K^{*2}\,C_P\,(T_w - T_\infty)}\left(\dfrac{\alpha\,Ra}{\bar{x}}\right)^{2-n}$ is the Brinkman number and $\Omega = \dfrac{T_w - T_\infty}{T_\infty}$ is the dimensionless temperature difference.

The above equation (3.11) can be split into two parts as $Ns = N_1 + N_2$,
where $N_1 = Ra\,\theta'^2$ and $N_2 = \dfrac{Br\,Ra}{\Omega}\xi\,[(f')^{n+1} + Gr^*(f')^3]$. The first part denotes the entropy generation due to heat transfer and the second part is responsible for the entropy generation due to fluid friction. To check the domination of fluid friction irreversibility over heat transfer irreversibility, one more irreversibility distribution parameter is defined which is the ratio of entropy generation due to heat transfer over total entropy generation and known as Bejan number (Be). The expression for the Bejan number can be given as

$$Be = \frac{N_1}{Ns} = \frac{\theta'^2}{\theta'^2 + \dfrac{Br}{\Omega}\xi\,[(f')^{n+1} + Gr^*(f')^3]} \in [0, 1]. \tag{3.12}$$

In particular, $Be = 0$ shows that the irreversibility due to fluid friction dominates, but $Be = 1$ reveals that the irreversibility due to heat transfer dominates. Further, the irreversibility due to fluid friction and heat transfer are equal in the process of entropy generation if $Be = 0.5$.

Results and Discussion

In this chapter (and further chapters in the entire thesis), the governing equations (3.6)-(3.7) along with the boundary conditions (3.8) are solved numerically using spectral local linearization method (SLLM) together with the non-similarity approach. Validation of the present problem can be done on comparison as it was done in the case (a) of *Chapter-2* by putting $\xi = 0$, $Ds = 0$, $\epsilon = 0$ and $\alpha_1 = 0$.

Here, the graphs in Figs. 3.2(a)-3.2(e) related to non-dimensional velocity and temperature profiles, heat transfer and entropy generation rates along with Bejan number respectively, are displayed. The effect of viscous dissipation parameter on these profiles and quantities, is analysed properly for pseudoplastic, Newtonian and dilatant fluids. In the physical sense, ϵ refers to the transformation of energy from the motion of fluid to the fluid's internal energy. Viscous dissipation is high in the regions of large gradients, e.g., boundary layers, shear layers etc. Velocity and temperature profiles are studied in respect of η and from Fig. 3.2(a), it is observed that the velocity in dilatant fluid flow is higher when compared to the pseudoplastic fluid flow. The presence of ϵ increases the velocity and temperature for each fluid, but the temperature is found to be higher in the case of pseudoplastic fluid as displayed in Fig. 3.2(b). The presence of ϵ makes the temperature of the system stable for all the fluids because viscous dissipation behaves like a source term in the fluid flow generating notable rise in the fluid temperature as the kinetic motion of fluid is converted to thermal energy. This observation has significance in the heat and fluid flow in microchannel having larger ratio of length to diameter. The non-dimensional heat transfer and entropy generation rates along with the Bejan number are analysed in respect of streamwise coordinate ξ and the variation in these quantities proves the non-similar nature of this problem. From Figs. 3.2(c)-3.2(e), it is seen that these quantities show decrements with increasing values of ϵ for all the fluids. As the streamwise coordinate increases, there is continuous increment in the heat transfer and entropy generation rates but opposite is observed with Bejan number. As expected, Bejan number approaches to zero for higher values of ξ. These smaller values of Bejan number indicate the domination of irreversibility due to fluid friction in the areas where streamwise coordinate is large. In all these three analyses, the dilatant fluid domi-

nates. The entropy generation minimization is very useful in the thermal engineering and design variable selection in many efficient fluid systems.

Here, the thermal dispersion parameter effect on the non-dimensional velocity and temperature profiles, Nusselt number, entropy generation rate and Bejan number is shown in Figs. 3.3(a)-3.3(e). The first two graphs show the variations in respect of η and the later three show in respect of ξ. The study of pseudoplastic, Newtonian and dilatant fluids are combined in single figure. Basically, this effect brings up the effectiveness of non-uniform pore level velocity on the temperature field inside the particular porous medium. As there are sufficiently high velocity due to the fluid flow through a porous medium, hence the molecular diffusion is dominated by the thermal dispersion. Also, it shows the significance of combined changes from the velocity and temperature to the heat transportation. From Figs. 3.3(a) and 3.3(b), it is observed that the presence of Ds enhances the velocity and temperature profiles for all the fluids and dilatant fluid dominates in the case of velocity profiles and pseudoplastic fluid dominates for the temperature profiles. It is found from the Fig. 3.3(c) that the heat transfer rate is increased in the presence of dispersion parameter for all these fluids and there is domination of dilatant fluid in this case too. There is slight change is the heat transfer rate with ξ in the absence of dispersion but variation is comparatively larger in its presence. In the Figs. 3.3(d) and 3.3(e), the impact of Ds on entropy generation and Bejan number is shown and both are decreased for its higher values. The values of entropy generation rate and Bejan number are more for dilatant fluid in comparison with pseudoplastic and Newtonian fluids. With higher streamwise coordinate, as expected, entropy generation rate increases and Bejan number decreases. This entropy generation and Bejan number analysis gives the idea of components and processes (mechanisms) of the system which provides real advantage in the improvement of the system efficiency by allocating proper engineering resources and efforts.

The non-dimensional velocity and temperature profiles, heat transfer and entropy generation rates along with the Bejan number respectively, are shown in the graphs in Figs. 3.4(a)-3.4(e). The nonlinear convection parameter effect on these profiles and quantities, is analysed properly for the pseudoplastic, Newtonian and dilatant fluids. This nonlinear con-

vection parameter deals with the nonlinearity in the density temperature relationship. Due to this reason, it is also termed as nonlinear density temperature parameter. In the physical sense, $\alpha_1 > 0$ refers to the relation $T_w > T_\infty$, so the surface of a truncated cone produces remarkable quantity of heat to the fluid flow region. Velocity and temperature profiles are studied in respect of η and from Fig. 3.4(a), continuous increment is noticed in the velocity profiles with increase in α_1 value for all the fluids but overall there is domination of dilatant fluid. On the other hand, pseudoplastic fluid dominates in the case of temperature profile and it decreases with increase in α_1 as displayed in Fig. 3.4(b). The non-dimensional heat transfer rate, entropy generation rate and Bejan number are analysed in respect of streamwise coordinate ξ. From Figs. 3.4(c)-3.4(e), it is found that the heat transfer and entropy generation rates increase with increasing values of α_1 but the Bejan number decreases for all the fluids. With the increasing values of streamwise coordinate, the continuous increment in heat transfer and entropy generation rates is seen but opposite is observed with the Bejan number. The Bejan number lies between 0 and 1 and approaches to zero for higher values of ξ. The higher values of Bejan number show the domination of irreversibility due to heat transfer in the case of small ξ. The Bejan number analysis is widely useful in various areas of heat transfer e.g., electronic cooling, contact melting, lubrication etc.

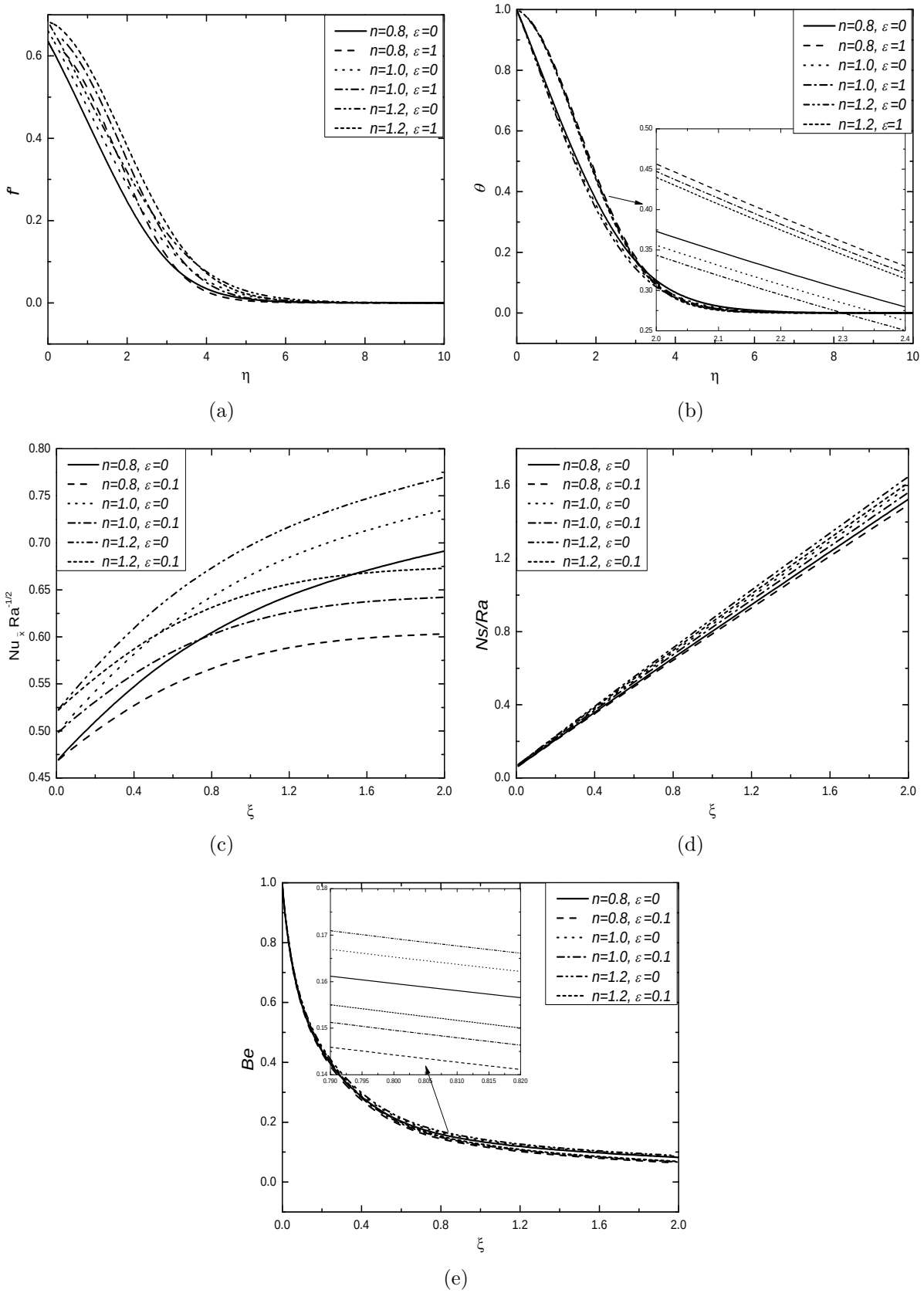

Figure 3.2: *Effect of* ϵ *on (a) velocity profiles, (b) temperature profiles, (c) Nusselt number, (d) entropy generation and (e) Bejan number with the fixed values* $Ds = 1.5$, $\alpha_1 = 0.1$, $Gr^* = 1.0$, $\xi = 1.0$ *(for (a),(b)),* $\frac{Br}{\Omega} = 1$.

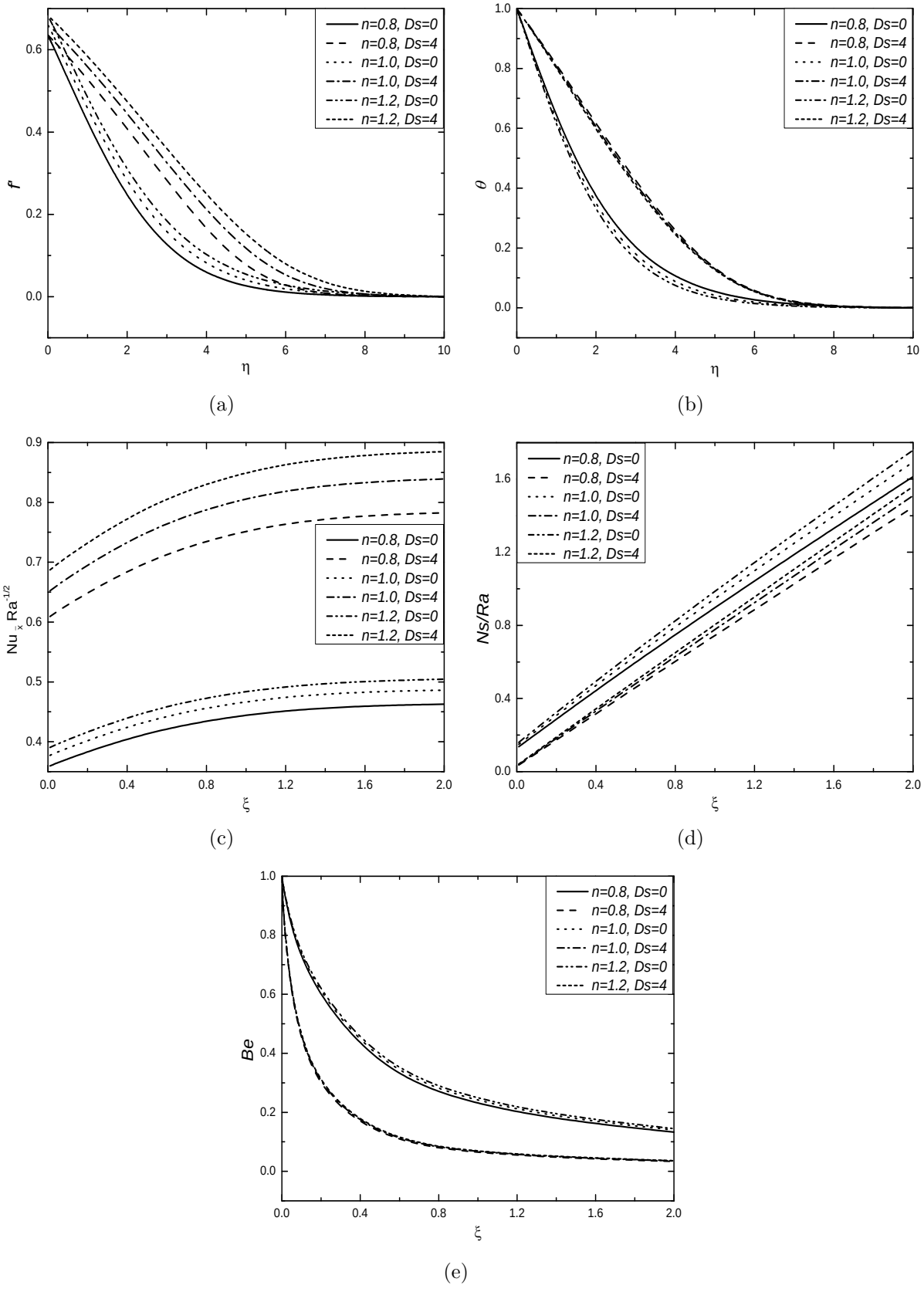

Figure 3.3: *Effect of Ds on (a) velocity profiles, (b) temperature profiles, (c) Nusselt number, (d) entropy generation and (e) Bejan number with the fixed values* $\alpha_1 = 0.1$, $Gr^* = 1.0$, $\epsilon = 0.1$, $\xi = 0.1$ *(for (a),(b)),* $\frac{Br}{\Omega} = 1$.

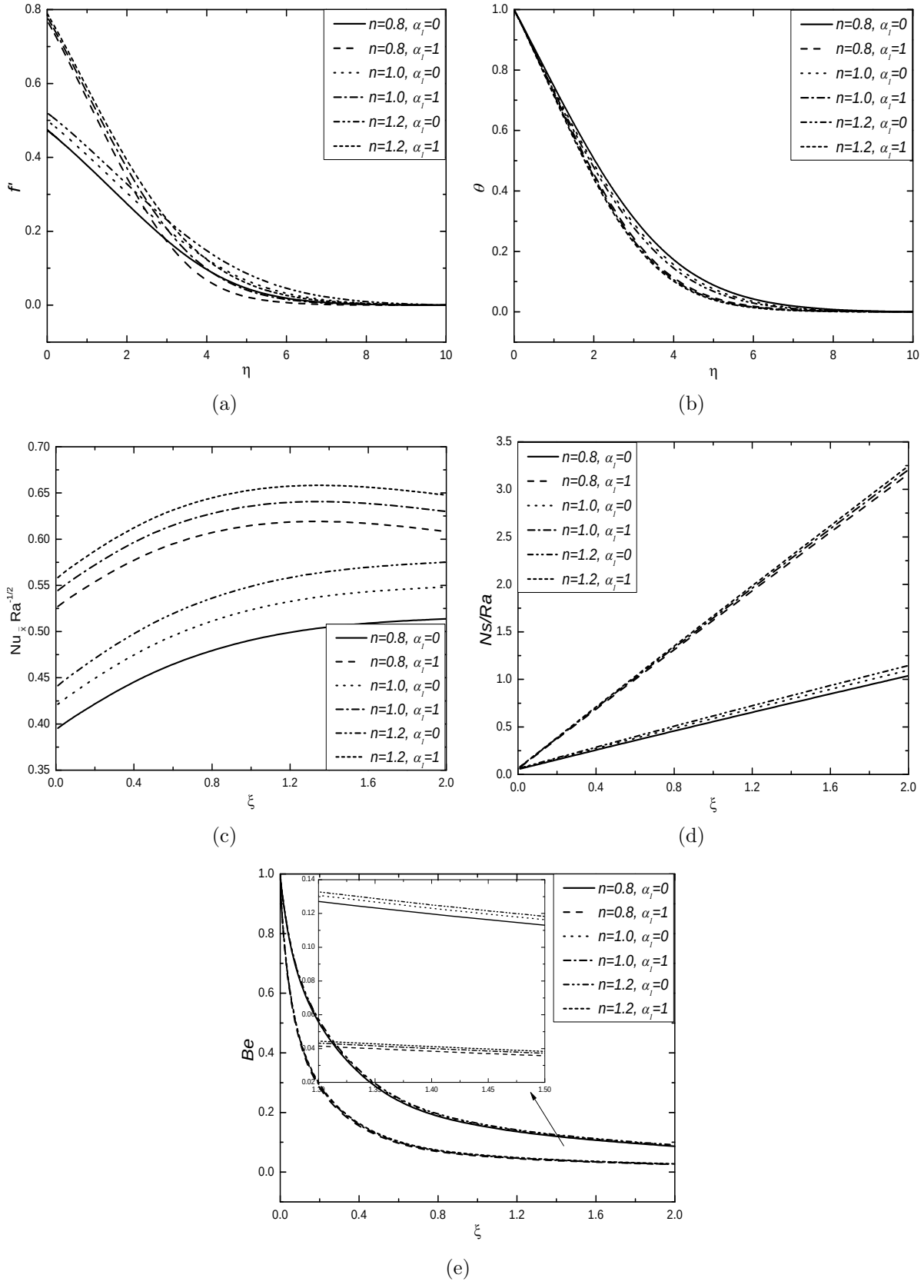

Figure 3.4: *Effect of* α_1 *on (a) velocity profiles, (b) temperature profiles, (c) Nusselt number, (d) entropy generation and (e) Bejan number with the fixed values* $Ds = 1.5$, $Gr^* = 2.0$, $\epsilon = 0.1$, $\xi = 0.2$ *(for (a),(b)),* $\frac{Br}{\Omega} = 1$.

3.2.2 Case(b): Mixed Convection

The mixed convective flow arises from both buoyancy forces and an external flow with the velocity u_∞. To get the non-dimensional form of the system of equations (3.2) - (3.3), the dimensionless transformations are given below

$$\xi = \frac{\bar{x}}{x_0}, \;\; \eta = \frac{y}{\bar{x}}\, Pe^{\frac{1}{2}}, \;\; \psi(\xi,\eta) = \alpha\, r\, Pe^{\frac{1}{2}}\, f(\xi,\eta), \;\; T(\xi,\eta) = T_\infty + (T_w - T_\infty)\, \theta(\xi,\eta), \quad (3.13)$$

where $Pe = \dfrac{u_\infty \bar{x}}{\alpha}$ is the local Peclet number.

Using these transformations (3.13) in the equations (3.2) to (3.3), the non-dimensional form of the above equations become

$$\left[n\, (f')^{n-1} + 2\, Fs\, f'\right] f'' = \lambda^n (1 + 2\,\alpha_1 \theta)\theta', \quad (3.14)$$

$$\begin{aligned}(1 + Ds\, f')\theta'' + \left[Ds\, f'' + \left(\frac{1}{2} + \frac{\xi}{\xi+1}\right) f\right] \theta' + \epsilon \xi f' \left[(f')^n + Fs\,(f')^2\right] \\ = \xi \left(\frac{\partial \theta}{\partial \xi} f' - \theta' \frac{\partial f}{\partial \xi}\right),\end{aligned} \quad (3.15)$$

subject to the transformed boundary conditions (3.4)

$$\begin{aligned}\frac{(\xi^2+\xi)}{(3\,\xi+1)} \left(\frac{\partial f}{\partial \xi}\right)_{\eta=0} + \frac{1}{2} f(\xi,0) = \; 0, \quad \theta(\xi,0) = 1, \\ f'(\xi,\eta) \to 1, \quad \theta(\xi,\eta) \to \; \epsilon(\xi+1)(1+Fs) \;\; as \;\; \eta \to \infty.\end{aligned} \quad (3.16)$$

Here, $\lambda = \dfrac{Ra}{Pe}$ is the mixed convection parameter, $Ra = \dfrac{\bar{x}}{\alpha} \left(\dfrac{\rho\, \beta_0\, g\, K^*\, cos\gamma\, (T_w - T_\infty)}{\mu}\right)^{\frac{1}{n}}$ is the local modified Darcy-Rayleigh number, $Fs = \dfrac{b\, K^*\, u_\infty^{2-n}}{\nu}$ is the non-Darcian parameter (Forchheimer number), $\epsilon = \dfrac{\nu\; u_\infty^n\; x_0}{K^*\; C_P\; (T_w - T_\infty)}$ is the viscous dissipation parameter, $\alpha_1 = \dfrac{\beta_1}{\beta_0}(T_w - T_\infty)$ is the nonlinear density-temperature parameter and $Ds = \dfrac{\chi d u_\infty}{\alpha}$ is the thermal dispersion parameter.

The non-dimensional form of Nusselt number $Nu_{\bar{x}} = -\dfrac{\bar{x}}{k}\dfrac{(k+k_d)}{(T_w - T_\infty)}\left[\dfrac{\partial T}{\partial y}\right]_{y=0}$ is given by

$$\frac{Nu_{\bar{x}}}{Pe^{\frac{1}{2}}} = -\left[1 + Ds\, f'(\xi,0)\right]\theta'(\xi,\, 0). \tag{3.17}$$

The non-dimensional form of entropy generation $Ns = \dfrac{S'''_g}{\left(S'''_g\right)_0}$ in this case, can be written as

$$\frac{Ns}{Pe} = \theta'^2 + \frac{Br}{\Omega}\xi\left[(f')^{n+1} + Fs(f')^3\right], \tag{3.18}$$

where $Br = \dfrac{\alpha\,\nu\,x_0\,u_\infty^n}{K^{*2}\,C_P\,(T_w - T_\infty)}$ is the Brinkman number and $\Omega = \dfrac{T_w - T_\infty}{T_\infty}$ is the dimensionless temperature difference.

The above equation (3.18) can be written into two parts as $Ns = N_1 + N_2$, where $N_1 = Pe\,\theta'^2$ and $N_2 = \dfrac{Br\,Pe}{\Omega}\xi\left[(f')^{n+1} + Fs(f')^3\right]$. The first part denotes entropy generation on account of heat transfer besides second part is responsible for the entropy generation because of fluid friction. In this case, the expression for Bejan number (Be) can be given as

$$Be = \frac{N_1}{N_s} = \frac{\theta'^2}{\theta'^2 + \dfrac{Br}{\Omega}\xi\left[(f')^{n+1} + Fs(f')^3\right]} \in [0,1]. \tag{3.19}$$

Results and Discussion

The governing equations (3.14)-(3.15) along with the boundary conditions (3.16) are solved numerically using spectral local linearization method (SLLM) together with the non-similarity approach. Validation of the present problem can be done on comparison as it was done in the case (b) of *Chapter-2* by putting $\xi = 0$, $Fs = 0$, $Ds = 0$, $\epsilon = 0$ and $\alpha_1 = 0$.

Figs. 3.5(a)-3.5(e) depict the ϵ influence on velocity, temperature, Nusselt number, entropy generation rate and Bejan number for aiding and opposing flows over a vertical truncated cone. In the first two graphs, study is done with respect to η and in the later three with respect to λ. The other physical parameters are fixed with certain relevant values and ϵ is varied. From Fig. 3.5(a), it is observed that the presence of ϵ lowers velocity profiles for

both the fluids and velocity is more for the aiding flow case in comparison with the opposing flow case due to the presence of favourable pressure gradient for the aiding flow. In Fig. 3.5(b), the viscous dissipation parameter impact on temperature profiles is shown and found to be same in both the flow cases. The presence of ϵ makes temperature of system stable to a non-zero value for both the fluids because the viscous dissipation behaves like an originator generating notable increase in the temperature of fluid as fluid's active shifting results into thermal energy. It has importance in the flow in microchannels having larger ratio of length to diameter. The variation in Nusselt number with respect to λ for different values of ϵ is shown in Fig. 3.5(c). Less variation is noticed in the opposing flow case when compared to the aiding flow and the pseudoplastic fluid constantly dominates over the dilatant fluid. It is seen from Fig. 3.5(d) that due to increment in ϵ, the entropy generation is decreased for both the fluids and influence is more for the aiding flow case. This entropy generation minimization is very much useful in thermal engineering and design variable selection in many efficient fluid systems. The study of Bejan number in respect of λ for both the fluids with different values of ϵ is shown in Fig. 3.5(e). This study shows that maximum value of Bejan number is obtained for $\lambda = 0$ (i.e., in the case of forced convection) and its effect is less in the case of aiding and opposing flows for every combination considered, and with increment in the viscous dissipation parameter, it is decreased effectively. It is observed that Bejan number is higher for the dilatant fluids. The small Bejan numbers specify domination of irreversibility due to fluid friction. The heat transfer is found to be less for higher values of the viscous dissipation parameter.

Figs. 3.6(a)-3.6(e) display the velocity and temperature profiles, Nusselt number, entropy generation and Bejan number for aiding and opposing flows with varying values of the thermal dispersion parameter Ds. The first two graphs show the variation in respect of η and the later three show in respect of λ. The other physical parameters are fixed with certain relevant values. The importance of combined changes in temperature and velocity to the heat transportation is shown by Ds parameter. From Fig. 3.6(a), it is observed that the presence of Ds enhances velocity profiles for both the fluids and the velocity is more for the aiding flow case as in previous effect. Fig. 3.6(b) shows the influence of thermal dispersion

on temperature profiles and found to be same in both the flow cases. The presence of Ds increases temperature profiles by the same amount irrespective of the nature of fluid and its flow. Fig. 3.6(c) displays the variation in Nusselt number and slight variation is noticed in both the aiding and opposing flows. But, the dilatant fluid dominates over the pseudoplastic fluid in aiding flow case, whereas the pseudoplastic fluid dominates in opposing flow case. The higher Nusselt number is observed with higher values of the thermal dispersion parameter. It is worth mentioning that entropy generation is much more for the aiding flow when compared with the opposing flow case which is evidently shown in Fig. 3.6(d). The Bejan number study in respect of λ, in Fig. 3.6(e), shows that the larger values are found for the dilatant fluids when compared to the pseudoplastic fluid for both the flow cases ($\lambda \neq 0$) and highest Bejan number is found for $\lambda = 0$.

Figs. 3.7(a)-3.7(e) depict the impact of α_1 on non-dimensional velocity and temperature profiles, Nusselt number, entropy generation and Bejan number for the aiding and opposing flows. The other physical parameters are fixed with certain relevant values and α_1 is varied. From Fig. 3.7(a), it is noted that the presence of α_1 makes huge impact on the velocity profiles and large increment is found in its presence for the aiding flow case. The Fig. 3.7(b) shows that α_1 slightly influences the temperature profiles. In its presence, the temperature is more for both the fluids in aiding and opposing flows. From Fig. 3.7(c), a completely different behaviour is noticed in the variation of Nusselt number for opposing and aiding flows. Lesser Nusselt number is observed in the aiding flow case when compared to the opposing flow case. It is seen from Fig. 3.7(d) that due to increment in α_1, the entropy generation is increased and the influence is more for the aiding flow and reverse nature is noticed in the opposing flow for both the fluids. In Fig. 3.7(e), the effect of α_1 on Bejan number is shown for both the fluids and it decreases in the presence of α_1 and higher Bejan number is noticed for the dilatant fluids when compared to the pseudoplastic fluids. The influence is similar for both the aiding and opposing flows but its range is wide for negative λs and maximum Bejan number is noticed for $\lambda = 0$.

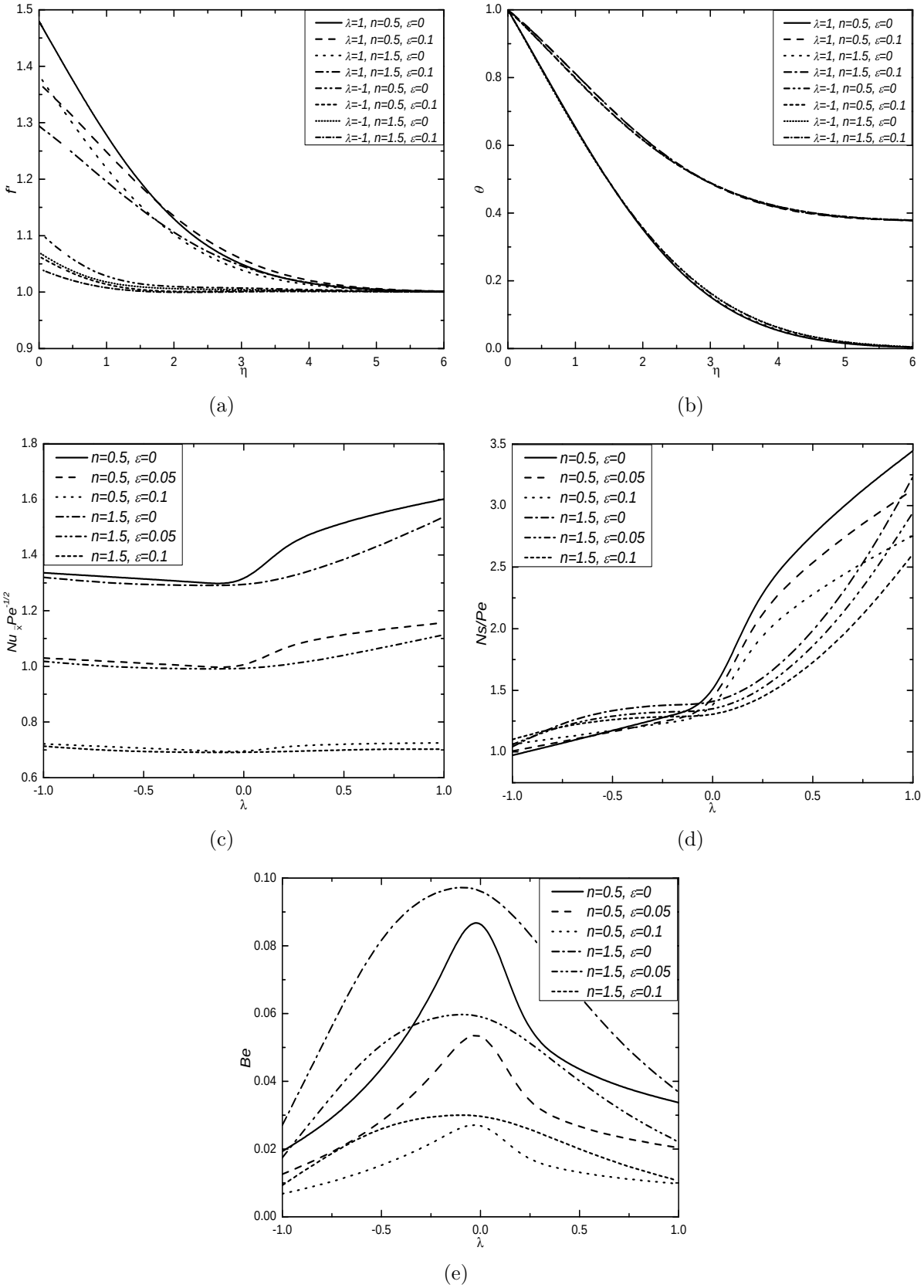

Figure 3.5: *Effect of ϵ on (a) velocity profiles, (b) temperature profiles, (c) Nusselt number, (d) entropy generation and (e) Bejan number with the fixed values $Ds = 2.5$, $\alpha_1 = 1.0$, $Fs = 1.5$, $\xi = 0.5$ and $\frac{Br}{\Omega} = 1$.*

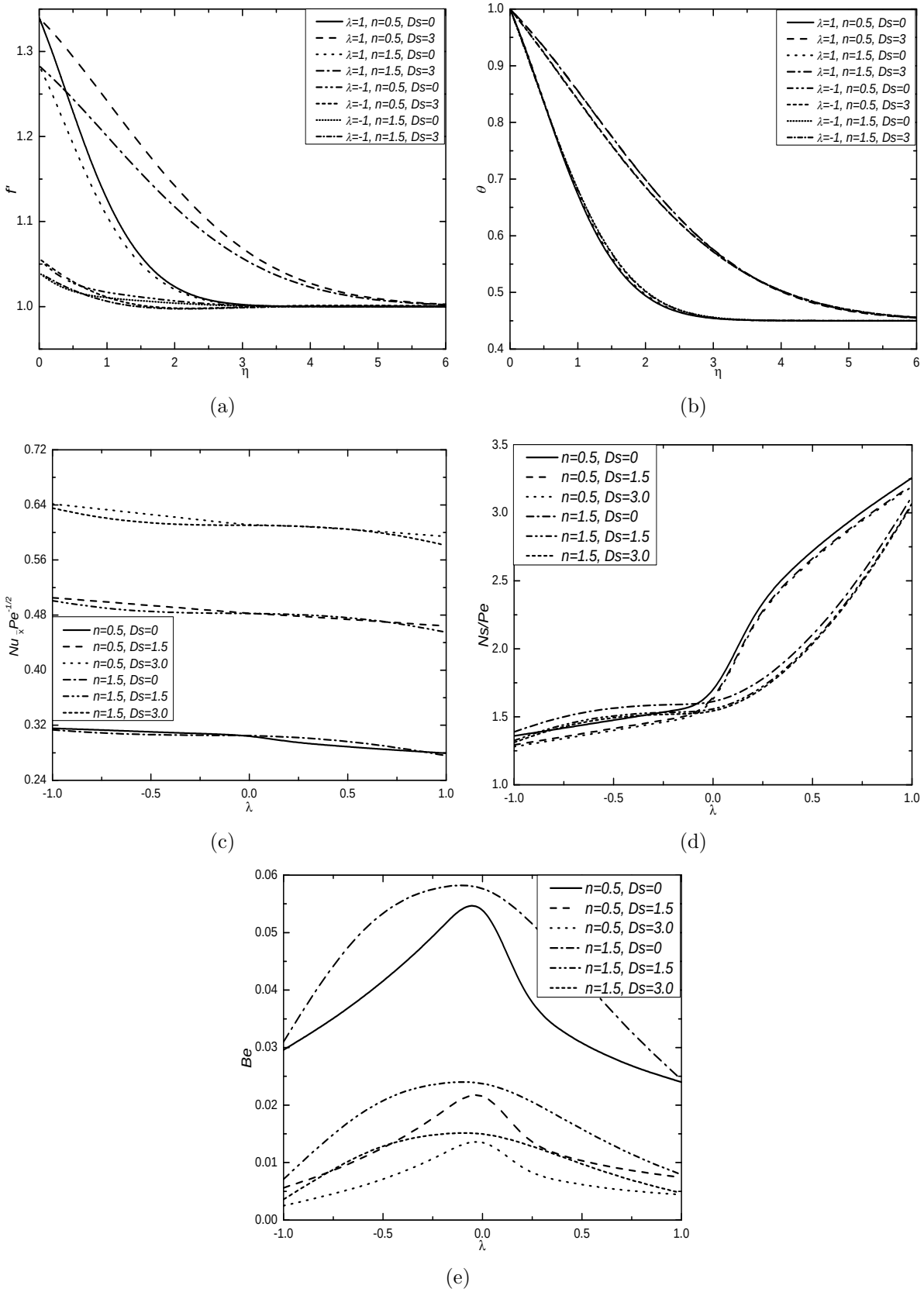

Figure 3.6: *Effect of Ds on (a) velocity profiles, (b) temperature profiles, (c) Nusselt number, (d) entropy generation and (e) Bejan number with the fixed values* $\epsilon = 0.1$, $\alpha_1 = 1.5$, $Fs = 2.0$, $\xi = 0.5$ *and* $\frac{Br}{\Omega} = 1$.

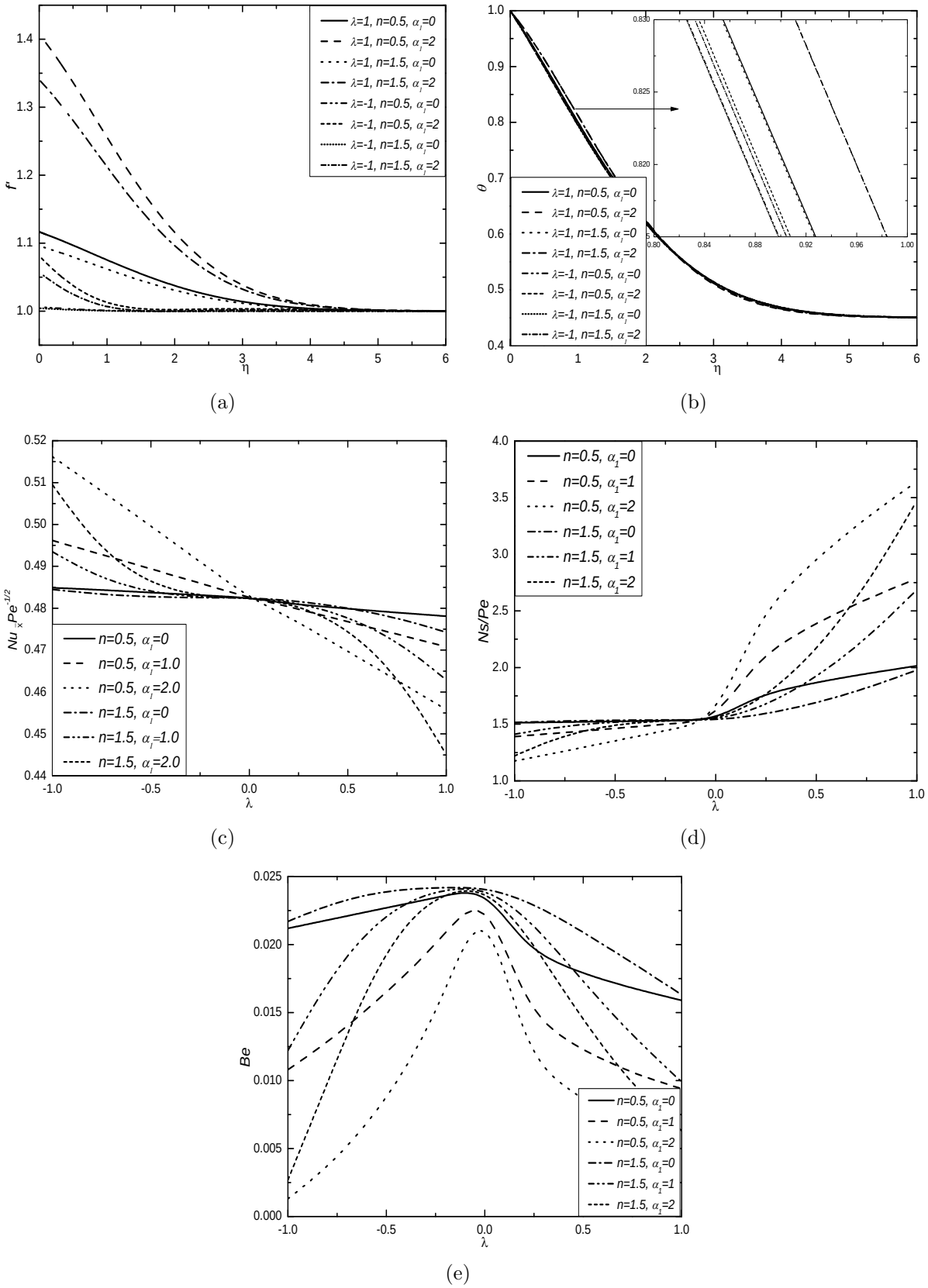

Figure 3.7: *Effect of* α_1 *on (a) velocity profiles, (b) temperature profiles, (c) Nusselt number, (d) entropy generation and (e) Bejan number with the fixed values* $\epsilon = 0.1$, $Ds = 1.5$, $Fs = 2.0$, $\xi = 0.5$ *and* $\frac{Br}{\Omega} = 1$.

3.3 Conclusions

In this chapter, the effect of viscous dissipation, thermal dispersion and nonlinear density-temperature parameters on the velocity and temperature profiles, heat transfer and entropy generation rates along with Bejan number for the power-law fluid flows over a truncated cone in a non-Darcy porous medium, is discussed in detail for the two cases: (a) natural convection and (b) mixed convection. The conclusive remarks of this work in both the cases (a) and (b) for physically suitable values of flow governing parameters, are:

Case (a): Natural Convection

- The higher values of viscous dissipation, thermal dispersion and non-linear convection parameters increase the velocity, and the dilatant fluid dominates over the Newtonian and pseudoplastic fluids.
- The temperature profiles are increased in the presence of viscous dissipation and thermal dispersion parameters and decreased with the higher values of non-linear convection parameter for all the fluids.
- The entropy generation and heat transfer rates increase with the streamwise coordinate (ξ) for all the fluids irrespective of presence and absence of all these parameters which shows that the heat transfer and entropy generation rates for a truncated cone are less than that for a full cone (higher values of ξ) and more than that for a vertical plate (ξ=0).
- The smaller values of Bejan number for higher values of ξ show the domination of irreversibility due to fluid friction in the case of a full cone.

Case (b): Mixed Convection

- The presence of viscous dissipation lowers velocity but the presence of thermal dispersion and non-linear convection increases velocity with considerable amount.

- Temperature profiles are enhanced in the existence of thermal dispersion and viscous dissipation, and very less impact of the non-linear convection is found on these profiles.
- Study of Bejan number and entropy generation gives idea about the stability of the system. Greater entropy generation results into a unstable system.
- This kind of work is very helpful in various technological fields which carry relation with the temperature dependent density as high temperature polymeric mixtures and aerosol technology.

Chapter 4

Numerical Estimations in a Non-Darcy Porous Medium Saturated by Power-law Fluids with Thermal Radiation: A Complete Case Study [1]

4.1 Introduction

The well-established importance of thermal radiation in solar exploration missions, space sectors and polymer processing industries make its analysis more significant. Its impact is also found to have more importance for the analysis of heat transfer in furnaces, combustion chambers, nuclear blast sites etc. Further, the impact of thermal radiation is more valuable when the difference between temperature of the surface and its ambient medium is huge in any flow problem. Apart from these, the literature shows that the distribution of temperature in thermal boundary layer flows is remarkably influenced by the thermal radiation at high temperatures.

[1] Case(a): Communicated to "**International Communications in Heat and Mass Transfer**", Case(b): Communicated to "**International Journal of Thermal Sciences**".

In view of all these applications, a good number of works on various flow studies related to either linear, quadratic or nonlinear radiation are performed in recent years. A boundary layer study related to the nonlinear thermal radiation on the fluid flow past a vertical wedge is done by Mansour and Gorla [70]. Grosan and Pop [41] studied the radiation effect using the Rosseland model for its simplification. A numerical investigation of non-Newtonian power-law fluid flows with the mass transfer and linear thermal radiation, is conducted by Tai and Char [122]. Mahapatra *et al.* [69] analysed a two-dimensional stagnation point flow of a power-law fluid in the presence of linear thermal radiation. Huang [49] obtained the non-similar solutions for non-Newtonian fluid flows past a permeable vertical plate with Rosseland diffusion approximation on thermal radiation. Impact of opposing and aiding flows on the mixed convection heat transfer, by incorporating the same approximation on radiation term, is examined by Manzur *et al.* [71]. Oyelakin *et al.* [91] studied about a non-Darcian mixed convective flow of a non-Newtonian power-law fluid by considering the nonlinear radiation and then demonstrated the applicability of a spectral method. Ahmad and Nadeem [1] performed thermal analysis numerically in a buoyancy driven flow in the presence of nonlinear radiation. Vasu *et al.* [125, 126] numerically investigated MHD natural convection-radiation interaction in a non-Darcy porous medium along with Soret/Dufour effects. But, very limited literature is available on the quadratic thermal radiation and its effect on boundary layer flows over a vertical plane surface is given by Mahanthesh *et al.* [68] (for more literature, refer the citations therein).

From the literature, it appears that the effect of thermal radiation on convective flow over a truncated cone immersed in a non-Darcy porous medium saturated by of power-law fluids, has not been investigated so far. To fulfil the above said gap and in view of its useful industrial and engineering applications, a novel aspect is attempted to analysis of power-law fluid flows over a truncated cone by inserting linear, quadratic and nonlinear thermal radiation effects one by one. Also, the details of various types of approximations on the thermal radiation are also provided.

4.2 Mathematical Analysis

The effect of thermal radiation on free and mixed convective flows of power-law fluids over a truncated cone immersed in a Forchheimer type of non-Darcy porous medium, is considered in this chapter. It deals with the linear, quadratic and nonlinear thermal radiation effects. The physical model with coordinate system is displayed in Fig. 4.1. The leading edge of the truncated cone is kept at a distance x_0 from the origin O, where x and y axes are taken along and normal to the surface of the truncated cone, respectively. The ambient medium and wall temperatures are taken as T_∞ and T_w respectively together with the modified streamwise coordinate $\bar{x}$, which is defined as $\bar{x} = x - x_0$ for the truncated cone.

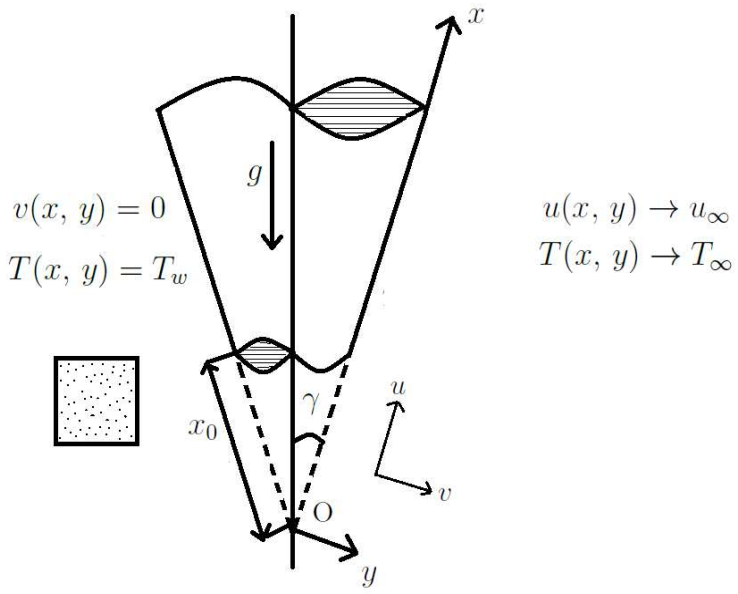

Figure 4.1: *Physical model and coordinate system.*

Taking the boundary layer hypothesis into the consideration along with the general and basic approximations and assumptions related to truncated cone as mentioned in *Chapter-2*, the governing equations for the fluid flow over a truncated cone can be written in the

following form

$$\frac{\partial(ru)}{\partial x} + \frac{\partial(rv)}{\partial y} = 0, \tag{4.1}$$

$$\frac{\partial u^n}{\partial y} + \frac{b\,K^*}{\nu}\frac{\partial u^2}{\partial y} = \frac{g\,\beta\,K^*\cos\gamma}{\nu}\frac{\partial T}{\partial y}, \tag{4.2}$$

$$u\frac{\partial T}{\partial x} + v\frac{\partial T}{\partial y} = \alpha\,\frac{\partial^2 T}{\partial y^2} + \frac{4\,\sigma}{3\,\rho\,C_P\,\bar{k}}\frac{\partial^2 T^4}{\partial y^2}, \tag{4.3}$$

along with the boundary conditions

$$\begin{aligned} v(x,\,y) = 0, \qquad & T(x,\,y) = T_w \qquad && \text{at} \qquad y = 0, \\ u(x,\,y) \to u_\infty, \qquad & T(x,\,y) \to T_\infty \qquad && \text{as} \qquad y \to \infty. \end{aligned} \tag{4.4}$$

where n is the power-law index ($n > 1$, $n = 1$ and $n < 1$ denote the dilatant, Newtonian and pseudoplastic nature), ρ is the density, ν is the kinematic viscosity, $\bar{k}$ is the mean absorption coefficient, β is the coefficient of thermal expansion, σ is the Stefan-Boltzmann constant, α is the thermal diffusivity constant and C_P is the specific heat capacity. Also, γ is the angle inclination, b is the empirical constant, g is the gravitational acceleration, T is the temperature and (u, v) are the Darcian velocities in x and y direction respectively. K^* indicates the improved permeability of a porous medium, which is a function of n.

Two types (cases) of problems with (a) free/natural convection and (b) mixed convection are considered in this chapter too, as specified in previous chapters.

4.2.1 Case(a): Natural Convection

The flow is assumed to be a natural convective flow which is caused by only buoyancy forces and without any external agent which implies zero velocity for the external flow ($i.e., u_\infty = 0$). The non-dimensional relations utilized to get the non-dimensional form of equations (4.2)-(4.4) are

$$\xi = \frac{\bar{x}}{x_0}, \;\; \eta = \frac{y}{\bar{x}}\,Ra^{\frac{1}{2}}, \;\; \theta(\xi,\eta) = \frac{T(\xi,\eta) - T_\infty}{(T_w - T_\infty)}, \;\; \psi(\xi,\eta) = \alpha\,r\,Ra^{\frac{1}{2}}\,f(\xi,\eta), \tag{4.5}$$

where $Ra = \dfrac{\bar{x}}{\alpha}\left(\dfrac{\beta\, g\, K^*\, cos\,\gamma\,(T_w - T_\infty)}{\nu}\right)^{\frac{1}{n}}$ is the local modified Darcy-Rayleigh number.

In order to simplify the radiation term, the Taylor series expansion of T about T_∞ yields

$$T^4 \;=\; {T_\infty}^4 \;+\; 4\,{T_\infty}^3\,(T - T_\infty) \;+\; 6\,{T_\infty}^2\,(T - T_\infty)^2 \;+ ..., \tag{4.6}$$

and its truncation up to first and second order gives equations (4.7) and (4.8) respectively.

$$T^4 \;=\; 4\,{T_\infty}^3\,T \;-\; 3\,{T_\infty}^4, \tag{4.7}$$

$$T^4 \;=\; 6\,{T_\infty}^2\,T^2 \;-\; 8\,{T_\infty}^3\,T \;+\; 3\,{T_\infty}^4, \tag{4.8}$$

Using the transformations (4.5) and the Taylor series expansions (4.6)-(4.8) in the equations (4.2) to (4.3), the non-dimensional form of the above equations becomes

$$\left[n\;(f')^{n-1} \;+ 2\,Gr^*\,f'\right] f'' - \theta' = 0, \tag{4.9}$$

Case (a): Linear Approximation (using equation (4.7))

$$\theta'' + \left(\frac{1}{2} \;+ \frac{\xi}{\xi + 1}\right) f\theta' \;+ \frac{4}{3}\,R_1\,\theta'' = \xi\left(f'\frac{\partial\theta}{\partial\xi} - \frac{\partial f}{\partial\xi}\theta'\right), \tag{4.10}$$

Case (b): Quadratic Approximation (using equation (4.8))

$$\theta'' + \left(\frac{1}{2} \;+ \frac{\xi}{\xi + 1}\right) f\theta' \;+ \frac{4}{3}\,R_2\,\left[\,\theta'' +\; 3\,(\theta_w - 1)\,\theta\,\theta'' \;+\; 3\,(\theta_w - 1)\,\theta'^2\right] = \xi\left(f'\frac{\partial\theta}{\partial\xi} - \frac{\partial f}{\partial\xi}\theta'\right), \tag{4.11}$$

Case (c): Nonlinear Approximation (using equation (4.5))

$$\theta'' + \left(\frac{1}{2} \;+ \frac{\xi}{\xi + 1}\right) f\theta' \;+ \frac{4}{3}\,R_3\,\left[3\,(\theta_w - 1)\,\{1 + (\theta_w - 1)\theta\}^2\,\theta'^2 \;+ \{1 + (\theta_w - 1)\theta\}^3\;\theta''\,\right] = \xi\left(f'\frac{\partial\theta}{\partial\xi} - \frac{\partial f}{\partial\xi}\theta'\right), \tag{4.12}$$

together with the transformed boundary conditions

$$f(\xi,0)+\frac{2\,\xi\,(\xi+1)}{3\,\xi+1}\left[\frac{\partial f}{\partial \xi}\right]_{\eta=0}=\ 0,\ \theta(\xi,0)=1,\ f'(\xi,\eta)\to 0,\ \theta(\xi,\eta)\to\ 0\ \text{ when }\ \eta\to\infty. \tag{4.13}$$

Here, the prime symbol represents differentiation in respect of η and the modified Grashof number is represented by $Gr^{*}=\dfrac{b\,K^{*}}{\nu}\left(\dfrac{\alpha}{\bar{x}}Ra\right)^{2-n}$. The linear, quadratic and nonlinear radiation parameters are denoted by R_1, R_2 and R_3 respectively and each parameter carry the value $\dfrac{4\,\sigma\,T_{\infty}^{3}}{k\,\bar{k}}$. The parameter $\theta_w=\dfrac{T_w}{T_\infty}$ represents the temperature ratio. With distinct values of ξ, the analysis for two geometries [viz., the vertical plate and full cone] can also be performed.

Non-dimensional form of the skin friction coefficient $C_f=\dfrac{2}{\rho\,u_{*}^{2}}\left[\mu\dfrac{\partial u}{\partial y}\right]_{y=0}$ is given by

$$\frac{1}{2}\frac{Ra^{\frac{1}{2}}}{Pr}C_f=f''(\xi,0), \tag{4.14}$$

where u_* and Pr are used to denote the characteristic velocity and the Prandtl number respectively

The heat transfer rates in terms of Nusselt number $Nu_{\bar{x}}=\dfrac{\bar{x}}{k\,(T_w-T_\infty)}\left[-k\dfrac{\partial T}{\partial y}-\dfrac{4\sigma}{3\bar{k}}\dfrac{\partial T^4}{\partial y}\right]_{y=0}$ for linear, quadratic and nonlinear cases of thermal radiation can be written as

$$\frac{Nu_{\bar{x}}}{Ra^{\frac{1}{2}}}=-\left[1+\frac{4}{3}R_1\right]\theta'(\xi,0), \tag{4.15}$$

$$\frac{Nu_{\bar{x}}}{Ra^{\frac{1}{2}}}=-\left[1+\frac{4}{3}R_2\,(1+3(\theta_w-1))\,\theta(\xi,0)\right]\theta'(\xi,0), \tag{4.16}$$

$$\frac{Nu_{\bar{x}}}{Ra^{\frac{1}{2}}}=-\left[1+\frac{4}{3}R_3\{(1+(\theta_w-1))\,\theta(\xi,0)\}^{3}\right]\theta'(\xi,0). \tag{4.17}$$

Results and Discussion

In this chapter also, the governing equations (4.9)-(4.12) along with the boundary conditions (4.13) are solved numerically using spectral local linearization method (SLLM) together with the non-similarity approach. Validation of the present problem can be done on comparison as it was done in the case (a) of *Chapter-2* in the absence of thermal radiation with $\xi = 0$.

Fig. 4.2 presents the velocity and temperature profiles along with Nusselt number and skin friction coefficient for different values of the linear radiation parameter R_1 when $Gr^* = 0.5$ and $\xi = 5.0$. It is observed from Fig. 4.2(a) that the non-dimensional velocity increases with enhancing values of R_1. It is significant to point out that the velocity for dilatant fluid dominates in comparison with the pseudoplastic fluid. The influence of R_1 is similar on both these fluids. The physical reason behind this increment in the velocity with R_1 enhancement is the weakening of bonds which hold the fluid particle components. As the thermal radiation R_1 increases, these bond split with more ease. This phenomenon is applicable in faster cooling process by reducing thermal radiation. Fig. 4.2(b) displays the temperature distribution with increasing values of R_1 for pseudoplastic and dilatant fluids. The dominance of pseudoplastic fluid is noticed when compared to that of the dilatant fluid for the temperature profiles. Increment is observed in the temperature with greater values of R_1. The enhanced values of radiation parameter make the boundary layer more thick and better thermal performance can be observed. The Nusselt number and skin friction coefficient are plotted with respect to streamwise coordinate (ξ) for pseudoplastic and dilatant fluids. As expected, Fig. 4.2(c) confirms the increment in the non-dimensional heat transfer rate or Nusselt number with increase in the R_1 values. The dominance of dilatant fluid over pseudoplastic fluid is observed for Nusselt number case. Fig. 4.2(d) shows that the magnitude of skin friction coefficient decreases with enhancing values of the linear radiation parameter. One more important point can be seen from Figs. 4.2(c) and 4.2(d) that the Nusselt number and skin friction coefficient become almost constant for higher values of ξ.

Figs. 4.3 and 4.4 portray the velocity and temperature profiles, Nusselt number and skin friction coefficient for different values of quadratic and nonlinear radiation parameters when

$Gr^* = 0.5$, $\theta_w = 0.1$ (quadratic), $\theta_w = 0.001$ (nonlinear) and $\xi = 5.0$. Figs. 4.3(a) and 4.4(a) display the non-dimensional velocity profiles with variation in the quadratic radiation parameter (R_2) and nonlinear radiation parameter (R_3). Similar to linear case, the velocity for dilatant fluid dominates in comparison with the pseudoplastic fluid. With increasing values of R_2 and R_3, there is enhancement in the velocity profiles. The temperature variation in the case of quadratic and nonlinear radiations are given in Figs. 4.3(b) and 4.4(b). These figures include both the pseudoplastic and dilatant fluids and the dominance of pseudoplastic fluid is again noticed as in the case of linear radiation. With increasing values of radiation parameters, the temperature profiles are enhanced. The increment in the Nusselt number with enhancing values R_2 and R_3 is again confirmed with the domination of dilatant fluid over the pseudoplastic fluid from the Figs. 4.3(c) and 4.4(c). It is assured from the fact that the enhancement in the thermal radiation parameter implies decay in mean absorption coefficient and hence enhances the radiative heat flux divergence. Therefore, the heat transfer rate increases and so the temperature of the fluid. Figs. 4.3(d) and 4.4(d) depict the skin friction coefficient variation with respect to the streamwise coordinate (ξ) for pseudoplastic and dilatant fluids. From Fig. 4.3(d), a decrement in the absolute value of skin friction is noticed for increase in R_2 and similar behaviour is also found in the Fig. 4.4(d).

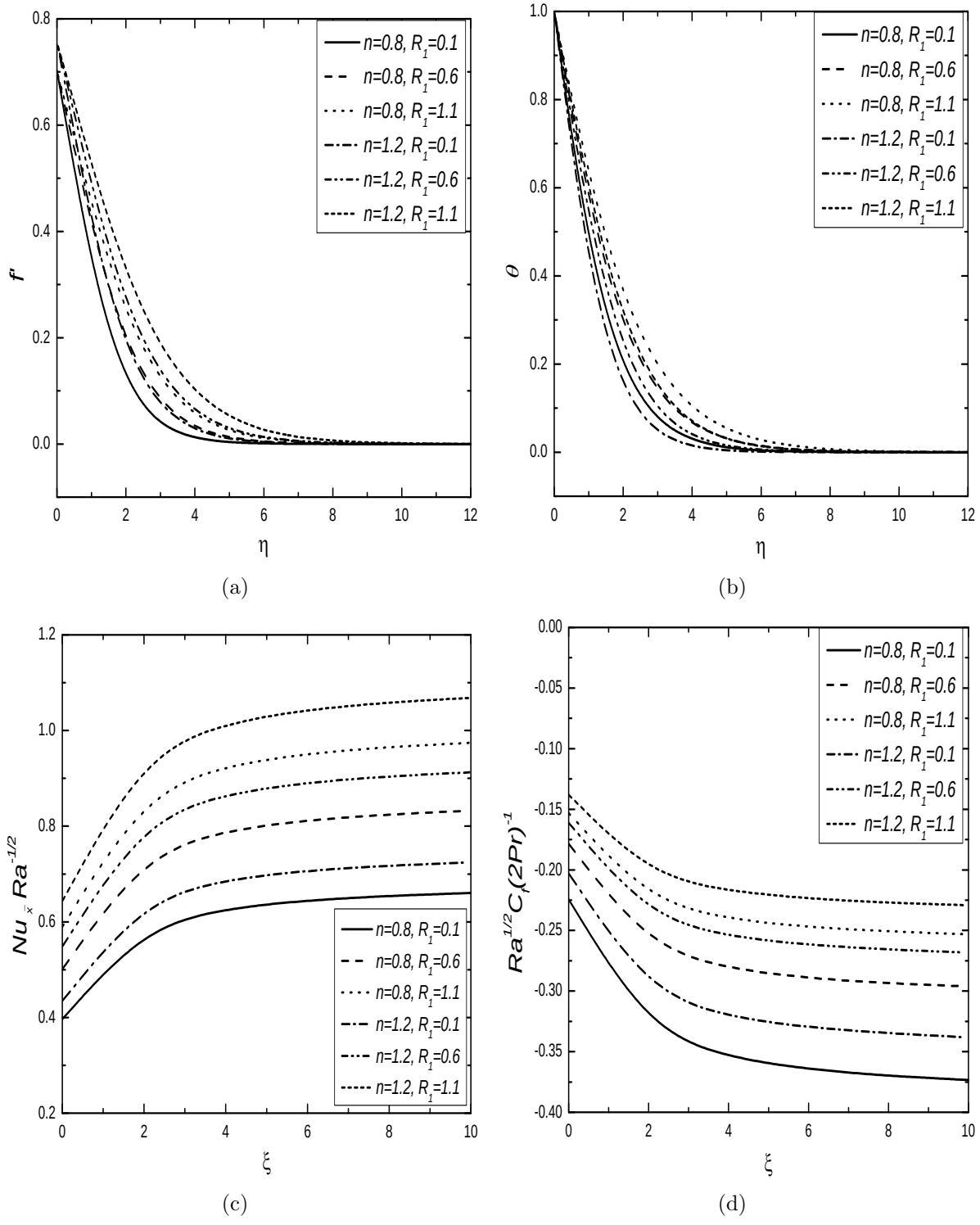

Figure 4.2: *Effect of linear radiation parameter (R_1) on (a) velocities, (b) temperatures, (c) Nusselt number and (d) skin friction coefficient.*

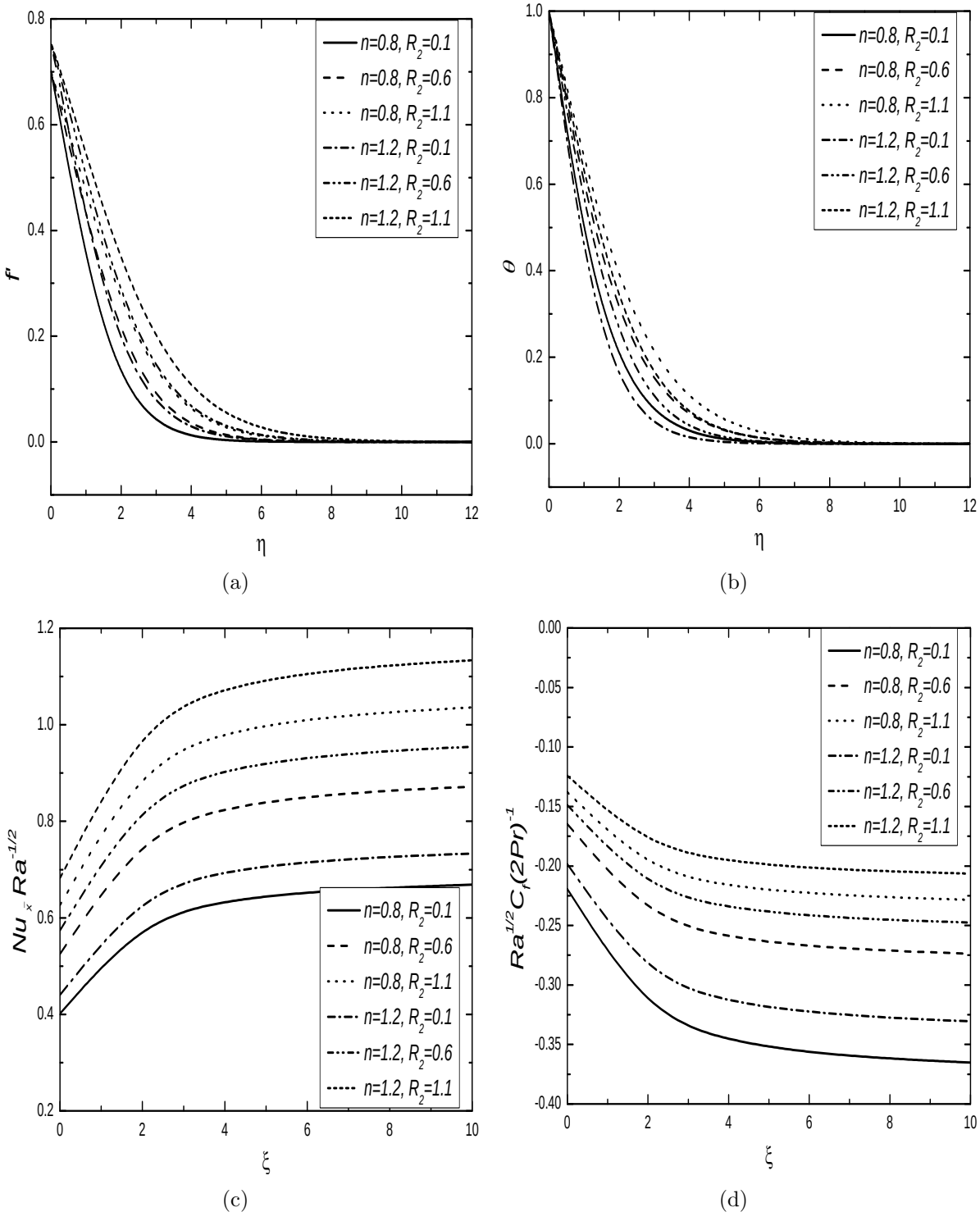

Figure 4.3: *Effect of quadratic radiation parameter (R_2) on (a) velocities, (b) temperatures, (c) Nusselt number and (d) skin friction coefficient.*

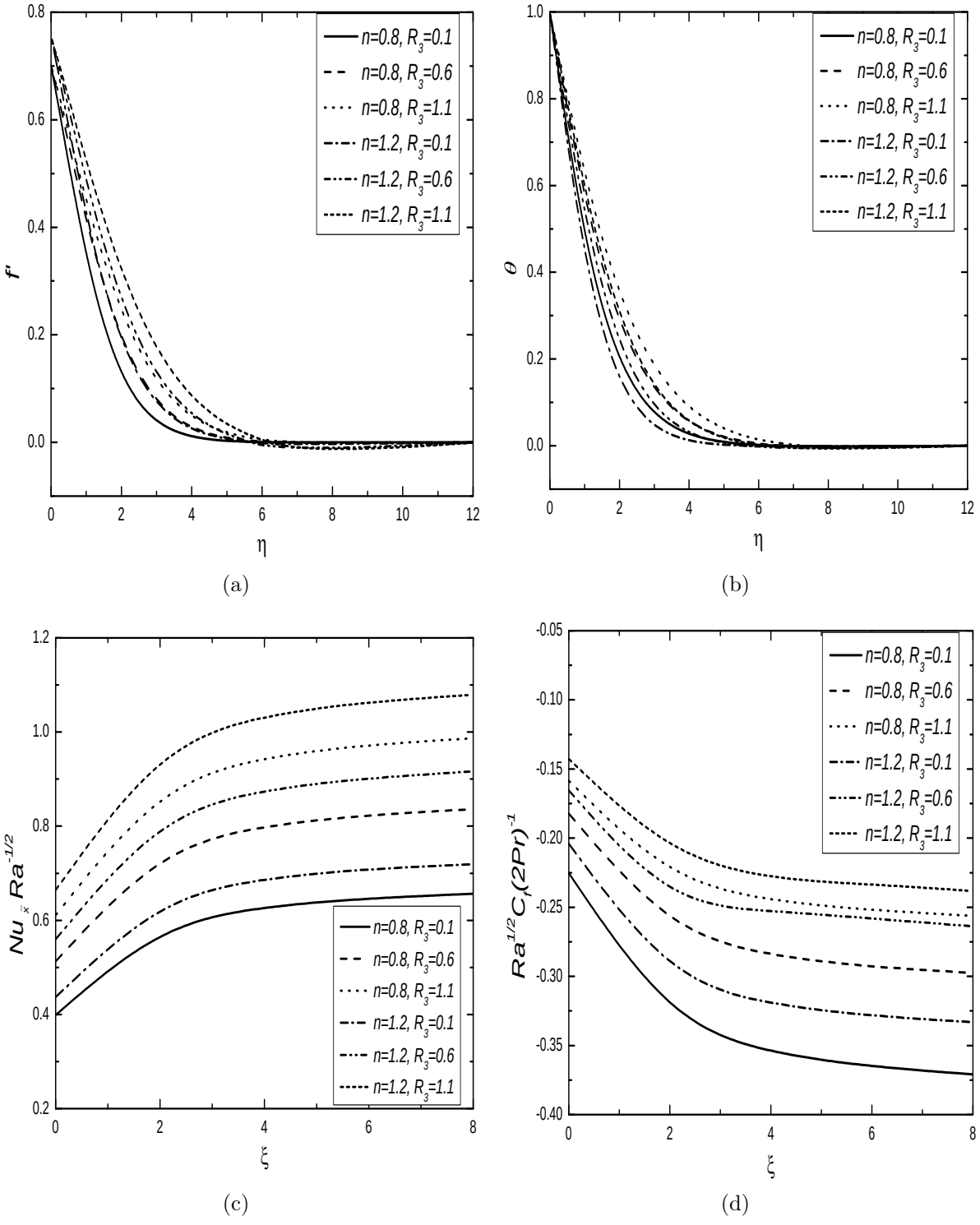

Figure 4.4: *Effect of nonlinear radiation parameter (R_3) on (a) velocities, (b) temperatures, (c) Nusselt number and (d) skin friction coefficient.*

4.2.2 Case(b): Mixed Convection

The flow is assumed to be a mixed convective flow, which arises from both buoyancy forces and an external flow with the velocity u_∞. To get the non-dimensional form of the system of equations (4.2) - (4.3), the dimensionless transformations are given below

$$\xi = \frac{\bar{x}}{x_0}, \;\; \eta = \frac{y}{\bar{x}}\, Pe^{\frac{1}{2}}, \;\; \theta(\xi,\eta) = \frac{T(\xi,\eta) - T_\infty}{(T_w - T_\infty)}, \;\; \psi(\xi,\eta) = \alpha\, r\, Pe^{\frac{1}{2}}\, f(\xi,\eta), \tag{4.18}$$

where $Pe = \dfrac{u_\infty \bar{x}}{\alpha}$ is the local Peclet number.

Using the transformations (4.18) and the Taylor series expansions (4.6)-(4.8) in the equations (4.2) to (4.3), the non-dimensional form of the above equations become

$$\left[n\, (f')^{n-1} + 2\, Fs\, f'\right] f'' - \lambda^n\, \theta' = 0, \tag{4.19}$$

Case (a): Linear Approximation (using equation (4.7))

$$\theta'' + \left(\frac{1}{2} + \frac{\xi}{\xi+1}\right) f\theta' + \frac{4}{3}\, R_1\, \theta'' = \xi \left(f' \frac{\partial \theta}{\partial \xi} - \frac{\partial f}{\partial \xi}\theta'\right), \tag{4.20}$$

Case (b): Quadratic Approximation (using equation (4.8))

$$\theta'' + \left(\frac{1}{2} + \frac{\xi}{\xi+1}\right) f\theta' + \frac{4}{3}\, R_2 \left[\theta'' + 3\,(\theta_w - 1)\,\theta\,\theta'' + 3\,(\theta_w - 1)\,\theta'^2\right] = \xi \left(f' \frac{\partial \theta}{\partial \xi} - \frac{\partial f}{\partial \xi}\theta'\right), \tag{4.21}$$

Case (c): Nonlinear Approximation (using equation (4.18))

$$\theta'' + \left(\frac{1}{2} + \frac{\xi}{\xi+1}\right) f\theta' + \frac{4}{3}\, R_3 \left[\{1 + (\theta_w - 1)\theta\}^3\, \theta'' + 3\,(\theta_w - 1)\,\{1 + (\theta_w - 1)\theta\}^2\, \theta'^2\right] = \xi \left(f' \frac{\partial \theta}{\partial \xi} - \frac{\partial f}{\partial \xi}\theta'\right). \tag{4.22}$$

The boundary conditions (4.4) in their transformed form can be written as

$$f(\xi,0)+\frac{2\,\xi\,(\xi+1)}{3\,\xi+1}\left[\frac{\partial f}{\partial \xi}\right]_{\eta=0}=\ 0,\ f'(\xi,\eta)\to 1,\ \theta(\xi,0)=1,\ \theta(\xi,\eta)\to\ 0\ \text{ when }\ \eta\to\infty. \tag{4.23}$$

Here, $Fs=\dfrac{b\,K^*\,u_\infty^{2-n}}{\nu}$ is the Forchheimer number (non-Darcian parameter). The mixed convection parameter is $\lambda=\dfrac{Ra}{Pe}$ whose negative and positive values correspond to opposing and aiding flows and $Ra=\dfrac{\bar{x}}{\alpha}\left(\dfrac{\beta\,g\,K^*\,cos\,\gamma\,(T_w-T_\infty)}{\nu}\right)^{\frac{1}{n}}$. The linear, quadratic and nonlinear radiation parameters are denoted by R_1, R_2 and R_3 respectively and each carry the value $\dfrac{4\,\sigma\,T_\infty^3}{k\,\bar{k}}$. The parameter $\theta_w=\dfrac{T_w}{T_\infty}$ represents temperature ratio.

Non-dimensional form of the skin friction coefficient $C_f=\dfrac{2}{\rho\,u_\infty^2}\left[\mu\dfrac{\partial u}{\partial y}\right]_{y=0}$ is given by

$$\frac{1}{2}\frac{Pe^{\frac{1}{2}}}{Pr}C_f=f''(\xi,0). \tag{4.24}$$

The heat transfer rates in terms of Nusselt number $Nu_{\bar{x}}=\dfrac{\bar{x}}{k\,(T_w-T_\infty)}\left[-k\dfrac{\partial T}{\partial y}-\dfrac{4\sigma}{3\bar{k}}\dfrac{\partial T^4}{\partial y}\right]_{y=0}$ for linear, quadratic and nonlinear cases of the thermal radiation can be written as

$$\frac{Nu_{\bar{x}}}{Pe^{\frac{1}{2}}}=-\left[1+\frac{4}{3}R_1\right]\theta'(\xi,0), \tag{4.25}$$

$$\frac{Nu_{\bar{x}}}{Pe^{\frac{1}{2}}}=-\left[1+\frac{4}{3}R_2\,(1+3(\theta_w-1))\,\theta(\xi,0)\right]\theta'(\xi,0), \tag{4.26}$$

$$\frac{Nu_{\bar{x}}}{Pe^{\frac{1}{2}}}=-\left[1+\frac{4}{3}R_3\{(1+(\theta_w-1))\,\theta(\xi,0)\}^3\right]\theta'(\xi,0). \tag{4.27}$$

Results and Discussion

The governing equations (4.19)-(4.22) along with the boundary conditions (4.23) are solved numerically using spectral local linearization method (SLLM) together with the local non-

similarity approach. Validation of the present problem can be done on comparison as it was done in the case (b) of *Chapter-2* in the absence of thermal radiation with $\xi = 0$ and $Fs = 0$.

Figs. 4.5 and 4.6 present the velocity, temperature, dimensionless heat transfer rate and skin friction coefficient variations for three values of linear radiation parameter R_1 when $Fs = 1.5$ and $\xi = 5.0$ for pseudoplastic and dilatant fluids respectively. It is observed from Figs. 4.5(a) and 4.6(a) that the non-dimensional velocity increases with enhancing values of R_1 in the aiding flow case and decreases in the opposing flow case for both type of fluids. The phenomenon of flow separation is clearly visible from these plots. The influence of thermal radiation is similar on both these fluids. The physical reason behind this increment in velocity with thermal radiation enhancement for the aiding flow case is the weakening of bonds which hold the fluid particle components. As thermal radiation increases, these bond split with more ease. This phenomenon is applicable in faster cooling process by reducing thermal radiation. Figs. 4.5(b) and 4.6(b) display the temperature distribution with increasing values of R_1 for pseudoplastic and dilatant fluids respectively. The dominance of temperature profiles is noticed for the aiding flow case when compared to the opposing flow case for both these fluids. Increment is observed in the temperature with greater values of R_1. The Nusselt number and skin friction coefficient variations are plotted with respect to streamwise coordinate (ξ) for opposing and aiding flow situations. As expected, Figs. 4.5(c) and 4.6(c) confirm the increment in the non-dimensional heat transfer rate with increase in R_1 values. Higher heat transfer rate is seen in the aiding flow case when compared with the opposing flow for both pseudoplastic and dilatant fluids. Figs. 4.5(d) and 4.6(d) depict that the magnitude of skin friction coefficient decreases with enhancing values of the linear radiation parameter in both opposing and aiding flow cases. The variations are more for higher values of ξ. One more important point can be seen from these figures that the skin friction coefficient and Nusselt number become almost constant for higher values of ξ as in case(a).

Figs. 4.7 and 4.8 portray the change in velocity, temperature, Nusselt number and skin friction coefficient for various values of the quadratic radiation parameter when $Fs = 1.5$, $\theta_w = 0.1$ and $\xi = 5.0$ for both pseudoplastic and dilatant fluids respectively. Figs. 4.7(a) and

4.8(a) display the non-dimensional velocity profiles with variation in the quadratic radiation parameter (R_2). Similar to the linear case, the velocity in aiding flow dominant in comparison with opposing flow. With increasing values of R_2, there is enhancement and diminution in the velocity profiles for aiding and opposing flows respectively. The temperature variation in pseudoplastic and dilatant fluid flows subject to quadratic radiation is given in Figs. 4.7(b) and 4.8(b). These figures include both the opposing and aiding flow cases. With increasing values of this radiation parameter, the temperature profiles are enhanced. The enhanced values of radiation parameter make the boundary layer more thick and better thermal performance can be observed. The increment in Nusselt number with enhancing values R_2 is again confirmed from the Figs. 4.7(c) and 4.8(c). The higher rate of heat transfer is clearly visible in the case aiding flow when compared to the opposing flow for both these fluids. Figs. 4.7(d) and 4.8(d) depict the skin friction coefficient variations with respect to the streamwise coordinate (ξ) for pseudoplastic and dilatant fluids respectively. From Fig. 4.7(d), a decrement in the magnitude of skin friction coefficient is noticed with increase in R_2 and similar behaviour is also found in the Fig. 4.8(d).

Similar to previous two cases, the influence of nonlinear thermal radiation parameter (R_3) on velocity and temperature profiles along with skin friction coefficient and Nusselt number are collected in the Figs. 4.9 and 4.10 for pseudoplastic and dilatant fluids respectively. The fixed values are $Fs = 1.5$, $\theta_w = 0.001$ and $\xi = 5.0$. Increment and decrement in velocity with increase in R_3 values are noticed from the Figs. 4.9(a) and 4.10(a) in aiding and opposing flow cases and also the occurrence of flow separation is seen. The increment in R_3 increases temperature profiles which are displayed in the Figs. 4.9(b) and 4.10(b) for pseudoplastic and dilatant fluids respectively and higher temperature is seen in aiding flow in comparison with the opposing flow. The study of Nusselt number and skin friction coefficient in respect of streamwise coordinate (ξ) for opposing and aiding flows is also included. The enhancement in Nusselt number with increasing values of the nonlinear radiation parameter is shown in the Figs. 4.9(c) and 4.10(c) for pseudoplastic and dilatant fluids respectively. This non-dimensional heat transfer rate carries higher values in aiding flow when compared to that of the opposing flow for both these fluids. It is assured from the fact that the

enhancement in thermal radiation parameter implies decay in mean absorption coefficient and hence enhances the radiative heat flux divergence. Therefore, the heat transfer rate increases and so the temperature of the fluid. The variations in the magnitude of skin friction coefficient with different values of the nonlinear radiation parameter are depicted in the Figs. 4.9(d) and 4.10(d) for pseudoplastic and dilatant fluids respectively and decrement is noticed with higher values of R_3 in both the opposing and aiding flow cases. Again, the variations are more for higher values of ξ.

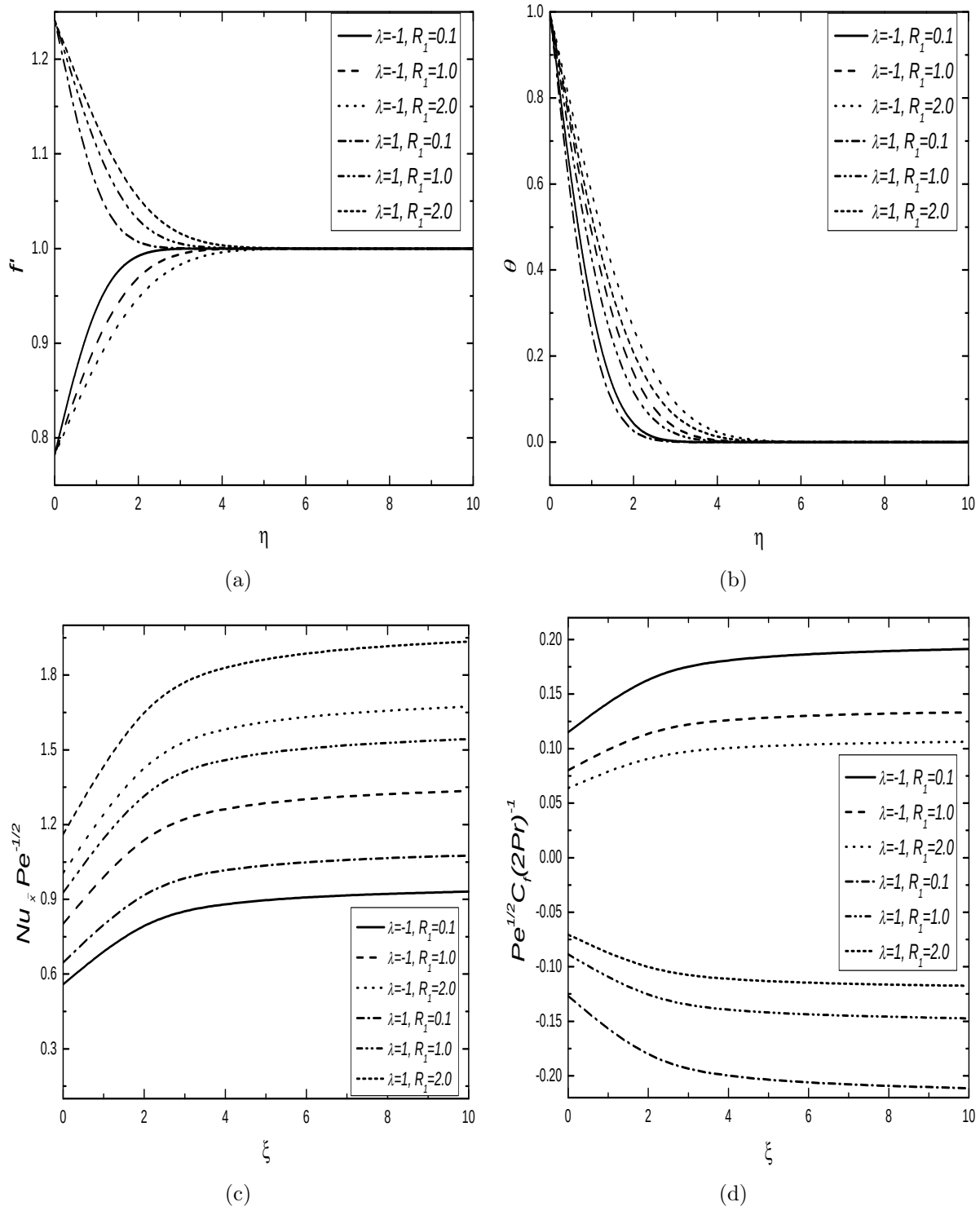

Figure 4.5: *Effect of linear radiation parameter (R_1) on (a) velocities, (b) temperatures, (c) Nusselt number and (d) skin friction coefficient for pseudoplastic fluid.*

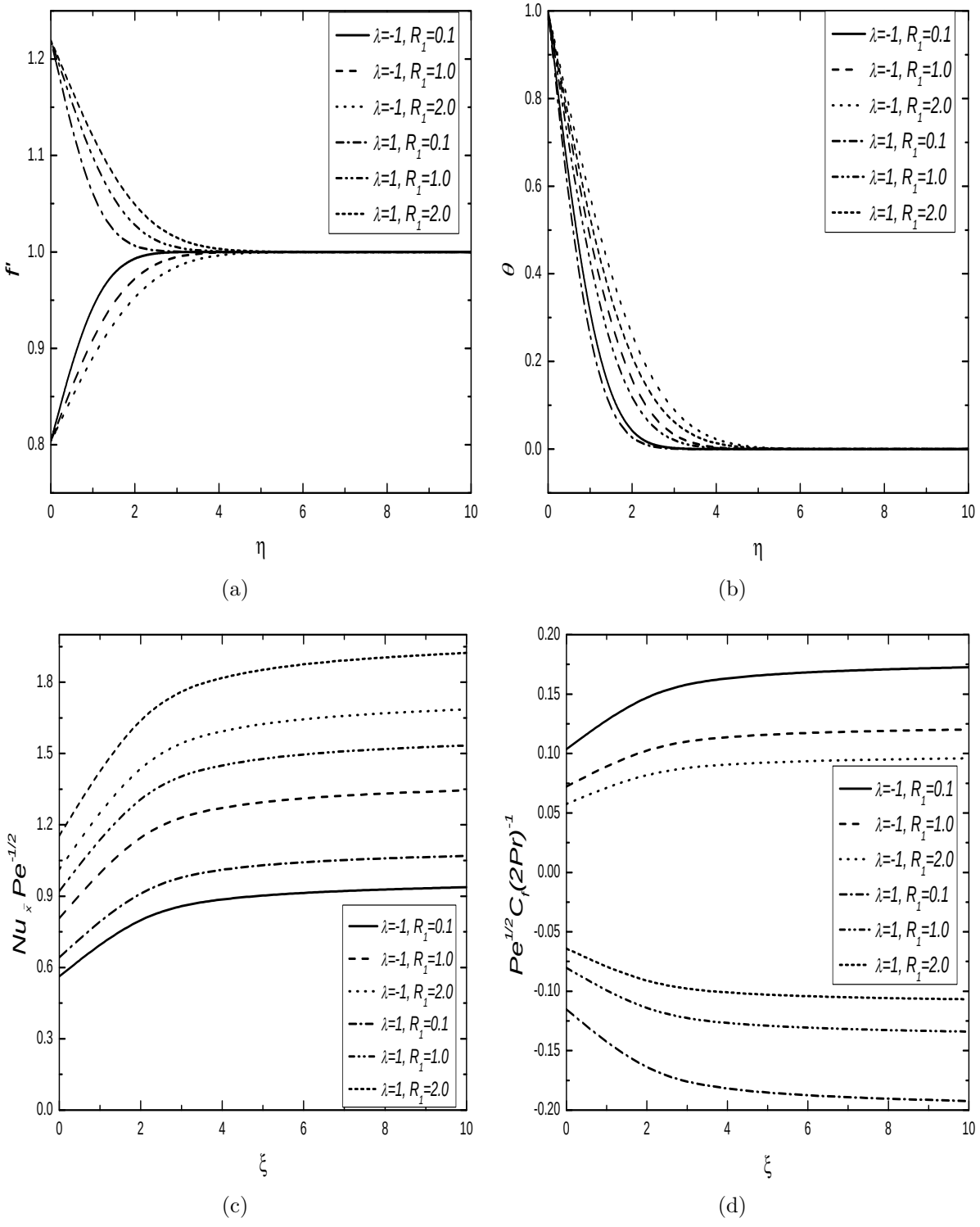

Figure 4.6: *Effect of linear radiation parameter (R_1) on (a) velocities, (b) temperatures, (c) Nusselt number and (d) skin friction coefficient for dilatant fluid.*

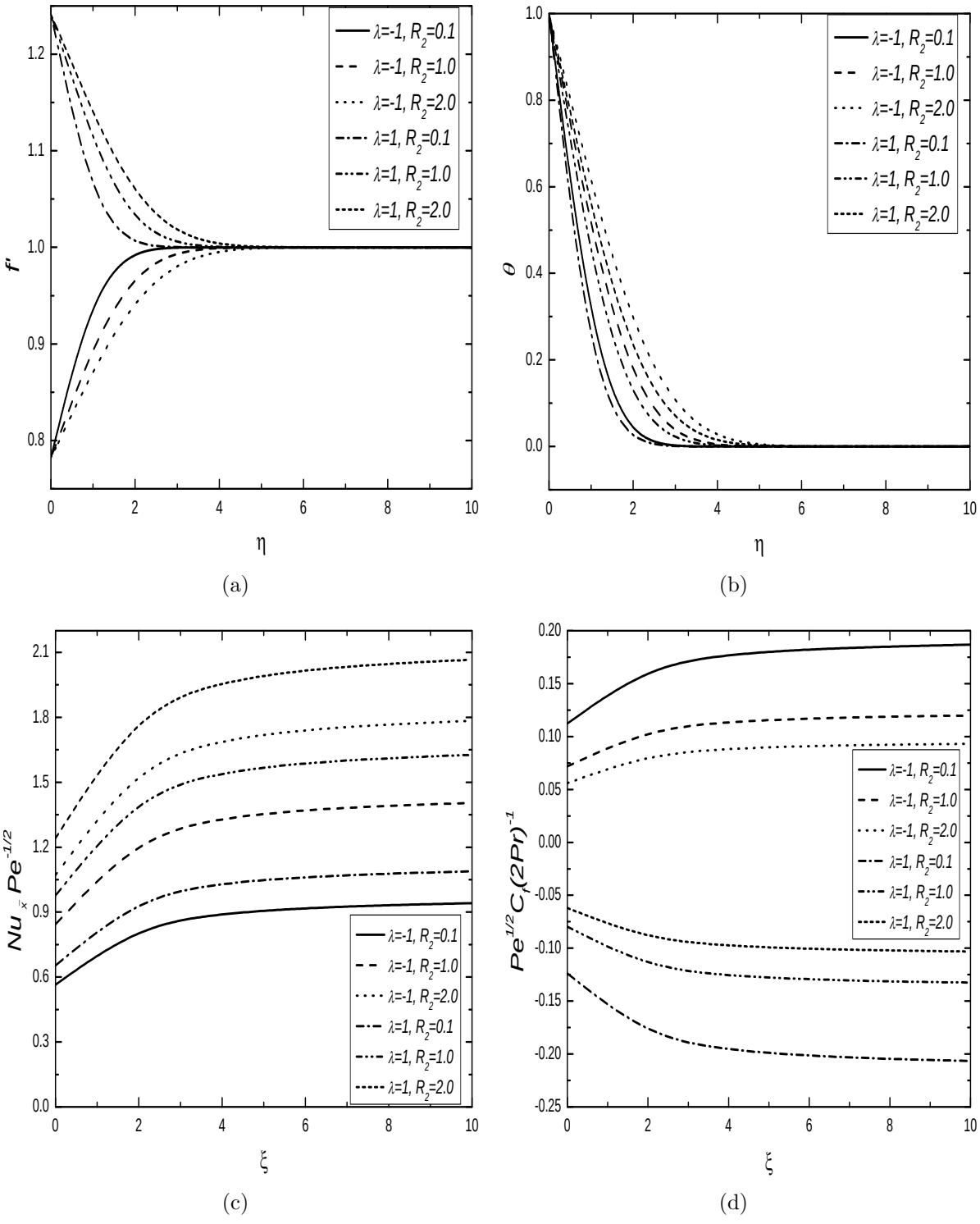

Figure 4.7: *Effect of quadratic radiation parameter (R_2) on (a) velocities, (b) temperatures, (c) Nusselt number and (d) skin friction coefficient for pseudoplastic fluid.*

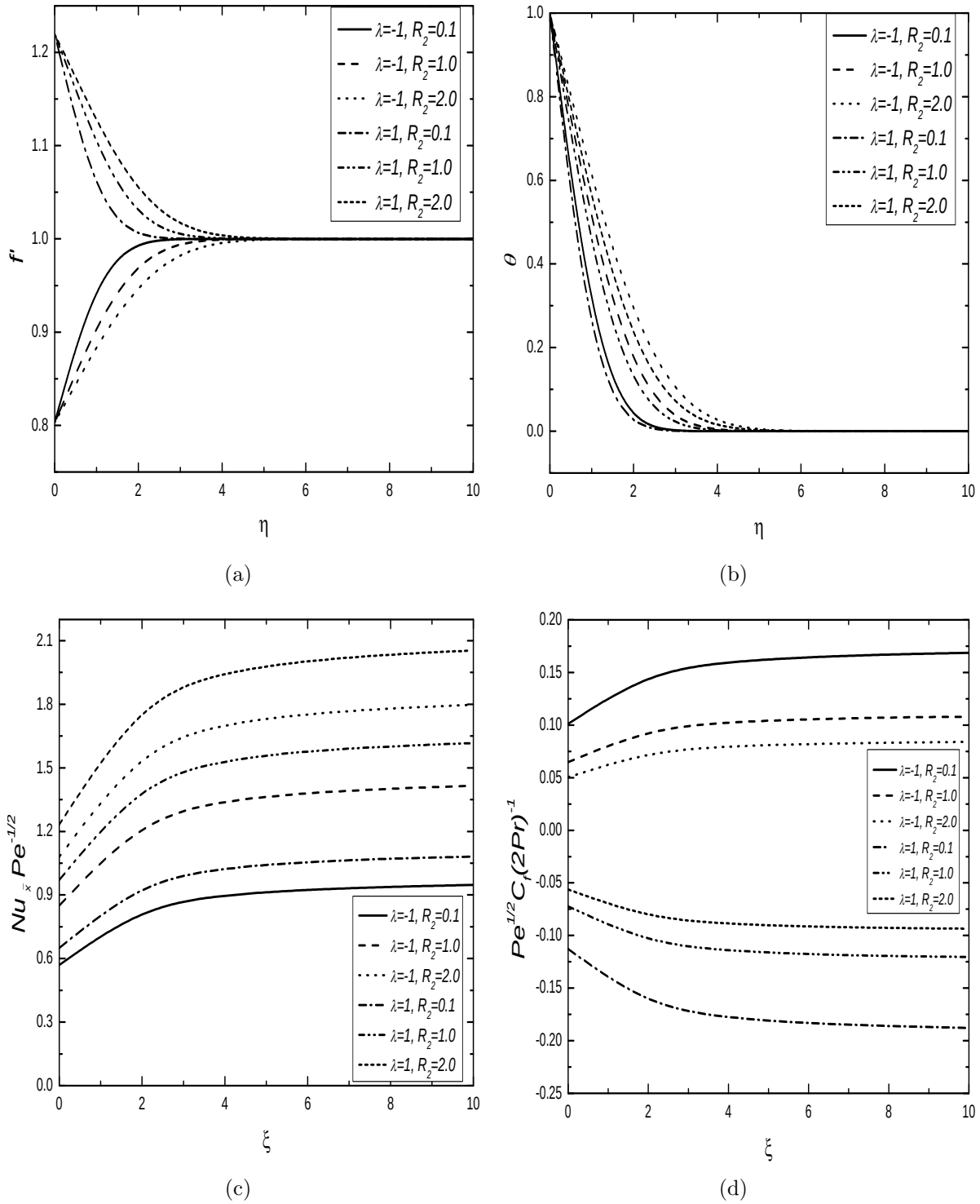

Figure 4.8: *Effect of quadratic radiation parameter (R_2) on (a) velocities, (b) temperatures, (c) Nusselt number and (d) skin friction coefficient for dilatant fluid.*

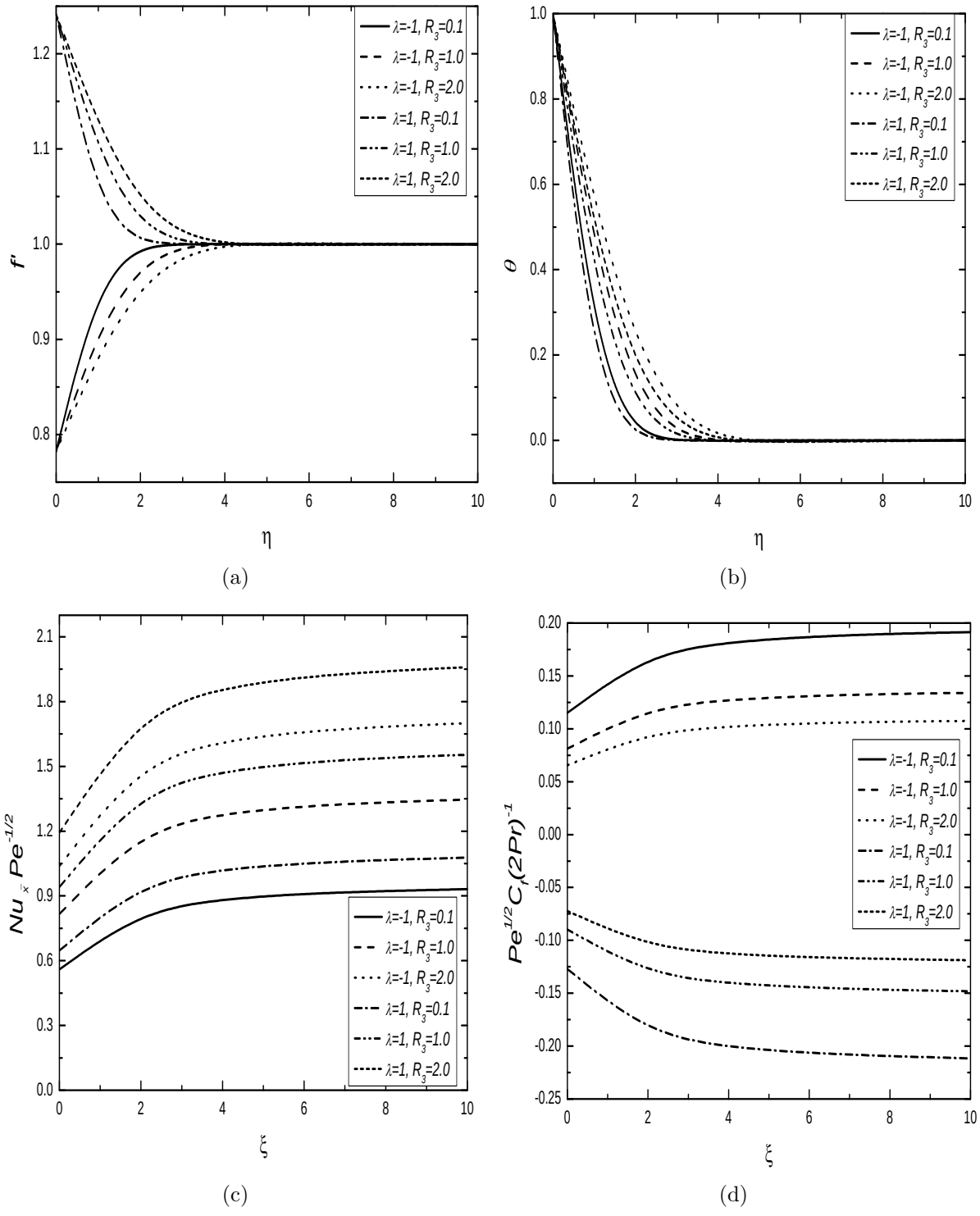

Figure 4.9: *Effect of nonlinear radiation parameter (R_3) on (a) velocities, (b) temperatures, (c) Nusselt number and (d) skin friction coefficient for pseudoplastic fluid.*

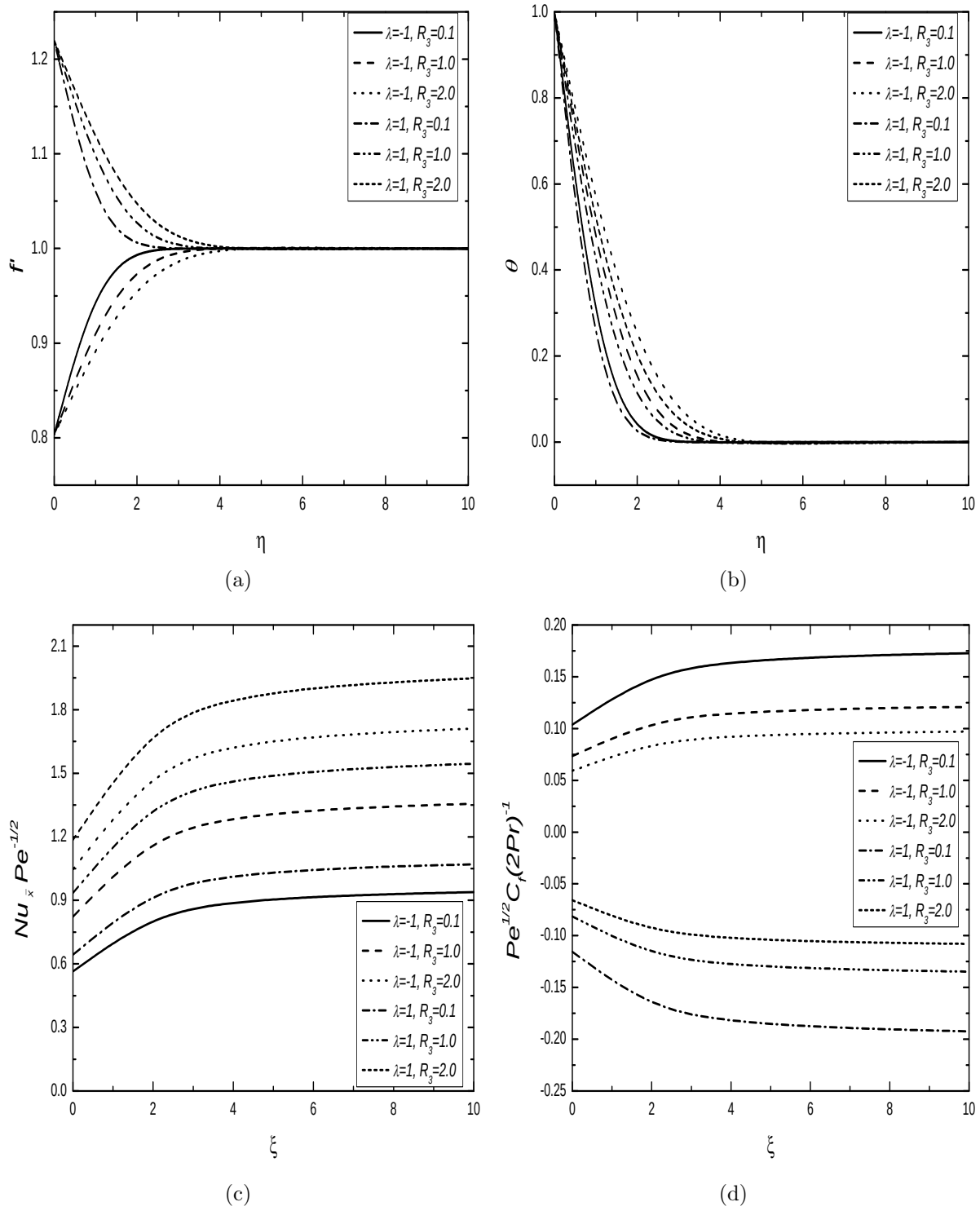

Figure 4.10: *Effect of nonlinear radiation parameter (R_3) on (a) velocities, (b) temperatures, (c) Nusselt number and (d) skin friction coefficient for dilatant fluid.*

4.3 Conclusions

In this chapter, the linear, quadratic and nonlinear radiation effects on power-law fluid flows past a truncated cone in a non-Darcy porous medium, are discussed in detail for the two cases: (a) natural convection and (b) mixed convection. The conclusive remarks of this work in both the cases (a) and (b) for physically suitable values of flow governing parameters, are:

Case (a): Natural Convection

- Higher velocity is obtained with increased values of the thermal radiation parameters in linear, quadratic and nonlinear cases along with the dominance of dilatant fluid over the pseudoplastic fluid.
- The dominance of pseudoplastic fluid over the dilatant fluid is noticed in the plots of temperature and it is higher for increment in all three radiation parameters.
- Larger absolute values of the skin friction is noticed for all the three cases of radiations for smaller values of R_1, R_2 and R_3. Here, quadratic radiation is more effective in this study.

Case (b): Mixed Convection

- The phenomenon of flow separation is observed between aiding and opposing flows for pseudoplastic and dilatant fluids in linear, quadratic and nonlinear radiation cases.
- The higher temperature is noticed in opposing flow when compared with the aiding flow case and the temperature is enhanced with increment in all three radiation parameters.
- The Nusselt number is greater for enhanced values of R_1, R_2 and R_3 with its dominance in the aiding flow case. For the quadratic and nonlinear radiation cases, the heat transfer rate is more in comparison with linear radiation case.

Chapter 5

Analysis of Ostwald-de Waele Power-law Nanofluid Flows over a Truncated Cone in a Non-Darcy Porous Medium [1]

5.1 Introduction

In modern days, several investigations in the field of nanotechnology have attracted many other researchers due to its broad-ranging applications. To understand the various aspects of experimental applications, different types of nanoparticles are introduced in Tiwari-Das nanofluid model and their efficiency is verified. For instance, Barnoon and Toghraie [5] investigated numerically the heat transfer and laminar flow of pseudoplastic non-Newtonian nanofluid (Al_2O_3 and Carboxy-Methyl-Cellulose) in a porous medium (also see the citations therein). But, the *Alloys* have distinct features among other nanoparticles and are defined as metals combined with one or other elements. A short description about different alloys

[1] Case(a): Accepted in "**Discontinuity, Nonlinearity, and Complexity**", January 2021, Case(b): Published in "**Indian Journal of Physics**", March 2021, DOI: 10.1007/s12648-021-02055-8.

with their usefulness and properties is provided in the papers [47, 92]. In particular, the Ti-alloys are mainly classified as α, $\alpha - \beta$ and β alloys. Among these, $\alpha - \beta$ alloys are most important and have multi-sector applications. The Ti6Al4V alloy which falls under $\alpha - \beta$ category, is frequently used in the manufacturing of aircraft turbines, engine components, high-performance automatic parts, sports equipment etc. Peters *et al.* [94] and Singh *et al.* [112] have given the details about applications of Titanium and its alloys in the aerospace sector. On the other hand, Multi Walled Carbon Nanotubes (MWCNTs) comprise many rolled layers of aligned nanotubes of graphene inside other nanotubes which are hollow and cylindrical in shape with high aspect ratio (length to diameter ratio). Its properties are also unique due to their complicated line-up and each aligned nanotube may be of distinct shape. It has a wide range of applications e.g., in drug delivery, filters and membrane, Li^+ batteries, sporting goods (bike rims, tennis rackets), aerospace materials, textiles, fibres and many more. Chougule and Sahu [22] analysed the thermal performance of radiators experimentally using Carbon nanotube-water nanofluid. Goodarzi *et al.* [38] performed a numerical simulation related to the free convective heat transfer involving three different nanoparticles (viz., Cu, MWCNT, and Al_2O_3) with water as the base fluid. The non-Newtonian nature of nanofluid containing MWCNT nanoparticles is experimentally verified by Liu *et al.* [66].

In this chapter, the Ostwald-de Waele power-law nanofluid flows over a vertical truncated cone embedded in a non-Darcy porous medium are investigated. From the literature, it is evident that the above said work is not received sufficient attention as per the best of authors' knowledge. Since the concept of using truncated cone in a nanofluid is relatively new, therefore there are not many well established applications but, there are several fields in which this geometry will be very helpful along with nanofluids. One such field is the study of nanofluid with gyrotactic microorganism over a truncated cone. Hence, it can be said that the consideration of these two nanoparticles for this fluid flow is noteworthy.

5.2 Mathematical Analysis

In this chapter, the free and mixed convective Ostwald-de Waele power-law nanofluid flows over a truncated cone in a non-Darcy porous medium, are considered. In addition, the Ti-alloy and Multi Walled Carbon Nanotubes (MWCNTs) are taken as nanoparticle one by one to form regular nanofluid model. The physical model with coordinate system is displayed in Fig. 5.1. The leading edge of the truncated cone is kept at a distance x_0 from the origin O, where x and y axes are taken along and normal to the surface of the truncated cone, respectively. The ambient medium and wall temperatures are taken as T_∞ and T_w respectively together with the modified streamwise coordinate $\bar{x}$, which is defined as $\bar{x} = x - x_0$ for the truncated cone.

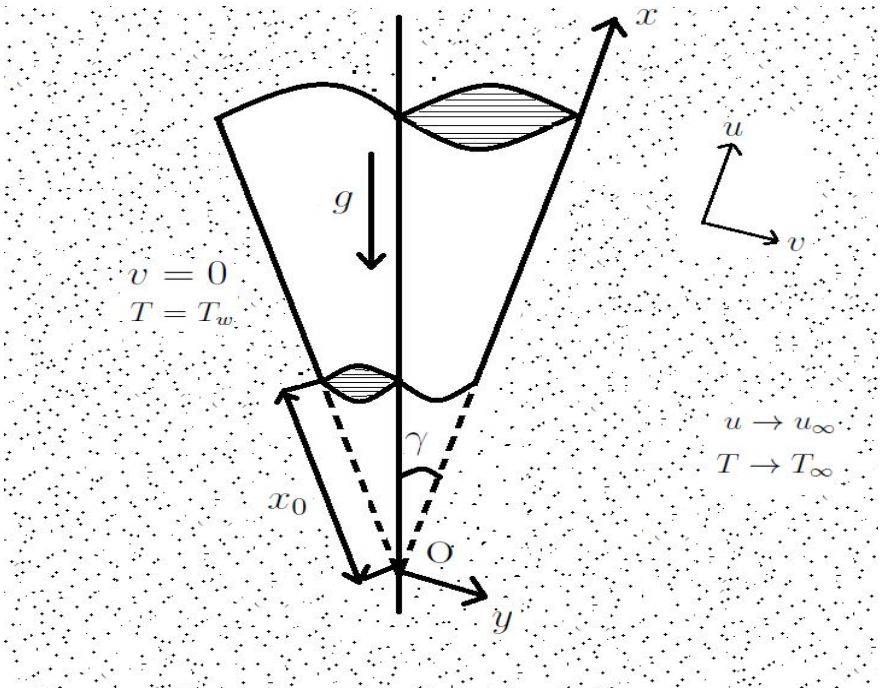

Figure 5.1: *Physical model and coordinate system.*

Taking the boundary layer hypothesis into the consideration along with the basic approximations and assumptions related to truncated cone as mentioned in *Chapter-2*, the

governing equations for the fluid flow over a truncated cone are given by

$$\frac{\partial(ru)}{\partial x}+\frac{\partial(rv)}{\partial y}=0, \tag{5.1}$$

$$\frac{\partial u^n}{\partial y}+\frac{b\,K^*\,\rho_{nf}}{\mu_{nf}}\frac{\partial u^2}{\partial y}=\frac{K^*\,g\,(\rho\,\beta)_{nf}\,\cos\gamma}{\mu_{nf}}\frac{\partial T}{\partial y}, \tag{5.2}$$

$$u\frac{\partial T}{\partial x}+v\frac{\partial T}{\partial y}=\frac{k_{nf}}{(\rho\,C_P)_{nf}}\frac{\partial^2 T}{\partial y^2}, \tag{5.3}$$

along with the boundary conditions

$$\begin{aligned} v(x,\,y)=0,\;\; T(x,\,y)=T_w \qquad & \text{at} \quad y=0 \\ u(x,\,y)\to u_\infty,\;\; T(x,\,y)\to T_\infty \qquad & \text{as} \quad y\to\infty. \end{aligned} \tag{5.4}$$

where ρ_{nf}, μ_{nf}, β_{nf}, k_{nf} and C_{Pnf} denote the density, dynamic viscosity, thermal expansion coefficient, thermal conductivity and specific heat capacity of the power-law nanofluid respectively. Also, b, g, γ, T, u_∞ and (u, v) are used for the empirical constant, acceleration due to gravity, inclination of angle, temperature, free stream and Darcian velocities respectively. K^* is the modified permeability of the porous medium which depends on power-law index n. The three values of the power-law index $n<1$, $n=1$ and $n>1$ denote the pseudoplastic, Newtonian and dilatant nanofluids respectively.

In this chapter also, two types (cases) of problems are considered: (a) free/natural convection and (b) mixed convection.

5.2.1 Case(a): Natural Convection

In this case, the flow is caused due to buoyancy forces only without the external flow velocities ($i.e., u_\infty=0$). By considering the above-said assumptions, the non-dimensional relations utilized to get the non-dimensional form of equations (5.2)-(5.4) are

$$\xi=\frac{\bar{x}}{x_0},\;\; \eta=\frac{y}{\bar{x}}\,Ra^{\frac{1}{2}},\;\; \psi(\xi,\eta)=\alpha_f\,r\,Ra^{\frac{1}{2}}\,f(\xi,\eta),\;\; T(\xi,\eta)=T_\infty+(T_w-T_\infty)\,\theta(\xi,\eta), \tag{5.5}$$

where $Ra = \dfrac{\bar{x}}{\alpha_f}\left(\dfrac{(\rho\,\beta)_f\, g\, K^*\, cos\,\gamma\,(T_w - T_\infty)}{\mu_f}\right)^{\frac{1}{n}}$ is the local modified Darcy-Rayleigh number and α_f is the thermal diffusivity of the base fluid.

On substituting the transformations (5.5) in the equations (5.2) to (5.3) and the boundary conditions (5.4), the non-dimensional form of the these equations and boundary conditions become

$$\begin{aligned} n\,(f')^{n-1}\,f'' + 2\left[(1-\phi)^{2.5}\left(\phi\,\frac{\rho_s}{\rho_f}\,+\,1-\phi\right)\right]Gr^*\,f'f'' \\ = \left[(1-\phi)^{2.5}\left(\phi\,\frac{(\rho\,\beta)_s}{(\rho\,\beta)_f}\,+\,1-\phi\right)\right]\theta', \end{aligned} \tag{5.6}$$

$$2A\,(\xi+1)\,\theta'' + (3\xi+1)\,f\theta' = 2\xi(\xi+1)\left(f'\frac{\partial\theta}{\partial\xi} - \frac{\partial f}{\partial\xi}\theta'\right), \tag{5.7}$$

$$\begin{aligned} f(\xi,0) + \frac{2\,\xi\,(\xi+1)}{3\,\xi+1}\left[\frac{\partial f}{\partial\xi}\right]_{\eta=0} = 0, \quad \theta(\xi,0) = 1, \\ f'(\xi,\eta)\to 0, \quad \theta(\xi,\eta)\to\ 0\ \ as\ \ \eta\to\infty, \end{aligned} \tag{5.8}$$

where the differentiation in respect of η is denoted by primes. $Gr^* = \dfrac{b\,K^*}{\nu_f}\left(\dfrac{\alpha}{\bar{x}}Ra\right)^{2-n}$ is the modified Grashof number, ν_f is the kinematic viscosity. Further, A depends on nanoparticle volume fraction and its expression can be written as:

$$A = \frac{1}{\left[\left(\phi\,\dfrac{(\rho\,C_P)_s}{(\rho\,C_P)_f}\,+\,1-\phi\right)\right]}\left[\frac{k_s + 2\,k_f - 2\,\phi\,(k_f - k_s)}{k_s + 2\,k_f + \phi\,(k_f - k_s)}\right].$$

Here, ϕ is the volume fraction of nanoparticles. The suffixes f and s are utilized to denote the base fluid and solid nanoparticle. In this work, Ti-alloy and MWCNTs nanoparticles are used and their different characteristics are discussed. The different thermo-physical properties associated to these nanoparticles and the base fluid are given in the Table (5.1).

Table 5.1: *Thermophysical Properties*

Properties	Ti-alloy[99]	MWCNTs[37]	Water[99]
$\rho\ (kg/m^3)$	4420	2100	997.1
$C_P\ (J/kgK)$	526.3	710	4179
$\beta\ (1/K) * 10^{-5}$	0.89	2.1	21
$k\ (W/mK)$	6.7	2000	0.613

With the help of this problem formulation, the Ostwald-de Waele power-law type of nanofluid flow over a full cone and along a vertical plate can also be studied directly just by assigning two different values of streamwise coordinate ξ. This property makes it very interesting and important. Very large values of ξ imply $x_0 = 0$ which leads the problem over a full cone. Similarly, this problem reduces to fluid flow problem over a vertical plate when $\xi = 0$ (i.e., $x = x_0$). These possible limiting cases and their comparative analysis is also presented through graphs in this chapter.

Non-dimensional form of the Nusselt number $Nu_{\bar{x}} = -\dfrac{\bar{x}}{(T_w - T_\infty)} \dfrac{k_{nf}}{k_f} \left[\dfrac{\partial T}{\partial y}\right]_{y=0}$ and the skin friction coefficient $C_f = \dfrac{2}{\rho\, u_*^2} \left[\mu_{nf} \dfrac{\partial u}{\partial y}\right]_{y=0}$ is given by

$$\frac{Nu_{\bar{x}}}{Ra^{\frac{1}{2}}} = -\frac{k_{nf}}{k_f}\theta'(\xi, 0), \;\; \frac{1}{2}\frac{Ra^{\frac{1}{2}}}{Pr} C_f = \frac{\mu_{nf}}{\mu_f} f''(\xi, 0), \tag{5.9}$$

where u_* and Pr are the characteristic velocity and the Prandtl number respectively.

Results and Discussion

As specified in the previous chapters, the flow governing equations (5.6)-(5.7) along with the boundary conditions (5.8) are solved numerically using spectral local linearisation method (SLLM) together with the non-similarity approach in this chapter. Validation of the present

problem can be done on comparison as it was done in the case (a) of *Chapter-2* by putting $\xi = 0$ and no volume fraction of Ti-alloy and MWCNTs are inserted.

The volume fraction of Ti-alloy and MWCNTs is denoted by ϕ_1 and ϕ_2 respectively to discuss the results undertaken. Also, $\phi_1 = 0.1$, $\phi_2 = 0.02$ and $\xi = 2.5$ are fixed throughout the computation otherwise mentioned specifically. Here, the influence of volume fraction of Ti-alloy (ϕ_1) and MWCNTs (ϕ_2) and graphical representation of non-dimensional velocity, temperature, Nusselt number and skin friction coefficient are discussed. Figs. 5.2 and 5.3 display the impact of volume fraction of Ti-alloy nanoparticle and MWCNTs nanoparticle respectively.

The influence of ϕ_1 and ϕ_2 on velocity profiles is displayed in Figs. 5.2(a) and 5.3(a) respectively. The domination of dilatant nanofluid over the pseudoplastic nanofluid is clearly visible from these graphs. The velocity is decreased with ϕ_1 and ϕ_2 increment and this variation is more for small change in the volume fraction of MWCNTs nanoparticle. One important observation is that all the profiles asymptotically satisfied the boundary conditions at infinity, so this is another way to show the accuracy of these numerical results. This asymptotic condition is satisfied by the temperature profiles too. The temperature profiles are increased with increment in volume fraction of both the nanoparticles ϕ_1 and ϕ_2 as displayed in Figs. 5.2(b) and 5.3(b) respectively. But, opposite to velocity profiles, there is domination of pseudoplastic nanofluid over the dilatant nanofluid. The physical reason behind this enhancement in temperature profiles with the nanoparticle volume fraction increment is the increased thermal conductivity when larger ϕ_1 and ϕ_2 are used. This happens due to the larger thermal conductivity of solid particles in comparison to the base fluid.

Effect of ϕ_1 and ϕ_2 on non-dimensional heat transfer rate (Nusselt number) for both the dilatant and pseudoplastic nanofluids, is presented in Figs. 5.2(c) and 5.3(c) respectively. Here, the analysis is done in respect of streamwise coordinate ξ. It is noticed that the heat transfer rate is decreased with the addition of volume fraction of nanoparticle. In this study, there is again domination of dilatant nanofluid over the pseudoplastic nanofluid. For very small values of ξ, the heat transfer is very less and there is rapid increment in the range near zero. For higher values (after $\xi = 5$), the Nusselt number becomes constant. In this way, it

is observed that the heat transfer rate over a truncated cone lies between the heat transfer rate over a vertical plate ($\xi = 0$) and full cone ($\xi \to \infty$).

The same kind of analysis is done for skin friction coefficient too. The impact of ϕ_1 and ϕ_2 variations on non-dimensional skin friction coefficient for both the dilatant and pseudoplastic nanofluids, are portrayed in Figs. 5.2(d) and 5.3(d) respectively. As the volume fraction of nanoparticle is increased, magnitude of the skin friction coefficient decreases for both Ti-alloy and MWCNTs cases. The magnitude of skin friction coefficient is more for dilatant nanofluid when compared to pseudoplastic nanofluid in the presence of nanoparticle volume fraction. A sharp increment in its magnitude is noted when ξ is nearly zero. For higher values, it almost becomes constant or change is negligible. So, it can be said that the skin friction coefficient in a fluid flow over a truncated cone lies between the vertical plate ($\xi = 0$) and full cone ($\xi \to \infty$) as in the case of heat transfer rate. In this way, all these profiles and their variations with nanoparticle volume fraction can be interpreted and these results are useful in daily life applications.

Figs. 5.4 and 5.5 are prepared to illustrate the significance of modified Grashof number on the velocity and temperature profiles, heat transfer rate and skin friction coefficient. The Grashof number plays the same role in natural convection which is played by the Reynolds number in forced convective flow. It depends on the dynamic, geometric and thermodynamic parameters of the heat transport problem. In the case of non-zero increasing values of Gr^*, there is reduction in the flow intensity and increment in the inertial effects which thickens the boundary layer and resist the heat transfer which is noticed in Figs. 5.4(c) and 5.5(c). In the Figs. 5.4(a) and 5.5(a), it is seen that the velocity profiles are also decreased with increment in the modified Grashof number. The domination of dilatant nanofluid is noted over the pseudoplastic nanofluid from these graphs. The temperature profiles are increased with an increment of modified Grashof number and the domination of pseudoplastic nanofluid is noticed as depicted in Figs. 5.4(b) and 5.5(b). The influence of Gr^* on magnitude of skin friction coefficient is shown in Figs. 5.4(d) and 5.5(d) and large decrement in its magnitude is readily visible with the domination of pseudoplastic nanofluid. Similar to the previous cases, this analysis is also helpful in the study the present problem with both full cone as

well as vertical plate geometries.

The variation in velocity and temperature profiles with respect to streamwise coordinate is shown in 5.6. It is observed that the velocity profiles are higher for dilatant nanofluid and there is decrement with higher values of ξ. The temperature profiles show similar trend too but, in this case, there is a domination of pseudoplastic nanofluid over dilatant nanofluid. It can be said from these graphs that the velocity and temperature in these kinds of flow over a truncated cone fall between the vertical plate and full cone geometries.

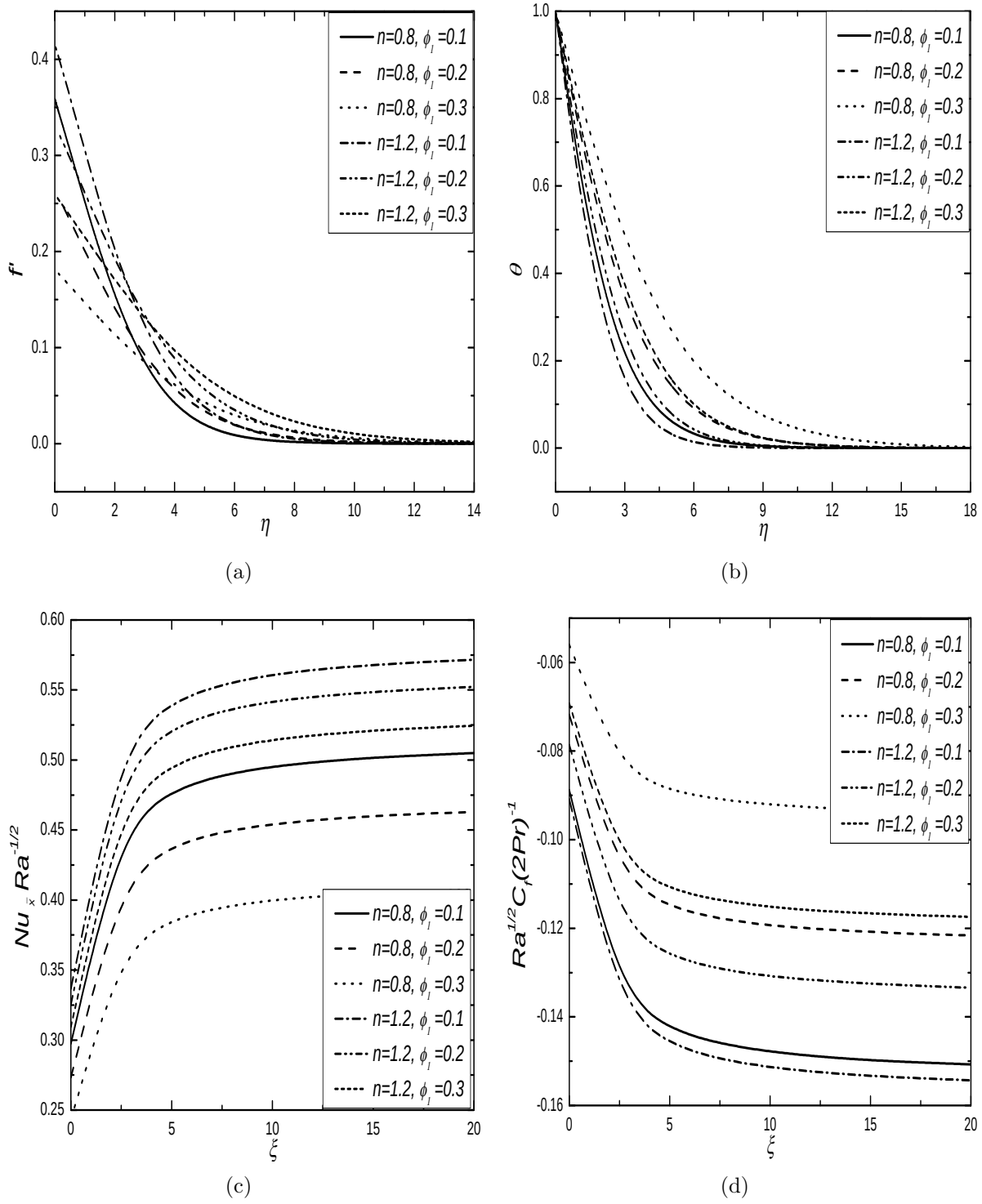

Figure 5.2: *Effect of volume fraction of Ti-alloy (ϕ_1) on (a) velocity and (b) temperature profiles, (c) Nusselt number and (d) skin friction coefficient for pseudoplastic and dilatant nanofluids.*

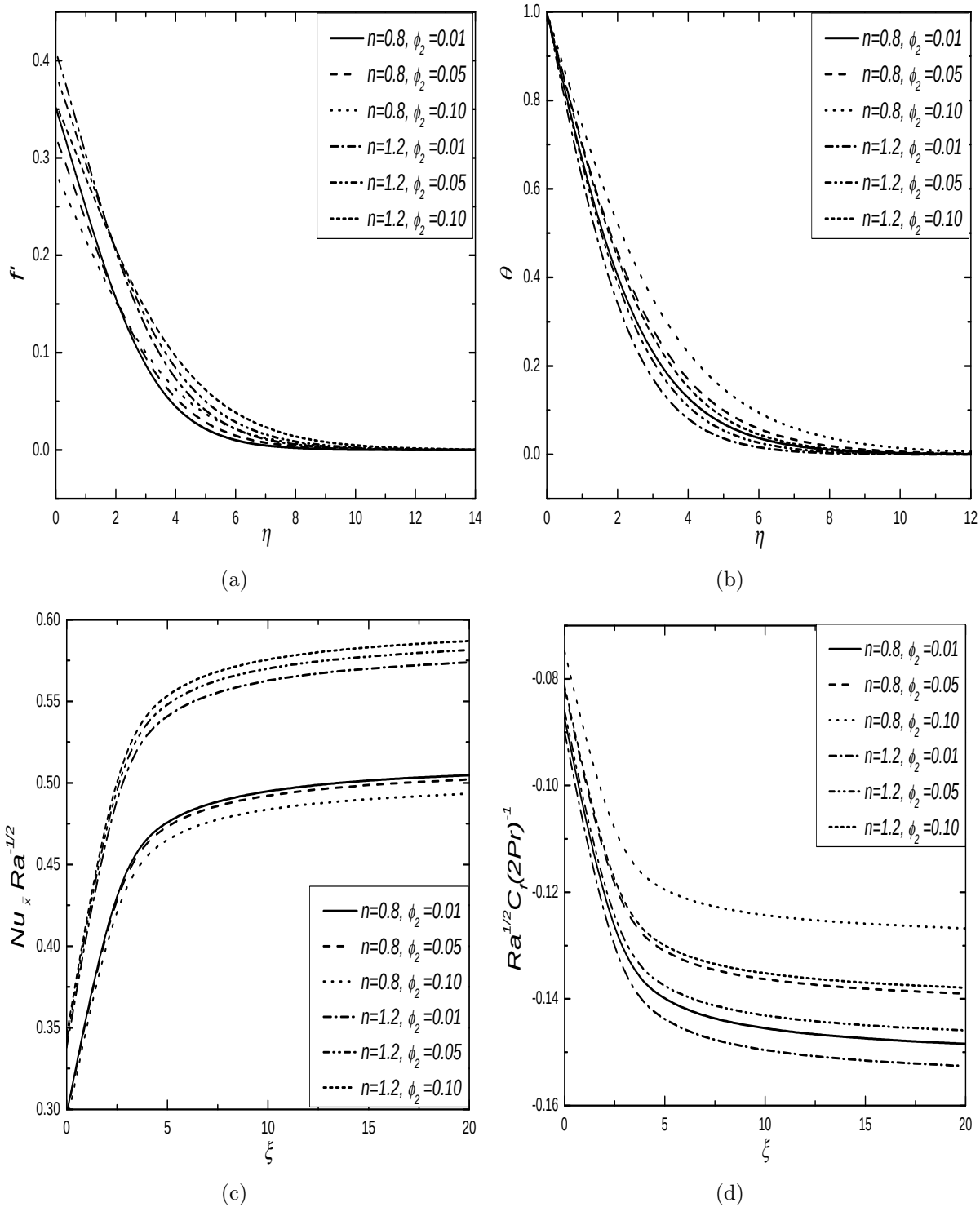

Figure 5.3: *Effect of volume fraction of MWCNTs (ϕ_2) on (a) velocity and (b) temperature profiles, (c) Nusselt number and (d) skin friction coefficient for pseudoplastic and dilatant nanofluids.*

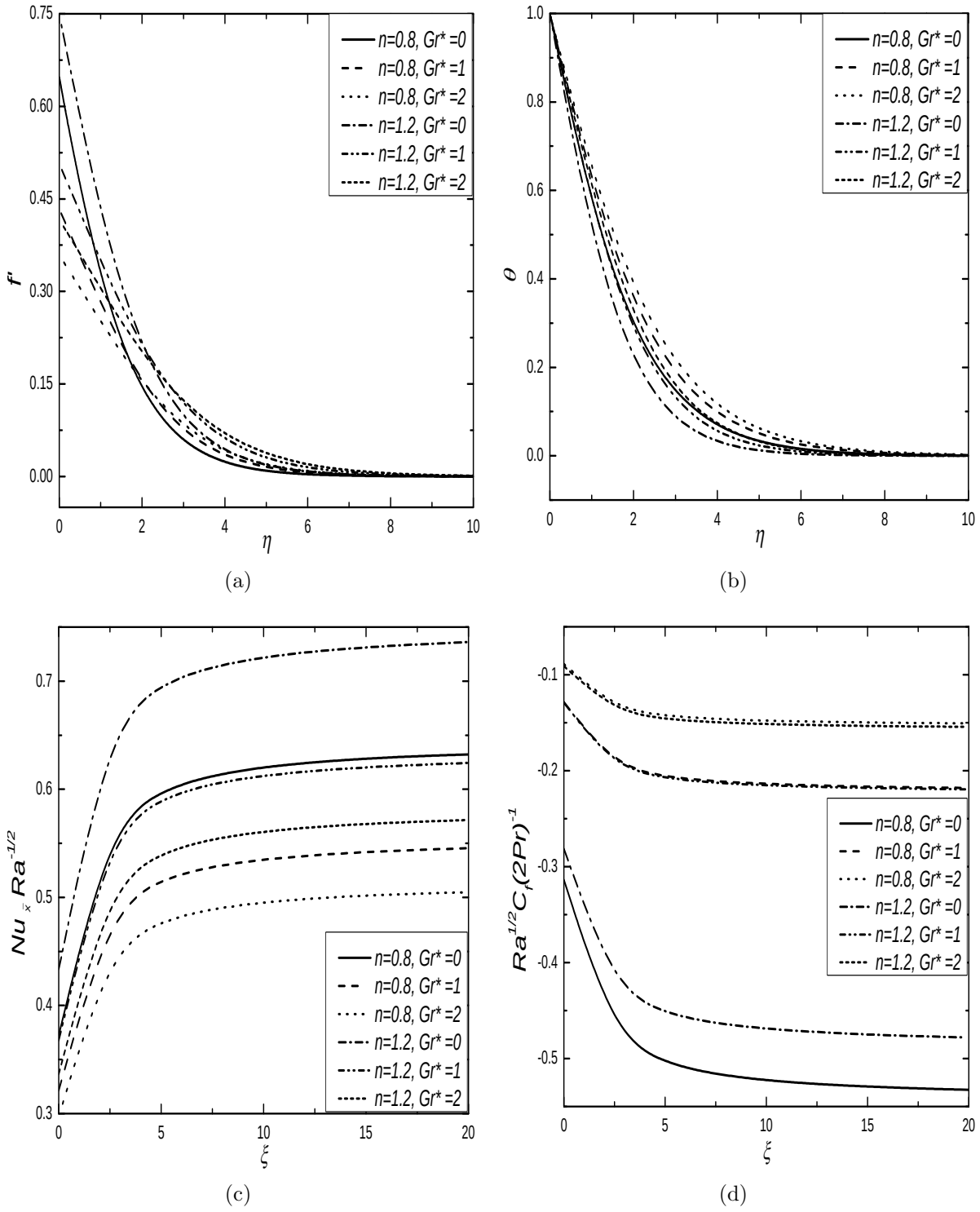

Figure 5.4: *Effect of Gr* on (a) velocity and (b) temperature profiles, (c) Nusselt number and (d) skin friction coefficient for pseudoplastic and dilatant nanofluids containing Ti-alloy nanoparticles.*

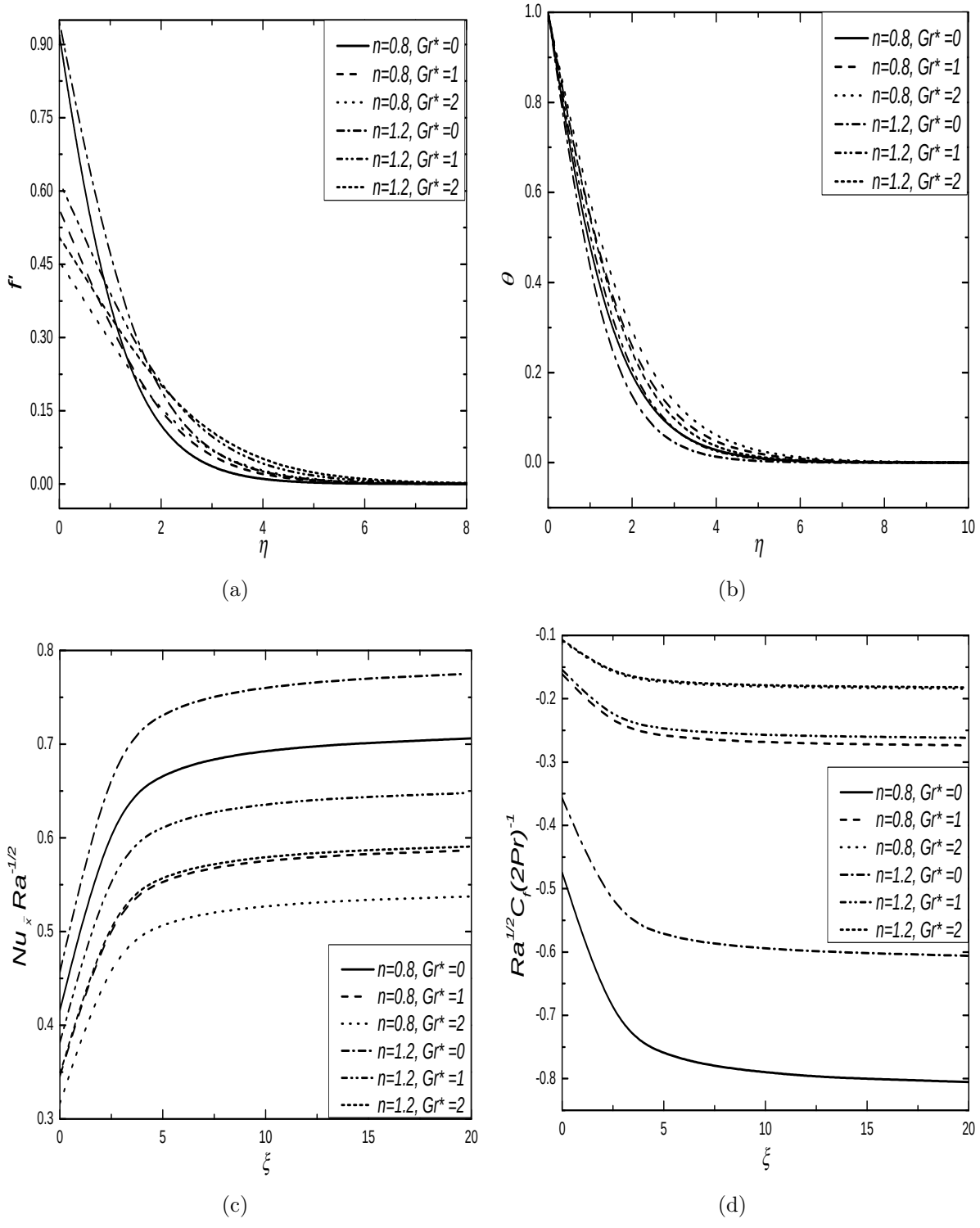

Figure 5.5: *Effect of Gr^* on (a) velocity and (b) temperature profiles, (c) Nusselt number and (d) skin friction coefficient for pseudoplastic and dilatant nanofluids containing MWCNTs nanoparticles.*

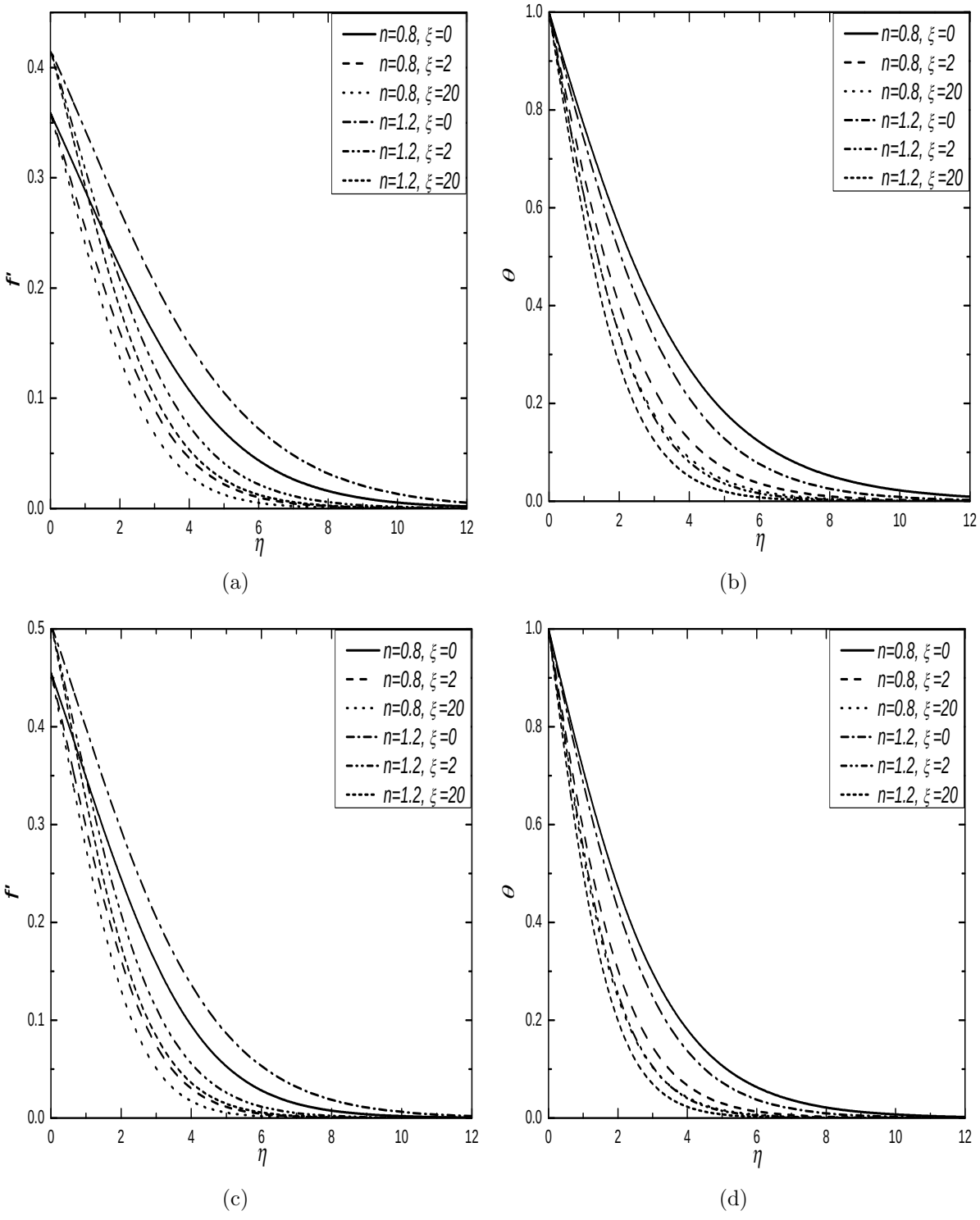

Figure 5.6: *Effect of ξ on velocity and temperature profiles for pseudoplastic and dilatant nanofluids containing Ti-alloy ((a), (b)) and MWCNTs nanoparticles ((c), (d)).*

5.2.2 Case(b): Mixed Convection

In this case, the flow arises due to buoyancy forces and external flow with the velocity u_∞. Taking the above-said points into consideration, the dimensionless transformations for the present setup are given by

$$\xi = \frac{\bar{x}}{x_0}, \;\; \eta = \frac{y}{\bar{x}}\, Pe^{\frac{1}{2}}, \;\; \psi(\xi,\eta) = \alpha_f\, r\, Pe^{\frac{1}{2}}\, f(\xi,\eta), \;\; T(\xi,\eta) = T_\infty + (T_w - T_\infty)\, \theta(\xi,\eta), \;\; (5.10)$$

where $Pe = \dfrac{u_\infty\, \bar{x}}{\alpha_f}$ is the local Peclet number and α_f is the thermal diffusivity of the base fluid.

Using these transformations (5.10) in the equations (5.2) to (5.3), the non-dimensional form of the above equations become

$$\begin{aligned} n\, (f')^{n-1}\, f'' + 2\, \left[(1-\phi)^{2.5} \left(\phi\, \frac{\rho_s}{\rho_f} \, + \, 1 - \phi\right)\right] Fs\, f' f'' \\ = \lambda^n \, \left[(1-\phi)^{2.5} \left(\phi\, \frac{(\rho\,\beta)_s}{(\rho\,\beta)_f} \, + \, 1 - \phi\right)\right] \theta', \end{aligned} \tag{5.11}$$

$$2A\,(\xi+1)\,\theta'' + (3\xi+1)\, f\theta' = 2\xi(\xi+1)\left(f' \frac{\partial\theta}{\partial\xi} - \frac{\partial f}{\partial\xi}\theta'\right). \tag{5.12}$$

The boundary conditions (5.4) in their transformed form can be written as

$$\begin{aligned} (3\,\xi+1) f(\xi,0) + 2\,\xi\,(\xi+1)\left(\frac{\partial f}{\partial\xi}\right)_{\eta=0} = \; 0, \quad \theta(\xi,0) = 1, \\ f'(\xi,\eta) \to 1, \quad \theta(\xi,\eta) \to \; 0 \;\; as \;\; \eta \to \infty, \end{aligned} \tag{5.13}$$

where primes indicate differentiation with respect to η, $Fs = \dfrac{b\,K^*\, u_\infty^{2-n}}{\nu_f}$, $\lambda = \dfrac{Ra}{Pe}$ and $Ra = \dfrac{\bar{x}}{\alpha_f}\left(\dfrac{(\rho\,\beta)_f\, g\, K^*\, cos\,\gamma\, (T_w - T_\infty)}{\mu_f}\right)^{\frac{1}{n}}$. Here, Fs is the non-Darcian parameter (Forchheimer number), ν_f is the kinematic viscosity and λ is the mixed convection parameter. The expression of A, which depend on nanoparticle volume fraction is given in Case (a) of this chapter.

Non-dimensional form of the Nusselt number $Nu_{\bar{x}} = -\dfrac{\bar{x}}{(T_w - T_\infty)} \dfrac{k_{nf}}{k_f} \left[\dfrac{\partial T}{\partial y}\right]_{y=0}$ and the skin friction coefficient $C_f = \dfrac{2}{\rho\, u_\infty^2} \left[\mu_{nf} \dfrac{\partial u}{\partial y}\right]_{y=0}$ is given by

$$\frac{Nu_{\bar{x}}}{Pe^{\frac{1}{2}}} = -\frac{k_{nf}}{k_f}\theta'(\xi, 0), \;\; \frac{1}{2}\frac{Pe^{\frac{1}{2}}}{Pr} C_f = \frac{\mu_{nf}}{\mu_f} f''(\xi, 0). \tag{5.14}$$

Results and Discussion

The governing equations (5.11)-(5.12) along with the boundary conditions (5.13) are solved numerically using spectral local linearisation method (SLLM) together with the non-similarity approach. Validation of the present problem can be done on comparison as it was done in the case (b) of *Chapter-2* by putting $\xi = 0$, $Fs = 0$ and no volume fraction of Ti-alloy and MWCNTs are inserted.

In this case also, the volume fraction of Ti-alloy and MWCNTs are denoted by ϕ_1 and ϕ_2 respectively to discuss the results. Also, $Fs = 0.5$, $\lambda = 3$ (for aiding flow), $\lambda = -3$ (for opposing flow) and $\xi = 2.5$ are fixed throughout the computation otherwise mentioned specifically. To understand the physical model of this fluid flow problem, the non-dimensional velocity, temperature, Nusselt number and skin friction coefficient in the opposing and aiding flow cases are graphically represented. The influence of volume fraction of Ti-alloy nanoparticles (ϕ_1) and MWCNTs nanoparticles (ϕ_2) is shown in Figs. 5.7-5.8 and 5.9-5.10 respectively.

In the aiding flow case, higher velocity is obtained in comparison with the opposing flow case (Figs. 5.7(a), 5.8(a) and 5.9(a), 5.10(a)). The domination of dilatant nanofluid over pseudoplastic nanofluid in both the flow cases is also noted. The velocity is decreased with ϕ_1 and ϕ_2 increments and this variation is more for small volume fraction of MWCNTs nanoparticles. It is observed again that all the profiles asymptotically satisfied the boundary conditions at infinity. The temperature profiles are almost similar in the opposing and aiding flow cases for respective values of ϕ_1 and ϕ_2 (Figs. 5.7(b), 5.8(b) and 5.9(b), 5.10(b)). But, opposite to the velocity profiles, there is domination of pseudoplastic nanofluid over

the dilatant nanofluid in this case. As the nanoparticle volume fraction increases, there is enhancement in temperature profiles. The physical reason behind this enhancement in temperature profiles with higher ϕ_1 and ϕ_2 is the increased thermal conductivity. This happens due to the reason that the solid particles have greater thermal conductivity in comparison to the base fluid.

In the Figs. 5.7(c), 5.8(c) and 5.9(c), 5.10(c), the impact of ϕ_1 and ϕ_2 variations on dimensionless heat transfer rate (Nusselt number) for both the dilatant and pseudoplastic nanofluids is presented. For this analysis, the opposing and aiding flow situations are taken into account. This study is done in respect of streamwise coordinate ξ. The heat transfer rate is higher in the case of aiding flow when compared to the opposing flow for both the fluids. When nanoparticle volume fraction is added further, it results into higher heat transfer due to larger thermal conductivity of Ti-alloy and MWCNTs. Also, in the physical sense, it is due to the increased collision among different nanoparticles which dissipates energy in the form of heat and results into increment of the heat transfer rate. In this study, there is again domination of dilatant nanofluid over the pseudoplastic nanofluid. For very small values of ξ, the heat transfer rate is very less and there is rapid increment in the range near zero. For higher values (after $\xi = 5$), the Nusselt number becomes constant. In this way, it is observed that heat transfer rate over a truncated cone lies between the heat transfer rate over vertical plate ($\xi = 0$) and full cone ($\xi \to 0$). Therefore, this additional analysis can also be done easily with the help of this physical model.

In the same way, the Figs. 5.7(d), 5.8(d) and 5.9(d), 5.10(d) show the impact of ϕ_1 and ϕ_2 variations on non-dimensional skin friction coefficient for both the dilatant and pseudoplastic nanofluids in the case of opposing and aiding flows respectively. This is also studied in respect of streamwise coordinate ξ. More negative skin friction coefficient is seen in the case of aiding flow when compared to the opposing flow for both these fluids. As volume fraction of the nanoparticles is increased, magnitude of skin friction coefficient decreases for both the Ti-alloy and MWCNTs. There is again domination of dilatant nanofluid over the pseudoplastic nanofluid as higher magnitude of skin friction coefficient is noted for dilatant nanofluid for all considered nanoparticle volume fractions. There is also a rapid increment in its magnitude

near zero. For higher values, it almost becomes constant or change is negligible. So, similar to heat transfer rate, it can be said that skin friction coefficient in a fluid flow over a truncated cone lies between its values over the vertical plate ($\xi = 0$) and full cone ($\xi \to 0$).

The velocity and temperature profiles with respect to streamwise coordinate ξ for both the dilatant and pseudoplastic nanofluids in the case of opposing and aiding flows are portrayed in Figs. (5.11) and (5.12) respectively. The first two graphs in each of these set of Figs. (5.11(a)-5.11(b) and 5.12(a)-5.12(b)) show the variation for nanofluids involving Ti-alloy nanoparticles and other graphs (5.11(c)-5.11(d) and 5.12(c)-5.12(d)) are for MWCNTs nanoparticles. It is readily visible from these figures that the velocity profiles are higher for dilatant nanofluid when compared to the pseudoplastic nanofluid but opposite is found for temperature profiles in both the flow cases. As ξ increases, all the profiles are decreased which implies the higher velocity and temperature in the case of flow over a vertical plate. So, these are minimum in the case of full cone and present study lies between them.

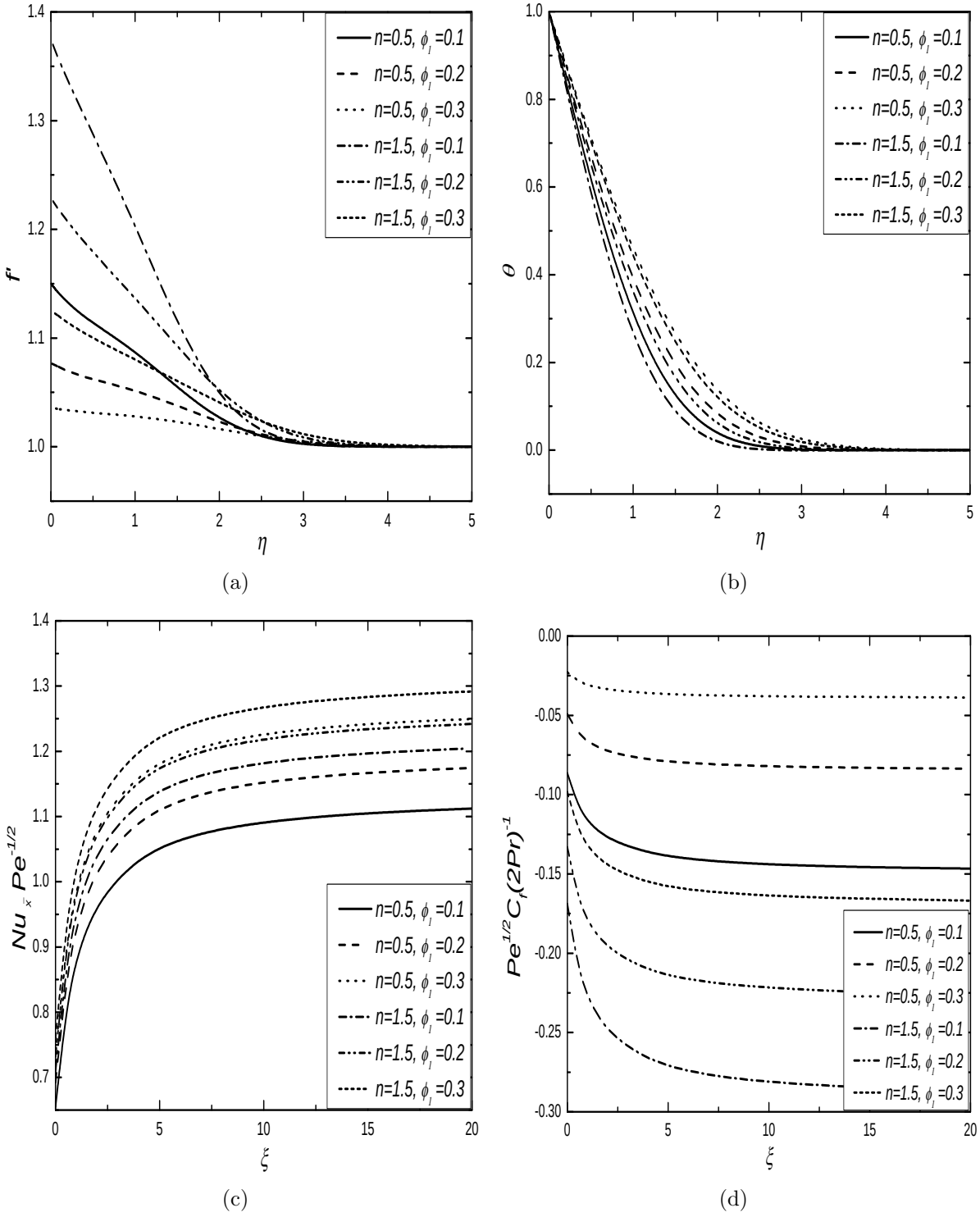

Figure 5.7: *Effect of volume fraction of Ti-alloy (ϕ_1) on (a) velocity and (b) temperature profiles, (c) Nusselt number and (d) skin friction coefficient for pseudoplastic and dilatant nanofluids in opposing flow case.*

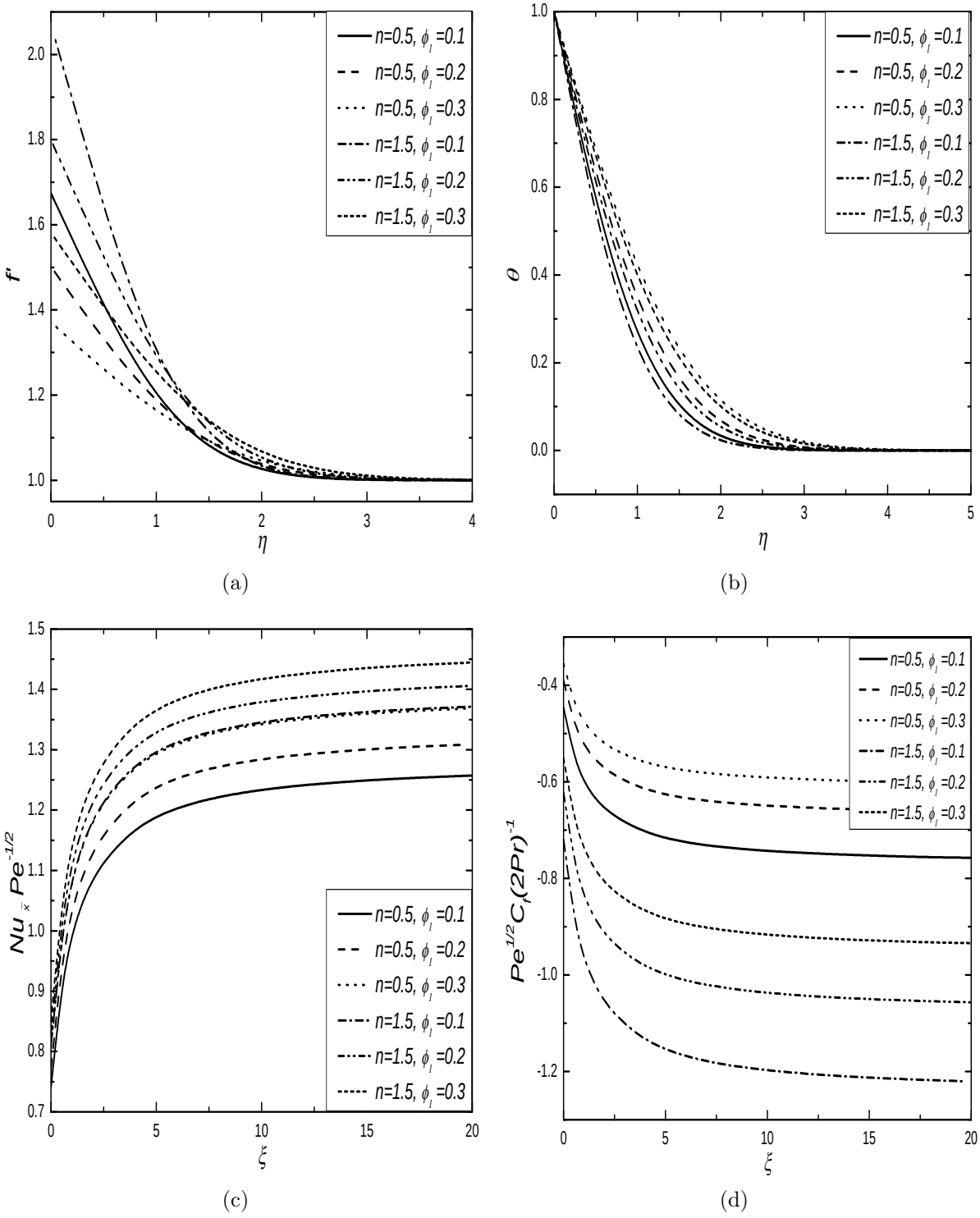

Figure 5.8: *Effect of volume fraction of Ti-alloy (ϕ_1) on (a) velocity and (b) temperature profiles, (c) Nusselt number and (d) skin friction coefficient for pseudoplastic and dilatant nanofluids in aiding flow case.*

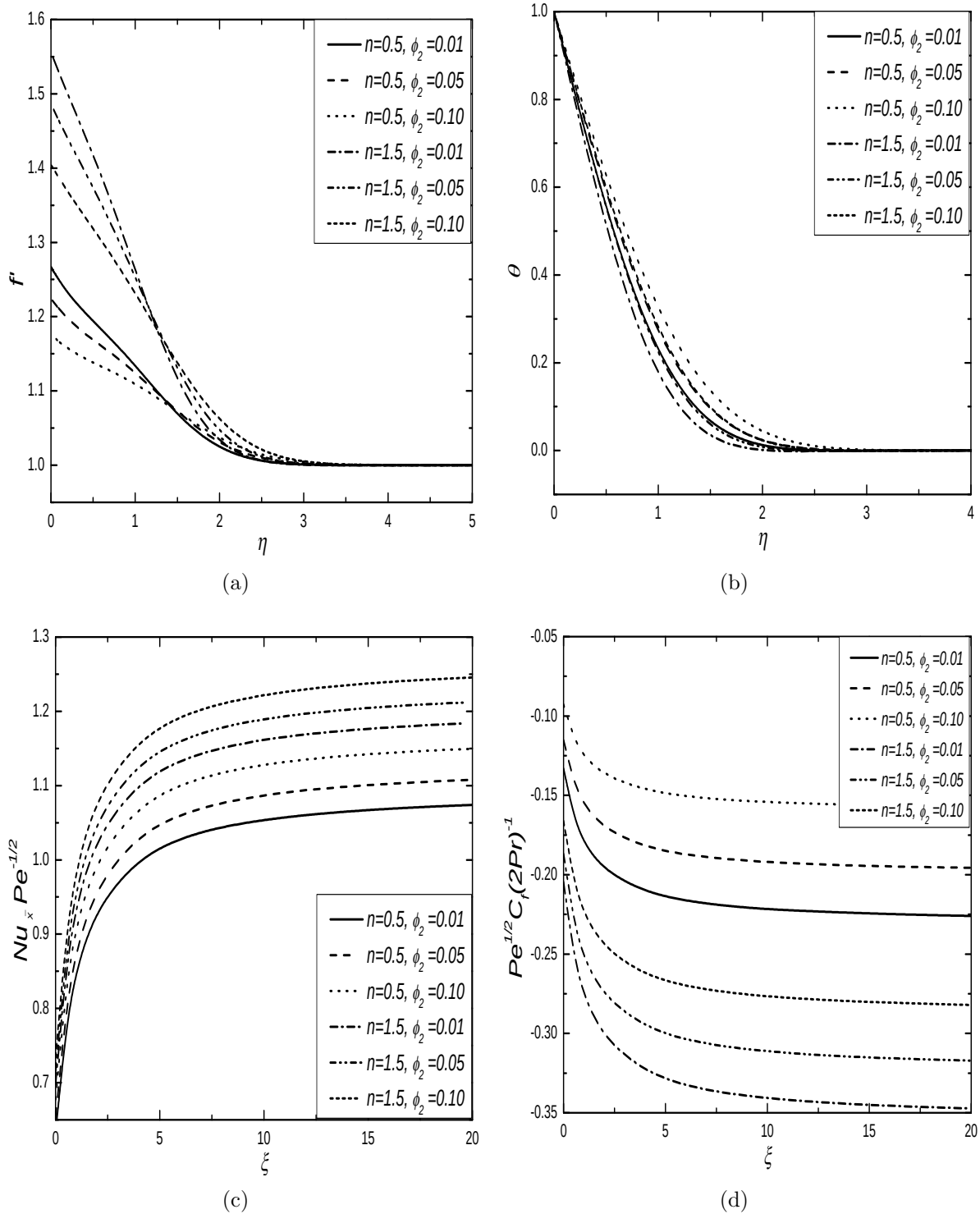

Figure 5.9: *Effect of volume fraction of MWCNTs (ϕ_2) on (a) velocity and (b) temperature profiles, (c) Nusselt number and (d) skin friction coefficient for pseudoplastic and dilatant nanofluids in opposing flow case.*

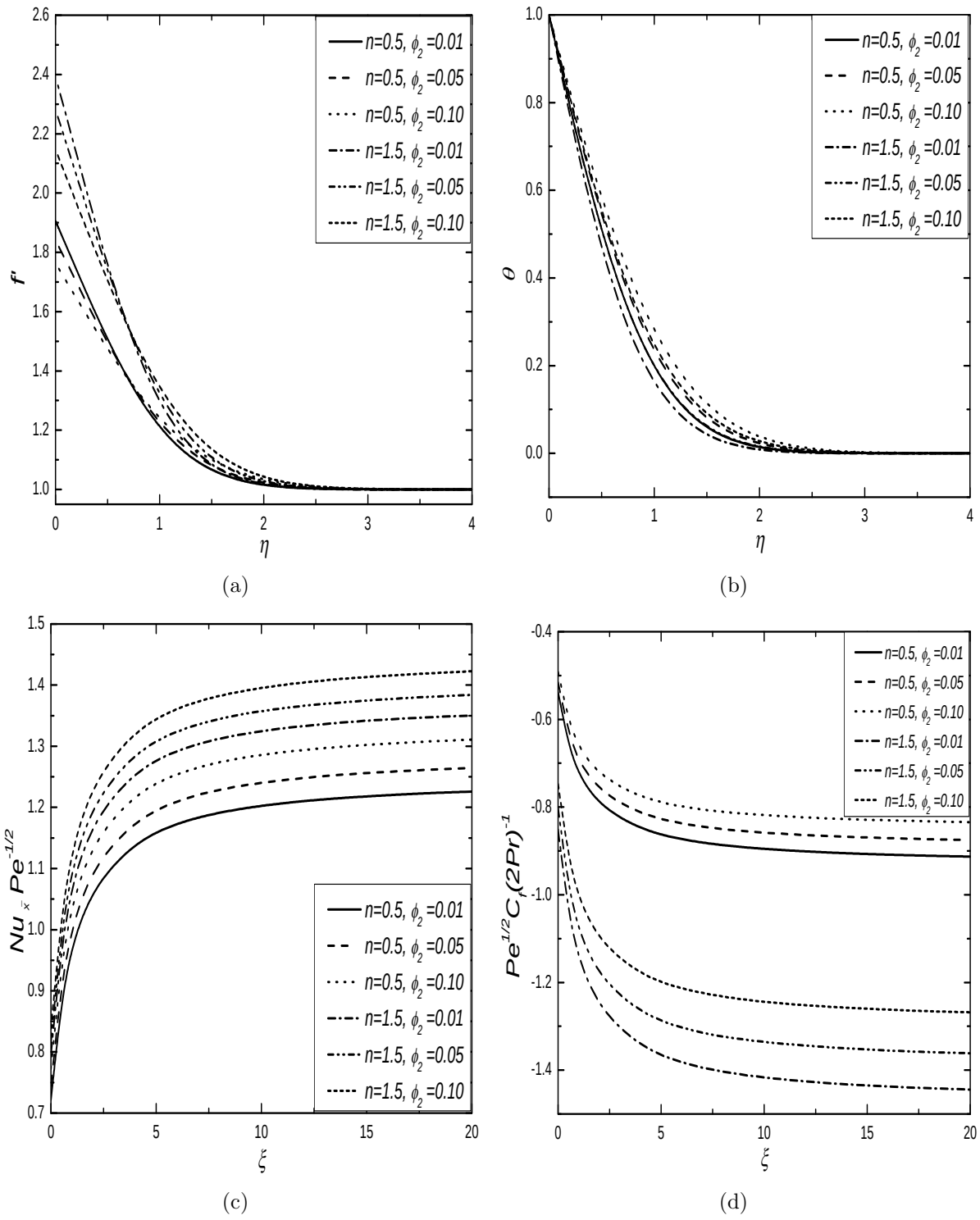

Figure 5.10: *Effect of volume fraction of MWCNTs (ϕ_2) on (a) velocity and (b) temperature profiles, (c) Nusselt number and (d) skin friction coefficient for pseudoplastic and dilatant nanofluids in aiding flow case.*

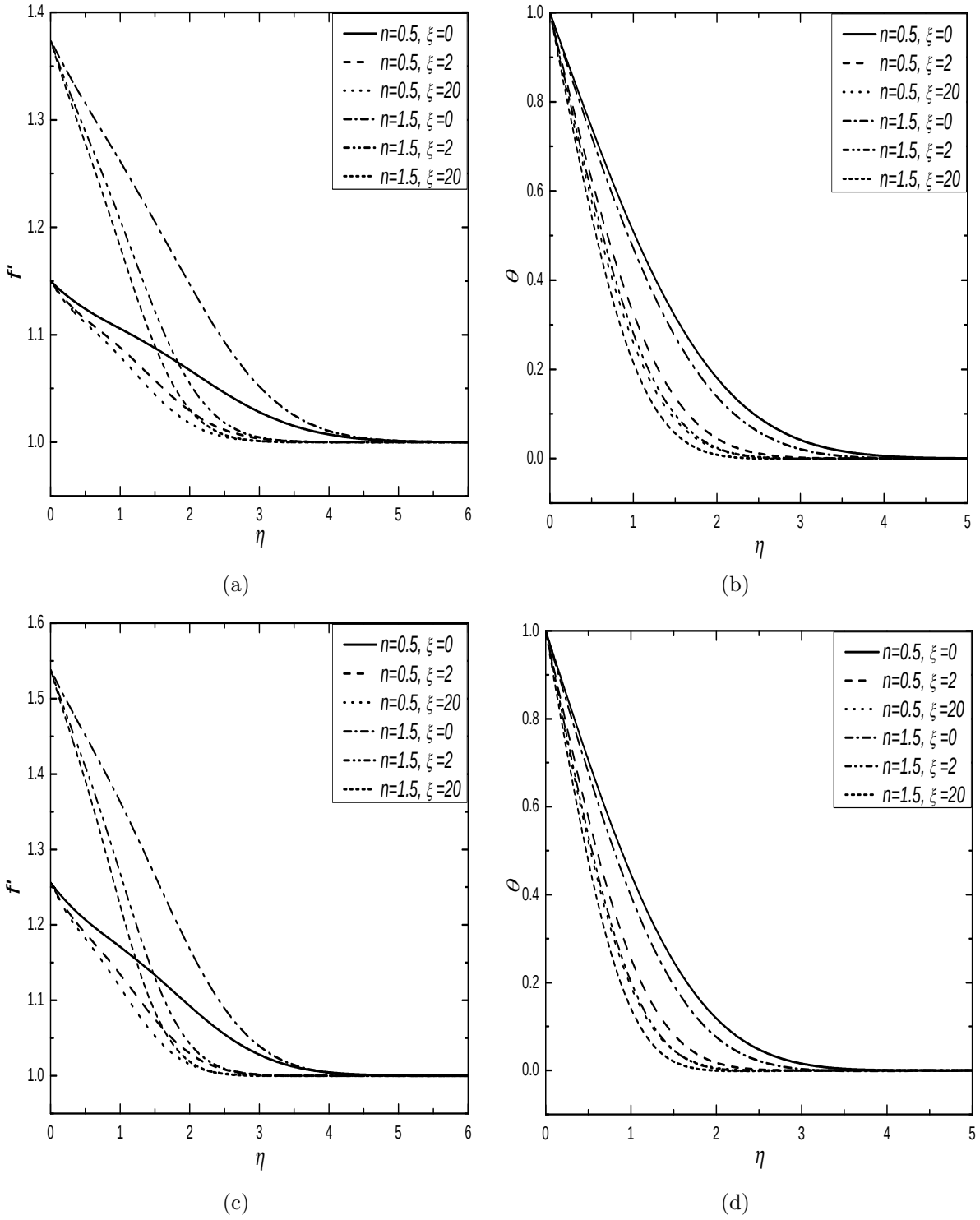

Figure 5.11: *Effect of ξ on velocity and temperature profiles for pseudoplastic and dilatant nanofluids involving Ti-alloy nanoparticles (a), (b) and MWCNTs nanoparticles (c), (d) in opposing flow case.*

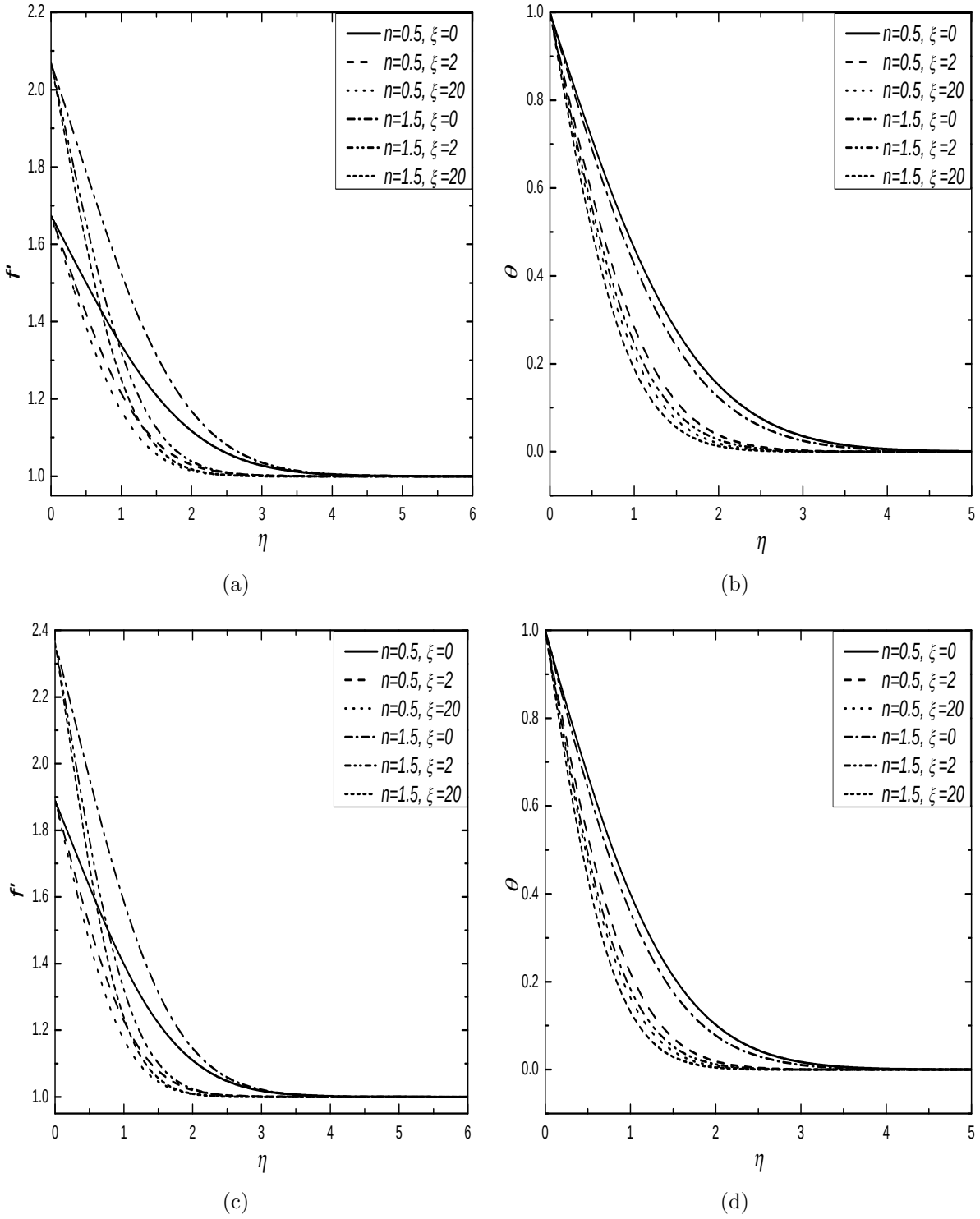

Figure 5.12: *Effect of ξ on velocity and temperature profiles for pseudoplastic and dilatant nanofluids involving Ti-alloy nanoparticles (a), (b) and MWCNTs nanoparticles (c), (d) in aiding flow case.*

5.3 Conclusions

In this chapter, the analysis of Ostwald-de Waele power-law nanofluid flows over a truncated cone situated in a non-Darcy porous medium, is done in detail for the two cases: (a) natural convection and (b) mixed convection. The Ti-alloy (Ti6Al4V) and multi walled Carbon nanotubes (MWCNTs) are used as nanoparticles in the base fluid water to get the power-law nanofluid model. The conclusive remarks of this work in both the cases (a) and (b) for physically suitable values of flow governing parameters, are:

Case (a): Natural Convection

- There is domination of pseudoplastic nanofluid over the dilatant nanofluid for the temperature profiles and the temperature is enhanced with increment in ϕ_1 and ϕ_2.
- The addition of nanoparticle volume fraction results into lower heat transfer rate and the dilatant nanofluid dominates.
- Higher magnitude of skin friction coefficient is observed for the dilatant nanofluid when compared to the pseudoplastic nanofluid for all values of ϕ_1 and ϕ_2.
- The change in all the profiles for various values of the streamwise coordinate show the non-similar nature of this problem.

Case (b): Mixed Convection

- There is domination of dilatant nanofluid over the pseudoplastic nanofluid in both the flow cases for velocity profiles and the velocity is decreased with increment in ϕ_1 and ϕ_2.
- Higher temperature is obtained for pseudoplastic nanofluid over the dilatant nanofluid in both the flow cases and the temperature is enhanced with ϕ_1 and ϕ_2 increments.
- The heat transfer rate is higher in the case of aiding flow when compared to opposing flow for both the fluids. The addition of nanoparticle volume fraction results into

higher heat transfer rate due to increased collision among different nanoparticles which dissipates energy in the form of heat.

- Nusselt number and magnitude of skin friction coefficient in the fluid flow over a truncated cone are found to be in between vertical plate and full cone.

Chapter 6

Flow of Aqueous Titanium Alloy-MWCNTs Hybrid Nanofluids in a Non-Darcy Porous Medium [1]

6.1 Introduction

In free and mixed convective flow mechanism, the heat transfer coefficient is comparatively lower to other mechanism which affects the performance of that thermal system. Thus, to increase this coefficient, the accompaniment of various nanoparticles in the base fluid is done and it is well established that this process increases the heat transfer property of resultant fluids (commonly known as nanofluids). Few mechanisms involved in the nanofluid heat transport are nanocluster, nanolayer, thermophoresis, Brownian motion etc. The thermal conductivity of nanofluids significantly relies on these mechanisms. This is due to its great capacity of enhancement in the flow characteristics and heat transfer. But, it has some drawbacks too, for example, increment in the pressure drop, long term stability of nanoparticles, etc. Hybrid nanofluids are made by the inserting two distinct type of nanoparticles in any

[1] Case(a): Published in "**Computational Thermal Sciences: An International Journal**" 13(5), 31–43, (2021), Case(b): Communicated to "**International Journal for Numerical Methods in Fluids**".

suitable base fluid. It consists of some additional properties in comparison to the regular nanofluids. The main idea behind its use is to increase the favourable properties of regular nanofluids and to overcome the drawbacks involved in regular nanofluid as much as possible. Following this concept, a few drawbacks can be resolved and this is the reason that hybrid nanofluid concept becomes more significant.

A detailed review of the preparation and thermal properties including friction factor and heat transfer is provided by Akilu *et al.* [2]. Hassan *et al.* [43] investigated hybrid nanoparticle impact on the thermal and momentum boundary layer flows over the wedge. Waini *et al.* [129] explained the mixed convective flow involving nanofluid based on hybrid structure in a porous medium. Recently, a new hybridity model is well developed by Dinarvand and Rostami [29] which involves the analysis of shape factor effects. From literature survey, it is noticed that the flow problem related to power-law hybrid nanofluids with truncated cone as a geometry is not properly explored though it carries a variety of applications. So, the aim of the present chapter is to analyse the basic impact of nanoparticle volume fraction on flow characteristics.

6.2 Mathematical Analysis

In this chapter, the free and mixed convective flows of a power-law hybrid nanofluids over a truncated cone in a non-Darcy porous medium, are considered. This chapter is an extension of previous chapter by taking both Ti-alloy and Multi Walled Carbon Nanotubes (MWCNTs) nanoparticles at a time. The physical model with coordinate system is taken as displayed in Fig. 5.1. Considering all the assumptions and approximations of previous chapter, the governing equations for the power-law hybrid nanofluid flows over a truncated cone are given by

$$\frac{\partial(ru)}{\partial x}+\frac{\partial(rv)}{\partial y}=0, \tag{6.1}$$

$$\frac{\partial u^n}{\partial y}+\frac{b\,K^*\,\rho_{hnf}}{\mu_{hnf}}\frac{\partial u^2}{\partial y}=\frac{K^*\,g\,(\rho\,\beta)_{hnf}\,\cos\gamma}{\mu_{hnf}}\frac{\partial T}{\partial y}, \tag{6.2}$$

$$u\frac{\partial T}{\partial x}+v\frac{\partial T}{\partial y}=\frac{k_{hnf}}{\rho_{hnf}\,(C_P)_{hnf}}\frac{\partial}{\partial y}\left[\frac{\partial T}{\partial y}\right], \tag{6.3}$$

subject to the boundary conditions

$$\begin{aligned} v(x,\,y)=0,\;\; T(x,\,y)=T_w \qquad & \text{at} \quad y=0 \\ u(x,\,y)\to u_\infty,\quad T(x,\,y)\to T_\infty \qquad & \text{as} \quad y\to\infty \end{aligned} \tag{6.4}$$

where ρ_{hnf}, μ_{hnf}, β_{hnf}, k_{hnf} and C_{Phnf} denote the density, dynamic viscosity, thermal expansion coefficient, thermal conductivity and specific heat capacity of the power-law hybrid nanofluid respectively. Also, b, g, γ, T, u_∞ and (u, v) is used for the empirical constant, acceleration due to gravity, inclination of angle, temperature, free stream and Darcian velocities individually. The three values of the power-law index $n<1$, $n=1$ and $n>1$ denote the pseudoplastic, Newtonian and dilatant hybrid nanofluids respectively. The modified permeability K^* of the porous medium which depends on power-law index n.

This chapter is analyzed for two types (cases) of problems: (a) free/natural convection and (b) mixed convection.

6.2.1 Case(a): Natural Convection

In this case, the flow is caused by only buoyancy forces and without any external velocity ($i.e., u_\infty=0$). Hence, the non-dimensional relations utilized to get the non-dimensional form of equations (6.2)-(6.4) are

$$\xi=\frac{\bar{x}}{x_0},\;\; \eta=\frac{y}{\bar{x}}\,Ra^{\frac{1}{2}},\;\; T(\xi,\eta)=T_\infty+(T_w-T_\infty)\;\theta(\xi,\eta),\;\; \psi(\xi,\eta)=\alpha_f\,r\,Ra^{\frac{1}{2}}\,f(\xi,\eta), \tag{6.5}$$

where $Ra=\dfrac{\bar{x}}{\alpha_f}\left(\dfrac{(\rho\,\beta)_f\,g\,K^*\,cos\,\gamma\,(T_w-T_\infty)}{\mu_f}\right)^{\frac{1}{n}}$ is the local modified Darcy-Rayleigh number and α_f is the base fluid's thermal diffusivity.

Using these transformations (6.5) in the equations (6.2) to (6.3) and the boundary con-

ditions (6.4), the resultant equations become

$$\left[n\ (f')^{n-1}\ + 2\,A_1\,Gr^*\,f'\right] f'' = A_2\,\theta', \tag{6.6}$$

$$2A_3\,(\xi+1)\,\theta'' + (3\xi+1)\,f\theta' = 2\xi(\xi+1)\left(f'\frac{\partial\theta}{\partial\xi} - \frac{\partial f}{\partial\xi}\theta'\right), \tag{6.7}$$

$$\begin{gathered} f(\xi,0) + \frac{2\,\xi\,(\xi+1)}{3\,\xi+1}\left[\frac{\partial f}{\partial\xi}\right]_{\eta=0} = 0, \quad \theta(\xi,0) = 1, \\ f'(\xi,\eta)\to 0, \quad \theta(\xi,\eta)\to\ 0\ \ as\ \ \eta\to\infty. \end{gathered} \tag{6.8}$$

where the differentiation in respect of η is denoted by primes and $Gr^* = \dfrac{b\,K^*}{\nu_f}\left(\dfrac{\alpha}{\bar{x}}Ra\right)^{2-n}$. Symbol ν_f is the kinematic viscosity and Gr^* is the modified Grashof number. The expressions of A_1, A_2 and A_3 which depend on nanoparticle volume fraction can be given as:

$$A_1 = \frac{\mu_f}{\mu_{hnf}}\left[(1-\phi_1)(1-\phi_2) + \phi_1(1-\phi_2)\frac{\rho_{s1}}{\rho_f} + \phi_2\frac{\rho_{s2}}{\rho_f}\right],$$

$$A_2 = \frac{\mu_f}{\mu_{hnf}}\left[(1-\phi_1)(1-\phi_2) + \phi_1(1-\phi_2)\frac{(\rho\,\beta)_{s1}}{(\rho\,\beta)_f} + \phi_2\frac{(\rho\,\beta)_{s2}}{(\rho\,\beta)_f}\right],$$

$$A_3 = \frac{\left[\dfrac{k_{s2}+2\,k_{nf}-2\,\phi_2\,(k_{nf}-k_{s2})}{k_{s2}+2\,k_{nf}+\phi_2\,(k_{nf}-k_{s2})}\right]\left[\dfrac{2\,k_f+k_{s1}-2\,\phi_1\,k_f+2\,\phi_1\,k_{s1}}{2\,k_f+k_{s1}+\phi_1\,k_f-\phi_1\,k_{s1}}\right]}{\left[(1-\phi_1)(1-\phi_2)+\phi_1\,(1-\phi_2)\,\dfrac{(\rho\,C_P)_{s1}}{(\rho\,C_P)_f} + \phi_2\dfrac{(\rho\,C_P)_{s2}}{(\rho\,C_P)_f}\right]},$$

where

$$k_{nf} = \left[\frac{2\,k_f+k_{s1}-2\,\phi_1\,k_f+2\,\phi_1\,k_{s1}}{2\,k_f+k_{s1}+\phi_1\,k_f-\phi_1\,k_{s1}}\right]k_f\ .$$

Here, ϕ_1 and ϕ_2 are the volume fraction of Ti-alloy and MWCNTs particles respectively. The suffixes *f*, *nf*, *s1* and *s2* are used to denote the base fluid, regular nanofluid, Ti-alloy and MWCNTs nanoparticles. The different thermo-physical properties associated to these nanoparticles together with the base fluid are given in the Table (5.1) of *Chapter-5*.

This problem can be utilized to study the Ostwald-de Waele power-law type of hybrid nanofluid flow over a full cone and along a vertical plate by considering two different values of streamwise coordinate ξ. Very large values of ξ imply $x_0 = 0$ which leads the problem over a full cone. Similarly, $\xi = 0$ (i.e., $x = x_0$) indicates flow problem along a vertical plate. These possible limiting cases and their comparative analysis is also presented through graphs in this chapter.

Non-dimensional form of the Nusselt number $Nu_{\bar{x}} = -\dfrac{\bar{x}}{(T_w - T_\infty)} \dfrac{k_{hnf}}{k_f} \left[\dfrac{\partial T}{\partial y}\right]_{y=0}$ and the skin friction coefficient $C_f = \dfrac{2}{\rho\, u_*^2} \left[\mu_{hnf} \dfrac{\partial u}{\partial y}\right]_{y=0}$ is given by

$$\frac{Nu_{\bar{x}}}{Ra^{\frac{1}{2}}} = -\frac{k_{hnf}}{k_f}\theta'(\xi, 0), \;\; \frac{1}{2}\frac{Ra^{\frac{1}{2}}}{Pr} C_f = \frac{\mu_{hnf}}{\mu_f} f''(\xi, 0), \tag{6.9}$$

where u_* and Pr represent the characteristic velocity and the Prandtl number respectively.

Results and Discussion

Utilizing the numerical procedure explained in Chapter-2, the governing equations (6.6)-(6.7) along with the boundary conditions (6.8) are solved in this chapter. In addition to this, the validation of present problem has been conducted as it was done in the case (a) of *Chapter-2* by putting $\xi = 0$ in the absence of nanoparticle volume fraction.

The volume fraction of Ti-alloy and MWCNTs are denoted by ϕ_1 and ϕ_2 respectively to discuss the results. Also, $\phi_1 = 0.1$, $\phi_2 = 0.02$ and $\xi = 2.5$ are fixed throughout the computation unless otherwise mentioned. Here, the detailed description about the influence of volume fraction of Ti-alloy and MWCNTs is given. It includes the graphs of non-dimensional velocity, temperature, Nusselt number and skin friction coefficient to get a proper understanding of ϕ_1 and ϕ_2 influences. Figs. 6.1 and 6.2 display the impact of volume fraction of Ti-alloy nanoparticle (ϕ_1) and MWCNTs nanoparticle (ϕ_2) respectively. These graphs also include the impact on dilatant and pseudoplastic hybrid nanofluids as specified in the figure itself.

The influence of ϕ_1 and ϕ_2 on velocity profiles is displayed in Figs. 6.1(a) and 6.2(a) respectively. The domination of dilatant hybrid nanofluid over the pseudoplastic hybrid nanofluid is also noted in both these graphs. The velocity is decreased with ϕ_1 and ϕ_2 increments and these variations are more for a small change in the volume fraction of MWCNTs nanoparticle. It is noticed that all the profiles asymptotically satisfied the boundary conditions at infinity, so this is another way to show the accuracy of these numerical results. This asymptotic condition is satisfied by the temperature profiles too. The temperature profiles are increased with increments in volume fraction of both the nanoparticles ϕ_1 and ϕ_2 as displayed in Figs. 6.1(b) and 6.2(b) respectively. But, opposite to the velocity profiles, there is domination of pseudoplastic hybrid nanofluid over dilatant hybrid nanofluid. The physical reason behind this enhancement in temperature profiles with the nanoparticle volume fraction increment is the increased thermal conductivity when larger ϕ_1 and ϕ_2 are used because solid particles have larger thermal conductivity in comparison with the base fluid.

In Figs. 6.1(c) and 6.2(c), the significance of ϕ_1 and ϕ_2 on non-dimensional heat transfer rate (Nusselt number) for both the dilatant and pseudoplastic hybrid nanofluids is presented. In this case, the analysis is done in respect of streamwise coordinate ξ. It is noticed that the heat transfer rate is decreased with the addition of volume fraction of nanoparticle. In the study, there is again domination of dilatant hybrid nanofluids over pseudoplastic hybrid nanofluids. For very small values of ξ, the heat transfer is very less and there is rapid increment in the range near zero. For higher values (after $\xi = 5$), the Nusselt number becomes constant. In this way, it is observed that heat transfer rate over a truncated cone lies between heat transfer rate over vertical plate ($\xi = 0$) and full cone ($\xi \to 0$) geometries.

The same kind of analysis is done for the skin friction coefficient too. The impact of ϕ_1 and ϕ_2 variations on non-dimensional skin friction coefficient for both the dilatant and pseudoplastic hybrid nanofluids is displayed in Figs. 6.1(d) and 6.2(d) respectively. As the volume fraction of nanoparticle is increased, the skin friction coefficient, in absolute values, decreases for both Ti-alloy and MWCNTs. The skin friction coefficient, in absolute values, is greater for dilatant hybrid nanofluid when compared to the pseudoplastic hybrid nanofluid for each nanoparticle volume fraction undertaken. A sharp increment in its magnitude is

noted when ξ is nearly zero. For higher values, it almost becomes constant or change is negligible. So, it can be said that the skin friction coefficient in a fluid flow over a truncated cone lies between the skin friction coefficient in flow over vertical plate ($\xi = 0$) and full cone ($\xi \to 0$) as in the case of heat transfer rate.

The three values of modified Grashof number are used to analyse its influence on velocity and temperature profiles, heat transfer rate and skin friction coefficient in this case. This influence is portrayed in Fig. 6.3. The Grashof number plays the same role in natural convection which is played by the Reynolds number in forced convective flow. It depends on the dynamic, geometric and thermodynamic parameters of the heat transport problem. In the case of non-zero increasing values of Gr^*, there is reduction in the flow intensity and increment in the inertial effects which thickens the boundary layer and resist the heat transfer which is noticed in Fig. 6.3(c). From the Fig. 6.3(a), it is seen that the velocity profiles are also decreased with increment in the modified Grashof number. The domination of dilatant hybrid nanofluid is noted over the pseudoplastic hybrid nanofluid from both these graphs. But, the temperature profiles are increased with its increment and pseudoplastic hybrid nanofluid dominates here in these profiles as depicted in Fig. 6.3(b). The influence of Gr^* on magnitude of skin friction coefficient is shown in Fig. 6.3(d) and large decrement in its magnitude is readily visible with the domination of pseudoplastic hybrid nanofluid. Similar to the previous cases, this analysis is also helpful in the study of fluid flow over full cone and vertical plate.

The variation in velocity and temperature profiles with respect to streamwise coordinate is shown in Fig. 6.4. It is observed that the velocity profiles are higher for dilatant hybrid nanofluid and there is decrement with higher values of ξ. The same trend is observed for temperature profiles too but in this case, there is domination of pseudoplastic hybrid nanofluid over the dilatant hybrid nanofluid. It can be said from these graphs that the velocity and temperature in these kind of flow over a truncated cone fall between the vertical plate and full cone.

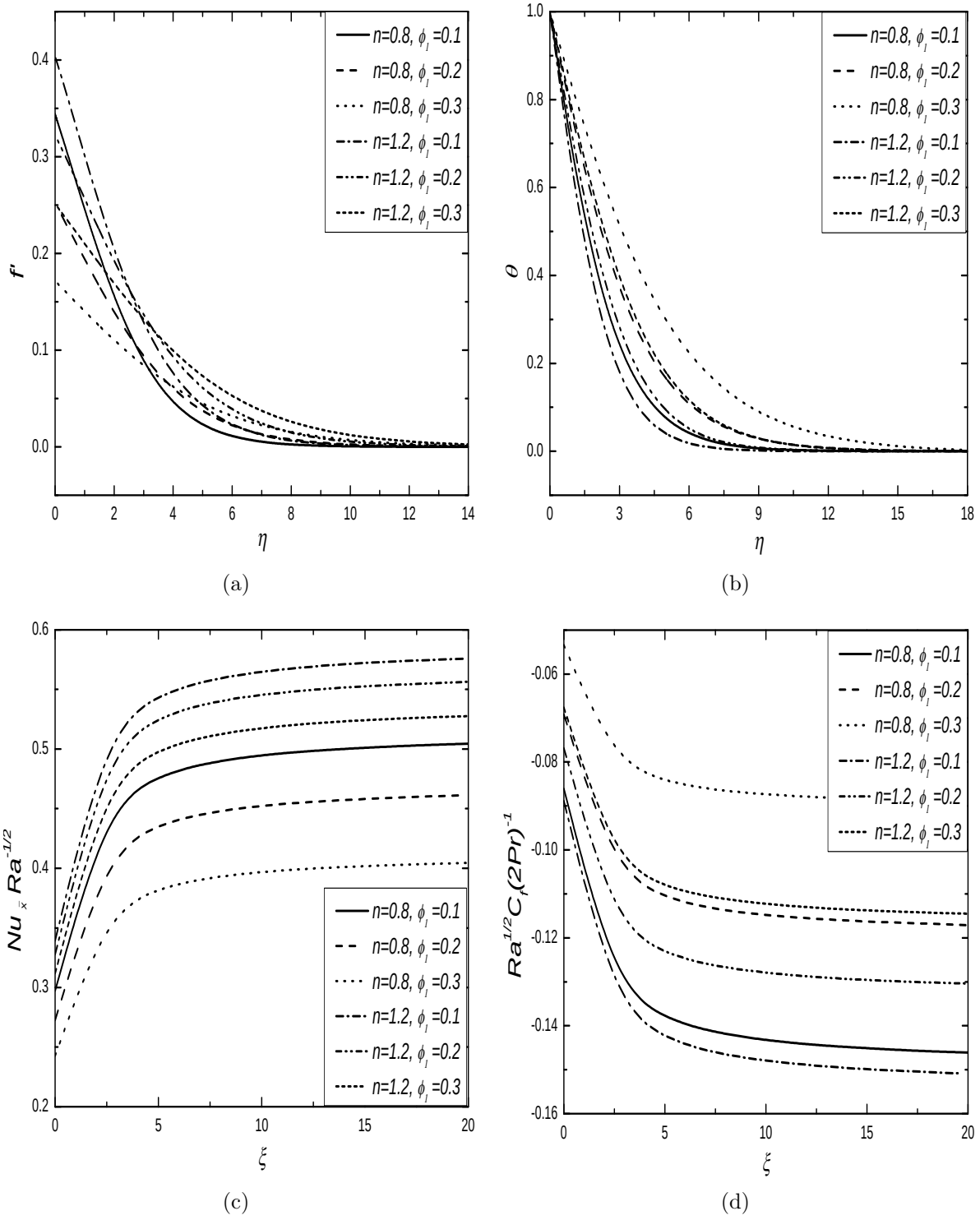

Figure 6.1: *Effect of volume fraction of Ti-alloy (ϕ_1) on (a) velocity and (b) temperature profiles, (c) Nusselt number and (d) skin friction coefficient for pseudoplastic and dilatant hybrid nanofluids.*

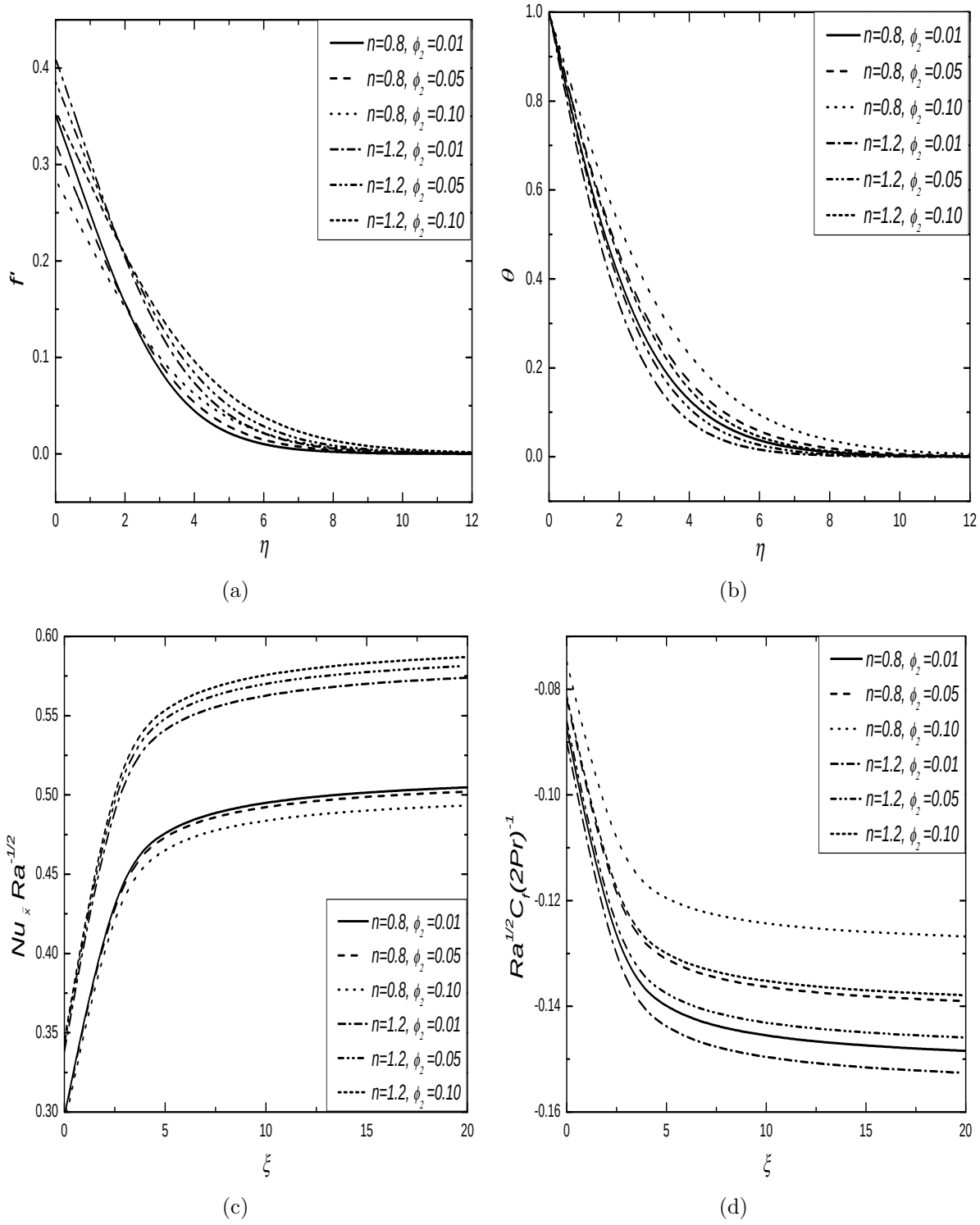

Figure 6.2: *Effect of volume fraction of MWCNTs (ϕ_2) on (a) velocity and (b) temperature profiles, (c) Nusselt number and (d) skin friction coefficient for pseudoplastic and dilatant hybrid nanofluids.*

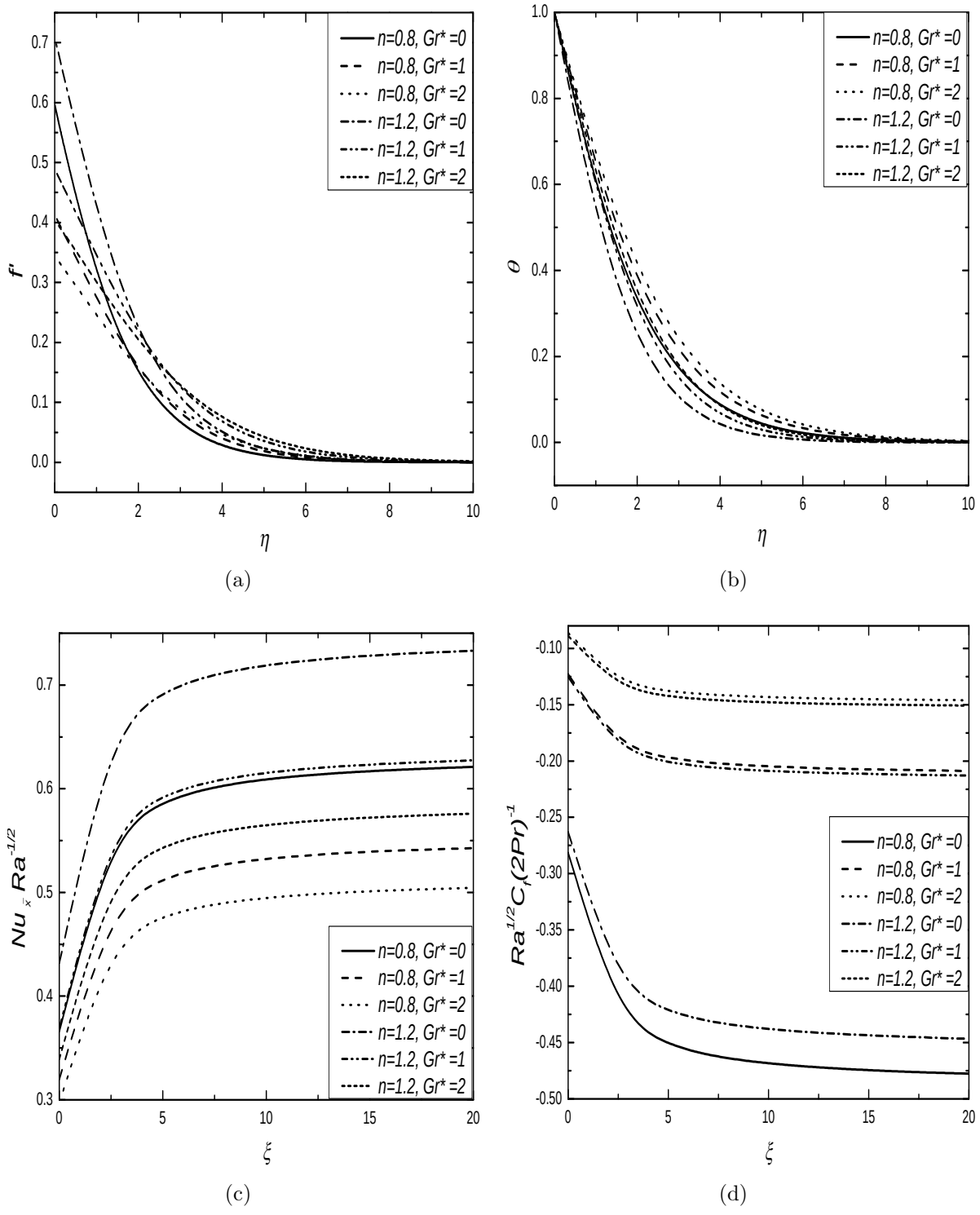

Figure 6.3: *Effect of Gr^* on (a) velocity and (b) temperature profiles, (c) Nusselt number and (d) skin friction coefficient for pseudoplastic and dilatant hybrid nanofluids.*

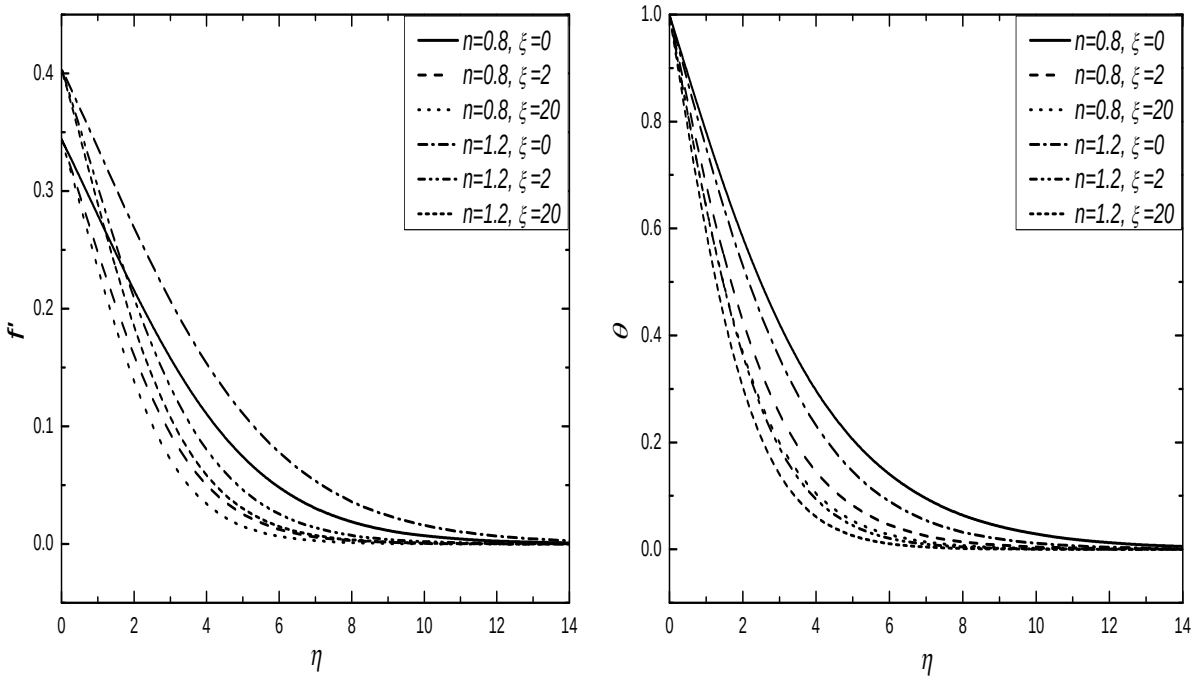

(a) (b)

Figure 6.4: *Effect of ξ on (a) velocity and (b) temperature profiles for pseudoplastic and dilatant hybrid nanofluids.*

6.2.2 Case(b): Mixed Convection

In this case, the flow arises from both buoyancy forces and an external flow with the velocity u_∞. To get the non-dimensional form of flow governing equations, the dimensionless transformations are given below

$$\begin{gathered}\xi = \frac{\bar{x}}{x_0}, \;\; \eta = \frac{y}{\bar{x}}\, Pe^{\frac{1}{2}}, \;\; \psi(\xi,\eta) = \alpha_f\, r\, Pe^{\frac{1}{2}}\, f(\xi,\eta), \\ T(\xi,\eta) = T_\infty + (T_w - T_\infty)\; \theta(\xi,\eta),\end{gathered} \tag{6.10}$$

where $Pe = \dfrac{u_\infty\, \bar{x}}{\alpha_f}$ is the local Peclet number and α_f is the thermal diffusivity of base fluid.

Using these transformations (6.10) in the equations (6.2) to (6.3) and boundary conditions (6.4), the non-dimensional form of equations become

$$n\, f''\; (f')^{n-1} \; + 2\, A_1\, Fs\, f''\, f' = \lambda^n\, A_2\, \theta', \tag{6.11}$$

$$2A_3\,(\xi+1)\,\theta'' + (3\xi+1)\, f\theta' = 2\xi(\xi+1)\left(f'\frac{\partial\theta}{\partial\xi} - \frac{\partial f}{\partial\xi}\theta'\right), \tag{6.12}$$

together with the resultant boundary conditions

$$f(\xi,0) + 2\,\frac{\xi\,(\xi+1)}{(3\,\xi+1)}\left[\frac{\partial f}{\partial\xi}\right]_{\eta=0} = 0,\;\; \theta(\xi,0) = 1, \;\; f'(\xi,\eta)\to 1,\, \theta(\xi,\eta)\to 0 \;\; as \;\; \eta\to\infty, \tag{6.13}$$

where primes denote differentiation in respect of η, $Ra = \dfrac{\bar{x}}{\alpha_f}\left(\dfrac{(\rho\,\beta)_f\, g\, K^*\, cos\,\gamma\,(T_w - T_\infty)}{\mu_f}\right)^{\frac{1}{n}}$, $\lambda = \dfrac{Ra}{Pe}$ and $Fs = \dfrac{b\,K^*\; u_\infty^{2-n}}{\nu_f}$. Here, Ra is the local modified Darcy-Rayleigh number, λ is the mixed convection parameter, ν_f is the kinematic viscosity, Fs is the non-Darcian parameter (Forchheimer number). The expressions of A_1, A_2 and A_3 which depend on nanoparticle volume fraction are given in Case (a) of this chapter.

Non-dimensional representation of the heat transfer rate $Nu_{\bar{x}} = -\dfrac{\bar{x}}{(T_w - T_\infty)}\dfrac{k_{hnf}}{k_f}\left[\dfrac{\partial T}{\partial y}\right]_{y=0}$

and the skin friction coefficient $C_f = \dfrac{2}{\rho\, u_\infty^2}\left[\mu_{hnf}\dfrac{\partial u}{\partial y}\right]_{y=0}$ is given by

$$\frac{Nu_{\bar{x}}}{Pe^{\frac{1}{2}}} = -\frac{k_{hnf}}{k_f}\theta'(\xi,0),\ \ \frac{1}{2}\frac{Pe^{\frac{1}{2}}}{Pr}C_f = \frac{\mu_{hnf}}{\mu_f}f''(\xi,0). \tag{6.14}$$

Results and Discussion

The governing equations (6.11)-(6.12) along with the boundary conditions (6.13) are solved numerically using spectral local linearisation method (SLLM) together with the non-similarity approach as explained in *Chapter-2*. Validation of the present problem has been conducted as it was done in the case (b) of *Chapter-2* by putting $\xi = 0$ and $Fs = 0$ in the absence of nanoparticle volume fraction.

The volume fraction of Ti-alloy and MWCNTs is denoted by ϕ_1 and ϕ_2 respectively to discuss the results. Also, $Fs = 0.5$, $\phi_1 = 0.1$, $\phi_2 = 0.02$, $\lambda = 3$ (for aiding flow), $\lambda = -3$ (for opposing flow) and $\xi = 2.5$ are unchanged during calculation otherwise described separately. A graphical representation of dimensionless velocity, temperature, heat transfer rate and skin friction coefficient for the opposing and aiding flows is provided to get a proper understanding of this physical model. Figs. 6.5-6.6 and 6.7-6.8 display the influence of ϕ_1 and ϕ_2 respectively.

As expected, the greater velocity is noticed for aiding flows in comparison to opposing flows (Figs. 6.5(a), 6.6(a) and 6.7(a), 6.8(a)). The dominance of dilatant hybrid nanofluid over the pseudoplastic hybrid nanofluid for these flows is also found. The velocity is reduced when ϕ_1 and ϕ_2 are increased and these changes are more in the case of smaller values of ϕ_2. There is slight variation in temperature profiles for opposing and aiding flows for respective values of ϕ_1 and ϕ_2 (Figs. 6.5(b), 6.6(b) and 6.7(b), 6.8(b)). The dominance of pseudoplastic hybrid nanofluid on dilatant hybrid nanofluid is noticed for the temperature profiles which is different from the velocity profiles. As ϕ_1 and ϕ_2 escalates, there is increase in the temperature profile because of the increased thermal conductivity when larger ϕ_1 and ϕ_2 are used. Physically, the solid particle has larger thermal conductivity in comparison with

the base fluid.

The influence of ϕ_1 and ϕ_2 alterations with respect to the streamwise coordinate ξ on Nusselt number in the case of dilatant and pseudoplastic hybrid nanofluids for both opposing and aiding flows, is presented in Figs. 6.5(c), 6.6(c) and 6.7(c), 6.8(c) respectively. Higher Nusselt number is noticed in the case of aiding flow for pseudoplastic and dilatant hybrid nanofluids. With further addition of ϕ_1 and ϕ_2, greater heat transfer is noticed because of higher thermal conductivity of Titanium alloy and MWCNTs. In physical aspect, collision of various nanoparticles is enhanced after insertion of ϕ_1 and ϕ_2. Therefore, the dissipation of energy takes place in the form of heat which results higher Nusselt number. Dominance of the dilatant hybrid nanofluid is again noticed in this case. With smaller ξ values, lesser Nusselt number is found and sharp increase is observed near zero. With grater values ($\xi = 5$ beyond), the heat transfer rate becomes stable. One important observation is that the Nusselt number in a flow past truncated cone lies between the Nusselt number in a flow past full cone ($\xi \to 0$) and vertical plate ($\xi = 0$).

Similar to the heat transfer rate, impact of ϕ_1 and ϕ_2 alterations on dimensionless skin friction coefficient in opposing and aiding flows for pseudoplastic and dilatant hybrid nanofluids, is presented in Figs. 6.5(d), 6.6(d) and 6.7(d), 6.8(d) respectively. Greater negative skin friction coefficient is observed for aiding flow in the case of pseudoplastic and dilatant fluids. With further addition of ϕ_1 and ϕ_2, its magnitude declines for Titanium alloy and MWCNTs. The dominance of dilatant hybrid nanofluid is retained as its smaller magnitude is noticed for pseudoplastic hybrid nanofluid for all the values of ϕ_1 and ϕ_2 undertaken. A sharp increase is observed near zero in this study too. With greater ξ values, the variation is very less. Again, it may be pointed out that the skin friction coefficient for fluid flow past a truncated cone lies between the skin friction coefficient for flow past a full cone ($\xi \to 0$) and vertical plate ($\xi = 0$) as in the case of heat transfer rate.

The Fig. 6.9 shows the variation in velocity and temperature in respect of ξ for opposing (Figs. 6.9(a)-6.9(b)) and aiding (Figs. 6.9(c)-6.9(d)) flows. Higher velocity in the case of dilatant hybrid nanofluid is noticed in comparison with pseudoplastic hybrid nanofluid. On the other hand, reverse nature is observed in the case of temperature profiles for opposing and

aiding flows. With ξ increments, there is decrement in each profile and hence it can be said that the velocity and temperature are higher for the flow past a vertical plate. Therefore, these are minimal for full cone and this study of flow past a truncated cone lies between them. It can be considered as an additional feature of this type of flow study which gives a feasibility of simultaneous study of flow field past full cone and vertical plate geometries. Also, the different profiles with respect to different ξ values prove the non-similar property of this considered flow.

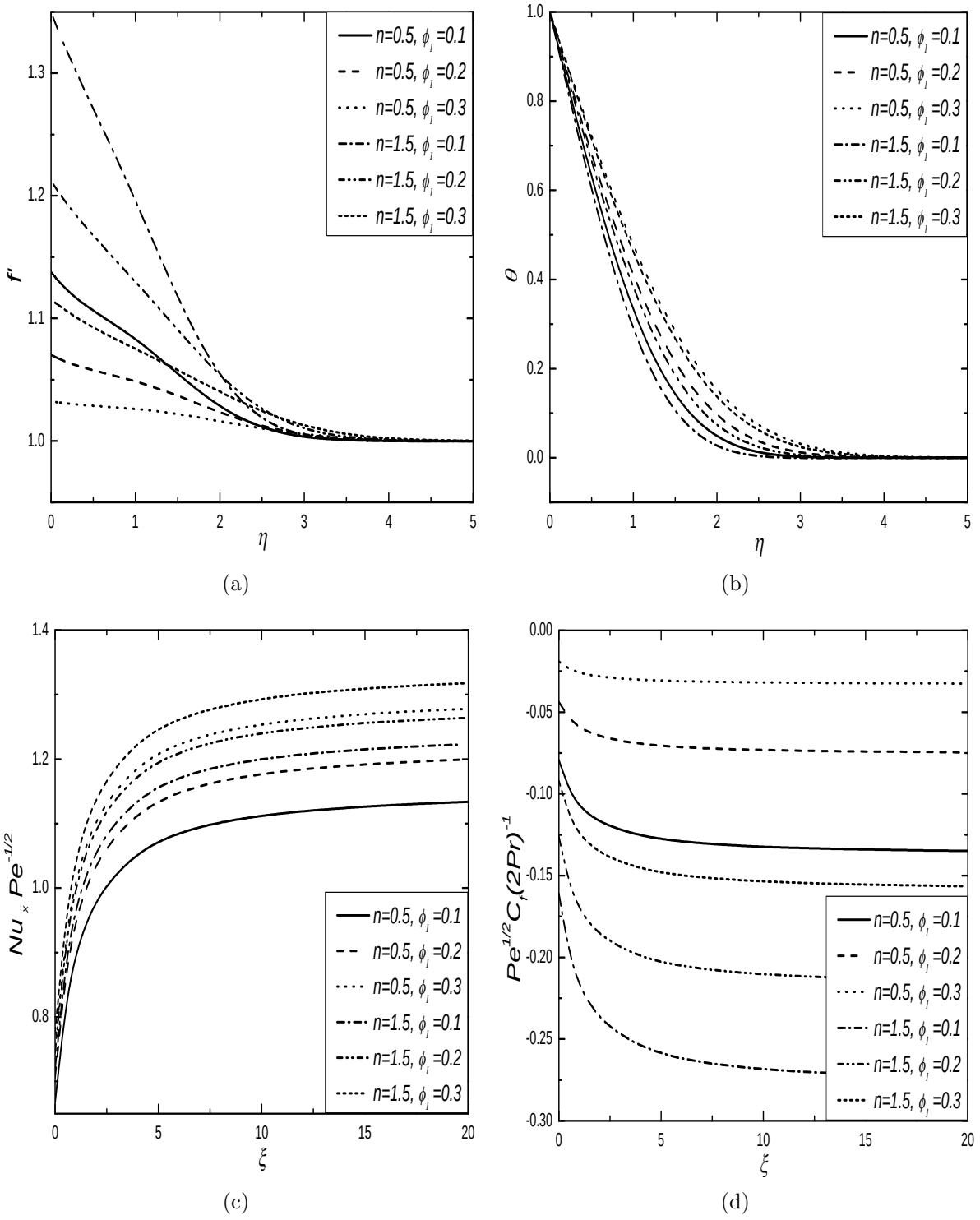

Figure 6.5: *Effect of volume fraction of Ti-alloy (ϕ_1) on (a) velocities, (b) temperatures, (c) Nusselt number and (d) skin friction coefficient for pseudoplastic and dilatant hybrid nanofluids in opposing flows.*

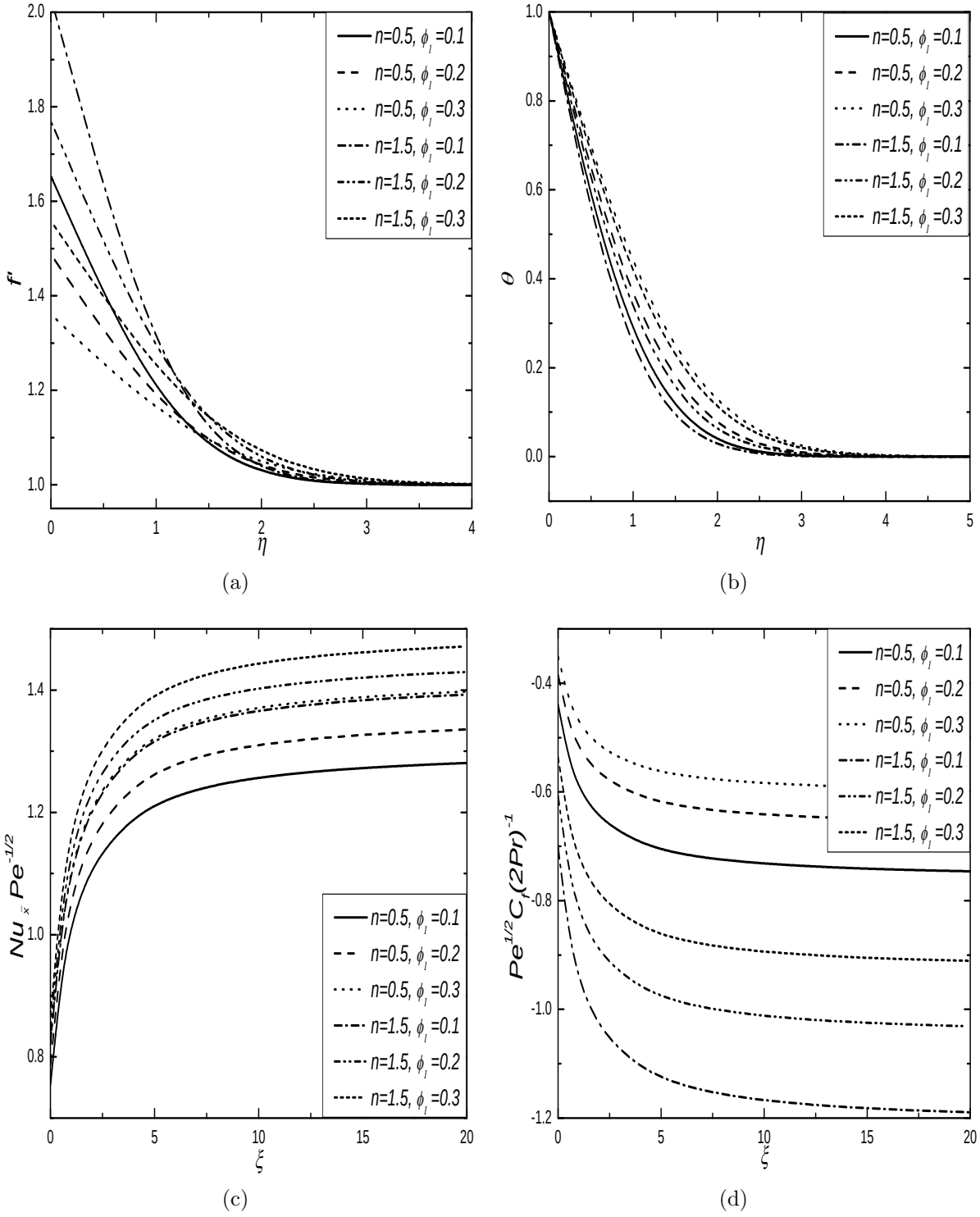

Figure 6.6: *Effect of volume fraction of Ti-alloy (ϕ_1) on (a) velocities, (b) temperatures, (c) Nusselt number and (d) skin friction coefficient for pseudoplastic and dilatant hybrid nanofluids in aiding flows.*

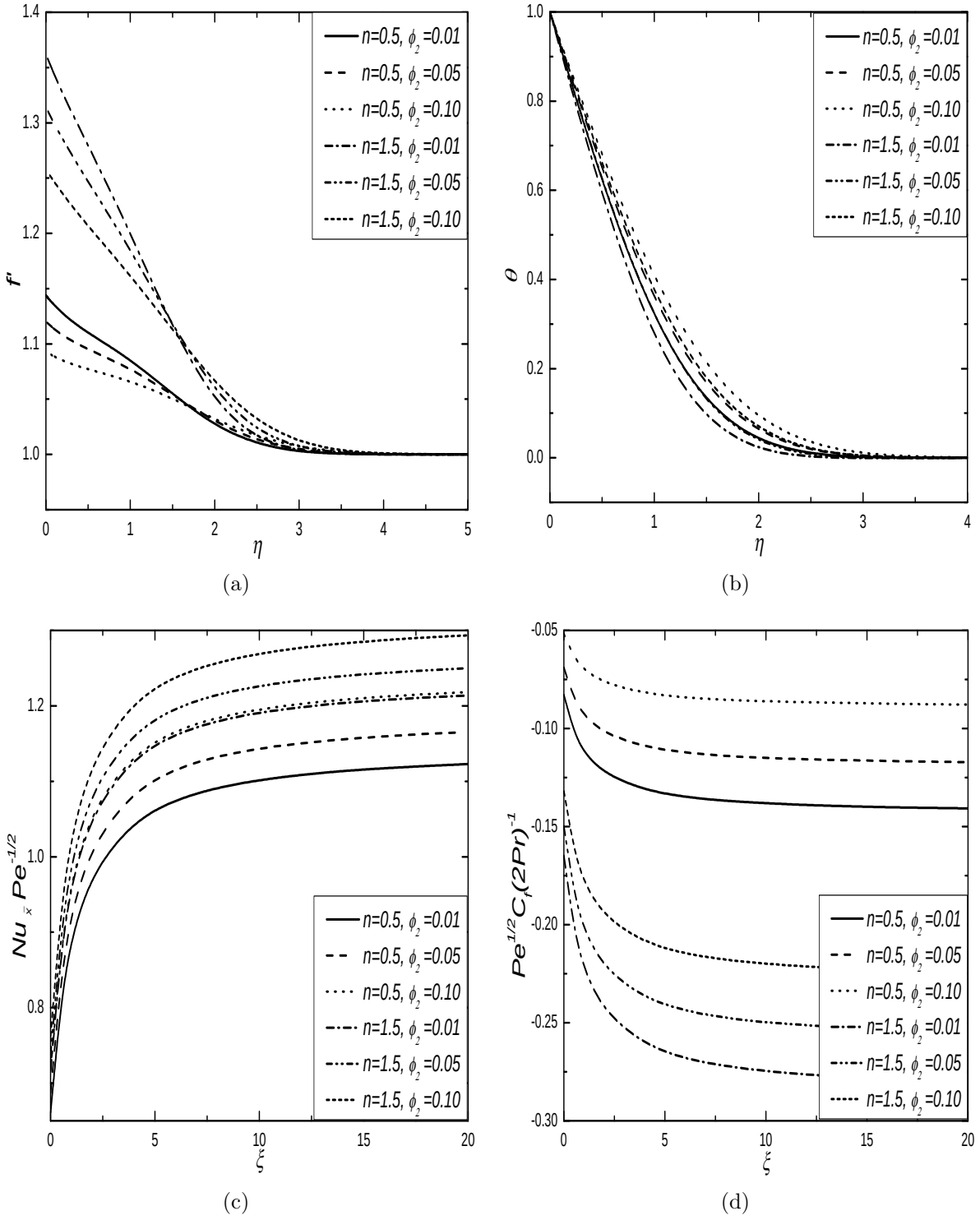

Figure 6.7: *Effect of volume fraction of MWCNTs (ϕ_2) on (a) velocities, (b) temperatures, (c) Nusselt number and (d) skin friction coefficient for pseudoplastic and dilatant hybrid nanofluids in opposing flows.*

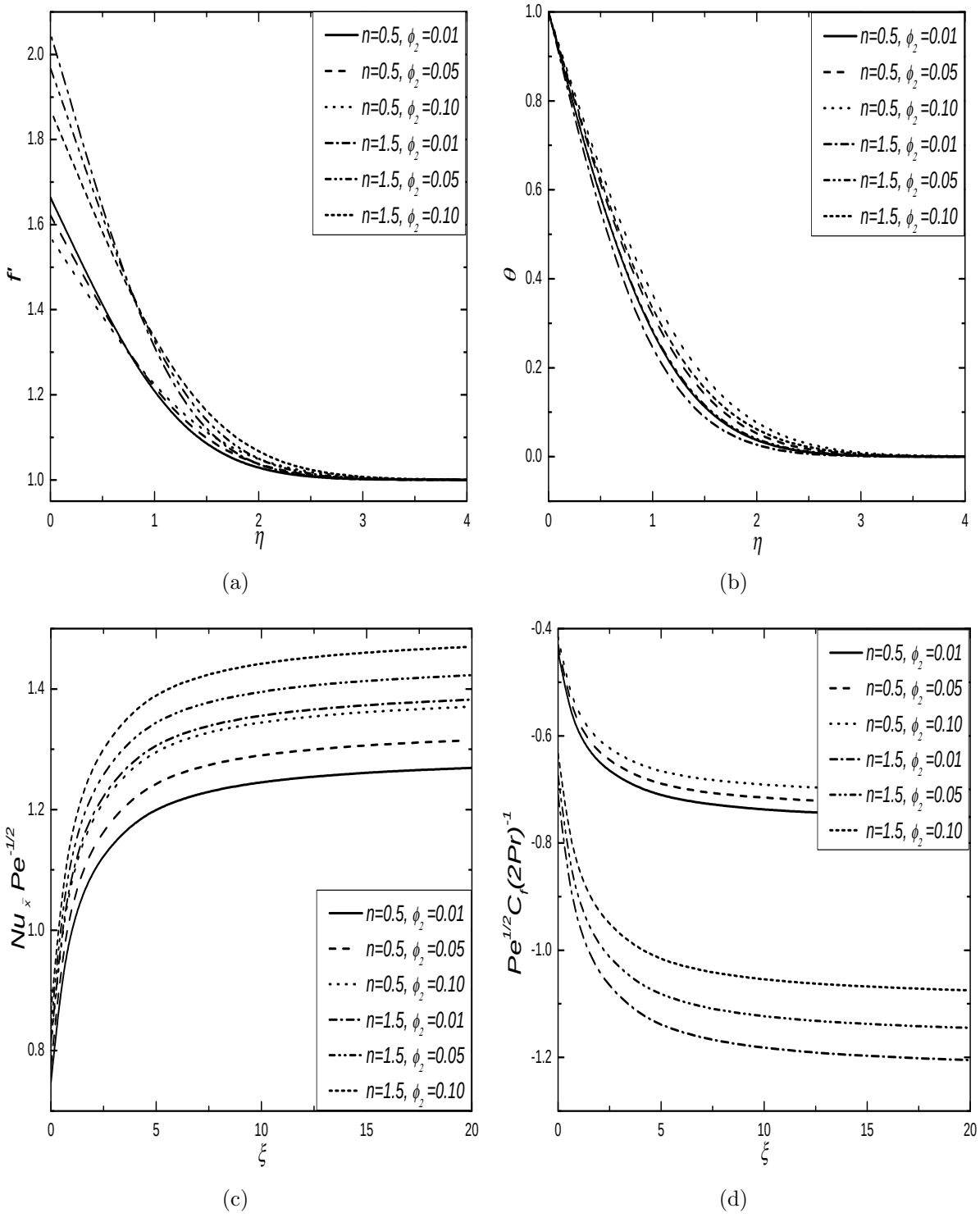

Figure 6.8: *Effect of volume fraction of MWCNTs (ϕ_2) on (a) velocities, (b) temperatures, (c) Nusselt number and (d) skin friction coefficient for pseudoplastic and dilatant hybrid nanofluids in aiding flows.*

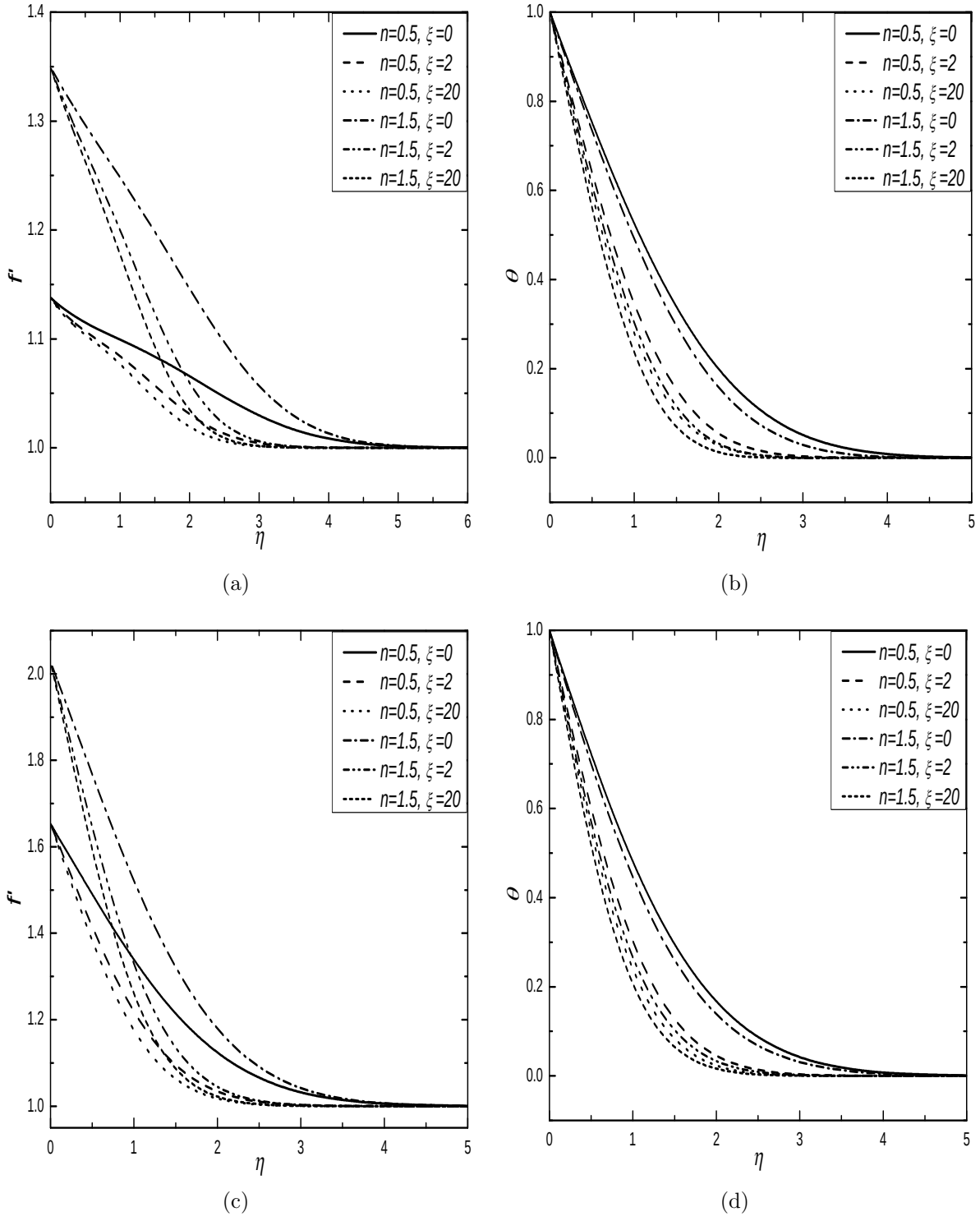

Figure 6.9: *Influence of* ξ *on velocities and temperatures for pseudoplastic and dilatant hybrid nanofluids in the case of (a), (b) opposing flows and (c), (d) aiding flows.*

6.3 Conclusions

In this chapter, a detailed analysis of power-law hybrid nanofluid flows over a truncated cone placed in a non-Darcy porous medium, is given for the two cases: (a) natural convection and (b) mixed convection. The Ti-alloy (Ti6Al4V) and multi walled carbon nanotubes (MWCNTs) are used together as nanoparticles in the base fluid water to get the power-law hybrid nanofluid model. The conclusive remarks of this work in both the cases (a) and (b) for physically suitable values of flow governing parameters, are:

Case (a): Natural Convection

- Higher velocity is obtained for the dilatant hybrid nanofluid over pseudoplastic hybrid nanofluid and the velocity is decreased with ϕ_1 and ϕ_2 increments.
- There is domination of pseudoplastic hybrid nanofluid over dilatant hybrid nanofluid for the temperature profiles and the temperature is enhanced with increment in ϕ_1 and ϕ_2.
- The addition of nanoparticle volume fraction results into lower heat transfer rate and again the dilatant hybrid nanofluid dominates.
- The changes in all the profiles for various values of streamwise coordinate ξ show the non-similar nature of this problem.

Case (b): Mixed Convection

- The dominance of pseudoplastic hybrid nanofluid over dilatant hybrid nanofluid for the temperature profiles is noticed and the temperature is enhanced with increment in ϕ_1 and ϕ_2.
- The Nusselt number is greater for aiding flows in the case of pseudoplastic and dilatant fluids. The further insertion of ϕ_1 and ϕ_2 increases Nusselt number values due to enhanced collision among nanoparticles which dissipates energy in the form of heat.

- Larger magnitude of skin friction coefficient is noticed in the case of dilatant hybrid nanofluid with each ϕ_1 and ϕ_2 value for opposing and aiding flows.
- The magnitude of skin friction coefficient and Nusselt number for this flow past truncated cone is observed between full cone and vertical plate geometries.

Chapter 7

Summary and Conclusions

The steady, two-dimensional natural and mixed convective flows of power-law fluids, power-law nanofluids and power-law hybrid nanofluids over a truncated cone in a non-Darcy porous medium have been investigated in this thesis. Ostwald-de Waele type of power-law fluids, namely the pseudoplastic and dilatant fluids, are taken into the consideration in all the chapters. Incorporating a suitable set of dimensionless variables, the governing equations are transformed into a system of nonlinear ordinary differential equations and then solved by using combined approach of local non-similarity technique and spectral local linearisation method. The attention is given to explain the effects of Biot number, thermal dispersion, thermal stratification, nonlinear convection, viscous dissipation, thermal radiation, nanoparticle volume fraction, streamwise coordinate, mixed convection and non-Darcy parameters on the various profiles and physical quantities. The important observations are as follows:

- The velocity, temperature and Nusselt number are increased but the skin friction coefficient is reduced with increasing values of Biot number (Bi) for the power-law fluids in both the natural and mixed convection cases. Further, the flow separation is identified and it is more in the pseudoplastic fluid in comparison with the dilatant fluid for larger values of the mixed convection parameter (λ).

- Thermal stratification parameter (S_T) decreases the temperature, velocity and rate of heat transfer with its higher values. But, the opposite trend is seen in the case of

skin friction coefficient for power-law fluids with increasing values of S_T. This analysis shows that the separation of flow is less in the thermally stratified power-law fluids but it is more in the thermally unstratified power-law fluids.

- The thermal dispersion parameter (Ds) enhances temperature, velocity, heat transfer rate and magnitude of skin friction coefficient for the power-law fluids. The variation in skin friction coefficient is more for the opposing flow case in comparison with the aiding flow case for enhancing values of Ds.

- Increasing values of the nonlinear convection parameter (α_1) give increment in the velocity profiles and decrement in the temperature profiles. Also, the heat transfer rate is less and skin friction is more for the power-law fluids when the linear Boussinesq approximation is employed in comparison with the nonlinear Boussinesq approximation.

- The increasing values of viscous dissipation parameter (ϵ) increases the velocity for natural convection case and the dilatant fluid dominates over the pseudoplastic fluid but it decreases the same in mixed convection. Further, the temperature profiles are increased with increasing values of ϵ for both the natural and mixed convection cases.

- The entropy generation and heat transfer rates increase with an enhancement in the streamwise coordinate (ξ) for power-law fluids which shows that the heat transfer and entropy generation rates for a truncated cone are less than that for a full cone (higher values of ξ) and more than that for a vertical plate (ξ=0). The smaller values of Bejan number (Be) for higher values of ξ show the domination of irreversibility due to fluid friction in the case of a full cone.

- In natural convection case, higher velocity and temperature are obtained with increased values of the linear, quadratic and nonlinear radiation parameters along with the dominance of dilatant fluid over the pseudoplastic fluid. The phenomenon of flow separation is observed between aiding and opposing flows of the power-law fluids for linear, quadratic and nonlinear radiation cases in mixed convective flow.

- The Nusselt number is greater for enhanced values of linear, quadratic and nonlinear radiation parameters with its dominance in the aiding flow case. For the quadratic

and nonlinear radiation cases, the heat transfer rate is more in comparison with linear radiation case.

- In natural and mixed convective flows of power-law nanofluid and power-law hybrid nanofluid, the velocity is decreased and temperature is increased with an increment in the volume fraction of Titanium alloy and multi wall Carbon nanotubes.
- The addition of nanoparticle volume fraction results into lower heat transfer rate in the natural convection case but it results into higher heat transfer rate in the mixed convective flow due to increased collision among different nanoparticles which dissipates energy in the form of heat.
- Larger magnitude of skin friction coefficient is noticed for dilatant nanofluid and dilatant hybrid nanofluid in comparison with respective pseudoplastic ones for each value of the nanoparticle volume fraction in both natural and mixed convective flows.
- In the case of non-zero increasing values of modified Grashof number, there is reduction in the flow intensity and increment in the inertial effects which thickens the boundary layer and resist the heat transfer.
- The change in all the profiles for various values of the streamwise coordinate shows the non-similar nature of this problem.
- Nusselt number and magnitude of skin friction coefficient in the power-law fluid flows over a truncated cone are found to be in between a vertical plate and a full cone.

The work presented in this thesis can be extended to investigate the effects of Joule heating, magnetic field, activation energy, etc. In addition, similar analysis can be done with various non-Newtonian fluids like micropolar fluids, couple stress fluids, visco-elastic fluids, Cassion fluids, etc. Further, this work can be extended for different combinations of nanoparticles to examine the flows of new power-law nanofluids and power-law hybrid nanofluids. Moreover, the stability analysis has attracted the curiosity of many researchers in the recent past. So, this work can be extended to perform the stability analysis too. Such a challenging study can be a rewarding experience though it is typical and time consuming.

Bibliography

[1] S. Ahmad and S. Nadeem. Thermal analysis in buoyancy driven flow of hybrid nanofluid subject to thermal radiation. *International Journal of Ambient Energy, DOI: 10.1080/01430750.2020.1861090*, 2020.

[2] S. Akilu, K.V. Sharma, A.T. Baheta, and R. Mamat. A review of thermophysical properties of water based composite nanofluids. *Renewable and Sustainable Energy Reviews*, 66:654–678, 2016.

[3] O. Aydin and A. Kaya. Mixed convection of a viscous dissipative fluid about a vertical flat plate embedded in a porous medium: Constant wall temperature case. *Journal of Porous Media*, 9(6):559–580, 2006.

[4] A. Aziz. A similarity solution for laminar thermal boundary layer over a flat plate with a convective surface boundary condition. *Communications in Nonlinear Science and Numerical Simulation*, 14(4):1064–1068, 2009.

[5] P. Barnoon and D. Toghraie. Numerical investigation of laminar flow and heat transfer of non-Newtonian nanofluid within a porous medium. *Powder Technology*, 325:78–91, 2018.

[6] H.T. Basha, R. Sivaraj, and I.L. Animasaun. Stability analysis on Ag-MgO/water hybrid nanofluid flow over an extending/contracting riga wedge and stagnation point. *Computational Thermal Sciences: An International Journal*, 12(6):491–508, 2020.

[7] C.K. Batchelor and G.K. Batchelor. *An Introduction to Fluid Dynamics*. Cambridge University Press, 2000.

[8] A. Bejan. Second-law analysis in heat transfer and thermal design. *Advances in Heat Transfer*, 15:1–58, 1982.

[9] A. Bejan. *Convection Heat Transfer*. John Wiley & Sons, 2013.

[10] A. Bejan. *Entropy Generation Minimization: The Method of Thermodynamic Optimization of Finite-size Systems and Finite-time Processes*. CRC press, 2013.

[11] J. Buongiorno. Convective transport in nanofluids. *Journal of Heat Transfer*, 128(3):240–250, 2006.

[12] C. Canuto, M.Y. Hussaini, A. Quarteroni, and T.A. Zang. *Spectral Methods*. Springer, 2006.

[13] A.J. Chamkha, A.M. Rashad, M.A. Mansour, T. Armaghani, and M. Ghalambaz. Effects of heat sink and source and entropy generation on MHD mixed convection of a Cu-water nanofluid in a lid-driven square porous enclosure with partial slip. *Physics of Fluids*, 29(5):052001, 2017.

[14] W. Chaoyang, T. Chuanjing, and Z. Xiaofen. Mixed convection of non-Newtonian fluids from a vertical plate embedded in a porous medium. *Acta Mechanica Sinica*, 6(3):214–220, 1990.

[15] C.H. Chen. Magneto-hydrodynamic mixed convection of a power-law fluid past a stretching surface in the presence of thermal radiation and internal heat generation/absorption. *International Journal of Non-Linear Mechanics*, 44(6):596–603, 2009.

[16] C.Y. Cheng. Double-diffusive natural convection along a vertical wavy truncated cone in non-Newtonian fluid saturated porous media with thermal and mass stratification. *International Communications in Heat and Mass Transfer*, 35(8):985–990, 2008.

[17] C.Y. Cheng. Combined heat and mass transfer in natural convection flow from a vertical wavy surface in a power-law fluid saturated porous medium with thermal and mass stratification. *International Communications in Heat and Mass Transfer*, 36(4):351–356, 2009.

[18] C.Y. Cheng. Natural convection heat and mass transfer from a vertical truncated cone in a porous medium saturated with a non-Newtonian fluid with variable wall temperature and concentration. *International Communications in Heat and Mass Transfer*, 36(6):585–589, 2009.

[19] C.Y. Cheng. Double diffusion from a vertical truncated cone in a non-Newtonian fluid saturated porous medium with variable heat and mass fluxes. *International Communications in Heat and Mass Transfer*, 37(3):261–265, 2010.

[20] C.Y. Cheng. Soret and Dufour effects on heat and mass transfer by natural convection from a vertical truncated cone in a fluid-saturated porous medium with variable wall temperature and concentration. *International Communications in Heat and Mass Transfer*, 37(8):1031–1035, 2010.

[21] P. Cheng. Thermal dispersion effects in non-Darcian convective flows in a saturated porous medium. *Letters in Heat and Mass Transfer*, 8(4):267–270, 1981.

[22] S.S. Chougule and S.K. Sahu. Thermal performance of automobile radiator using carbon nanotube-water nanofluid experimental study. *Journal of Thermal Science and Engineering Applications*, 6(4):041009, 2014.

[23] R.H. Christopher and S. Middleman. Power-law flow through a packed tube. *Industrial & Engineering Chemistry Fundamentals*, 4(4):422–426, 1965.

[24] J.M.K. Dake and D.R.F. Harleman. Thermal stratification in lakes: Analytical and laboratory studies. *Water Resources Research*, 5(2):484–495, 1969.

[25] H. Darcy. *The Flow of Homogeneous Fluids Through Porous Media*. Victor Dalmont, Paris, 1856.

[26] S. Das and R.N. Jana. Entropy generation in an unsteady MHD channel flow with navier slip and asymmetric convective cooling. *International Journal of Industrial Mathematics*, 9(2):149–160, 2017.

[27] S.K. Das, S.U. Choi, W. Yu, and T. Pradeep. *Nanofluids: Science and Technology*. John Wiley & Sons, 2007.

[28] R.V. Dharmadhikari and D.D. Kale. Flow of non-Newtonian fluids through porous media. *Chemical Engineering Science*, 40(3):527–529, 1985.

[29] S. Dinarvand and M.N. Rostami. Three-dimensional squeezed flow of aqueous magnetite–graphene oxide hybrid nanofluid: a novel hybridity model with analysis of shape factor effects. *Proceedings of the Institution of Mechanical Engineers, Part E: Journal of Process Mechanical Engineering*, 234(2):193–205, 2020.

[30] A.S. Dogonchi and D.D. Ganji. Effect of Cattaneo–Christov heat flux on buoyancy MHD nanofluid flow and heat transfer over a stretching sheet in the presence of Joule heating and thermal radiation impacts. *Indian Journal of Physics*, 92(6):757–766, 2018.

[31] M.C. Ece and E. Büyük. Similarity solutions for free convection to power-law fluids from a heated vertical plate. *Applied Mathematics Letters*, 15(1):1–5, 2002.

[32] M.R. Eid. Thermal characteristics of 3D nanofluid flow over a convectively heated riga surface in a Darcy-Forchheimer porous material with linear thermal radiation: an optimal analysis. *Arabian Journal for Science and Engineering*, 45(11):9803–9814, 2020.

[33] M.F. El-Amin, M.A. El-Hakiem, and M.A. Mansour. Effects of viscous dissipation on a power-law fluid over plate embedded in a porous medium. *Heat and Mass Transfer*, 39(10):807–813, 2003.

[34] M.F. El-Amin, A. Salama, S. Sun, and R.S.R. Gorla. Development of flow and heat transfer in the vicinity of a vertical plate embedded in a porous medium with viscous dissipation effects. *Special Topics & Reviews in Porous Media: An International Journal*, 3(2):169–175, 2012.

[35] E.M.A. Elbashbeshy, T.G. Emam, and E.A.A. Sayed. Effect of thermal radiation on free convection flow and heat transfer over a truncated cone in the presence of pressure work and heat generation/absorption. *Thermal Science*, 20(2):555–565, 2016.

[36] J. Fan and L. Wang. Review of heat conduction in nanofluids. *Journal of Heat Transfer*, 133(4):040801, 2011.

[37] S.O. Giwa, M. Sharifpur, and J.P. Meyer. Experimental study of thermo-convection performance of hybrid nanofluids of Al_2O_3-MWCNT/water in a differentially heated square cavity. *International Journal of Heat and Mass Transfer*, 148:119072, 2020.

[38] H. Goodarzi, O.A. Akbari, M.M. Sarafraz, M.M. Karchegani, M.R. Safaei, S. Sheikh, and A. Gholamreza. Numerical simulation of natural convection heat transfer of nanofluid with Cu, MWCNT, and Al_2O_3 nanoparticles in a cavity with different aspect ratios. *Journal of Thermal Science and Engineering Applications*, 11(6):061020, 2019.

[39] R.S.R. Gorla, V. Krishnan, and I. Pop. Free convection of a power-law fluid over the vertical frustum of a cone. *International Journal of Engineering Science*, 32(11):1791–1800, 1994.

[40] D. Gottlieb and S.A. Orszag. *Numerical Analysis of Spectral Methods: Theory and Applications*. SIAM, 1977.

[41] T. Grosan and I. Pop. A note on the effect of radiation on free convection over a vertical flat plate embedded in a non-Newtonian fluid saturated porous medium. *Applied Mechanics and Engineering*, 11(3):715, 2006.

[42] F.M. Hady, M.R. Eid, M.R. Abd-Elsalam, and M.A. Ahmed. Soret effect on natural convection boundary-layer flow of a non-Newtonian nanofluid over a vertical cone embedded in a porous medium. *IOSR Journal of Mathematics*, 8(4):51–61, 2013.

[43] M. Hassan, A. Faisal, I. Ali, M.M. Bhatti, and M. Yousaf. Effects of Cu–Ag hybrid nanoparticles on the momentum and thermal boundary layer flow over the wedge. *Proceedings of the Institution of Mechanical Engineers, Part E: Journal of Process Mechanical Engineering*, 233(5):1128–1136, 2019.

[44] T. Hayat, M. Mustafa, and S. Obaidat. Simultaneous effects of MHD and thermal radiation on the mixed convection stagnation-point flow of a power-law fluid. *Chinese Physics Letters*, 28(7):074702, 2011.

[45] T. Hayat and S. Nadeem. Heat transfer enhancement with Ag–CuO/water hybrid nanofluid. *Results in Physics*, 7:2317–2324, 2017.

[46] T. Hayat, M. Waqas, S.A. Shehzad, and A. Alsaedi. Mixed convection radiative flow of Maxwell fluid near a stagnation point with convective condition. *Journal of Mechanics*, 29(3):403–409, 2013.

[47] C.M. Hogan. Density of states of an insulating ferromagnetic alloy. *Physical Review*, 188(2):870, 1969.

[48] J.T. Hong, Y. Yamada, and C.L. Tien. Effects of non-Darcian and nonuniform porosity on vertical-plate natural convection in porous media. *Journal of Heat Transfer*, 109(2):356–362, 1987.

[49] C.J. Huang. Influence of non-Darcy and MHD on free convection of non-Newtonian fluids over a vertical permeable plate in a porous medium with Soret/Dufour effects and thermal radiation. *International Journal of Thermal Sciences*, 130:256–263, 2018.

[50] F.S. Ibrahim, S.M. Abdel-Gaid, and R.S.R. Gorla. Non-Darcy mixed convection flow along a vertical plate embedded in a non-Newtonian fluid saturated porous medium with surface mass transfer. *International Journal of Numerical Methods for Heat & Fluid Flow*, 10(4):397–408, 2000.

[51] D.B. Ingham and I. Pop. *Transport Phenomena in Porous Media III*. Elsevier, 2005.

[52] F. Irgens. *Rheology and non-Newtonian Fluids*, volume 190. Springer, 2014.

[53] R.R. Kairi. Free convection around a slender paraboloid of non-Newtonian fluid in a porous medium. *Thermal Science*, 23(5 Part B):3067–3074, 2019.

[54] R.R. Kairi and P.V.S.N. Murthy. Free convection in a thermally stratified non-Darcy porous medium saturated with a non-Newtonian fluid. *International Journal of Fluid Mechanics Research*, 36(5):414–423, 2009.

[55] R.R. Kairi and P.V.S.N. Murthy. Effect of viscous dissipation on natural convection heat and mass transfer from vertical cone in a non-Newtonian fluid saturated non-Darcy porous medium. *Applied Mathematics and Computation*, 217(20):8100–8114, 2011.

[56] S. Kakaç and A. Pramuanjaroenkij. Review of convective heat transfer enhancement with nanofluids. *International Journal of Heat and Mass Transfer*, 52(13-14):3187–3196, 2009.

[57] P.K. Kameswaran, P. Sibanda, M.K. Partha, and P.V.S.N. Murthy. Thermophoretic and nonlinear convection in non-Darcy porous medium. *Journal of Heat Transfer*, 136(4):042601, 2014.

[58] M. Khan and W.A. Khan. MHD boundary layer flow of a power-law nanofluid with new mass flux condition. *AIP Advances*, 6(2):025211, 2016.

[59] W.A. Khan and R.S.R. Gorla. Mixed convection of power-law fluids along a vertical wedge with convective boundary condition in a porous medium. *Journal of Mechanical Science and Technology*, 24(9):1919–1925, 2010.

[60] W.A. Khan and R.S.R. Gorla. Entropy generation in non-Newtonian fluids along horizontal plate in porous media. *Journal of Thermophysics and Heat Transfer*, 25(2):298–303, 2011.

[61] A.A. Khidir, M. Narayana, P. Sibanda, and P.V.S.N. Murthy. Natural convection from a vertical plate immersed in a power-law fluid saturated non-Darcy porous medium with viscous dissipation and Soret effects. *Afrika Matematika*, 26(7):1495–1518, 2015.

[62] S. Knudsen and S. Furbo. Thermal stratification in vertical mantle heat-exchangers with application to solar domestic hot-water systems. *Applied Energy*, 78(3):257–272, 2004.

[63] W. Kozicki, C.J. Hsu, and C. Tiu. Non-Newtonian flow through packed beds and porous media. *Chemical Engineering Science*, 22(4):487–502, 1967.

[64] S. Kumar and C. Diwakar. A mathematical model of power law fluid with an application of blood flow through an artery with stenosis. *Advances in Applied Mathematically Bio-Sciences*, 4(2):51–61, 2013.

[65] F.C. Lai and F.A. Kulacki. Non-Darcy mixed convection along a vertical wall in a saturated porous medium. *Journal of Heat Transfer*, 113(1):252–255, 1991.

[66] X. Liu, H.I. Mohammed, A.Z. Ashkezari, A. Shahsavar, A.K. Hussein, and S. Rostami. An experimental investigation on the rheological behavior of nanofluids made by suspending multi-walled Carbon nanotubes in liquid paraffin. *Journal of Molecular Liquids*, 300:112269, 2020.

[67] E. Magyari, I. Pop, and B. Keller. New similarity solutions for boundary-layer flow on a horizontal surface in a porous medium. *Transport in Porous Media*, 51(2):123–140, 2003.

[68] B. Mahanthesh, J. Mackolil, M. Radhika, and W. Al-Kouz. Significance of quadratic thermal radiation and quadratic convection on boundary layer two-phase flow of a dusty nanoliquid past a vertical plate. *International Communications in Heat and Mass Transfer*, 120:105029, 2021.

[69] T.R. Mahapatra, S. Mondal, and D. Pal. Heat transfer due to magnetohydrodynamic stagnation-point flow of a power-law fluid towards a stretching surface in the presence of thermal radiation and suction/injection. *International Scholarly Research Notices*, 2012:1–9, 2012.

[70] M.A. Mansour and R.S.R. Gorla. Mixed convection–radiation interaction in power-law fluids along a non–isothermal wedge embedded in a porous medium. *Transport in Porous Media*, 30(1):113–124, 1998.

[71] M. Manzur, M. Khan, and M. Rahman. Mixed convection heat transfer to cross fluid with thermal radiation: effects of buoyancy assisting and opposing flows. *International Journal of Mechanical Sciences*, 138:515–523, 2018.

[72] A.M. Megahed. Flow and heat transfer of a non-Newtonian power-law fluid over a non-linearly stretching vertical surface with heat flux and thermal radiation. *Meccanica*, 50(7):1693–1700, 2015.

[73] A.M. Megahed and M.G. Reddy. Numerical treatment for MHD viscoelastic fluid flow with variable fluid properties and viscous dissipation. *Indian Journal of Physics*, 95(4):673–679, 2021.

[74] W.J. Minkowycz and E.M. Sparrow. Local nonsimilar solutions for natural convection on a vertical cylinder. *Journal of Heat Transfer*, 96(2):178–183, 1974.

[75] W.J. Minkowycz, E.M. Sparrow, and J.P. Abraham. *Nanoparticle Heat Transfer and Fluid Flow IV*. CRC press, 2012.

[76] S.S. Motsa. A new spectral local linearization method for nonlinear boundary layer flow problems. *Journal of Applied Mathematics*, 2013:1–15, 2013.

[77] S.S. Motsa, F.G. Awad, Z.G. Makukula, and P. Sibanda. The spectral homotopy analysis method extended to systems of partial differential equations. *Abstract and Applied Analysis*, 2014:1–11, 2014.

[78] S.S. Motsa, C. RamReddy, and C.V. Rao. Non-similarity solution for Soret effect on natural convection over the vertical frustum of a cone in a nanofluid using new bivariate pseudo-spectral local linearisation method. *Applied Mathematics and Computation*, 314:439–455, 2017.

[79] P.V.S.N. Murthy. Effect of double dispersion on mixed convection heat and mass transfer in non-Darcy porous medium. *Journal of Heat Transfer*, 122(3):476–484, 2000.

[80] P.V.S.N. Murthy, S. Mukherjee, D. Srinivasacharya, and P.V.S.S.S.R. Krishna. Combined radiation and mixed convection from a vertical wall with suction/injection in a non-Darcy porous medium. *Acta Mechanica*, 168(3):145–156, 2004.

[81] P.V.S.N. Murthy, C. RamReddy, A.J. Chamkha, and A.M. Rashad. Magnetic effect on thermally stratified nanofluid saturated non-Darcy porous medium under convective boundary condition. *International Communications in Heat and Mass Transfer*, 47:41–48, 2013.

[82] T.Y. Na and J.P. Chiou. Laminar natural convection over a frustum of a cone. *Applied Scientific Research*, 35(5):409–421, 1979.

[83] A. Nakayama, T. Kokudai, and H. Koyama. An integral treatment for non-Darcy free convection over a vertical flat plate and cone embedded in a fluid-saturated porous medium. *Wärme-und Stoffübertragung*, 23(6):337–341, 1988.

[84] R. Nandkeolyar, P.K. Kameswaran, S. Shaw, and P. Sibanda. Heat transfer on nanofluid flow with homogeneous–heterogeneous reactions and internal heat generation. *Journal of Heat Transfer*, 136(12):122001, 2014.

[85] M. Narayana, A.A. Khidir, P. Sibanda, and P.V.S.N. Murthy. Viscous dissipation and thermal radiation effects on mixed convection from a vertical plate in a non-Darcy porous medium. *Transport in Porous Media*, 96(2):419–428, 2013.

[86] P.A.L. Narayana, P.V.S.N. Murthy, P.V.S.S.S.R. Krishna, and A. Postelnicu. Free convective heat and mass transfer in a doubly stratified porous medium saturated with a power-law fluid. *International Journal of Fluid Mechanics Research*, 36(6):524–537, 2009.

[87] M.K. Nayak, A.K.A. Hakeem, B. Ganga, M.I. Khan, M. Waqas, and O.D. Makinde. Entropy optimized MHD 3D nanomaterial of non-Newtonian fluid: A combined approach to good absorber of solar energy and intensification of heat transport. *Computer Methods and Programs in Biomedicine*, 186:105131, 2020.

[88] D.A. Nield and A. Bejan. *Convection in Porous Media, 4^{th} Ed.* Springer-Verlag, New York, 2013.

[89] S. Noreen and Q.U. Ain. Entropy generation analysis on electroosmotic flow in non-Darcy porous medium via peristaltic pumping. *Journal of Thermal Analysis and Calorimetry*, 137(6):1991–2006, 2019.

[90] W. Ostwald and R. Auerbach. About the viscosity of colloidal solutions in the structure, laminar and turbulence area. *Colloid Journal*, 38:261–280, 1926.

[91] I.S. Oyelakin, S. Mondal, and P. Sibanda. A multi-domain spectral method for non-Darcian mixed convection flow in a power-law fluid with viscous dissipation. *Physics and Chemistry of Liquids*, 56(6):771–789, 2018.

[92] P. Parayanthal and F.H. Pollak. Raman scattering in alloy semiconductors: "Spatial correlation" model. *Physical Review Letters*, 52(20):1822–1825, 1984.

[93] M.K. Partha. Nonlinear convection in a non-Darcy porous medium. *Applied Mathematics and Mechanics*, 31(5):565–574, 2010.

[94] M. Peters, J. Kumpfert, C.H. Ward, and C. Leyens. Titanium alloys for aerospace applications. *Advanced Engineering Materials*, 5(6):419–427, 2003.

[95] C. Ping. Combined free and forced convection flow about inclined surfaces in porous media. *International Journal of Heat and Mass Transfer*, 20(8):807–814, 1977.

[96] O.A. Plumb. The effect of thermal dispersion on heat transfer in packed bed boundary layers. In *ASME/JSME Thermal Engineering Joint Conference*, volume 2, pages 17–21, 1983.

[97] O.A. Plumb and J.C. Huenefeld. Non-Darcy natural convection from heated surfaces in saturated porous media. *International Journal of Heat and Mass Transfer*, 24(4):765–768, 1981.

[98] I. Pop and D.B Ingham. *Convective Heat Transfer: Mathematical and Computational Modelling of Viscous Fluids and Porous Media*. Elsevier, 2001.

[99] C.S.K. Raju, N. Sandeep, and V. Sugunamma. Unsteady magneto-nanofluid flow caused by a rotating cone with temperature dependent viscosity: A surgical implant application. *Journal of Molecular Liquids*, 222:1183–1191, 2016.

[100] C. RamReddy, P.A.L. Narayana, and S.S. Motsa. A spectral relaxation method for linear and non-linear stratification effects on mixed convection in a porous medium. *Applied Mathematics and Computation*, 268:991–1000, 2015.

[101] C. RamReddy and P. Naveen. Analysis of activation energy and thermal radiation on convective flow of a power-law fluid under convective heating and chemical reaction. *Heat TransferAsian Research*, 48(6):2122–2154, 2019.

[102] A.M. Rashad, T. Armaghani, A.J. Chamkha, and M.A. Mansour. Entropy generation and MHD natural convection of a nanofluid in an inclined square porous cavity: Effects of a heat sink and source size and location. *Chinese Journal of Physics*, 56(1):193–211, 2018.

[103] A. Salama. On the Brinkman equation and the concept of viscous dissipation in porous media. *Special Topics & Reviews in Porous Media: An International Journal*, 2(2):83–89, 2011.

[104] S. Saleem and M.A. El-Aziz. Entropy generation and convective heat transfer of radiated non-Newtonian power-law fluid past an exponentially moving surface under slip effects. *The European Physical Journal Plus*, 134(4):184, 2019.

[105] J. Sarkar, P. Ghosh, and A. Adil. A review on hybrid nanofluids: recent research, development and applications. *Renewable and Sustainable Energy Reviews*, 43:164–177, 2015.

[106] F. Selimefendigil and A.J. Chamkha. Natural convection of a hybrid nanofluid-filled triangular annulus with an opening. *Computational Thermal Sciences: An International Journal*, 8(6):555–566, 2016.

[107] N.S. Shashikumar, B.J. Gireesha, B. Mahanthesh, B.C. Prasannakumara, and A.J. Chamkha. Entropy generation analysis of magneto-nanoliquids embedded with alu-

minium and Titanium alloy nanoparticles in microchannel with partial slips and convective conditions. *International Journal of Numerical Methods for Heat & Fluid Flow*, 29(10):3638–3658, 2019.

[108] S. Shaw, A.S. Dogonchi, M.K. Nayak, and O.D. Makinde. Impact of entropy generation and nonlinear thermal radiation on Darcy-Forchheimer flow of $MnFe_2O_4$-Casson/water nanofluid due to a rotating disk: application to brain dynamics. *Arabian Journal for Science and Engineering*, 45(7):5471–5490, 2020.

[109] M. Sheikholeslami, M. Jafaryar, A. Shafee, and Z. Li. Nanofluid heat transfer and entropy generation through a heat exchanger considering a new turbulator and CuO nanoparticles. *Journal of Thermal Analysis and Calorimetry*, 134(3):2295–2303, 2018.

[110] A.V. Shenoy. Darcy-Forchheimer natural, forced and mixed convection heat transfer in non-Newtonian power-law fluid-saturated porous media. *Transport in Porous Media*, 11(3):219–241, 1993.

[111] N.A.C. Sidik, I.M. Adamu, M.M. Jamil, G.H.R. Kefayati, R. Mamat, and G. Najafi. Recent progress on hybrid nanofluids in heat transfer applications: A comprehensive review. *International Communications in Heat and Mass Transfer*, 78:68–79, 2016.

[112] P. Singh, H. Pungotra, and N.S. Kalsi. On the characteristics of Titanium alloys for the aircraft applications. *Materials Today: Proceedings*, 4(8):8971–8982, 2017.

[113] P. Singh, V. Radhakrishnan, and K.A. Narayan. Non-similar solutions of free convection flow over a vertical frustum of a cone for constant wall temperature. *Ingenieur-Archiv*, 59(5):382–389, 1989.

[114] A. Sözen, K. Martin, İ. Aytaç, and Ç. Filiz. Upgrading the performance of heat recovery unit containing heat pipes by using a hybrid (CuO+ ZnO)/water nanofluid. *Heat Transfer Research*, 51(14):1289–1300, 2020.

[115] E.M. Sparrow and H.S. Yu. Local non-similarity thermal boundary-layer solutions. *Journal of Heat Transfer*, 93(4):328–334, 1971.

[116] D. Srinivasacharya and K.H. Bindu. Entropy generation in a micropolar fluid flow through an inclined channel with slip and convective boundary conditions. *Energy*, 91:72–83, 2015.

[117] D. Srinivasacharya, J. Pranitha, and C. RamReddy. Magnetic and double dispersion effects on free convection in a non-Darcy porous medium saturated with power-law fluid. *International Journal for Computational Methods in Engineering Science and Mechanics*, 13(3):210–218.

[118] D. Srinivasacharya, J. Pranitha, and C. RamReddy. MHD and radiation effects on non-Darcy mixed convection. *International Journal of Nonlinear Science*, 10(1):61–69, 2010.

[119] D. Srinivasacharya and G.S. Reddy. Mixed convection heat and mass transfer over a vertical plate in a power-law fluid-saturated porous medium with radiation and chemical reaction effects. *Heat Transfer–Asian Research*, 42(6):485–499, 2013.

[120] D. Srinivasacharya and G.S. Reddy. Chemical reaction and radiation effects on mixed convection heat and mass transfer over a vertical plate in power-law fluid saturated porous medium. *Journal of the Egyptian Mathematical Society*, 24(1):108–115, 2016.

[121] L.S. Sundar, K.V. Sharma, M.K. Singh, and A.C.M. Sousa. Hybrid nanofluids preparation, thermal properties, heat transfer and friction factor–a review. *Renewable and Sustainable Energy Reviews*, 68:185–198, 2017.

[122] B.C. Tai and M.I. Char. Soret and Dufour effects on free convection flow of non-Newtonian fluids along a vertical plate embedded in a porous medium with thermal radiation. *International Communications in Heat and Mass Transfer*, 37(5):480–483, 2010.

[123] R.K. Tiwari and M.K. Das. Heat transfer augmentation in a two-sided lid-driven differentially heated square cavity utilizing nanofluids. *International Journal of Heat and Mass transfer*, 50(9-10):2002–2018, 2007.

[124] K. Vafai. *Handbook of Porous Media*. CRC Press, 2015.

[125] B. Vasu, R.S.R. Gorla, P.V.S.N. Murthy, V.R. Prasad, O.A. Bég, and S. Siddiqa. MHD free convection-radiation interaction in a porous medium-part I: Numerical investigation. *International Journal of Applied Mechanics and Engineering*, 25(1):198–218, 2020.

[126] B. Vasu, R.S.R. Gorla, P.V.S.N. Murthy, V.R. Prasad, O.A. Beg, and S. Siddiqa. MHD free convection-radiation interaction in a porous medium-part II: Soret/Dufour effects. *International Journal of Applied Mechanics and Engineering*, 25(2):157–175, 2020.

[127] B. Vasu, C. RamReddy, P.V.S.N. Murthy, and R.S.R. Gorla. Entropy generation analysis in nonlinear convection flow of thermally stratified fluid in saturated porous medium with convective boundary condition. *Journal of Heat Transfer*, 139(9):091701, 2017.

[128] A. Waele. *Viscometry and Plastometry*. Oil and Colour Chemists' Association, 1923.

[129] I. Waini, A. Ishak, T. Groşan, and I. Pop. Mixed convection of a hybrid nanofluid flow along a vertical surface embedded in a porous medium. *International Communications in Heat and Mass Transfer*, 114:104565, 2020.

[130] L. Zhang, M.M. Bhatti, and E.E. Michaelides. Electro-magnetohydrodynamic flow and heat transfer of a third-grade fluid using a Darcy-Brinkman-Forchheimer model. *International Journal of Numerical Methods for Heat & Fluid Flow*, 31(8):2623–2639, 2020.